

**Development of a twin-cuvette  
measurement system for trace gas flux  
measurements and its application to  
various gas species under laboratory  
conditions**

Dissertation  
zur Erlangung des Grades

“Doktor der Naturwissenschaften”

im Promotionsfach Chemie  
am Fachbereich Chemie, Pharmazie und Geowissenschaften  
der Johannes Gutenberg-Universität  
in Mainz

Shang Sun  
geb. in Shaanxi, Volksrepublik China

Mainz, den 24.11.2016

Dekan: Prof. Dr. Dirk Schneider

Berichterstatter:

1. Berichterstatter: Prof. Dr. Thorsten Hoffmann
2. Berichterstatter: Prof. Dr. Jürgen Kesselmeier

Tag der mündlichen Prüfung: 22.11.2016

# Ehrenwörtliche Erklärung

**(§ 10 Abs. 3d – aa der Promotionsordnung)**

Hiermit erkläre ich eidesstattlich, dass ich die Dissertation selbständig verfasst und keine anderen als die von mir angegebenen Quellen und Hilfsmittel benutzt habe.

**(§ 10 Abs. 3d – bb der Promotionsordnung)**

Hiermit erkläre ich eidesstattlich, dass ich die vorliegende Dissertation nicht als Prüfungsarbeit für eine andere Prüfung eingereicht habe.

**(§ 10 Abs. 3d – cc der Promotionsordnung)**

Hiermit erkläre ich eidesstattlich, dass ich die gleiche oder Teile der Dissertation noch nicht bei einer anderen Fakultät oder einem anderen Fachbereich eingereicht habe.

Datum, Ort:

Unterschrift des Verfassers:



# Summary

Ozone (O<sub>3</sub>), Peroxyacetyl nitrate (PAN) and trimethylamine (TMA) are reactive gases in the atmosphere and play an important role in atmospheric chemistry as well as for particle formation. They have an impact on the air quality, human health and ecosystems. Therefore, understanding their sources and sinks is essential for the determination of global atmospheric budgets and for the improvement of the environmental quality.

It is well-known that O<sub>3</sub> and PAN are taken up by terrestrial vegetation. But the mechanism determining their non-stomatal deposition process is not totally understood. Especially, the influence of humidity on the non-stomatal deposition pathway is mainly deduced from field measurements. But for the understanding of their underlying mechanisms more systematical investigations of the processes are required. The role of TMA in the atmosphere is a special topic, which becomes more important in view of its impact on new particle formation (NPF). The contribution of its emission from terrestrial vegetation is poorly understood and needs more investigations to estimate the contribution to the chemical and physical processes.

Within this thesis a twin-cuvette measurement system to analyze the exchange fluxes of reactive gases as O<sub>3</sub> and PAN with plants under controlled environmental conditions has been developed. The resolution of the mixing ratio difference measured with this cuvette setup was high, so that even small differences in the range of few hundred ppt O<sub>3</sub> and several ppt PAN could be differentiated in the measurement data. With a special focus on the investigations of the flux partitioning, i.e. the discrimination between stomatal and non-stomatal deposition of O<sub>3</sub> and PAN, such a measurement system with high precision to resolve the mixing ratio difference was required. A main feature of the setup was the Automatic Temperature Regulated Air Humidification System (ATRAHS), which allows a precise regulation (0.3 %) of the relative humidity within the dynamic cuvette in a range of 40 – 90 %. This feature is essential for the investigation of the impact of humidity on the deposition process of O<sub>3</sub> and PAN.

In the first case study, the influence of liquid surface films on the O<sub>3</sub> and PAN deposition was investigated. We observed a clear relationship between the O<sub>3</sub> deposition on plants (*Quercus ilex*) and the relative humidity (*RH*). In the presence of light, the opening of leaf stomata were

responsible for the increasing  $O_3$  deposition, while during the absence of light the liquid surface films were the reason for  $O_3$  deposition as shown by closing stomata by the addition of abscisic acid (ABA). Therefore, the liquid surface film significantly contributes to the total deposition of  $O_3$ . Additionally, we demonstrated that the formation of the liquid surface film on leaves as well as the non-stomatal  $O_3$  deposition are depending on the chemical composition of the particles deposited on the leaf cuticles as has been previously proposed by Fuentes and Gillespie (1992). In the case of PAN, a similar correlation between the deposition flux and  $RH$  was found in the presence of light, indicating the dominance of stomatal uptake. In the dark period, no relationship with  $RH$  was found, which may be related to the lower rate of aqueous partitioning for PAN than  $O_3$ . A contribution of non-stomatal PAN deposition was found to be  $\sim 20\%$ , which was not affected by liquid surface films. Therefore, the ratio of the  $O_3$  and PAN deposition velocities is not constant when relative humidity changes, as assumed in many models.

In the second case study, we investigated the emission of TMA by *Chenopodium vulvaria*. The analysis of the leaf anatomy showed that the emission of TMA can be related to the epidermal gland vesicles, which were well distributed on both sides of the plant leaf. Additionally, we could show that mechanical stimuli such as slight air streams were able to destroy these gland vesicles, which led to a high emission of TMA up to  $8 \text{ nmol m}^{-2} \text{ s}^{-1}$  or a local mixing ratio of 100 ppb. Also, environmental factors as temperature and relative humidity seem to be a driving force for the emission of TMA from that plant, which is in agreement with the suggestion from Cromwell (1949). Additionally, a screening of different flowering plants showed that plant emissions of TMA might not be restricted to specialized plants. Furthermore, their potential impact on the atmospheric new particle formation could be demonstrated qualitatively by the ternary nucleation systems with sulfuric acid – TMA –  $H_2O$  and formic acid – TMA –  $H_2O$ . Sulfuric acid was used to test if enhanced formation can be reproduced according to recent publications (e.g. Almeida et al., 2013). A new approach was to study the nucleation with organic acids. For formic acid, the particle concentration was about 3 orders of magnitude less than for sulfuric acid, whereas for the other tested organic acids (acetic acid and tartaric acid) no particle formation was observed.

# Zusammenfassung

Ozon ( $O_3$ ), Peroxyacetylnitrat (PAN) und Trimethylamin (TMA) sind reaktive Gase in der Atmosphäre und spielen eine wichtige Rolle in der Atmosphärenchemie sowie bei der Partikelneubildung. Sie beeinflussen die Luftqualität, menschliche Gesundheit und das Ökosystem. Daher sind Kenntnisse über ihre Quellen und Senken von entscheidender Bedeutung für die Bestimmung des globalen atmosphärischen Budgets und die Verbesserung der Umweltqualität.

Es ist wohlbekannt, dass  $O_3$  und PAN von der Vegetation aufgenommen werden. Jedoch ist dabei der Mechanismus, der ihre nicht-stomatäre Deposition bestimmt, noch nicht ausreichend geklärt. Besonders der Einfluss der Feuchte auf die nicht-stomatäre Deposition ist ein Effekt, der fast ausschließlich und immer wieder in Feldmessungen beobachtet wird. Um jedoch den dahinterliegenden Mechanismus zu verstehen, sind weitere systematische und prozessorientierte Untersuchungen nötig. Die Rolle von TMA in der Atmosphäre ist von großem Interesse wegen seines Einflusses auf die Partikelneubildung (PNF). Der Beitrag der Emission durch die Vegetation ist dabei weitgehend unklar und benötigt weitere, differenzierte Untersuchungen, um die Einflüsse auf chemische und physikalische Prozesse abschätzen zu können.

Diese Doktorarbeit beschreibt die Entwicklung eines Doppelküvettenmesssystems, um die Austauschflüsse von reaktiven Gasen wie  $O_3$  und PAN mit Pflanzen unter konstanten Umweltbedingungen zu analysieren. Die Auflösung der gemessenen Mischungsverhältnisdifferenz ist so hoch, dass in den Messdaten für  $O_3$  bereits im Bereich von wenigen Hundert ppt und PAN im Bereich von einigen ppt unterschieden werden kann. Besonders für die Untersuchung von Flusspartitionierung zwischen stomatärer und nicht-stomatärer Deposition von  $O_3$  und PAN wird solch ein Messsystem benötigt, das in der Lage ist, kleinste Flussdifferenzen aufzulösen. Ein Hauptmerkmal des Setups ist das Automatic Temperature Regulated Air Humidification System (ATRAHS), welches in der Lage ist, mit einer hohen Präzision von 0.3 % die relative Feuchte in der Küvette im Bereich von 40 – 90 % zu steuern. Dies ist entscheidend für die Untersuchung des Einflusses der Feuchte auf den Depositionsprozess von  $O_3$  und PAN.

In der ersten Fallstudie wurde der Einfluss von oberflächigen Wasserfilmen auf die Deposition von  $O_3$  und PAN untersucht. Wir beobachteten einen klaren Zusammenhang zwischen der  $O_3$  Deposition an Pflanzen (*Quercus ilex*) und der relativen Feuchte (RH). In der

Anwesenheit von Licht konnte der Anstieg der O<sub>3</sub> Deposition auf die geöffneten Spaltöffnungen zurückgeführt werden, während in der Abwesenheit von Licht die oberflächigen Wasserfilme der Grund für die O<sub>3</sub> Deposition war, wie sich durch das künstliche Verschließen der Spaltöffnungen mittels Abscisinsäure (ABA) zeigte. Somit tragen oberflächige Wasserfilme zur Gesamtdeposition von O<sub>3</sub> signifikant bei. Zusätzlich fanden wir heraus, dass sowohl die Bildung von Wasserfilmen auf Blattoberflächen als auch die nicht-stomatäre Deposition von O<sub>3</sub> von der chemischen Zusammensetzung der deponierten Partikeln auf der Blattoberfläche abhängt, wie eine frühere Studie von Fuentes and Gillespie (1992) bereits vermutet hatte. Für PAN wurde ein ähnlicher Zusammenhang zwischen der Deposition und *RH* in der Anwesenheit von Licht festgestellt, was die Dominanz der stomatären Aufnahme zeigte. In der Dunkelperiode wurde keine Abhängigkeit zu *RH* festgestellt, was eventuell mit der niedrigeren Wasserlöslichkeit von PAN im Vergleich zu O<sub>3</sub> in Verbindung gebracht werden kann. Dabei wurde ein nicht-stomatärer Beitrag von ca. 20 % festgestellt, welcher nicht durch Wasserfilme beeinflusst wurde. Man kann daher nicht davon ausgehen, dass das Verhältnis der Depositionsgeschwindigkeit von O<sub>3</sub> und PAN bei Feuchteänderung konstant bleibt, was bisher von vielen Berechnungsmodellen angenommen wird.

In der zweiten Fallstudie wurde die Emission von TMA durch *Chenopodium vulvaria* untersucht. Die Analyse der Blattanatomie zeigte, dass die Emission von TMA in Zusammenhang mit den epidermalen Drüsenhaaren gebracht werden kann, welche homogen auf beiden Blattseiten verteilt waren. Zusätzlich konnten wir durch mechanische Stresstests zeigen, dass bereits die geringste Beeinflussung, wie beispielsweise ein leichter Luftstrom, diese Drüsenhaare zerstören kann und somit zu einer hohen Emissionsrate von über 8 nmol m<sup>-2</sup> s<sup>-1</sup> oder einem lokalen Mischungsverhältnis von 100 ppb an TMA führen kann. Ebenfalls scheint es so, dass Umweltfaktoren wie Temperatur und Luftfeuchte die Emission von TMA durch diese Pflanze beeinflussen kann, was im Einklang mit der Vermutung von Cromwell (1949) steht. Zusätzlich zeigte ein Screening-Experiment von verschiedenen Spezies an Blütenpflanzen, dass die Emission von TMA nicht zwangsläufig auf bestimmte Pflanzenarten beschränkt ist. Darüber hinaus konnte ihr potentieller Einfluss auf die atmosphärische Partikelneubildung qualitativ anhand von ternären Nukleationssystemen wie Schwefelsäure – TMA – H<sub>2</sub>O und Ameisensäure – TMA – H<sub>2</sub>O gezeigt werden. Schwefelsäure wurde verwendet, um zu testen, ob die erhöhte Partikelbildung nach den aktuellen Publikationen reproduziert werden kann (siehe Almeida et al., 2013). Ein neues Vorgehen war es, die Nukleation mit organischen Säuren zu studieren. Bei Ameisensäure zeigte sich dabei eine um 3 Größenordnungen niedrigere Partikelkonzentration als bei Schwefelsäure, wobei für die anderen getesteten organischen Säuren (Essigsäure und Weinsäure) keine Partikelneubildung beobachtet wurde.



# List of manuscripts

This dissertation is written in a cumulative form and includes three individual manuscripts. One manuscript has been published in a scientific journal. The second manuscript has been submitted to a peer-reviewed journal. The third manuscript will be submitted.

## Published manuscript

Sun, S., Moravek, A., von der Heyden, L., Held, A., Sörgel, M. and Kesselmeier, J.: Twin-cuvette measurement technique for investigation of dry deposition of O<sub>3</sub> and PAN to plant leaves under controlled humidity conditions, *Atmospheric Measurement Techniques*, 9, 599-617, doi:10.5194/amt-9-599-2016, 2016.

## Accepted manuscript

Sun, S., Moravek, A., Trebs, I., Kesselmeier, J. and Sörgel, M.: Investigation of the influence of liquid surface films on O<sub>3</sub> and PAN deposition to plant leaves coated with organic / inorganic solution, *Journal of Geophysical Research: Atmospheres*, DOI: 10.1002/2016JD025519, 2016

## Manuscript to be submitted

Shang S., Neftel, A., Sintermann, J., Sauvage, C., Derstroff, B., Bohley, K., Kadereit, G., Williams, J., Pöhlker, C., Kesselmeier, J. and Sörgel, M.: Emission of trimethylamine from *Chenopodium vulvaria* - first results from quantifying plant emissions of amines and their potential effects on the atmospheric new particle formation







# Table of contents

Ehrenwörtliche Erklärung .....	3
Summary .....	5
Zusammenfassung .....	7
List of manuscripts .....	9
Table of contents .....	13
Table of figures .....	19
List of abbreviations .....	21
1 Introduction .....	23
1.1 The fate of tropospheric O <sub>3</sub> .....	23
1.2 The important role of PAN in the global nitrogen cycle .....	25
1.3 The emission of amines from terrestrial vegetation and its influence on new atmospheric particle formation.....	28
1.4 Purposes of the thesis .....	29
2 Methods .....	31
2.1 The methodology of cuvette measurement system.....	31
3 Results .....	35
3.1 Development and performance of the twin-cuvette measurement system .....	35
3.1.1 Setup.....	35
3.1.2 Performance .....	37
3.1.2.1 Residence time .....	37
3.1.2.2 Loss of O <sub>3</sub> and PAN within the twin-cuvette system .....	37
3.1.2.3 Accuracy of the twin-cuvette measurement system.....	38

---

3.1.2.4	Humidification .....	38
3.2	Case study: Investigation of the influence of liquid surface films on O <sub>3</sub> and PAN deposition to plant leaves coated with organic / inorganic solution .....	39
3.2.1	Flux partitioning .....	40
3.2.2	Impact of leaf surface composition and water films on the non-stomatal deposition of O <sub>3</sub> and PAN .....	41
3.2.3	Deposition velocity ratio of O <sub>3</sub> and PAN .....	42
3.3	Case study: Emission of Trimethylamine from <i>Chenopodium vulvaria</i> - first results from quantifying plant emissions of amines and their potential effects on atmospheric new particle formation .....	43
3.3.1	Leaf anatomic structure and reservoir for TMA .....	44
3.3.2	Screening experiment over different plant species .....	44
3.3.3	Emission of TMA from <i>Chenopodium vulvaria</i> .....	45
3.3.4	Impact on atmospheric new particle formation .....	46
4	Conclusions & Outlook .....	47
	References .....	51
	Appendix A .....	59
	Appendix B .....	63
	Abstract .....	64
1	Introduction .....	64
2	Material and Methods .....	67
2.1	Setup of dual dynamic cuvette system .....	67
2.1.1	General setup .....	67
2.1.2	Dynamic cuvette .....	69
2.1.3	Automatic Temperature Regulated Air Humidification System (ATRAHS) .....	71
2.1.4	Leaf wetness sensor .....	72
2.2	Test experiment with O <sub>3</sub> and PAN .....	73
2.2.1	Plant material and growth conditions .....	73
2.2.2	Plant cabinet conditions .....	73
2.2.3	Determination of the leaf area .....	74

---

2.2.4 Application of abscisic acid .....	74
2.2.5 Calculation of fluxes and plant exchange parameters .....	74
2.3 System characterization and quality assurance .....	76
2.3.1 Evaluation of the twin-cuvette system and O <sub>3</sub> and PAN loss .....	76
2.3.2 Calibration procedure .....	76
2.3.3 Random flux error calculation and statistical significance .....	77
3 Results .....	78
3.1 Performance of the twin-cuvette system .....	78
3.1.1 Quality of O <sub>3</sub> and PAN measurements .....	78
Comparison between the empty sample and reference cuvettes .....	78
Precision and detection limit (LOD) of the cuvette system .....	79
3.1.2 Quality of the humidity regulation with ATRAHS .....	80
3.1.3 Loss of O <sub>3</sub> and PAN within the system .....	81
3.2 Flux measurements under laboratory conditions .....	83
3.2.1 Test run and flux rates .....	83
3.2.2 Correlation between ambient mixing ratio and uptake of O <sub>3</sub> and PAN .....	85
3.2.3 Application of abscisic acid (ABA) .....	86
3.2.4 Influence of RH on electrical surface conductance .....	88
4 Discussion .....	89
4.1 Performance of the twin-cuvette system .....	89
4.1.1 Accuracy and consistency of O <sub>3</sub> and PAN measurements .....	89
4.1.2 ATRAHS .....	90
4.2 Flux measurements under laboratory conditions .....	91
5 Conclusions .....	93
Acknowledgements .....	<b>Fehler! Textmarke nicht definiert.</b>
References .....	94
Appendix C .....	99
Abstract .....	100
1 Introduction .....	100

---

2 Material and Methods.....	103
2.1 Plant Material and Growth .....	103
2.2 O <sub>3</sub> and PAN flux measurements.....	103
2.3 Flux experiment 1: stomatal and non-stomatal flux partitioning under outdoor air conditions .....	106
2.4 Flux experiment 2: effect of liquid surface film composition on non-stomatal deposition .....	107
3 Results .....	108
3.1 Flux experiment 1: stomatal and non-stomatal flux partitioning under outdoor air conditions .....	108
3.2 Flux experiment 2: effect of liquid surface film composition on non-stomatal deposition .....	111
4 Discussion .....	114
4.1 Stomatal and non-stomatal deposition after exposure to outdoor air conditions .....	114
4.2 Influence of leaf surface and liquid surface films on non-stomatal deposition .....	120
5 Conclusion.....	123
Acknowledgement.....	<b>Fehler! Textmarke nicht definiert.</b>
References .....	124
Appendix D .....	133
Abstract .....	134
1 Introduction .....	134
2 Material and Methods.....	136
2.1 Plant growth condition .....	136
2.2 Leaf sectioning of <i>Chenopodium vulvaria</i> and extraction of the sap of bladder cells for chemical identification of TMA .....	136
2.3 TMA-emission measurement with GC-NCD.....	136
2.3.1 Performance of the GC-NCD and peak identification .....	136
2.3.2 Screening experiment.....	137
2.4 TMA-emission measurement with PTR-TOF-MS.....	138
2.4.1 Performance of the PTR-TOF-MS .....	138



---

2.4.2 Twin-cuvette setup .....	138
2.4.3 TMA-Emission experiment with <i>Chenopodium vulvaria</i> .....	139
2.5 Investigation of new particle formation .....	140
2.5.1 Setup of the flow reactor .....	140
2.5.2 Nucleation experiment .....	142
3 Results .....	142
3.1 Leaf anatomic structure and reservoir for TMA .....	142
3.2 Chemical identification of TMA within bladder cells .....	142
3.3 Identification of TMA .....	143
3.4 Screening experiment with GC-NCD .....	144
3.5 Emission of TMA from <i>Chenopodium vulvaria</i> .....	145
3.6 Influence of TMA on atmospheric new particle formation.....	147
4 Discussion .....	148
4.1 Leaf anatomic structure and reservoir for TMA .....	148
4.2 Screening experiment with different plant species and their potential contribution to the emission of volatile TMA.....	149
4.3 Emission of TMA from <i>Chenopodium vulvaria</i> .....	150
4.4 Influence of TMA on atmospheric new particle formation.....	151
5 Conclusion.....	152
Acknowledgements .....	<b>Fehler! Textmarke nicht definiert.</b>
References .....	153
Appendix E.....	157
Curriculum vitae.....	157



## Table of figures

<i>Fig. 1: Formation of O<sub>3</sub> and its sources, sinks and transport in the troposphere. ....</i>	24
<i>Fig. 2: PAN formation and its sources, sinks and transport in the troposphere, relating to the anthropogenic influence. ....</i>	27
<i>Fig. 3: Flow chart of the dual cuvette system. 1 plant cabinet, 2 water storage tank, 3 ATRAHS, 4 Temperature and relative humidity sensor for humidity, 5 mass flow controller (MFC), 6 dynamic cuvette (reference), 7 dynamic cuvette (sample), 8 Temperature and relative humidity sensor for monitoring, 9 Teflon- valve block, 10 MFC for gas addition, 11 O<sub>3</sub> – primary standard, 12 PAN – calibration unit, 13 mixing vessel, 14 overflow, 15 Teflon membrane pump (Sun et al., 2016a, Appendix B). ....</i>	36
<i>Fig. 4: Flow chart of the automatic temperature regulated air humidification system (ATRAHS). 1 deionized water supply; 2 water storage tank; 3 humidifier tank; 4 float valve; 5 V25 control device; 6 T/RH sensor (initial regulation); 7 T/RH sensor (monitoring); 8 dynamic cuvette; 9 heat element. ....</i>	39
<i>Fig. 5: Calculated partitioning ratio <math>R_{nsto/sto}</math> between non-stomatal and stomatal deposition flux (left) and <math>R_{nsto/tot}</math> between non-stomatal and total deposition flux (right) of O<sub>3</sub> (black) and PAN (red) versus RH. The red and grey uncertainty areas of the partitioning ratios were propagated considering the errors of the stomatal and non-stomatal fluxes of O<sub>3</sub> and PAN (Sun et al., 2016b, Appendix C). ....</i>	41
<i>Fig. 6: O<sub>3</sub>, PAN flux and electrical surface conductance G at various RH (5 % - 80 %) during the dark period under ABA induced stomatal closure. Cleaned leaf surface (column a), exposed with outdoor air (column b), treated with inorganic solution (column c), treated with humic acid (column d) and treated with Cl, Br (column e). The increasing trend was fitted with an exponential growth function. ....</i>	42
<i>Fig. 7: Deposition velocity ratio between PAN and O<sub>3</sub> of different deposition pathways <math>nsto+sto</math> (black), <math>sto</math> (red) and <math>nsto</math> (blue) in relation to RH compared with various modelled deposition velocity ratio as GEOS-chem (orange dashed), EMEP (green, dashed) and <math>D_{PAN}/D_{O_3}</math> (blue, dashed). The shaded uncertainty areas of the deposition velocity ratios were</i>	

---

*propagated considering the errors of the stomatal and non-stomatal fluxes and deposition velocities of O<sub>3</sub> and PAN (Sun et al., 2016b, Appendix C). ..... 43*

*Fig. 8: Glandular hairs on the bottom of the leaf surface of *Chenopodium vulvaria* (left) and the leaf cross section of *Chenopodium vulvaria* (right). These glandular hairs emerge from the top and bottom leaf epidermis. They are specialised trichomes consisting of a thin stalk and a large globular vesicle..... 44*

*Fig. 9: TMA screening experiment over four different plant species. *Crataegus monogyna*, *Sorbus aucuparia* and *Pyrus communis* were measured at flowering period. Emitted substances were characteristic for their retention time (RT). ■ RT 2.13, ● RT 2.29, ▲ RT 2.34, ▼ RT 2.37(acetonitrile), ◆ RT 2.65, ◀ RT 3.35 (assumed to be TMA). ..... 45*

*Fig. 10: Emitted trimethylamine (TMA) from *Chenopodium vulvaria*. Mixing ratio (left) and emission flux (right). Plant samples growth under various fertilization levels low (black line), middle (blue line) and high (red line). ..... 46*

# List of abbreviations

ABA	Abscisic acid
ATRAHS	Automatic Temperature Regulated Air Humidification System
C <sub>2</sub> H <sub>4</sub> O <sub>3</sub>	Peracetic acid radicals
CO	Carbon monoxide
DMA	Dimethylamine
DMS	Dimethyl sulphide
ECD	Electron capture detector
EMEP	European Monitoring and Evaluation Programme
FEP	Fluorinated ethylene propylene
G	Electrical surface conductance
GC	Gas chromatography
GEOS	Goddard Earth Observing System
LOD	Limit of detections
M	Collision partner
MA	Methylamine
MFC	Mass flow controller
MMA	Monomethylamine
N	Nitrogen
NCD	Nitrogen chemiluminescence detector
NH <sub>3</sub>	Ammonia
N <sub>2</sub> O	Nitrous oxide
NO <sub>x</sub>	Nitrogen oxides
NO <sub>2</sub>	Nitrogen dioxide
NO	Nitrogen monoxide
NPF	New particle formation
N <sub>r</sub>	Reactive nitrogen species

O	Oxygen radical
O(3P)	Exited oxygen atom in triplet state
O <sub>3</sub>	Ozone
PAN	Perxoyacetyl nitrate
PFA	Perfluoroalkoxy alkanes
ppt	Parts per trillion
ppb	Parts per billion
RH	Relative humidity
RO <sub>2</sub>	organic peroxy radical
SO <sub>2</sub>	Sulfur dioxide
T	Temperature
TMA	Trimethylamine
UV	Ultraviolet
VOCs	Volatile organic compounds

# 1 Introduction

## 1.1 The fate of tropospheric O<sub>3</sub>

O<sub>3</sub> is an important trace gas in the troposphere. Due to its high reactivity, it controls (mostly in the form of OH-radicals) a wide variety of photochemical reactions in the atmosphere (Ravishankara et al., 1998), such as the oxidation of hydrocarbons, carbon monoxide, dimethyl sulphide, and sulfuric acid (Johnson et al., 1990; Stehr et al., 2002; Watanabe et al., 2005). O<sub>3</sub> is a secondary air pollutant, which can have negative impacts on natural ecosystems (Paoletti, 2009) and human health (Lippman, 1989). Many previous studies showed that the dominant sources of O<sub>3</sub> in the troposphere are the downward transport from the stratosphere on the one hand and photochemical reactions on the other hand. The latter involves reactions of other pollutants such as volatile organic compounds (VOCs), carbon monoxide (CO) and nitrogen oxides (NO<sub>x</sub>) in the presence of sunlight (see R1-R3 and Fig. 1) (Crutzen, 1974; Liu et al., 1980), which account for ~20 % and ~80 % of the production of global tropospheric O<sub>3</sub> (Crutzen et al., 1999; Lelieveld and Crutzen, 1994; Ganguly and Tzanis, 2011).



R1 - R3 constitute a zero cycle, which creates and destroys ozone at the same time. This zero ozone cycle is disturbed indirectly by oxidation of VOCs, which produce peroxyradicals that converts NO to NO<sub>2</sub> without destroying O<sub>3</sub> and leads to a net production of tropospheric O<sub>3</sub> (see Fig. 1). In urban areas these precursors are associated with vehicular emissions (esp. for NO<sub>x</sub>) and make O<sub>3</sub> to a major component of urban smog (Sillman, 2003).

Tropospheric O<sub>3</sub> is known as a threat for ecosystems due to its plant toxicity (Fuhrer et al., 1997). This negative effect on plants, especially crops, results in yield losses, which are associated with economic losses. A global impact assessment for major agriculture crops estimated annual production losses of \$US 14-74 billion under present air quality legislation

(Van Dingenen et al., 2009). Furthermore, Madronich et al. (2015) showed that a higher exposure to air pollutants such as  $O_3$  leads to an increasing risk of cardiovascular and respiratory diseases in humans and is associated with several million deaths annually. Hence, there is a general interest in the knowledge about the flux of  $O_3$  between the atmosphere and terrestrial ecosystems.

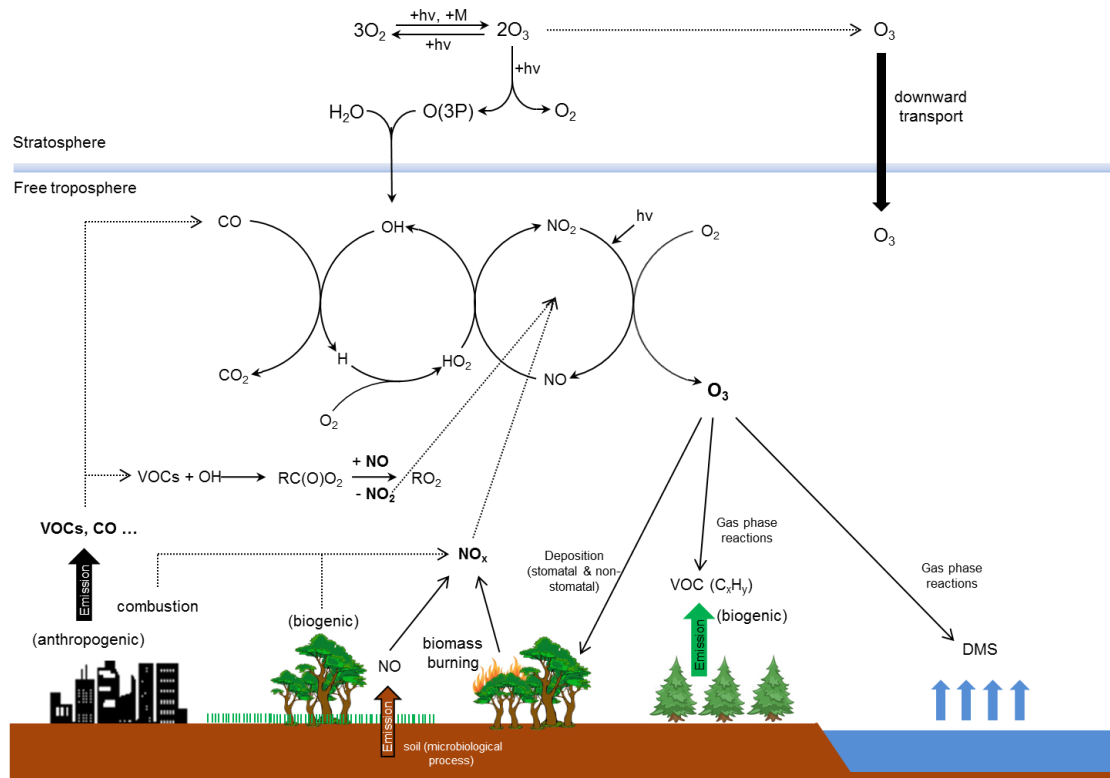


Fig. 1: Formation of  $O_3$  and its sources, sinks and transport in the troposphere.

Besides other removal processes of  $O_3$  in the atmosphere such as photolysis and gas phase reactions with VOCs and NO, the terrestrial surfaces represent the main sink for boundary layer  $O_3$  (Simpson, 1992). The sink intensity is depending on the combination of all removal pathways including stomatal as well as non-stomatal deposition (Fares et al., 2012). Non-stomatal  $O_3$  deposition on plants includes various pathways such as deposition on leaf cuticle, soil, stems and gas phase reactions. On the one hand, Loreto and Fares (2007) concluded the stomatal uptake by plant leaves to be the dominant contribution to the total  $O_3$  deposition for ecosystems in typical European regions during daytime. On the other hand, Hogg et al. (2007) showed for a hardwood forest during daytime that the non-stomatal  $O_3$  conductance accounted for  $\sim 66\%$  of the canopy conductance and the non-stomatal sink represented  $63\%$  of the  $O_3$  flux. However, several studies had shown that the contribution of non-stomatal deposition to the total  $O_3$  deposition is not necessarily constant and varied diurnally (Coe et al., 1995; Granat and Richter, 1995; Gerosa et al., 2005). The variations of the non-stomatal



partition has been attributed to physicochemical processes such as surface reaction, gas phase reaction, and environmental factors like temperature, light, wind speed and relative humidity. Fuentes and Gillespie (1992) found that the O<sub>3</sub> deposition was enhanced by leaf surface wetness in the form of a dew layer or raindrops. Additionally, Altimir et al. (2006) found a clear correlation between the non-stomatal O<sub>3</sub> deposition and ambient relative humidity over 70 % in the boreal zone. Their suggestion that the non-stomatal O<sub>3</sub> deposition on the leaf cuticle was influenced by the leaf surface water film was in line with the conclusion of Fuentes and Gillespie (1992). Further, Rudich et al. (2000) found that the formation of liquid films on organic surfaces is depending on the chemical composition and corrugation degree of the surface. Fuentes and Gillespie (1992) came to the similar conclusion that the increased O<sub>3</sub> deposition may be ascribed mainly to the presence of compounds in aqueous form, which scavenge O<sub>3</sub> by chemical reactions.

Conclusively, investigations on the flux partitioning of O<sub>3</sub> are important to quantify the global sinks of atmospheric O<sub>3</sub>. This topic is covered by many field studies, which measured O<sub>3</sub> fluxes at the canopy of forests to estimate the overall non-stomatal O<sub>3</sub> deposition. But, systematical investigations, especially in relation to the environmental humidity are very limited. This aspect of the O<sub>3</sub> deposition shows the importance of the accurate determination of the stomatal as well as the non-stomatal deposition pathway, which also improves the knowledge about the real O<sub>3</sub> tolerance of plants. Further, it plays a key role for estimations of the global O<sub>3</sub> budget and is essential for taking action against the environmental pollution. As it was shown, the sources and sinks of tropospheric O<sub>3</sub> are strongly influenced by both, anthropogenic and biogenic activities. Therefore, knowledge about the interaction between the biosphere and atmosphere is required for the understanding of the atmospheric chemistry and the fate of O<sub>3</sub> in the global trace gas cycle.

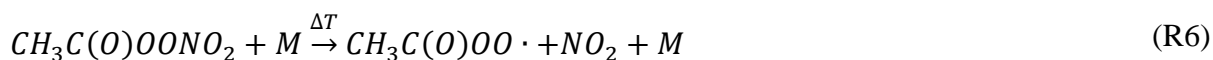
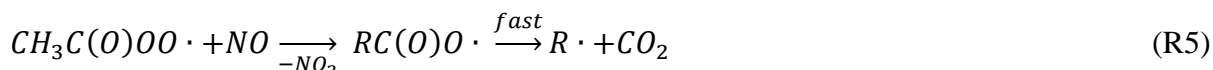
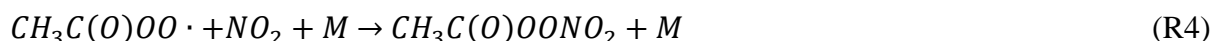
### **1.2 The important role of PAN in the global nitrogen cycle**

Nitrogen (N) is one of the most important elements which are crucial for life on earth and essential for the growth and functioning of plants, animals and humans (Hatfield and Follett, 2008). In the atmosphere, nitrogen compounds have effects on the chemical processes such as tropospheric O<sub>3</sub> production or particle formation. Only a small fraction of the large reservoir of unreactive molecular nitrogen (N<sub>2</sub>) in the atmosphere is available for uptake by plants and microorganisms, which transform the molecular N<sub>2</sub> to reactive nitrogen species (N<sub>r</sub>) by biological fixation (Fowler et al., 2013). Further biogenic sources of atmospheric N<sub>r</sub> are biomass burning and lightning (Erisman et al., 2013). Due to the limitation of natural N<sub>r</sub> related to increasing growth of the world population, the demand of nitrogen as a key

component for food production led to the development of synthetic fertilizers by industrial fixation of molecular  $N_2$  (Erisman et al., 2008; Galloway et al., 2003; Smil, 2001). The additional anthropogenic release of  $N_r$  to the atmosphere, which becomes nowadays greater than all natural terrestrial systems (Galloway et al., 2003), is responsible for the increase of negative effects for the environment and human health in the last century. The amount of  $N_r$  used for food production is on average 10-fold higher than needed, due to the inefficiencies in the production, processing, and consumption (Sutton et al., 2011; Galloway et al., 2008, 2003). Further anthropogenic sources such as agriculture, combustion process for energy production, transport, and industry contribute to the emission of millions of tons  $N_r$  ( $NO_x$ ,  $N_2O$ ,  $NH_3$ ) to the atmosphere annually (Erisman et al., 2003).  $N_r$  is highly mobile and can enter the environment and be transported via different media (air, water and terrestrial ecosystems). Being once arrived, it can take negative effects on the environment, human health and climate change (Galloway et al., 2003, 2008). Therefore, it is important to understand the interaction of the  $N_r$  in the atmosphere with the biosphere and its potential sources and sinks.

In the last decades, the knowledge about processes within the global nitrogen cycle has been improved significantly (Galloway et al., 2013). But the atmospheric organic nitrogen is still a poorly understood component of the atmospheric nitrogen deposition flux (Jickells et al., 2013, Cape et al., 2011). Jickells et al. (2013) suggests the organic nitrogen flux to be 25 % of the total nitrogen deposition flux. Closely related to their solubilities and chemical properties, organic nitrogen species can be found in aqueous, gaseous and particulate phases. While the removal of soluble organic nitrogen species in the atmosphere is determined by wet deposition pathways, the fate of insoluble species such as peroxyacetyl nitrate (PAN) is subject to conditions such as chemical transformation or dry deposition. Since PAN plays an important role in the global nitrogen transport system and is toxic to plants, a deeper understanding of its uptake efficiency by ecosystems in relation to  $O_3$  is required.

PAN is a secondary trace gas, which is produced in the atmosphere by photochemical oxidation of volatile organic substances to peracetic acid radicals ( $C_2H_4O_3$ ) in the presence of nitrogen dioxide (see Fig. 2 and R4) (Tuazon et al., 1991). Besides the formation of PAN, a further reaction pathway (R5) competes with the PAN formation by reaction of  $RO_2$  with  $NO$ .



Atmospheric PAN mixing ratios vary from several ppt to few ppb. While in the northern free troposphere, a PAN mixing ratio of 100 ppt could be observed (Singh, 1987), the PAN mixing

ratio could exceed several tens of ppb or even higher under urban conditions (Rubio et al., 2007).

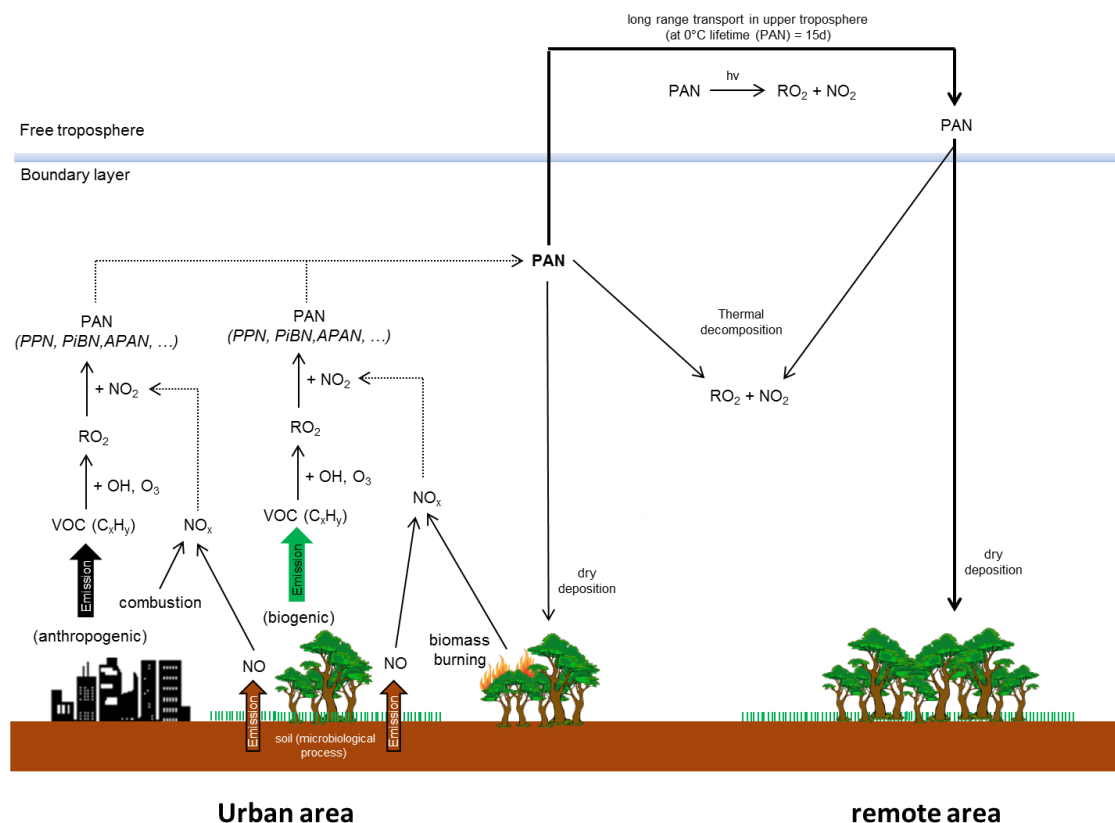


Fig. 2: PAN formation and its sources, sinks and transport in the troposphere, relating to the anthropogenic influence.

As shown in Fig. 2, the precursors required for the formation of RO<sub>2</sub> are VOCs emitted from both biogenic and anthropogenic sources. The produced PAN can reach the upper troposphere by convection, where the main removal process for PAN under low temperature is mainly depending on the UV photolysis. This is regarded as an important process above 7 km (Talukdar et al., 1995). Under these conditions PAN is able to bind and transport RO<sub>2</sub> and NO<sub>2</sub> over long distances (> 10000 km). Below 7 km the lifetime of PAN is determined by its thermal decomposition (Talukdar et al., 1995). In combination, these two processes affect a release of NO<sub>2</sub> into remote areas with lower atmospheric NO<sub>x</sub> concentration. For that reason, PAN can serve as a source of reactive nitrogen species in the remote area and influences the local atmospheric chemistry such as tropospheric ozone production (Zhang et al., 2009, Fischer et al., 2011).

Further deposition processes including dry and wet deposition also play an important role as a loss mechanism of PAN to the terrestrial surfaces. The low water solubility of PAN excludes wet deposition as an important removal process (Kames et al., 1991). Also in many previous studies the contribution of the wet deposition to the total PAN deposition was concluded as

negligible because of its lower water solubility (Hill, 1971, Garland and Penkett, 1976, Doskey et al., 2004, Teklemariam and Sparks, 2004). Of high importance with regard to dry and wet deposition is the uptake of PAN by ecosystems. Sparks (2009) found the surface uptake of the atmospheric  $N_r$  by plants to be a major source of global atmospheric nitrogen into the ecosystems. On the one hand, several lab studies showed the PAN deposition flux to be clearly related to the stomatal conductance, and concluded the stomatal uptake of PAN by plant leaves to be the dominant pathway (Okano et al. 1990, Sparks et al. 2003, Teklemariam and Sparks 2004). On the other hand, many field studies have also reported about the existence and significant contribution of non-stomatal deposition of PAN, which is suggested to be related to the leaf cuticles (Turnipseed et al., 2006, Wolfe et al., 2009, Moravek et al., 2015).

Conclusively, the influence of the role of the relationship between ecosystems and PAN deposition has not been totally understood (Shepson et al., 1992, Schrimpf et al., 1996).

### **1.3 The emission of amines from terrestrial vegetation and its influence on new atmospheric particle formation**

Within the group of atmospheric organic compounds, amines are unique in their acid-neutralizing capacity and comprise a wide range of nitrogen organic compounds such as monomethylamine (MMA), dimethylamine (DMA) and trimethylamine (TMA), which are the most common species found in the atmosphere (Ge et al., 2011a). Amines are semi-volatile and can exist in both gas and particle phase. Their major sources are both natural and anthropogenic. Schade and Crutzen (1995) concluded that TMA could be the species which is predominantly emitted by agriculture. But other amine species could also be released. Further, biodegradation of organic matter could also serve as a major source of amines (Ge et al., 2011a). Many marine plants and bacteria contain MA (MMA, DMA and TMA), which can be produced within secondary metabolism (Wang and Lee, 1994, Calderón et al., 2007). On the global scale, the knowledge about the flux of most amines is limited (Ge et al., 2011a). Schade and Crutzen (1995) suggest the animal husbandry, ocean and biomass burning to be the major emission sources of MA. Additionally, terrestrial vegetation is also assumed to be a potential source for amines (Schade and Crutzen, 1995, Ge et al., 2011a). There exist few studies from the end of the 19<sup>th</sup> century until 1975, which described high amounts of MA-emission from certain plant species, which was associated with their plant tissues or with blossoms during flowering (Smith, 1971, 1975). As the one of the first scientists, Wicke (1862) had described the emission of TMA from the plant species *Chenopodium vulvaria*. By incubation under a glass dome, he observed a kind of “fog”- forming close to the plant in the

presence of HCl exposed air. This report can be regarded as one of the first to observe a new aerosol particle formation (NPF) under controlled environmental conditions.

Despite the low atmospheric concentration of amines (DMA = 0.5 ppb (Okita, 1970), TMA = 0.6 -1.6 ppb (Fujii and Kitai, 1987)), previous studies have already shown that amines play an important role in the NPF (Almeida et al., 2013, Glasoe et al., 2015, and summarized by Sintermann and Neftel, 2015). In the atmosphere, NPF occurs frequently from gas-phase precursors. High uncertainty exists in the estimation of the global secondary aerosols budget, which is caused by the uncertain contribution of the gas-phase precursors to the NPF (Spracklen et al., 2011). Instead of a binary system of sulfuric acid and water, a ternary system of sulfuric acid, water and a neutralizing compound such as  $\text{NH}_3$  or amines can be regarded as the key to understanding NPF (Chen et al., 2012, Almeida et al., 2013, Kurten et al., 2014). Furthermore, the contribution of organic acids in combination with amines cannot be neglected. For example, Dawson et al. (2012) found that amines are able to form stable clusters with methane sulfonic acid. Also oxidation products of organic compounds can contribute to NPF (Riccobono et al., 2014). However, such kind of vegetation dependent amine emission in relation to its key role in the NPF has not been elucidated yet (Sintermann and Neftel, 2015).

### 1.4 Purposes of the thesis

The purpose of this work is to develop a measurement method to investigate special scientific questions, such as the influence of leaf wetness on the deposition of  $\text{O}_3$  and PAN to plant leaves on the one hand and the emission of TMA by plants and their potential impact on atmospheric new particle formation on the other hand. Thereby, the focus of the technical method development is set on the modification and optimization of the measurement system to achieve high precision and accuracy for investigations of the non-stomatal/stomatal flux partitioning. According to that, the aim of this thesis is separated into three stages:

- (1) Development and optimization of a twin-cuvette-measurement system for investigation of reactive trace gas deposition under controlled conditions (light, temperature, humidity, gas concentration)
- (2) Application of the system on the flux partitioning of  $\text{O}_3$  and PAN between stomatal and non-stomatal deposition and influences of liquid water films on the deposition flux
- (3) Investigation of the emission of TMA by *Chenopodium vulvaria*.

The performance of the measurement system was essential to work on the following scientific

questions:

- (a) How is the deposition of O<sub>3</sub> and PAN related to the formation of liquid water films on plant leaf surfaces?
- (b) What is the influence of the chemical composition of the leaf's cuticular water films on the O<sub>3</sub> and PAN deposition?
- (c) To what extent may the emission of TMA by *Chenopodium vulvaria* contribute to new atmospheric particle formation?

The first part of this thesis is focused on the development of the twin-cuvette-measurement system, which includes the design, technical development and the validation of the system with two reactive substances, O<sub>3</sub> and PAN. To investigate the mentioned scientific questions, the cuvette measurement system should be able to perform long term measurements under laboratory conditions autonomously. The system itself has to be able to measure small gaseous mixing ratio differences between two dynamic cuvettes with a high resolution to determine the exchange flux. Additionally, all environmental parameters have to be controllable with high precision. All these requirements led to the development of the following general features, which the whole system is based on.

- Twin-cuvette setup to discard disturbing effects such as wall deposition of sample gases
- Humidification system to control the relative humidity inside the cuvettes (see Sun et al., 2016a, Appendix B)
- Development of a software to combine all control and data acquisition elements of the measurement system

In the second part, the influence of liquid films on the deposition of O<sub>3</sub> and PAN was investigated to determine the ratio of stomatal/non-stomatal deposition flux of O<sub>3</sub> and PAN. Furthermore, the deposition velocity ratio between PAN and O<sub>3</sub> for the respective deposition pathway was a subject of interest to improve recent model applications for estimation of the PAN deposition. Additionally, the leaf surfaces were coated with different chemicals to investigate the relationship between the deposition flux and chemical composition of the liquid films at various humidities. Finally, the importance and dependency of the O<sub>3</sub> and PAN deposition on the relative humidity were discussed in Sun et al., (2016b, Appendix C).

In the third part (Appendix D), the emission of TMA by *Chenopodium vulvaria* was measured to investigate potential sources of atmospheric amine and its influences on new atmospheric particle formation. These preliminary results will contribute to a better understanding of the emission mechanism of TMA by *Chenopodium vulvaria*.

## 2 Methods

### 2.1 The methodology of cuvette measurement system

The understanding of atmosphere-biosphere exchange of trace gases is crucial for atmospheric chemistry and the calculation of global trace gas budgets. The interest in the mechanism of trace gas exchange of ecosystems led to the development of different methods to determine the exchange flux of trace gases in the field and under controlled laboratory conditions. For flux measurements on ecosystem level micrometeorological methods such as the eddy covariance or gradient method are used, causing only minimal disturbance (Horst and Weil, 1995). However, to understand mechanism and processes of the interaction between the plant and the atmosphere in more detail, measurement on the plant and leaf scale under controlled environment conditions are often used. Therefore, enclosure techniques are mainly used to perform experiments under constant environmental conditions but also under field conditions for investigation of volatile organic compounds (Kesselmeier et al., 1993, 1996, 1998; Dindorf et al., 2006 ), sulfur compounds (Kuhn et al., 2000; Sandoval-Soto et al., 2012) as well as nitrogen compounds (Chaparro et al., 2011; Breuninger et al., 2012; Breuninger et al., 2013). For such process studies, it is of advantage to control the environmental conditions such as radiation, humidity, temperature and the trace gas concentration not only to ensure an optimum of plant physiological activity (Pape et al., 2009) but also to get close to reproducible environmental conditions and plant reactions. Especially for flux measurements of trace gases whose exchange processes are predominantly controlled by the leaf stomata, such reproducible preconditions should be achieved.

A commonly used technique for the measurement of trace gas uptake and release on plant and leaf scale is the dynamic cuvette technique (e.g. Breuninger et al., 2012). In the field, it can be ensured that the inner trace gas concentration and other related quantities are constant and close to the ambient conditions outside of the cuvette by the continuous renewal of the air inside the cuvette. For laboratory measurements, the dynamic cuvette leads to a temporally constant trace gas mixing ratio inside the cuvette. Typically, systems employ one single dynamic cuvette, where the trace gas concentration is measured at the entrance position of the cuvette and inside the cuvette to retrieve the trace gas flux. One disadvantage of such cuvette systems are potential adsorption and/or desorption effects on the cuvette walls, which is critical especially for reactive trace gases (Kulmala et al. 1999, Pape et al., 2009).

Furthermore, the influence of humidity is an important factor for the surface deposition of various water soluble trace gas species (e.g.  $\text{NH}_3$ ,  $\text{SO}_2$ ,  $\text{NO}$ ,  $\text{NO}_2$ , organic and inorganic acids and oxygenated monoterpenes such as linalool and 1,8-cineole) in the atmosphere (Kruit et al., 2008, Niinemets et al., 2011). Even substances with less water solubility (e.g.  $\text{O}_3$ ) can be affected by higher air humidity resulting in a water film on the leaf surface (Altimir et al., 2006, Fuentes and Gillespie, 1992).

In this work, we present the use of a twin cuvette system, which was designed to perform long term flux measurements under controlled laboratory conditions. The setup is based on a cuvette system which was previously used for measurements of volatile organic compounds (VOCs) and  $\text{NO}_2$  (Kesselmeier et al., 1996, Chaparro-Suarez et al., 2011, Breuninger et al., 2012). To account for wall effects and other systematic uncertainties, a main feature of the system was the employment of a second, empty cuvette, which was used as a reference. To control the humidity in both cuvettes we developed a new humidification system, which allowed for a precise regulation of the humidity inside the cuvettes. This allows us to investigate important questions such as the relationship between humidity and the trace gas deposition on vegetation surfaces with high reliability.

The twin-cuvette system was first developed for the plant-atmosphere exchange of PAN and  $\text{O}_3$ . While previous investigations mainly focused on the effect of inorganic nitrogen containing trace gases, particularly  $\text{NO}_2$  to plants (Hill, 1971, Sparks et al., 2001, Ortega et al., 2008, Breuninger et al., 2012), studies on the uptake of gaseous organic nitrogen species such as PAN under laboratory conditions are rare. An overview is given in Sun et al., 2016a, Appendix A. Laboratory studies which were designed to compare the PAN deposition with  $\text{O}_3$  deposition have not been performed up to now. Both Okano et al. (1990) and Teklemariam and Sparks (2004) used relatively high PAN mixing ratios (up to 190 ppb) for fumigation, which do not correspond to the PAN mixing ratios found under typical environmental conditions. Furthermore, the obtained deposition velocities in these studies differed considerably (see Table 1), which might be attributed to the use of different plant species and measurement methods. With adapting the cuvette conditions as closely as possible to the ones found in natural environments, our dual cuvette system is convenient to investigate the deposition mechanism of  $\text{O}_3$  and PAN on plants concerning their reactivity and potential wall effect with plant surface as well as the wall material.



Table 1: List of previous studies in the research field of O<sub>3</sub> and PAN flux measurement on plants under laboratory conditions.

Reference	Gas species	Plant species	Instrument	Method	Inlet mixing ratio	Regulated Humidification	Deposition velocity mm s <sup>-1</sup>
Fares et al. (2008)	O <sub>3</sub>	<i>Quercus ilex</i> , <i>Populus nigra</i>	O <sub>3</sub> -Analyzer Model 49	Plant chamber, gas phase reaction chamber	100 ppb	Not mentioned	0.9 – 1.8
Fares et al. (2010)	O <sub>3</sub>	<i>Citrus limon</i> , <i>Citrus reticulata</i> , <i>Citrus sinensis</i>	O <sub>3</sub> -Analyzer DASIBI mod. 1008-AH	Branch dynamic enclosure	40 – 160 ppb	No	2 - 5
Wang et al. (1995)	O <sub>3</sub>	<i>Populus trichocarpa</i> , <i>Populus deltoides</i> , <i>Phaseolus vulgaris</i> , <i>Cucurbita sativus</i> , <i>Cucurbita pepo</i>	O <sub>3</sub> -Analyzer Dasibi 1003	Single dynamic chamber (inlet & outlet measurement)	< 200 ppb	No	0.02 – 0.05
Van Hove et al. (1999)	O <sub>3</sub>	<i>Populus nigra</i> , <i>P.brandaris</i> , <i>P.robusta</i>	O <sub>3</sub> -Analyzer	Leaf chamber (inlet & outlet measurement)	30 – 100 ppb	No	---
Teklemariam & Sparks (2004)	PAN	<i>Zea mays</i> , <i>Triticum aestivum</i> , <i>Helianthus annuus</i> , <i>Catharanthus roseus</i>	GC (ECD) Limit 5 ppt, precision better than 1% > 200ppt	Single dynamic chamber (inlet & outlet measurement)	0.8 – 18 ppb	No	0.03 – 0.3
Okano et al. (1990)	PAN	<i>Herbaceous species</i>	2x GC (ECD) For inlet and outlet	Single dynamic chamber (inlet & outlet measurement)	190 ppb	No	0.3 – 3.1
Sparks et al. (2003)	PAN	<i>Zea mays</i> , <i>Phaseolus vulgaris</i> , <i>Pinus contorta</i> , <i>Mangifera indica</i> , <i>Quercus velutina</i> , <i>Quercus rubra</i> , <i>Abies grandis</i> , <i>Picea engelmannii</i>	GC (ECD) Limit 5 ppt, precision better than 1% > 200ppt	Single dynamic chamber (inlet & outlet measurement)	250 ppt	No	1.8 – 4.9
This study	PAN, O <sub>3</sub>	<i>Quercus ilex</i>	O <sub>3</sub> -Analyzer Model 49i, GC (ECD) LOD 1 ppt, precision 2% < 800ppt	Dual dynamic cuvette system (4 position measurement)	O <sub>3</sub> : 60 ppb PAN: 280 ppt	Yes 40-90%	See Sect. 3.2.1



# 3 Results

## 3.1 Development and performance of the twin-cuvette measurement system

### 3.1.1 Setup

The experimental setup consisted of two dynamic cuvettes with a respective volume of 70 liters. One of the cuvettes was empty and kept as reference. The sample cuvette enclosed the part of the entire plant above the soil. The wall material of the cuvettes was made of FEP to minimize wall effects for the measured trace gases. Additionally, all tubing and tubing connections which were in contact with the air flow consisted of PFA-Teflon<sup>®</sup>. A fan, also coated with Teflon<sup>®</sup> was installed inside both cuvettes to assure well-mixed conditions in order to reduce the aerodynamic resistance for the trace gas fluxes (Gut et al., 2002).

The flow chart (see Fig. 3) describes the operation process of the entire cuvette system. The pressurized air flow was provided by a compressor and purified by different filter cartridges to remove interfering gaseous compounds as O<sub>3</sub>, NO, NO<sub>2</sub> and PAN. The purified air stream (20 L min<sup>-1</sup> for each cuvette) was regulated by two mass flow controllers (MFC) and humidified to a predefined humidity value. The addition of O<sub>3</sub> and PAN into the main air stream occurred under atmospheric pressure downstream of the humidification step. The purified air stream supplied with a certain mixing ratio of O<sub>3</sub> and PAN reached the inner cuvette through the inlet PFA-tube. The surplus of the air stream effused at the vent situated at the bottom of the cuvette. To prevent ambient air from entering the cuvette, the flow rates were adjusted such that the cuvettes were slightly over-pressurized. A valve block consisted of three Teflon-valves were used to switch between inlet and outlet of both cuvettes for the analysis of O<sub>3</sub> and PAN mixing ratios (see Fig. 3, No. 9). The PAN mixing ratio was continuously measured by an automatic gas chromatograph with electron capture detector (GC-ECD). The O<sub>3</sub> mixing ratio was measured by a UV photometric analyzer. After inserting the plant into the sample cuvette, the relative difference of O<sub>3</sub> and PAN mixing ratios between

the sample and the reference cuvette corresponded to  $O_3$  and PAN uptake by the leaves, respectively. The valve switching between both cuvettes was controlled automatically with an interval of 10 minutes, which matched to the measurement cycle of the PAN GC-ECD. Inlet mixing ratios of both cuvettes were monitored once per hour over the entire experiment. The cuvettes were located inside a plant cabinet to keep the environmental temperature constant during the experiments. In addition,  $CO_2$  and  $H_2O$  concentrations were measured with an infrared gas analyzer to determine plant photosynthesis and transpiration. For further detailed description see Sun et al. (2016a, Appendix B)

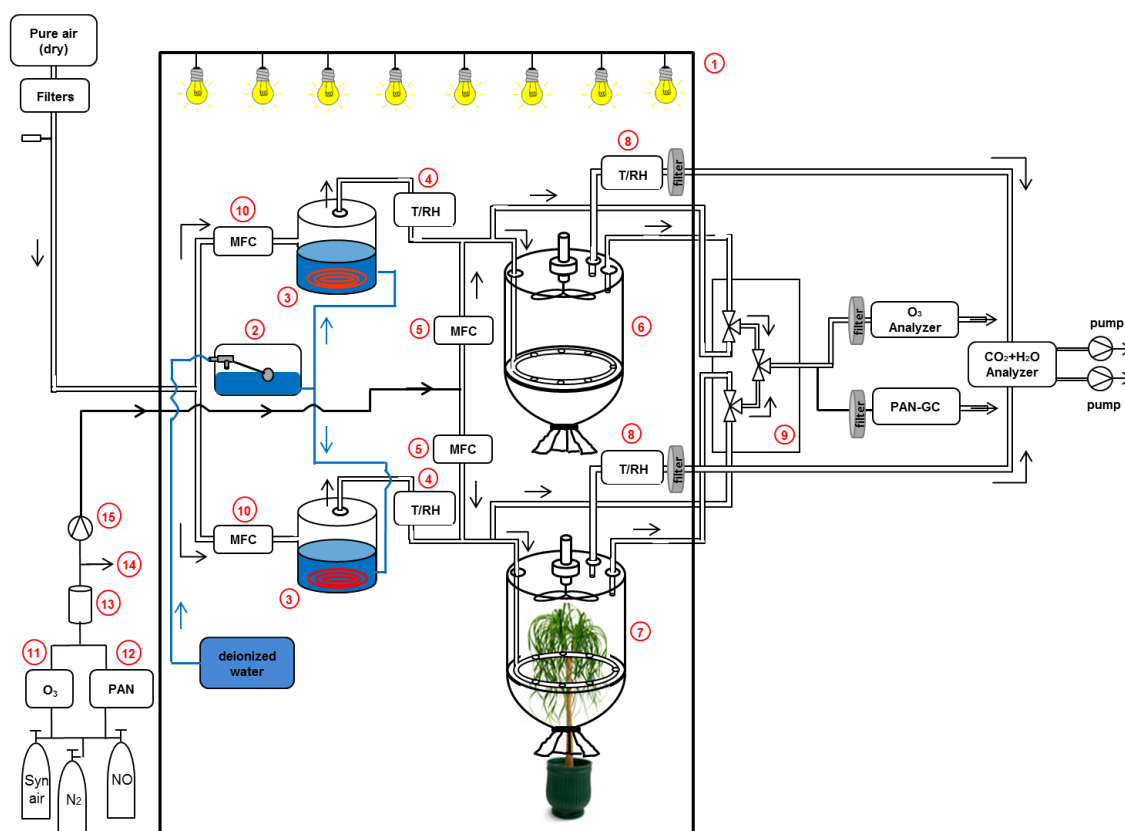


Fig. 3: Flow chart of the dual cuvette system. 1 plant cabinet, 2 water storage tank, 3 ATRAHS, 4 Temperature and relative humidity sensor for humidity, 5 mass flow controller (MFC), 6 dynamic cuvette (reference), 7 dynamic cuvette (sample), 8 Temperature and relative humidity sensor for monitoring, 9 Teflon- valve block, 10 MFC for gas addition, 11  $O_3$  – primary standard, 12 PAN – calibration unit, 13 mixing vessel, 14 overflow, 15 Teflon membrane pump (Sun et al., 2016a, Appendix B).

### 3.1.2 Performance

#### 3.1.2.1 Residence time

For an accurate operation of a dynamic cuvette system for exchange flux measurements, the choice of an appropriate residence time in the cuvette is required. On the one hand, it should be short enough to exclude chemical reactions in the cuvette and to follow potential fast changes in the environmental conditions. In the case of PAN, the thermal decomposition under higher temperature is the limiting factor and made it necessary to keep the residence time as short as possible. But, as the lifetime of PAN was about 5 hours at a cuvette temperature of 25 °C (calculated from the rate coefficient suggested by Atkinson et al., (2006)) the thermal decomposition of PAN did not affect the uptake measurements by the leaves. On the other hand, the residence time has to be high enough to receive a sufficient mixing ratio difference caused by the enclosed leaf material that can be resolved by the analytical system. With a cuvette volume of 70 L and an operating air flow of about 20 L min<sup>-1</sup> for each cuvette the residence time inside the cuvette was 3.4 minutes, which was sufficient for our flux measurements.

#### 3.1.2.2 Loss of O<sub>3</sub> and PAN within the twin-cuvette system

The calibration of O<sub>3</sub> and PAN including the total cuvette setup showed a weaker slope than calibrating the analyzers without the setup. This indicates a loss of O<sub>3</sub> and PAN inside the setup, caused by different components such as tubing, connectors, MFCs, valves, pumps, and the cuvette itself. The overall loss measured at the different sampling positions was 18 % for O<sub>3</sub> and 16 % for PAN mixing ratios. For O<sub>3</sub>, the difference between the inlet and outlet positions was not significant, indicating the major O<sub>3</sub> loss not to be caused by the cuvettes themselves. For PAN, a 5% difference between the cuvette inlet and outlet was found, which is most likely associated with deposition of PAN to the foil surface. To determine the loss of O<sub>3</sub> and PAN which was not caused by the cuvette walls, the mixing ratios were measured downstream of the Teflon membrane pump, the MFCs, the cuvettes, and the Teflon valves (see Fig. 3). For O<sub>3</sub>, the highest loss of 9.7 % occurred at the gas stream passing through the MFCs, where O<sub>3</sub> most likely reacted with the inner surface of the MFC consisting of stainless steel. For PAN, the highest loss of 9.5 % was induced by the Teflon pump. As the air inside the Teflon pump heated up to 50 °C, thermal decomposition of PAN could be responsible for the higher loss of PAN.

Furthermore, the finding that the wall deposition rates for both gases were not significantly different comparing both cuvettes supports the use of a twin cuvette system with an identical construction. For further details see Sun et al. (2016a) in Appendix B.

### 3.1.2.3 Accuracy of the twin-cuvette measurement system

With the presented twin cuvette system it is possible to ensure stable O<sub>3</sub> and PAN mixing ratios over long time periods under controlled environmental conditions. The resolution of the mixing ratio difference was quite high, so that even small differences in the range of few hundred ppt O<sub>3</sub> and several ppt PAN could be differentiated in the measurement data. The minimal resolvable mixing ratio difference of O<sub>3</sub> was  $0.01 \pm 0.33$  ppb and for PAN it was  $0.68 \pm 9.35$  ppt. As these mixing ratio differences are used to calculate the fluxes, the fluxes could be determined with a high sensitivity as well. Especially for the investigations on the flux partitioning, i.e. the discrimination between stomatal and non-stomatal deposition of O<sub>3</sub> and PAN, a measurement system with high precision to resolve the mixing ratio difference was required.

The mixing ratios used during the long-term flux experiments (57 ppb O<sub>3</sub> and 280 ppt PAN) as well as the mixing ratios inside the sample cuvette (58.8 ppb O<sub>3</sub> and 307.6 ppt PAN) were far above the measured detection limits of the twin cuvette setup (0.9 ppb for O<sub>3</sub> and 1.3 ppt for PAN), but representative for ambient conditions.

Furthermore, the twin cuvette system was tested to be a more precise method to perform flux measurements with reactive trace gas species under controlled laboratory conditions than a single cuvette system. The results indicate some overestimation at least for PAN when relying on inlet/outlet measurements with a single cuvette system. The flux overestimation with a single cuvette system is caused by an underestimation of the O<sub>3</sub> and PAN deposition on the cuvette foil, which had to be considered during the flux calculation with the single cuvette system. For the twin cuvette system, such a correction is not needed. For further detailed information see Sun et al. (2016a) in Appendix B.

### 3.1.2.4 Humidification

To investigate the uptake of trace gases by plant leaves under controlled laboratory conditions, the simulation of environmental parameters such as light, temperature and relative humidity inside the cuvettes is essential (Niinemets et al., 2011). An automatic humidification system was required for the twin-cuvette system to optimize long term flux measurements and achieve our scientific objectives (Fig. 4). Due to the high operating flow rate of 20 L min<sup>-1</sup> and the resulting short residence time of the dry air stream inside the humidifier tank for each cuvette, we chose to humidify the main dry air stream directly with the challenge to obtain high humidification efficiency. Our Automatic temperature regulated air humidification system (ATRAHS) provided an opportunity to humidify the air stream inside the cuvette very precisely (0.3 % of the adjusted *RH*) with a wide humidity range of 40 – 90 %.

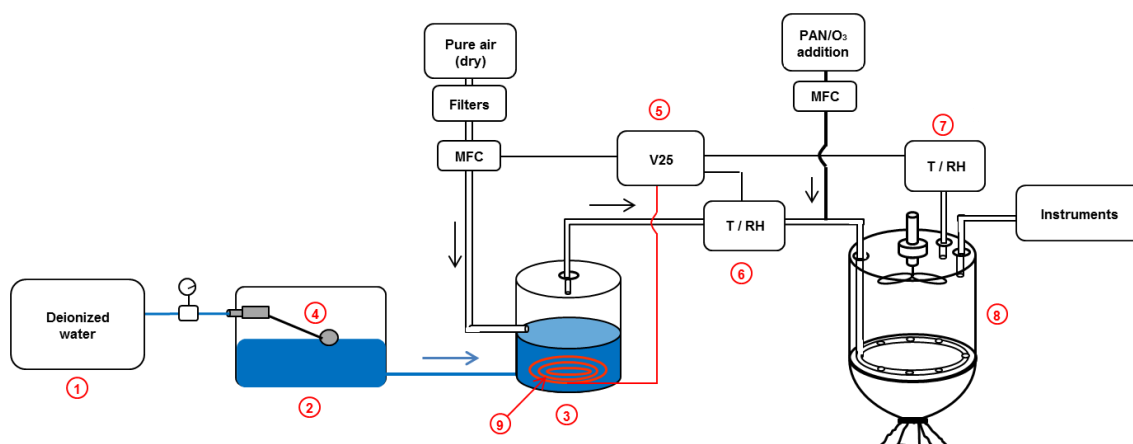


Fig. 4: Flow chart of the automatic temperature regulated air humidification system (ATRAHS). 1 deionized water supply; 2 water storage tank; 3 humidifier tank; 4 float valve; 5 V25 control device; 6 T/RH sensor (initial regulation); 7 T/RH sensor (monitoring); 8 dynamic cuvette; 9 heat element.

### 3.2 Case study: Investigation of the influence of liquid surface films on O<sub>3</sub> and PAN deposition to plant leaves coated with organic / inorganic solution

The formation of surface water films and its influence on the deposition of trace gases was discussed in many previous studies (van Hove et al., 1989, Fuentes and Gillespie, 1992, Burkhardt and Eiden, 1994, Grantz et al., 1995, Hakan et al., 1995, Burkhardt et al., 1999, Flechard et al., 1999, Klemm et al., 2002). But, comparable systematical laboratory experiments to investigate the impact of surface water films on the deposition of O<sub>3</sub> and PAN were not performed up to now. The aim of this study is to contribute to a better understanding of underlying mechanisms determining the non-stomatal deposition process of O<sub>3</sub> and PAN to terrestrial vegetation. We investigate the influence of leaf surface liquid films on the O<sub>3</sub> and PAN deposition as well as the partitioning of stomatal and non-stomatal fluxes of O<sub>3</sub> and PAN under controlled laboratory conditions. The presented twin-cuvette system (Sun et al. 2016a, Appendix B) was used to simulate environmental variables such as light, temperature, and humidity. Furthermore, the leaf surface was treated with various organic and inorganic solutions to investigate the electrical surface conductance of the leaves at various relative humidity values. Based on these experiments the surface deposition of O<sub>3</sub> and PAN was investigated depending on the leaf surface properties and the influence of soluble compounds.

### 3.2.1 Flux partitioning

The partitioning between stomatal and non-stomatal deposition of O<sub>3</sub> and PAN was investigated (see Sun et al., 2016b, Appendix C). For O<sub>3</sub>, we observed a clear correlation between the deposition to plants (*Quercus ilex*), the relative humidity and the stomatal conductance at both light and dark conditions. During the light period, the increase of the O<sub>3</sub> deposition was mostly explained by opening of leaf stomata under rising *RH*. As already known, leaf stomata were induced to open under elevated humidity conditions caused to the decrease of peristomatal water loss, which led to a restitution of the turgescence (Lange et al., 1971). Under dark conditions the contribution of stomatal uptake of O<sub>3</sub> is expected to be negligible (Mikkelsen et al., 2004) due to the low stomatal activity, which could be confirmed by our results as O<sub>3</sub> deposition flux did not correlate with  $g_{s,calc}(H_2O)$  (see Sun et al., 2016, Fig. 2c, Appendix C). During the absence of light, liquid surface films were responsible for the enhancement of the O<sub>3</sub> deposition. Fuentes and Gillespie (1992) observed a correlation between the O<sub>3</sub> deposition flux and the leaf surface moisture. Our experiments confirm the observed enhancement of the O<sub>3</sub> deposition with rising *RH*. The observed electrical surface conductance (*G*) correlated with *RH*, which indicated the formation of liquid surface films on the leaves above 40 – 50 % *RH*.

In the case of PAN, a similar linear correlation with *RH* was found in the presence of light, which was mostly due to the stomatal uptake of PAN. In the dark period, we found a non-stomatal contribution of ~20 % to the total PAN deposition, which is not correlated with *RH* (Fig. 5). This could be explained by the lower aqueous partitioning for PAN. Generally, the contribution of the non-stomatal deposition of PAN is still controversial. While studies where the PAN deposition was concluded as mainly stomatal controlled were performed under laboratory conditions (Okano et al., 1990, Sparks et al., 2003, Teklemariam and Sparks, 2004), significant contribution of non-stomatal PAN deposition was observed in the field (Turnipseed et al., 2006, Wolfe et al., 2009, Moravek et al., 2015). These different conclusions suggest that the deposition of PAN is dependent on many environmental parameters such as light, relative humidity, temperature and consistency of natural surfaces. Indeed, the environmental conditions in the field are much more complex than can be simulated in the laboratory. Hence, the challenge for future studies is to understand the complex background for the observed non-stomatal PAN deposition in the field. Enclosure (cuvette) studies can discern between stomatal and non-stomatal exchange related to leaf surfaces. Field study results, however, are affected by non-stomatal exchange outside plant/leaf surfaces.



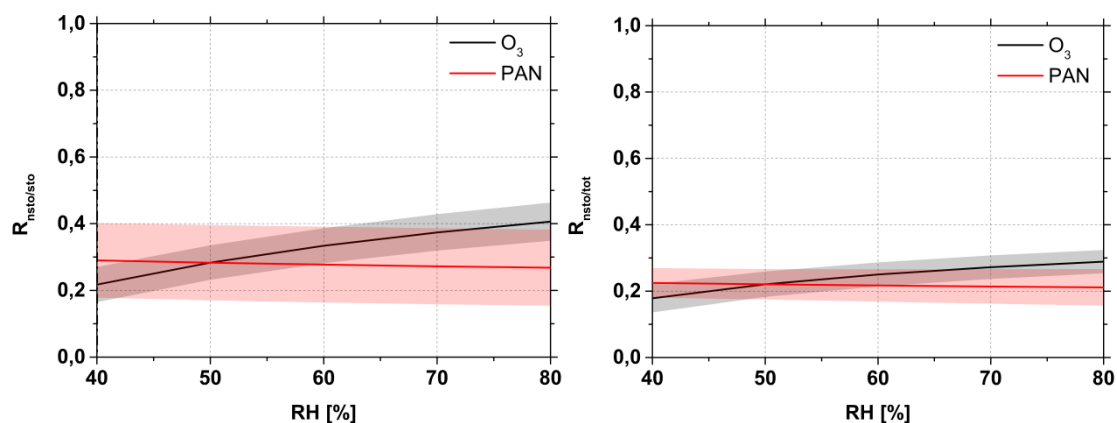


Fig. 5: Calculated partitioning ratio  $R_{nsto/sto}$  between non-stomatal and stomatal deposition flux (left) and  $R_{nsto/tot}$  between non-stomatal and total deposition flux (right) of O<sub>3</sub> (black) and PAN (red) versus  $RH$ . The red and grey uncertainty areas of the partitioning ratios were propagated considering the errors of the stomatal and non-stomatal fluxes of O<sub>3</sub> and PAN (Sun et al., 2016b, Appendix C).

### 3.2.2 Impact of leaf surface composition and water films on the non-stomatal deposition of O<sub>3</sub> and PAN

Based on the findings by Fuentes and Gillespie (1992), who argued that dissolved substances in the water film are able to scavenge O<sub>3</sub> via chemical reactions, we treated the leaf surface of sample branches with various inorganic and organic chemical compounds (see Sun et al., 2016b, Appendix C) and measured the deposition flux of O<sub>3</sub> and PAN under light and dark conditions as well as at various  $RH$ . To exclude/demonstrate the influence of stomatal deposition, the plant material was treated with abscisic acid. The experimental results showed a clear exponential relationship for O<sub>3</sub> to rising  $RH$ . The strongest increase could be observed at the plant sample exposed to outdoor air condition, which led to the conclusion that ambient particles deposited on the leaf surface dissolved in the liquid phase and served as a chemical sink for atmospheric O<sub>3</sub>. Additionally, artificial leaf surface coatings consisting of inorganic and organic compounds showed a significant impact on the O<sub>3</sub> non-stomatal deposition in relation to  $RH$  (Fig. 6).

For PAN, the results revealed a contribution of non-stomatal deposition, but no clear relationship between the deposition flux and  $RH$  was found for the different leaf surface coatings. On the other hand, a larger non-stomatal deposition pathway has been observed in past field experiments. As an additional sink for atmospheric PAN, gas phase reactions with PAN are also possible and may contribute to the larger non-stomatal PAN deposition. For example, reaction of PAN with aldehydes was reported by Wendschuh et al. (1973). It was concluded that the addition of aldehydes to PAN resulted in the oxidation of the aldehyde to the corresponding acid with a yield of approximately 85 %. Nevertheless, in our laboratory

measurements we found no evidence for additional PAN loss in the liquid phase.

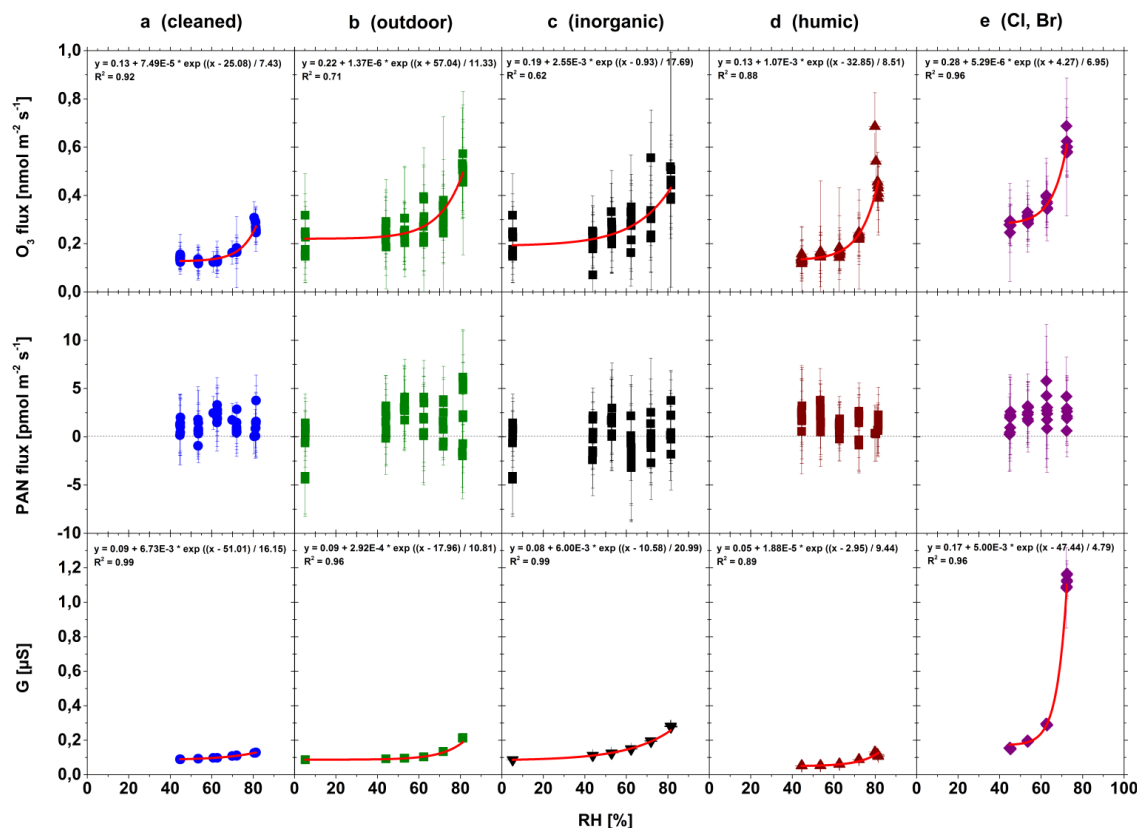


Fig. 6:  $O_3$ , PAN flux and electrical surface conductance  $G$  at various  $RH$  (5 % - 80 %) during the dark period under ABA induced stomatal closure. Cleaned leaf surface (column a), exposed with outdoor air (column b), treated with inorganic solution (column c), treated with humic acid (column d) and treated with Cl, Br (column e). The increasing trend was fitted with an exponential growth function.

### 3.2.3 Deposition velocity ratio of $O_3$ and PAN

The deposition velocity ratio between PAN and  $O_3$  for the respective deposition pathway was investigated to improve the recent model application for estimation of the PAN deposition. In recent applied regional and global deposition models the non-stomatal PAN deposition is typically derived assuming a certain reactivity of PAN with the underlying surface. For the non-stomatal deposition pathway the EMEP model estimation based on the non-stomatal conductance of  $SO_2$  ( $G_{ns,SO_2}$ ) and  $O_3$  ( $G_{ns,O_3}$ ) is given by the following equation from Simpson et al. (2012):

$$G_{ns}(PAN) = 10^{-5} \times H_{*,PAN} \times G_{ns}(SO_2) + f_{0,PAN} \times G_{ns}(O_3) \quad (1)$$

$f_{0,PAN}$  is a reactivity index. Most models suggested  $f_{0,PAN}$  to be lower than  $f_{0,O_3}$ , but, depending on the used  $f_0$ -factors, the results differ considerably. Furthermore, all of the deposition

models did not consider the influence of the relative humidity. As Fig. 7 shows, the non-stomatal  $V_d$ -ratio between PAN and  $O_3$  varied considerably depending on  $RH$ , which was due to the  $RH$ -related non-stomatal deposition flux of  $O_3$ . Therefore, the estimation of the non-stomatal conductance of PAN in the deposition models should be improved by considering the  $RH$ -related non-stomatal  $O_3$  deposition.

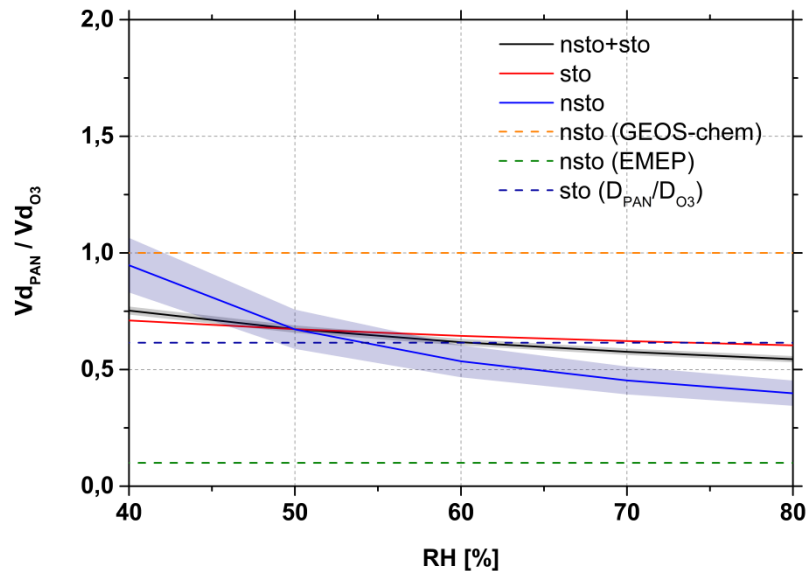


Fig. 7: Deposition velocity ratio between PAN and  $O_3$  of different deposition pathways nsto+sto (black), sto (red) and nsto (blue) in relation to  $RH$  compared with various modelled deposition velocity ratio as GEOS-chem (orange dashed), EMEP (green, dashed) and  $D_{PAN}/D_{O_3}$  (blue, dashed). The shaded uncertainty areas of the deposition velocity ratios were propagated considering the errors of the stomatal and non-stomatal fluxes and deposition velocities of  $O_3$  and PAN (Sun et al., 2016b, Appendix C).

### 3.3 Case study: Emission of Trimethylamine from *Chenopodium vulvaria* - first results from quantifying plant emissions of amines and their potential effects on atmospheric new particle formation

In this study, we investigate the TMA emission from *Chenopodium vulvaria*, which is well known as a strong TMA-emitter (Dessaignes, 1856). As TMA plays a key role in the atmospheric NPF and its emission rates from that plant species have not been determined systematically up to now, the results should give a perception of the contribution of the TMA emission from the terrestrial vegetation to the global NPF. Additionally, we have screened several typical European plant species at their flowering state with a GC-NCD to determine

further potential TMA-emitter qualitatively. Furthermore, we investigate in a nucleation tube system the NPF-process of a ternary nucleation system based on inorganic / organic acids, water and TMA. For further detailed information see Sun et al. (2016c) in Appendix D.

### 3.3.1 Leaf anatomic structure and reservoir for TMA

In the case of *Chenopodium vulvaria*, TMA is released by gland vesicles at the leaf surface, which makes the determination difficult (Cromwell, 1949). The factors controlling the release of TMA from the gland vesicles have not yet been fully investigated (Cromwell, 1949), but a mechanical rupture seems to be the most plausible explanation. Our leaf anatomic study (see Fig. 8) showed the gland vesicles to be well distributed at both sides of the plant leaf. The glands were very fragile and easily ruptured by handling or even slight air streams. Additionally, the connection between the gland vesicles and the leaf epidermis is very fragile as well, whose destruction could lead to a splitting of the entire gland vesicle. In both cases, the contained liquid TMA can be released easily into the atmosphere.

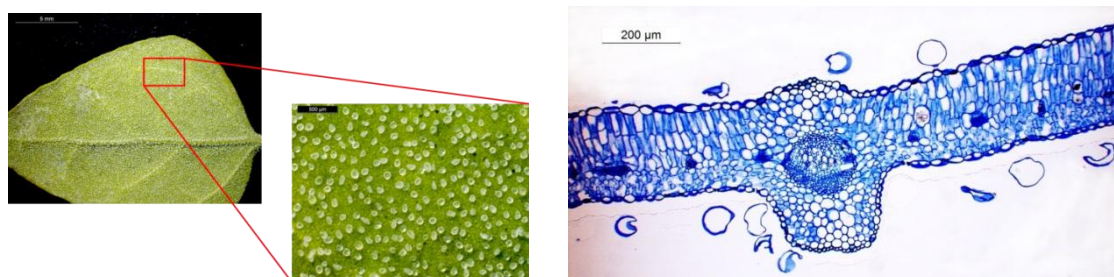


Fig. 8: Glandular hairs on the bottom of the leaf surface of *Chenopodium vulvaria* (left) and the leaf cross section of *Chenopodium vulvaria* (right). These glandular hairs emerge from the top and bottom leaf epidermis. They are specialised trichomes consisting of a thin stalk and a large globular vesicle.

### 3.3.2 Screening experiment over different plant species

Four different plant species (*Crataegus monogyna*, *Sorbus aucuparia*, *Pyrus communis* and *Chenopodium vulvaria*) were analyzed with a GC-NCD to investigate the TMA emission qualitatively. For the first three plant species the measurement was performed during their flowering period (see Fig. 9). It has been observed by former studies that various groups of plant species emit high amounts of MA from blossoms during the flowering period (Smith, 1971, 1975). Accordingly, our screening experiment showed that all of the investigated plant species emit an amount of TMA, assuming the identification of the TMA peak with GC-NCD was correct (see Appendix D for details). Already in the middle of the 19<sup>th</sup> century, Wicke (1862) concluded that TMA can be found in the blossoms of these mentioned species above.

But such in-situ measurement of volatile TMA in the gas phase was not possible at that time and even until nowadays conclusive studies of TMA-emission by plants are very limited.

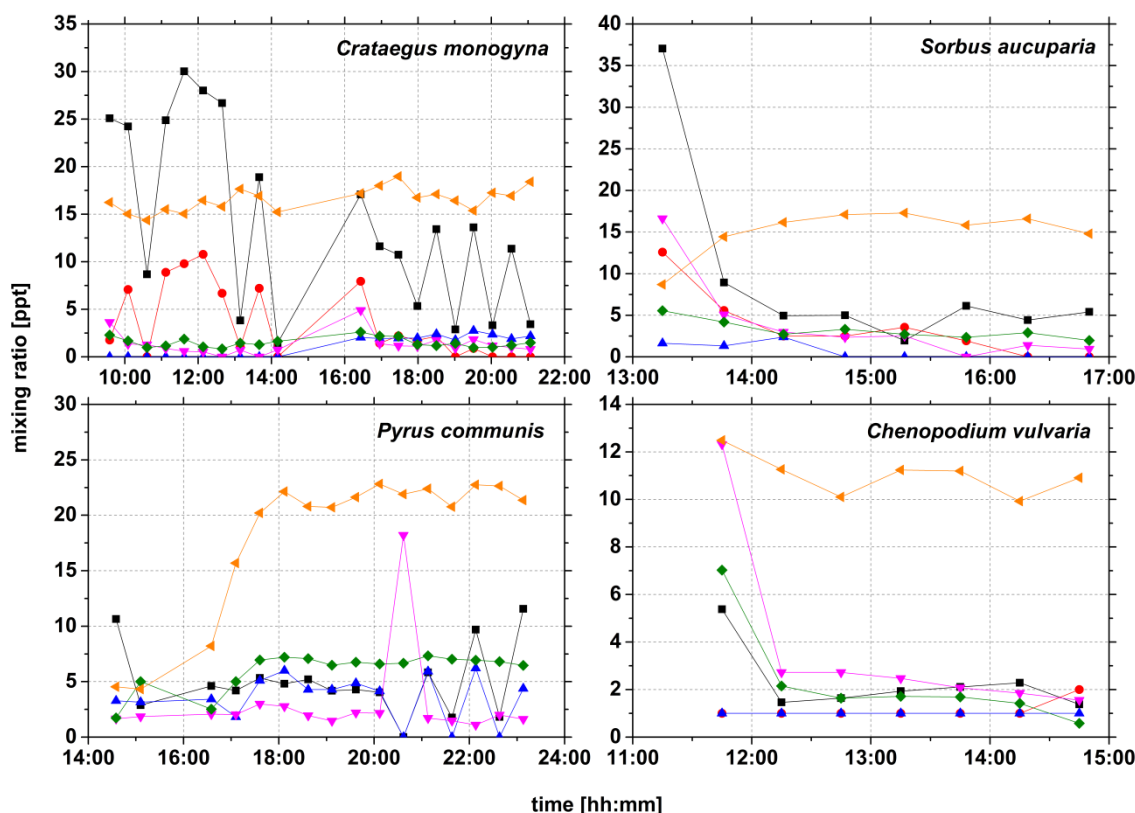


Fig. 9: TMA screening experiment over four different plant species. *Crataegus monogyna*, *Sorbus aucuparia* and *Pyrus communis* were measured at flowering period. Emitted substances were characteristic for their retention time (RT). ■ RT 2.13, ● RT 2.29, ▲ RT 2.34, ▼ RT 2.37(acetonitrile), ◆ RT 2.65, ◀ RT 3.35 (assumed to be TMA).

### 3.3.3 Emission of TMA from *Chenopodium vulvaria*

In this study, flux experiments were performed with *Chenopodium vulvaria* to determine the emission of TMA from the plant to the atmosphere. We could observe a strong influence of the emission of TMA by mechanical stimuli, which can be realized from the emission peaks that occurred upon introducing the plant into the cuvettes (Fig. 10). The gland vesicles were very fragile and could easily be destroyed by handling, which led to an emission increase of TMA resulting in atmospheric concentrations of more than 100 ppb. Additionally, we could observe further TMA emission peaks, which were not related to the mechanical stimuli of the plant (Sun et al. 2016c; Appendix D). We assumed that the occurrence of these emission peaks was due to the changes in environmental parameters such as light and *RH*, which occurred during the transition from light to dark period. This is in accordance with the suggestion of Cromwell (1949), who assumed the relative humidity and temperature to be the

driving factors of the emission of TMA.

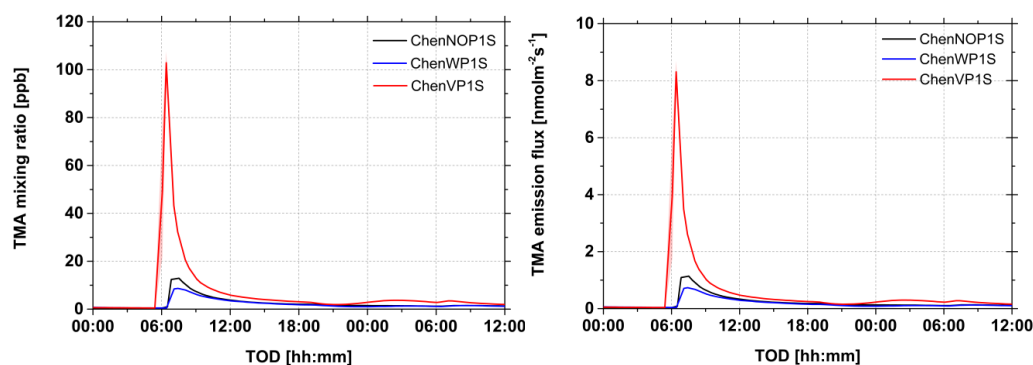


Fig. 10: Emitted trimethylamine (TMA) from *Chenopodium vulvaria*. Mixing ratio (left) and emission flux (right). Plant samples growth under various fertilization levels low (black line), middle (blue line) and high (red line).

### 3.3.4 Impact on atmospheric new particle formation

The important role of amines in relationship with the new aerosol particle formation (NPF) was investigated by recent studies as Almeida et al., 2013, Kurten et al., 2014 and Glasoe et al., 2015. Almeida et al. (2013) found that DMA could influence the atmospheric new particle formation more efficiently than ammonia. Glaseo et al. (2015) investigated the effect of various amines on the sulfuric acid nucleation process and found that in the case of TMA the effect on the particle formation rate was the strongest followed by DMA and MMA. The aim of our nucleation experiments was to gain a first insight into the ternary nucleation process, which could be potentially induced by organic substances such as formic acid, acetic acid and tartaric acid.

We used sulfuric acid to validate our nucleation reactor. The results confirmed the previous studies and the enhancing effect of TMA by the ternary nucleation process with sulfuric acid. In the case of the nucleation experiment with formic acid and TMA an enhancement of the particle formation could be observed as well, but less intensively than with sulfuric acid. For the other tested organic acids, no significant enhancement of the particle formation was observed in our experiments (For details see Sun et al., 2016c; Appendix D)

## 4 Conclusions & Outlook

The understanding of atmosphere-biosphere exchange of trace gases is essential for atmospheric chemistry. To investigate its processes in more detail on a process level, cuvette techniques are mainly used to perform measurements on the plant and leaf scale under controlled environment conditions. Typically, many systems employ one single cuvette to retrieve the trace gas flux with the disadvantage of potential adsorption and/or desorption effects on the cuvette walls. Furthermore, the influence of humidity is an important factor for the surface deposition of various trace gas species in the atmosphere (Kruit et al., 2008, Niinemets et al., 2011). Therefore, the main focus of this thesis was the adaptation of a twin-dynamic cuvette system and its application on our specific scientific questions.

Due to the presented results of this thesis, the following major conclusions could be achieved:

- (a) Conclusions of the twin-cuvette system and its performance (Sun et al., 2016a; Appendix B)
  - The comparison of fluxes between a single and the twin - cuvette system revealed an overestimation of fluxes by the single-cuvette system for both O<sub>3</sub> (8.3 %) and PAN (21.4 %), which is due to unconsidered effects of wall deposition. Consequently, the dual cuvette system represents a more precise method to perform flux measurements with reactive trace gas species under controlled laboratory conditions.
  - With ATRAHS, the relative humidity inside the cuvette could be controlled with a high precision of 0.3 % RH. According to our experimental data, ATRAHS is suitable for cuvette systems operated with higher flow rates (> 20 L min<sup>-1</sup>), but it could also be used for lower flow rates (> 5 L min<sup>-1</sup>), and where humidity values up to 100 % are required. Due to the automatic water-filling mechanism, an interruption to refill the water for humidification during long-term measurements is not necessary, which improves the performance of the entire measurement system and prevents data gaps.

- By using O<sub>3</sub> mixing ratios between 32 and 105 ppb and PAN mixing ratios between 100 and 350 ppt, a linear dependency of the O<sub>3</sub> flux as well as the PAN flux to its ambient mixing ratio could be observed, which showed a constant deposition velocity over the mixing ratio range.
- We are able to observe and characterize the formation of a water film on the leaf surface. An exponential relationship was observed between the electrical surface conductance and the ambient humidity.

The combination of all these features of the presented twin-cuvette system will give the opportunity to investigate further scientific questions such as flux partitioning between stomatal and non-stomatal deposition of O<sub>3</sub> and PAN and the influence of liquid films on a leaf surface.

(b) Conclusions of the system application on the case study: influence of surface water films on the deposition of O<sub>3</sub> and PAN (Sun et al., 2016b; Appendix C)

- We observed a clear correlation between the O<sub>3</sub> deposition to plants (*Quercus ilex*), the relative humidity and the stomatal conductance at both light and dark conditions. During the light period the increase of the O<sub>3</sub> deposition was partly explained by the opening of leaf stomata under rising *RH*, while during the absence of light, liquid surface films were responsible for the enhancement of the O<sub>3</sub> deposition as proved by experiments with plants treated with ABA.
- In the case of PAN, a similar linear correlation with *RH* was found in the presence of light, which was mostly due to the stomatal uptake of PAN. In the dark period, no relationship with *RH* was found, which showed that the PAN deposition was not significantly affected by liquid surface films. Therefore, the variation of the deposition of PAN to plants appears to be mostly stomatal controlled, which is in line with other laboratory studies.
- The flux partitioning ratio between non-stomatal and stomatal deposition as well as between non-stomatal and total deposition was found to be  $R_{nsto/sto} = (0.21 - 0.40) \pm 0.05$ ,  $R_{nsto/tot} = (0.18 - 0.30) \pm 0.04$  for O<sub>3</sub> and  $R_{nsto/sto} = (0.26 - 0.29) \pm 0.11$ ,  $R_{nsto/tot} = (0.21 - 0.23) \pm 0.10$  for PAN at 40 – 80 % *RH*. As in our laboratory setup environmental variables (light, temperature, and humidity) were controlled and the residence time of air inside the cuvette was low, the change in fluxes could be related to stomatal opening and the formation of liquid water films.
- The determined  $V_d$ -ratios between PAN and O<sub>3</sub> for the different deposition pathways: non-stomatal = 0.40 – 0.95, stomatal = 0.61 – 0.71 and total = 0.55 – 0.75, in relation to the relative humidity would improve the model estimation



of the deposition velocity of PAN.

- The formation of the leaf surface films was found to be depending on the chemical composition of the particles deposited on the leaf cuticles. Accordingly, the O<sub>3</sub> deposition was also influenced by the species of the deposited particles dissolved in the liquid surface films, which provide a chemical loss pathway in the liquid phase.

(c) Conclusions of the system application on the case study: emission of Trimethylamine from *Chenopodium vulvaria* (Sun et al., 2016c; Appendix D)

- The emission of TMA was located to the epidermal gland vesicles, which were evenly distributed on both sides of the leaf. Due to its fragility, the contained liquid TMA can be easily released by handling or even slight air streams causing high amounts of TMA (> 100 ppb) to be emitted by the plant. Thus, under the natural conditions which led to mechanical stimuli of *Chenopodium vulvaria*, this mechanism could be the key factor for a high emission of TMA. Additionally, environmental factors such as temperature and relative humidity could be assumed as a potential driver for TMA emission, which may not impact the release of the TMA from the gland vesicles, but the release of the adsorbed TMA on the leaf surface.
- Further TMA emitting plant species (*Crataegus monogyna*, *Sorbus aucuparia*, *Pyrus communis* and *Chenopodium vulvaria*) were analyzed by screening experiments. For the first three species, the emission of TMA occurred at the flowering period. All these plant species represent an emission source of volatile TMA. Because of their wide geographical distribution and depending on the flowering period, a potential contribution to the global budget of volatile TMA can be assumed.
- The impact of volatile TMA on the atmospheric new particle formation could be qualitatively demonstrated by a ternary nucleation system with sulfuric acid – TMA – H<sub>2</sub>O and formic acid – TMA – H<sub>2</sub>O. The enhancing effect of volatile TMA on the particle formation was 3 orders of magnitude higher in the case of sulfuric acid than with formic acid. For the other tested organic acids (acetic acid and tartaric acid) no significant enhancement of the particle formation was observed. However, for formic acid a small effect on the particle formation could be observed. Thus, an influence of TMA on organic acid induced new particle formation could not be completely excluded.

The features of the measurement setup were developed especially for our experimental requirements. Additionally, the results of the case studies contribute to a better understanding

of the underlying mechanism of the surface wetness deposition of O<sub>3</sub> and PAN on the one side and the emission of TMA from *Chenopodium vulvaria* on the other side. The presented results of these studies open up further interesting scientific questions. The ideas listed below should give a direction to future studies and improvement of the cuvette setup:

- The lowest adjustable humidification limit of ATRAHS was 50 % at a temperature of 19.5 °C and flow rate of 20 L min<sup>-1</sup>, which was sufficient for our experiments. To achieve the range below 50 % *RH* with ATRAHS in the current setup, a cooling system would be needed for the humidifier tank to reach a lower water temperature.
- For the first case study it would be interesting to investigate the flux partitioning ratio on different plant species. As we showed in the cuvette experiment, the surface deposition of O<sub>3</sub> is only depending on the formation of surface water films and the leaf surface composition. Thus, the contribution of water films to the non-stomatal deposition in relation to the total deposition of O<sub>3</sub> should vary among different plant species cause to the variation of their stomatal conductance.
- For PAN it is important to investigate the discrepancy between the flux partitioning ratio determined in the laboratory and the field. Since many previous studies showed higher partitioning ratios in the field, which indicated further potential dependent factors for the non-stomatal deposition of PAN, future investigations should focus on the identification of these factors.
- For the second case study, we quantified the TMA emission flux from *Chenopodium vulvaria* and located its emission area on the leaf cuticles. That leads to a better understanding of its emission mechanism. In the future work it would be interesting to investigate the production processes of TMA within the plant. That would be important to understand how the plant metabolism works for TMA and its relation to the global nitrogen cycle.

## References

- Almeida, J. et al.: Molecular understanding of sulphuric acid–amine particle nucleation in the atmosphere, *Nature*, 502, 359–363, 2013.
- Altimir, N., Kolari, P., Tuovinen, J.P., Vesala, T., Bäck, J., Suni, T., Kulmala, M. and Hari, P.: Foliage surface ozone deposition: a role for surface moisture?, *Biogeosciences*, 3, 1-20, 2006.
- Atkinson, R., Baulch, D. L., Cox, R. A., Crowley, J. N., Hampson, R. F., Hynes, R. G., Jenkin, M. E., Rossi, M. J., Troe, J., and IUPAC Subcommittee: Evaluated kinetic and photochemical data for atmospheric chemistry: Volume II – gas phase reactions of organic species, *Atmos. Chem. Phys.*, 6, 3625–4055, doi:10.5194/acp-6-3625-2006, 2006.
- Breuninger, C., Oswald, R., Kesselmeier, J., and Meixner, F. X.: The dynamic chamber method: trace gas exchange fluxes (NO, NO<sub>2</sub>, O<sub>3</sub>) between plants and the atmosphere in the laboratory and in the field, *Atmospheric Measurement Techniques*, 5(5), 955-989, 2012.
- Breuninger, C., Meixner, F. X., and Kesselmeier, J.: Field investigations of nitrogen dioxide (NO<sub>2</sub>) exchange between plants and the atmosphere. *Atmos. Chem. Phys.*, 13, 773–790, doi:10.5194/acp-13-773-2013.
- Burkhardt, J. and Eiden, R.: Thin water films on coniferous needles, *Atmospheric Environment*, 28(12), 2001-2011, 1994.
- Burkhardt, J., Kaiser, H., Goldbach, H., and Kappen, L.: Measurements of electrical leaf surface conductance reveal recondensation of transpired water vapour on leaf surfaces, *Plant Cell and Environment*, 22, 189–196, 1999.
- Calderón, S.M., Poor, N.D. and Campbell, S.W.: Estimation of the particle and gas scavenging contributions to wet deposition of organic nitrogen. *Atmospheric Environment*, 41, 4281-4290, 2007.
- Cape, J. N., Cornell, S. E., Jickells, T. D. and Nemitz, E.: Organic nitrogen in the atmosphere - Where does it come from? A review of sources and methods. *Atmospheric Research*, 102(1), 30-48, 2011.
- Chaparro-Suarez, I. G., Meixner, F. X., and Kesselmeier, J.: Nitrogen dioxide (NO<sub>2</sub>) uptake by vegetation controlled by atmospheric concentrations and plant stomatal aperture, *Atmos. Environ.*, 45, 5742–5750, 2011.
- Chen, M., Titcombe, M., Jiang, J., Jen, C., Kuang, C., Fischer, M. L., Eisele, F. L., Siepmann, J. I., Hanson, D. R., Zhao, J., and McMurry, P. H.: Acid-base chemical reaction model for nucleation rates in the polluted atmospheric boundary layer, *Proceedings of the National Academy of Sciences*, 109, 18 713–18 718, 2012.
- Coe, H., Gallagher, M. W., Choularton, T. W., & Dore, C.: Canopy scale measurements of stomatal and cuticular O<sub>3</sub> uptake by sitka spruce, *Atmospheric Environment*, 29(12), 1413-

- 1423, 1995.
- Cromwell, B. T.: The Micro-estimation and Origin of Trimethylamine in *Chenopodium vulvaria* L., *Biochem. J.*, 45, 84, 1949.
- Crutzen, P. J.: Photochemical reactions initiated by and influencing ozone in unpolluted tropospheric air, *Tellus*, 26(1-2), 47-57, 1974.
- Crutzen, P. J., Lawrence, M. G. and Pöschl, U.: On the background photochemistry of tropospheric ozone, *Tellus A*, 51(1), 123-146, 1999.
- Dawson, M. L., Varner, M. E., Perraud, V., Ezell, M. J., Gerber, R. B., and Finlayson-Pitts, B. J.: Simplified mechanism for new particle formation from methanesulfonic acid, amines, and water via experiments and abinitio calculations, *Proceedings of the National Academy of Sciences*, 109, 18719–18724, 2012.
- Dessaignes, M.: Trimethylamine obtenue de l'urine humaine, *C. R. Acad. Sci. (Paris)*, 43, 670-671, 1856.
- Dindorf, T., Kuhn, U., Ganzeveld, L., Schebeske, G., Ciccioli, C., Holzke, C., Köble, R., Seufert, G., and Kesselmeier, J.: Significant light and temperature dependent monoterpene emissions from European beech (*Fagus sylvatica* L.) and their potential impact on the European VOC budget. *J. Geophys. Res.*, VOL. 111, (D16):16305. doi:10.1029/2005JD006751, 2006.
- Doskey, P. V., Kotamarthi, V. R., Fukui, Y., Cook, D. R., Breitbeil, F. W., and Wesely, M. L.: Air–surface exchange of peroxyacetyl nitrate at a grassland site, *J. Geophys. Res.-Atmos.*, 109, D10310, doi:10.1029/2004JD004533, 2004.
- Erismann, J. W., Grennfelt, P. and Sutton, M.: The European perspective on nitrogen emission and deposition, *Environment International*, 29(2), 311-325, 2003.
- Erismann, J. W., Sutton, M. A., Galloway, J., Klimont, Z. and Winiwarter, W.: How a century of ammonia synthesis changed the world, *Nature Geoscience*, 1(10), 636-639, 2008.
- Erismann, J. W., Galloway, J. N., Seitzinger, S. P., Bleeker, A. D., Dise, N. B., Petrescu, A. M. R., Leach, A. M. and de Vries, W.: Consequences of human modification of the global nitrogen cycle, *Philosophical Transactions of the Royal Society B: Biological Sciences*, 368(1621), 2013.
- Fares, S., Loreto, F., Kleist, E., and Wildt, J.: Stomatal uptake and stomatal deposition of ozone in isoprene and monoterpene emitting plants, *Plant Biol.*, 10, 44–54, 2008.
- Fares, S., Park, J. H., Ormeno, E., Gentner, D. R., McKay, M., Loreto, F., Karlik, J. and Goldstein, A. H.: Ozone uptake by citrus trees exposed to a range of ozone concentrations, *Atmos. Environ.*, 44(28), 3404-3412, doi:10.1026/j.atmosenv.2010.06.010, 2010
- Fares, S., Weber, R., Park, J. H., Gentner, D., Karlik, J. and Goldstein, A. H.: Ozone deposition on orange orchard: Partitioning between stomatal and non-stomatal sinks, *Environmental Pollution*, 169, 258-266, 2012.
- Fischer, E. V., Jaffe, D. A. and Weatherhead, E. C.: Free tropospheric peroxyacetyl nitrate (PAN) and ozone at Mount Bachelor: potential causes of variability and timescale for trend detection, *Atmospheric Chemistry and Physics*, 11(12), 5641-5654, 2011.
- Flechard, C. R., Fowler, D., Sutton, M. A. and Cape, J. N.: A dynamic chemical model of bi-directional ammonia exchange between semi-natural vegetation and the atmosphere, *Quarterly Journal of the Royal Meteorology Society*, 125, 2611–2641, 1999.

- Fowler, D., et al.: The global nitrogen cycle in the twenty-first century, *Philosophical Transactions of the Royal Society B: Biological Sciences*, 368(1621), 2013.
- Fuentes, J. D. and Gillespie, T. J.: A gas-exchange system to study the effects of leaf surface wetness on the deposition of ozone, *Atmospheric Environment*, 26(6), 1165-1173, 1992.
- Fuhrer, J., Skärby, L. and Ashmore, M.R.: Critical levels for ozone effects on vegetation in Europe, *Environmental Pollution*, 97(1-2), 91-106, 1997.
- Fujii, T. and Kitai, T.: Determination of trace levels of trimethylamine in air by gas chromatography/surface ionization organic mass spectrometry, *Analytical Chemistry*, 59, 379-382, 1987.
- Galloway, J. N., Aber, J. D., Erisman, J. W., Seitzinger, S. P., Howarth, R. W., Cowling, E. B. and Cosby, B. J.: The nitrogen cascade, *Bioscience*, 53(4), 341-356, 2003.
- Galloway, J. N., Townsend, A. R., Erisman, J. W., Bekunda, M., Cai, Z., Freney, J. R., Martinelli, L. A., Seitzinger, S. P. and Sutton, M. A.: Transformation of the nitrogen cycle: recent trends, questions, and potential solutions, *Science*, 320(5878), 889-892, 2008.
- Galloway, J. N., Leach, A. M., Bleeker, A., & Erisman, J. W.: A chronology of human understanding of the nitrogen cycle, *Philosophical Transactions of the Royal Society of London B: Biological Sciences*, 368(1621), 20130120, doi:10.1098/rstb.2013.0120, 2013.
- Ganguly, N. D. and Tzanis, C.: Study of Stratosphere-troposphere exchange events of ozone in India and Greece using ozonesonde ascents, *Meteorological applications*, 18(4), 467-474, 2011.
- Garland, J. A. and Penkett, S. A.: Absorption of peroxyacetyl nitrate and ozone by natural surfaces, *Atmos. Environ.*, 10, 1127-1131, 1976.
- Ge, X., Wexler, A. S. and Clegg, S. L.: Atmospheric amines – Part I. A review, *Atmospheric Environment*, 45, 524-546, 2011.
- Gerosa, G., Vitale, M., Finco, A., Manes, F., Denti, A. B. and Cieslik, S.: Ozone uptake by an evergreen Mediterranean Forest (*Quercus ilex*) in Italy. Part I: Micrometeorological flux measurements and flux partitioning, *Atmospheric Environment*, 39(18), 3255-3266, 2005.
- Glasoe, W. A., Volz, K., Panta, B., Freshour, N., Bachman, R., Hanson, D. R., McMurry, P. H. Jen, C.: Sulfuric acid nucleation: An experimental study of the effect of seven bases, *Journal of Geophysical Research-Atmospheres*, 120(5), 1933-1950, 2015.
- Granat, L. and Richter, A.: Dry deposition to pine of sulphur dioxide and ozone at low concentration, *Atmospheric Environment*, 29(14), 1677-1683, 1995.
- Grantz, D. A., Zhang, X. J., Massman, W. J., Den Hartog, G., Neumann, H. H. and Pederson, J. R.: Effects of stomatal conductance and surface wetness on ozone deposition in field-grown grape, *Atmospheric Environment*, 29(21), 3189-3198, 1995.
- Hakan, P., Karlsson, G. P., Danielsson, H. and Selldén, G.: Surface wetness enhances ozone deposition to a pasture canopy, *Atmospheric Environment*, 29(22), 3391-3393, 1995.
- Hatfield, J. L. and Follett, R. F. (Eds.): *Nitrogen in the Environment: Sources, Problems, and Management*, Elsevier, 2008.
- Hill, A. C.: Vegetation: a sink for atmospheric pollutants, *JAPCA J. Air Waste Ma.*, 21, 341-346, 1971.
- Hogg, A., Uddling, J., Ellsworth, D., Carroll, M. A., Pressley, S., Lamb, B. and Vogel, C.: Stomatal and non-stomatal fluxes of ozone to a northern mixed hardwood forest, *Tellus*

- Series B-Chemical and Physical Meteorology, 59(3), 514-525, 2007.
- Horst, T. W. and Weil, J. C.: How far is far enough – The fetch requirements for micrometeorological measurement of surface fluxes (Vol 11, PG 1018, 1994), *J. Atmos. Ocean. Tech.*, 12, 447–447, 1995.
- Jickells, T., Baker, A. R., Cape, J. N., Cornell, S. E. and Nemitz, E.: The cycling of organic nitrogen through the atmosphere. *Philosophical Transactions of the Royal Society of London B: Biological Sciences*, 368(1621), 20130115, doi: 10.1098/rstb.2013.0115, 2013.
- Johnson, J. E., Gammon, R. H., Larsen, J., Bates, T. S., Oltmans, S. J. and Farmer, J. C.: Ozone in the marine boundary layer over the Pacific and Indian Oceans: Latitudinal gradients and diurnal cycles, *J. Geophys. Res.*, 95(D8), 11847–11856, doi:10.1029/JD095iD08p11847, 1990.
- Kames, J., Schweighöfer, S. and Schurath, U.: Henrys law constant and hydrolysis of Peroxyacetyl nitrate (PAN), *Journal of Atmospheric Chemistry*, 12(2), 169-180, 1991.
- Kesselmeier, J., Meixner, F. X., Hofmann, U., Ajavon, A., Leimbach, S., and Andreae, M. O.: Reduced sulfur compound exchange between the atmosphere and tropical tree species in southern Cameroon, *Biogeochemistry* 23, 23–45, 1993.
- Kesselmeier, J., Schäfer, L., Ciccioli, P., Brancaleoni, E., Cecinato, A., Frattoni, M., Foster, P., Jacob, V., Denis, 5 J., Fugit, J. L., Dutaur, L., and Torres, L.: Emission of monoterpenes and isoprene from a Mediterranean oak species *Quercus ilex* L measured within the BEMA (Biogenic Emissions in the Mediterranean Area) project, *Atmos. Environ.*, 30, 1841–1850, 1996.
- Kesselmeier, J., Bode, K., Gerlach, C., and Jork, E. M.: Exchange of atmospheric formic and acetic acids with trees and crop plants under controlled chamber and purified air conditions, *Atmos. Environ.*, 32, 1765–1775, 1998.
- Klemm, O., Milford, C., Sutton, M. A., Spindler, G. and van Putten, E.: Aclimatology of leaf surface wetness, *Theoretical and Applied Climatology*, 71, 107–117, 2002.
- Kruit, R. J. W., Jacob, A. F. G., and Holtslaga, A. A. M.: Measurements and estimates of leaf wetness over agricultural grassland for dry deposition modeling of trace gases, *Atmos. Environ.*, 42, 5304–5316, 2008.
- Kuhn, U., Wolf, A., Gries, C., Nash, T. H., and Kesselmeier, J.: Field measurements on the exchange of carbonyl sulfide between lichens and the atmosphere, *Atmos. Environ.*, 34, 4867–4878, 2000.
- Kulmala, M., Hienola, J., Pirjola, L., Vesala, T., Shimmo, M., Altimir, N. and Hari, P.: A model for NO<sub>x</sub>-O<sub>3</sub>-terpene chemistry in chamber measurements of plant gas exchange, *Atmos. Environ.*, 33, 2145-2156, 1999.
- Kurten, A. et al.: Neutral molecular cluster formation of sulfuric acid-dimethylamine observed in real time under atmospheric conditions, *Proceedings of the National Academy of Sciences*, 111, 15019–15024, 2014.
- Lange, O. L., Lösch, R., Schulze, E.-D. and Kappen, L.: Response of stomatal to changes in humidity, *Planta*, 100(1), 76-86, 1971.
- Lelieveld, J. and Crutzen, P. J.: Role of deep cloud convection in the ozone budget of the troposphere, *Science*, 264(5166), 1759-1761, 1994.
- Lippmann, M.: Health effects of ozone a critical review, *Japca*, 39(5), 672-695, 1989.

- Liu, S. C., Kley, D., McFarland, M., Mahlman, J. D. and Levy, H.: On the origin of tropospheric ozone, *Journal of Geophysical Research: Oceans*, 85(C12), 7546-7552, 1980.
- Loreto, F. and Fares, S.: Is ozone flux inside leaves only a damage indicator? Clues from volatile isoprenoid studies, *Plant Physiology*, 143, 1096-1100, 2007.
- Madronich, S., Shao, M., Wilson, S. R., Solomon, K. R., Longstreth, J. D. and Tang, X. Y.: Changes in air quality and tropospheric composition due to depletion of stratospheric ozone and interactions with changing climate: implications for human and environmental health, *Photochemical & Photobiological Sciences*, 14(1), 149-169, 2015.
- Mikkelsen, T. N., Ro-Poulsen, H., Hovmand, M. F., Jensen, N. O., Pilegaard, K., and Egeløv, A. H.: Five-year measurements of ozone fluxes to a Danish Norway spruce canopy, *Atmospheric Environment*, 38, 2361–2371, 2004.
- Moravek, A., Stella, P., Foken, T. and Trebs, I.: Influence of local air pollution on the deposition of peroxyacetyl nitrate to a nutrient-poor natural grassland ecosystem, *Atmospheric Chemistry and Physics*, 15, 899-911, 2015.
- Niinemets, Ü., Kuhn, U., Harley, P. C., Staudt, M., Arneth, A., Cescatti, A., Ciccioli, P., Copolovici, L., Geron, C., Guenther, A., Kesselmeier, J., Lerdau, M. T., Monson, R. K., and Peñuelas, J.: Estimations of isoprenoid emission capacity from enclosure studies: measurements, data processing, quality and standardized measurement protocols, *Biogeosciences*, 8, 2209–2246, doi:10.5194/bg-8-2209-2011, 2011.
- Okano, K., Tobe, K., and Furukawa, A.: Foliar uptake of peroxyacetyl nitrate (PAN) by herbaceous species varying in susceptibility to this pollutant, *New Phytol.*, 114, 139–145, 1990.
- Okita, T.: Filter method for the determination of trace quantities of amines, mercaptans, and organic sulphides in the atmosphere, *Atmospheric Environment*, 4, 93-102 1970.
- Ortega, J. and Helmig, D.: Approaches for quantifying reactive and low-volatility biogenic organic compound emissions by vegetation enclosure techniques – Part A, *Chemosphere*, 72(3), 343-364, doi: 10.1016/j.chemosphere.2007.11.020, 2008
- Paoletti, E.: Ozone and Mediterranean ecology: Plants, people, problems, *Environmental Pollution*, 157(5), 1397-1398, 2009.
- Pape, L., Ammann, C., Nyfeler-Brunner, A., Spirig, C., Hens, K., and Meixner, F. X.: An automated dynamic chamber system for surface exchange measurement of non-reactive and reactive trace gases of grassland ecosystems, *Biogeosciences*, 6, 405–429, doi:10.5194/bg- 6-405-2009, 2009.
- Ravishankara, A. R., Hancock, G., Kawasaki, M. and Matsumi, Y.: Photochemistry of Ozone: Surprises and Recent Lessons, *Science*, 280(5360), 60-61, doi: 10.1126/science.280.5360.60, 1998.
- Riccobono, F. et al.: Oxidation Products of Biogenic Emissions Contribute to Nucleation of Atmospheric Particles, *Science*, 344, 717–721, 2014.
- Rubio, M. A., Gramsch, E., Lissi, E. and Villena, G.: Seasonal dependence of peroxyacetyl nitrate (PAN) concentrations in downtown Santiago, Chile, *Atmósfera*, 20(4), 319-328, 2007.
- Rudich, Y., Benjamin, I., Naaman, R., Thomas, E., Trakhtenberg, S., Ussyshkin, R.: Wetting of hydrophobic organic surfaces and its implications to organic aerosols in the atmosphere, *J. Phys. Chem. A*, 104, 5238–5245, 2000.

- Sandoval-Soto, L., Kesselmeier, M., Schmitt, V., Wild, A. and Kesselmeier, J.: Observations of the uptake of Carbonyl sulfide (COS) by trees under elevated atmospheric carbon dioxide concentrations. *Biogeosciences*, 9, 2935–2945, 2012.
- Schade, G.W. and Crutzen, P.J.: Emission of aliphatic amines from animal husbandry and their reactions: potential source of N<sub>2</sub>O and HCN, *Journal of Atmospheric Chemistry*, 22, 319-346, 1995.
- Schrimpf, W., Lienaerts, K., Müller, K. P., Rudolph, J., Neubert, R., Schüßler, W. and Levin, I., Dry deposition of peroxyacetyl nitrate (PAN): Determination of its deposition velocity at night from measurements of the atmospheric PAN and (222) Radon concentration gradient, *Geophysical Research letters*, 23(24). 3599-3602, 1996.
- Shepson, P. B., Bottenheim, J. W., Hastie, D. R. and Venkatram, A.: Determination of the relative Ozone and PAN deposition velocities at night, *Geophysical Research Letters*, 19(11), 1121-1124, 1992.
- Sillman, S.: Tropospheric ozone and photochemical smog, *Environmental geochemistry*, 9, 407-31, 2003.
- Simpson, D.: Long-period modelling of photochemical oxidants in Europe. Model calculations for July 1985, *Atmospheric Environment*, 26(9), 1609-1634, 1992.
- Simpson, D., Benedictow, A., Berge, H., Bergström, R., Emberson, L. D., Fagerli, H., Flechard, C. R., Hayman, G. D., Gauss, M., Jonson, J. E., Jenkin, M. E., Nyríri, A., Richter, C., Semeena, V.S., Tsyro, S., Tuovinen, J.-P., Valdebenito, Á. and Wind, P.: The EMEP MSC-W chemical transport model – technical description, *Atmos. Chem. Phys.*, 12, 7825-7865, doi:10.5194/acp-12-7825-2012, 2012.
- Singh, H. B.: Reactive nitrogen in the troposphere, *Environmental science & technology*, 21(4), 320-327, 1987.
- Sintermann, J. and Neftel, A.: Ideas and perspectives: on the emission of amines from terrestrial vegetation in the context of new atmospheric particle formation, *Biogeosciences*, 12(11), 3225-3240, 2015.
- Spracklen, D. V., Jimenez, J. L., Carslaw, K. S., Worsnop, D. R., Evans, M. J., Mann, G. W., Zhang, Q., Canagaratna, M. R., Allan, J., Coe, H., McFiggans, G., Rap, A., and Forster, P.: Aerosol mass spectrometer constraint on the global secondary organic aerosol budget, *Atmospheric Chemistry and Physics*, 11, 12 109–12 136, 2011.
- Smil, V.: *Feeding the world: A challenge for the twenty-first century*, MIT press., 2001.
- Smith, T. A.: The occurrence, metabolism and functions of amines in plants, *Biological Reviews*, 46, 201–241, 1971.
- Smith, T. A.: Recent advances in the biochemistry of plant amines, *Phytochemistry*, 14, 865–890, 1975.
- Sparks, J. P., Monson, R. K., Sparks, K. L., and Lerdau, M.: Leaf uptake of nitrogen dioxide (NO<sub>2</sub>) in a tropical wet forest: implications for tropospheric chemistry, *Oecologia*, 127, 214 221, 2001.
- Sparks, J. P., Roberts, J. M. and Monson, R. K.: The uptake of gaseous organic nitrogen by leaves: A significant global nitrogen transfer process, *Geophysical Research Letters*, 30(23), 2189, 2003
- Sparks, J. P.: Ecological ramifications of the direct foliar uptake of nitrogen, *Oecologia*, 159(1), 1-13, 2009.



- Stehr, J. W., Ball, W. P., Dickerson, R. R., Doddridge, B. G., Piety, C. A. and Johnson, J. E.: Latitudinal gradients in O<sub>3</sub> and CO during INDOEX 1999, *J. Geophys. Res.*, 107(D19), 8016, doi:10.1029/2001JD000446, 2002.
- Sun, S., Moravek, A., von der Heyden, L., Held, A., Sörgel, M. and Kesselmeier, J.: Twin-cuvette measurement technique for investigation of dry deposition of O<sub>3</sub> and PAN to plant leaves under controlled humidity conditions, *Atmospheric Measurement Techniques in press*, 8, 12051-12104, doi:10.5194/amtd-8-12051-2016, 2016.
- Sutton, M. A. et al. (Eds.): *The European nitrogen assessment: sources, effects and policy perspectives*, Cambridge University Press., 2011.
- Talukdar, R. K., Burkholder, J. B., Schmoltner, A. M., Roberts, J. M., Wilson, R. R. and Ravishankara, A. R.: Investigation of the loss processes for Peroxyacetyl nitrate in the atmosphere - UV photolysis and reaction with OH, *Journal of Geophysical Research – Atmospheres*, 100(D7), 144163-14173, 1995.
- Teklemariam, T. A. and Sparks, J. P.: Gaseous fluxes of peroxyacetyl nitrate (PAN) into plant leaves, *Plant Cell and Environment*, 27(9), 1149-1158, 2004.
- Tuazon, E. C., Carter, W. P. L. and Atkinson, R.: Thermal-decomposition of peroxyacetyl nitrate and reactions of acetylperoxy-radicals with NO and NO<sub>2</sub> over the temperature-range 283-313 K, *Journal of Physical Chemistry*, 95(6), 2434-2437, 1991.
- Turnipseed, A. A., Huey, L. G., Nemitz, E., Stickel, R., Higgs, J., Tanner, D. J., Slusher, D. L., Sparks, J. P., Flocke, F. and Guenther, A.: Eddy covariance fluxes of peroxyacetyl nitrates (PANs) and NO<sub>y</sub> to a coniferous forest, *Journal of Geophysical Research-Atmospheres*, 111(D9), D09304, 2006.
- Van Dingenen, R., Dentener, F. J., Raes, F., Krol, M. C., Emberson, L. and Cofala, J.: The global impact of ozone on agricultural crop yields under current and future air quality legislation, *Atmospheric Environment*, 43(3), 604-618, 2009.
- Van Hove, L.W.A., Bossen, M. E., de Bok, F. A. M. and Hooijmaijers, C. A. M.: The uptake of O<sub>3</sub> by poplar leaves: the impact of a long-term exposure to low O<sub>3</sub>-concentrations, *Atmos. Environ.*, 33, 907-917. 1999
- Wang, X.C. and Lee, C.: Sources and distribution of aliphatic amines in salt marsh sediment. *Organic Geochemistry*, 22, 1005-1021, 1994.
- Wang, D., Hinckley, T. M., Cumming, A. B. and Braatne, J.: A comparison of measured and modeled ozone uptake into plant leaves, *Environ. Pollut.* 89(3), 247-254, 1995.
- Watanabe, K., Nojiri, Y. and Kariya, S.: Measurements of ozone concentrations on a commercial vessel in the marine boundary layer over the northern North Pacific Ocean, *J. Geophys. Res.*, 110(D11310), doi:10.1029/2004JD005514, 2005.
- Wendschuh, P. H., Pate, C. T. and Pitts, Jr. J. N.: The reaction of peroxyacetyl nitrate with aldehydes, *Tetrahedron Letters*, 31, 2931-2934, 1973.
- Wicke, W.: Beobachtungen an *Chenopodium vulvaria* über die Ausscheidung von Trimethylamin, *Annalen der Chemie und Pharmacie*, 124, 338–340, 1862.
- Wolfe, G. M., Thornton, J. A., Yatavelli, R. L. N., McKay, M., Goldstein, A. H., LaFranchi, B., Min, K. E. and Cohen, R. C.: Eddy covariance fluxes of acyl peroxy nitrates (PAN, PPN and MPAN) above a Ponderosa pine forest, *Atmospheric Chemistry and Physics*, 9(2), 615-634, 2009.

Zhang, J. M., Wang, T., Ding, A. J., Zhou, X. H., Xue, L. K., Poon, C. N., Wu, W. S., Gao, J., Zuo, C., Chen, J. M., Zhang, X. C. and Fan, S. J.: Continuous measurement of peroxyacetyl nitrate (PAN) in suburban and remote areas of western China, *Atmospheric Environment*, 43(2), 228-237, 2009.

# Appendix A

## List of publications and individual contribution

This cumulative dissertation consists of the following listed publications and manuscripts, which evolved from close collaboration with other scientists and colleagues of the Max-Planck-Institute for Chemistry, Johannes Gutenberg-University Mainz, University of Bayreuth, and Agroscope. The individual contributions to the respective publications and manuscripts are specified below:

### Appendix B

Sun, S., Moravek, A., von der Heyden, L., Held, A., Sörgel, M. and Kesselmeier, J.: Twin-cuvette measurement technique for investigation of dry deposition of O<sub>3</sub> and PAN to plant leaves under controlled humidity conditions, Atmospheric Measurement Techniques, 9, 599-617, doi:10.5194/amt-9-599-2016, 2016.

- My contribution was focused on the development of the entire cuvette measurement system, which includes the design and construction of the cuvettes and the software development for data acquisition and monitoring. Thereafter, the cuvette system was tested and optimized for the required conditions including the development of the humidification system. Furthermore, all data analysis and the writing of the manuscript belong to my task.
- Alexander Moravek was my scientific colleague, who was involved mostly in the implementation of the PAN-GC. He was essential for the technical performance of the PAN-GC and helping me with the O<sub>3</sub> and PAN flux measurements. Furthermore, he was involved in discussion of the results and gave useful comments on the manuscript.
- Lisa von der Heyden and Andreas Held offered the leaf wetness sensor and helped with the technical description of that device. Additionally they wrote the technical part of the leaf wetness sensor for the manuscript.
- Matthias Sörgel is my daily-supervisor. He was involved in all decisions and stages of my work. He supported me with helpful advice and discussions of the results. Additionally, he gave essential comments on the manuscript.
- Jürgen Kesselmeier is my co-supervisor. He was a co-initiator of this work and

allocates the laboratory and plant materials to me. Additionally, he provides me with technical materials and equipment. Furthermore, he was also involved in all decisions and stages of my research work and helped me with useful advice and comments to the manuscript.

## Appendix C

Sun, S., Moravek, A., Trebs, I., Kesselmeier, J. and Sörgel, M.: Investigation of the influence of liquid surface films on O<sub>3</sub> and PAN deposition to plant leaves coated with organic / inorganic solution, submitted to Journal of Geophysical Research: Atmospheres, 2016

- I wrote the manuscript and developed the concept of the experiments. Additionally, I prepared the plant samples for the liquid film experiments and performed the flux measurements of O<sub>3</sub> and PAN. Furthermore, I analyzed all the measurement data and incorporated it into the manuscript.
- Alexander Moravek was involved in the discussion of the results. He helped me with useful comments on the manuscript and was essential for its completion.
- Ivonne Trebs was my initial-supervisor. She gave valuable comments on the manuscript and initiated the research.
- Jürgen Kesselmeier is my co-supervisor. He allocates the laboratory and plant materials to me. Additionally, he provides me with technical materials and equipment. Furthermore, he was also involved in all decisions and stages of my research work and helped me with useful advice and comments to the manuscript.
- Matthias Sörgel is my daily-supervisor. He initiated this research topic and was involved in all decisions and stages of my work. He supported me with helpful advice and discussions of the results. Additionally, he gave essential comments on the manuscript.

## Appendix D

Sun S., Neftel, A., Sintermann, J., Sauvage, C., Derstroff, B., Bohley, K., Kadereit, G., Williams, J., Pöhlker, C., Kesselmeier, J. and Sörgel, M.: Emission of Trimethylamine from *Chenopodium vulvaria* - first results from quantifying plant emissions of amines and their potential effects on the atmospheric new particle formation, to be submitted.

- I am the major author and wrote the main part of the manuscript. I designed and constructed the small cuvette system for the screening experiment and optimized the twin-cuvette system for the TMA flux measurement. Additionally, I designed and constructed the nucleation chamber setup and performed the particle formation experiments. Furthermore, I performed the emission flux measurement with the twin-

cuvette system, analyzed the emission flux data and pooled all other analyzed data for incorporating into the manuscript.

- Albrecht Neftel and Joerg Sintermann initiated this research topic and shared their experience. They helped with useful ideas for the experiments and comments on the manuscript.
- Carina Sauvage performed the screening experiment and analyzed all of the corresponding data. Additionally, she wrote the technical description of the GC-NCD for the manuscript.
- Bettina Derstroff was involved in the emission flux measurement with the twin-cuvette system. She was responsible for the performing of the PTR-TOF-MS. Additionally, she analyzed all of the corresponding data and wrote the technical description of the PTR-TOF-MS for the manuscript.
- Katharina Bohley prepared the leaf cross section of the plant material and performed the microscopic analysis. Additionally, she wrote the method description of the leaf cross section analysis.
- Gudrun Kadereit was responsible for the plant samples. She grew the seeds and cultivated the plants. Additionally, she helped with useful plant physiological knowledge.
- Jonathan Williams provided the PTR-TOF-MS for the flux measurement and helped with useful advice for the data analyzing
- Christopher Pöhlker provided the laboratory and equipment for the nucleation experiments. He was involved in the performance and construction of the nucleation chamber. Furthermore, he helped with useful advice for the nucleation experiments.
- Jürgen Kesselmeier is my co-supervisor. He allocates the laboratory and plant materials to me. Additionally, he provided me with technical materials and equipment. Furthermore, he was also involved in all decisions and stages of my research work and helped me with useful advice and comments to the manuscript.
- Matthias Sörgel is my daily-supervisor. He was involved in all decisions and stages of my work. He supported me with helpful advice and discussions of the results. Additionally, he gave essential comments on the manuscript.



# Appendix B

## **Twin-cuvette measurement technique for investigation of dry deposition of O<sub>3</sub> and PAN to plant leaves under controlled humidity conditions**

Shang Sun<sup>1</sup>, Alexander Moravek<sup>2</sup>, Lisa von der Heyden<sup>3</sup>, Andreas Held<sup>3,4</sup>, Matthias Sörgel<sup>1</sup>, Jürgen Kesselmeier<sup>1</sup>

<sup>1</sup>Max Planck Institute for Chemistry, Biogeochemistry Department, P.O. Box 3060, 55128 Mainz, Germany

<sup>2</sup>University of Toronto, Department of Chemistry, 80 St. George St, M5S 3H6, Toronto, Canada

<sup>3</sup>University of Bayreuth, Atmospheric Chemistry, 95440 Bayreuth, Germany

<sup>4</sup>University of Bayreuth, Bayreuth Center of Ecology and Environmental Research, 95440 Bayreuth, Germany

Correspondence to: S.Sun (shang.sun@mpic.de)

Published in Atmospheric Measurements Techniques

Received: 5 October 2015 – Revised: 28 January 2016 – Accepted: 9 February 2016 –  
Published: 23 February 2016

Published by Copernicus Publications on behalf of the European Geosciences Union.

Atmos. Meas. Tech., 9, 599–617, doi:10.5194/amt-9-599-2016, 2016

## Abstract

We present a dynamic twin-cuvette system for quantifying the trace-gas exchange fluxes between plants and the atmosphere under controlled temperature, light and humidity conditions. Compared with a single-cuvette system, the twin-cuvette system is insensitive to disturbing background effects such as wall deposition. In combination with a climate chamber, we can perform flux measurements under constant and controllable environmental conditions. With an Automatic Temperature Regulated Air Humidification System (ATRAHS) we are able to regulate the relative humidity inside both cuvettes between 40 % to 90 % with a high precision of 0.3 %. Thus, we could demonstrate that for a cuvette system operated with a high flow rate ( $> 20 \text{ L min}^{-1}$ ) such a temperature-regulated humidification system as ATRAHS is an accurate method for air humidification of the flushing air. Furthermore, the fully automatic progressive fill-up of ATRAHS based on a floating valve improved the performance of the entire measurement system and prevented data gaps. Two reactive gas species, ozone ( $\text{O}_3$ ) and peroxyacetyl nitrate (PAN), were used to demonstrate the quality and performance of the twin-cuvette system.  $\text{O}_3$  and PAN exchange with *Quercus ilex* was investigated over a 14 day measurement period under controlled climate chamber conditions. By using  $\text{O}_3$  mixing ratios between 32 - 105 ppb and PAN mixing ratios between 100 - 350 ppt a linear dependency of the  $\text{O}_3$  flux as well as the PAN flux in relation to its ambient mixing ratio could be observed. At relative humidity (RH) of 40%, the deposition velocity ratio of  $\text{O}_3$  and PAN was determined to be 0.45. At that humidity, the deposition of  $\text{O}_3$  to the plant leaves was found to be only controlled by the leaf stomata. For PAN an additional resistance inhibited the uptake of PAN by the leaves. Furthermore, the formation of water films on the leaf surface of plants inside the chamber could be continuously tracked with our custom built leaf wetness sensors. Using this modified leaf wetness sensor measuring the electrical surface conductance on the leaves, an exponential relationship between the ambient humidity and the electrical surface conductance could be determined.

## 1 Introduction

The atmosphere-biosphere exchange of various trace gas species plays an important role for the climate and ecosystem interaction. The removal and emission of trace gases by the biosphere represents a significant factor, and its understanding is essential for atmospheric chemistry and the calculation of global trace gas budgets. While there is an increasing interest in the underlying mechanism of trace gas exchange of plants, various methods to determine the exchange flux of trace gases exist – in the field and under controlled laboratory



conditions. For flux measurements on ecosystem level micrometeorological methods such as the eddy covariance or gradient method are used, causing only minimal disturbance (Horst and Weil, 1995). However, to understand the mechanism and processes in more detail, measurement on the plant and leaf scale under controlled environment conditions are often used. Therefore, enclosure techniques are mainly used to perform experiments under constant environmental conditions for investigation of the interaction between the plant and the atmosphere with higher resolution and reliability. For these experiments, it is important to minimize the disturbance of the environmental conditions such as radiation, humidity, temperature, and the trace gas concentration to ensure an optimum of plant physiological activity (Pape et al., 2009). Especially for flux measurements of trace gases whose exchange processes are predominantly controlled by the leaf stomata, such reproducible preconditions should be achieved.

A commonly used technique for the measurement of trace gas uptake and release on plant and leaf scale is the dynamic cuvette technique (e.g., Breuninger et al., 2012). In the field, it can be ensured that the inner trace gas concentration and other related quantities are constant and close to the ambient conditions outside of the cuvette by the continuous renewal of the air inside the cuvette. For laboratory measurements, the dynamic cuvette leads to a temporally constant trace gas mixing ratio inside the cuvette. Typically, systems employ one single dynamic cuvette, in which the trace gas concentration is measured at the entrance position of the cuvette and inside the cuvette to retrieve the trace gas flux. One disadvantage of such cuvette systems is the potential adsorption and/or desorption effects on the cuvette walls, which is critical, especially for reactive trace gases (Kulmala et al. 1999, Pape et al., 2009). Furthermore, the influence of humidity is an important factor for the surface deposition of various water soluble trace gas species (e.g.,  $\text{NH}_3$ ,  $\text{SO}_2$ ,  $\text{NO}$ ,  $\text{NO}_2$ , organic and inorganic acids and oxygenated monoterpenes such as linalool and 1,8-cineole) in the atmosphere (Kruit et al., 2008, Niinemets et al., 2011). Even substances with less water solubility (e.g.,  $\text{O}_3$ ) can be affected by higher air humidity resulting in a water film on the leaf surface (Altimir et al., 2006, Fuentes and Gillespie, 1992). In this paper, we present the use of a twin-cuvette system, which was designed to perform long-term flux measurements under controlled laboratory conditions. The setup is based on a cuvette system which was previously used for measurements of volatile organic compounds (VOCs) and  $\text{NO}_2$  (Kesselmeier et al., 1996, Chaparro-Suarez et al., 2011, Breuninger et al., 2012). To account for wall effects and other systematic uncertainties, a main feature of the system was the employment of a second, empty cuvette, which was used as a reference. To control the humidity in both cuvettes, we developed a new humidification system, which allowed for a precise regulation of the humidity inside the cuvettes. This allows to investigate important questions such as the relationship between humidity and the trace gas deposition on vegetation surfaces with high reliability. The twin-cuvette system was first developed for the plant-atmosphere exchange of

PAN (peroxyacetyl nitrate) and O<sub>3</sub>. While previous investigations mainly focused on the effect of inorganic nitrogen containing trace gases, particularly NO<sub>2</sub> to plants (Hill, 1971, Sparks et al., 2001, Ortega et al., 2008, Breuninger et al., 2012), studies on the uptake of gaseous organic nitrogen species such as PAN under laboratory conditions are rare. An overview is given in Table 1.

Table 1: List of previous studies in the research field of O<sub>3</sub> and PAN flux measurement on plants under laboratory conditions.

Reference	Gas species	Plant species	Instrument	Method	Inlet mixing ratio	Regulated Humidification	Deposition velocity mm s <sup>-1</sup>
Fares et al. (2008)	O <sub>3</sub>	<i>Quercus ilex</i> , <i>Populus nigra</i>	O <sub>3</sub> -Analyzer Model 49	Plant chamber, gas phase reaction chamber	100 ppb	Not mentioned	0.9 – 1.8
Fares et al. (2010)	O <sub>3</sub>	<i>Citrus limon</i> , <i>Citrus reticulata</i> , <i>Citrus sinensis</i>	O <sub>3</sub> -Analyzer DASIBI mod. 1008-AH	Branch dynamic enclosure	40 – 160 ppb	No	2 – 5
Wang et al. (1995)	O <sub>3</sub>	<i>Populus trichocarpa</i> , <i>Populus deltoides</i> , <i>Phaseolus vulgaris</i> , <i>Cucurbita sativus</i> , <i>Cucurbita pepo</i>	O <sub>3</sub> -Analyzer Dasibi 1003	Single dynamic chamber (inlet & outlet measurement)	< 200 ppb	No	0.02 – 0.05
Van Hove et al. (1999)	O <sub>3</sub>	<i>Populus nigra</i> , <i>P.brandaris</i> , <i>P.robusta</i>	O <sub>3</sub> -Analyzer	Leaf chamber (inlet & outlet measurement)	30 – 100 ppb	No	---
Teklemariam & Sparks (2004)	PAN	<i>Zea mays</i> , <i>Triticum aestivum</i> , <i>Helianthus annuus</i> , <i>Catharanthus roseus</i>	GC (ECD) Limit 5 ppt, precision better than 1% > 200ppt	Single dynamic chamber (inlet & outlet measurement)	0.8 – 18 ppb	No	0.03 – 0.3
Okano et al. (1990)	PAN	<i>Herbaceous species</i>	2x GC (ECD) For inlet and outlet	Single dynamic chamber (inlet & outlet measurement)	190 ppb	No	0.3 – 3.1
Sparks et al. (2003)	PAN	<i>Zea mays</i> , <i>Phaseolus vulgaris</i> , <i>Pinus contorta</i> , <i>Mangifera indica</i> , <i>Quercus velutina</i> , <i>Quercus rubra</i> , <i>Abies grandis</i> , <i>Picea engelmannii</i>	GC (ECD) Limit 5 ppt, precision better than 1% > 200ppt	Single dynamic chamber (inlet & outlet measurement)	250 ppt	No	1.8 – 4.9
This study	PAN, O <sub>3</sub>	<i>Quercus ilex</i>	O <sub>3</sub> -Analyzer Model 49i, GC (ECD) LOD 1 ppt, precision 2% < 800ppt	Dual dynamic cuvette system (4 position measurement)	O <sub>3</sub> : 60 ppb PAN: 280 ppt	Yes 40-90%	See Sect. 3.2.1

Laboratory studies which were designed to compare the PAN deposition with O<sub>3</sub> deposition have not been performed up to now (Table 5). Both Okano et al. (1990) and Teklemariam and Sparks (2004) used relatively high PAN mixing ratios (up to 190 ppb) for fumigation, which do not correspond to the PAN mixing ratios found under typical environmental conditions. Furthermore, the obtained deposition velocities in these studies differed considerably (see Table 1), which might be attributed to the use of different plant species and measurement methods. With adapting the cuvette conditions as closely as possible to the ones found in natural environments, our dual cuvette system is convenient for investigating the deposition mechanism of O<sub>3</sub> and PAN on plants concerning their reactivity and potential wall effect with

plant surface as well as the wall material.

## 2 Material and Methods

### 2.1 Setup of dual dynamic cuvette system

#### 2.1.1 General setup

The experimental setup consisted of two dynamic cuvettes (Kesselmeier et al., 1996, Chaparro-Suarez et al., 2011, Breuninger et al., 2012) (see Fig. 1+Fig. 2). The entire plant sample above the soil was introduced into the sample cuvette. The leaf temperature was measured by thermocouples (Type E, OMEGA Engineering, Inc., USA) at four different positions of the plant. Pressurized air flow was provided by a compressor and was purified by different filter cartridges filled with glass wool (Merck, Germany), silica gel (2-5mm Merck, Germany), Purafil<sup>®</sup> (KMnO<sub>4</sub>/Al<sub>2</sub>O<sub>3</sub>, Purafil Inc., USA) and active charcoal (LS–Labor Service, Germany), producing air free of O<sub>3</sub>, NO, NO<sub>2</sub> and PAN. The purified air stream (20 L min<sup>-1</sup> for each cuvette) was regulated by two mass flow controllers (MFC) (MKS Instruments, USA) and humidified to a predefined RH value (ATRAHS see, Sect. 2.1.3). The addition of O<sub>3</sub> and PAN into the main air stream occurred under atmospheric pressure downstream of the humidification step. To perform exchange flux measurements under controlled laboratory conditions, the pure air had to be enriched by known amounts of both O<sub>3</sub> and PAN. PAN was produced by a calibration unit (Meteorologie Consult GmbH, Germany) via gas phase photolysis of acetone in the presence of NO (see Sect. 2.3.2) (Patz et al., 2002). O<sub>3</sub> was produced by a primary standard device (Model 49C Primary Standard, Thermo Fisher Scientific, USA) via photolysis of O<sub>2</sub> in the synthetic air stream. A precise addition of the O<sub>3</sub> and PAN to the pure air stream was obtained by the use of MFCs. Both calibration devices had to be operated at atmospheric pressure at their outlet. Therefore, a Teflon membrane pump (KNF Neuberger GmbH, Germany) was implemented to deliver an over pressure of nearly 1.6 bar, which was needed to operate the MFCs (see Fig. 1, No.11-15) for providing a controlled stream of the gas mixture to the system. With this additional setup, stable mixing ratio levels of O<sub>3</sub> and PAN within both cuvettes could be achieved. Downstream of the cuvettes, three Teflon-valves (Entegris, Inc. USA) were used to switch between inlet and outlet of both cuvettes for the analysis of O<sub>3</sub> and PAN mixing ratios (see Fig. 1, No. 9). The PAN mixing ratio was continuously measured by an automatic gas chromatograph with electron capture detection (GC-ECD) (Meteorologie Consult GmbH, Germany, see also Volz-Thomas et al., 2002). PAN was pre-concentrated over a duration of 5 min on a capillary

column, which was thermally controlled at 2 °C. This enhanced the detection limit of the PAN analyzer to less than 5 ppt (see Sect. 3.1.1) and leads to PAN mixing ratios which represented average conditions over the 5 min period in contrast to a single point measurement. At the same time, the pre-concentration unit was operated in the saturation mode to reduce the susceptibility to lower flow rate and pressure fluctuation (Moravek et al., 2014). The flow rate through the pre-concentration column was 9 mL min<sup>-1</sup> to optimize the saturation time of the column. A Nafion dryer was used to prevent water condensation in the pre-concentration column. The design and characteristics of the pre-concentration unit is described in further detail elsewhere (Moravek et al., 2014). The O<sub>3</sub> mixing ratio was measured by a UV photometric analyzer (Model 49i, Thermo Fisher Scientific, USA).

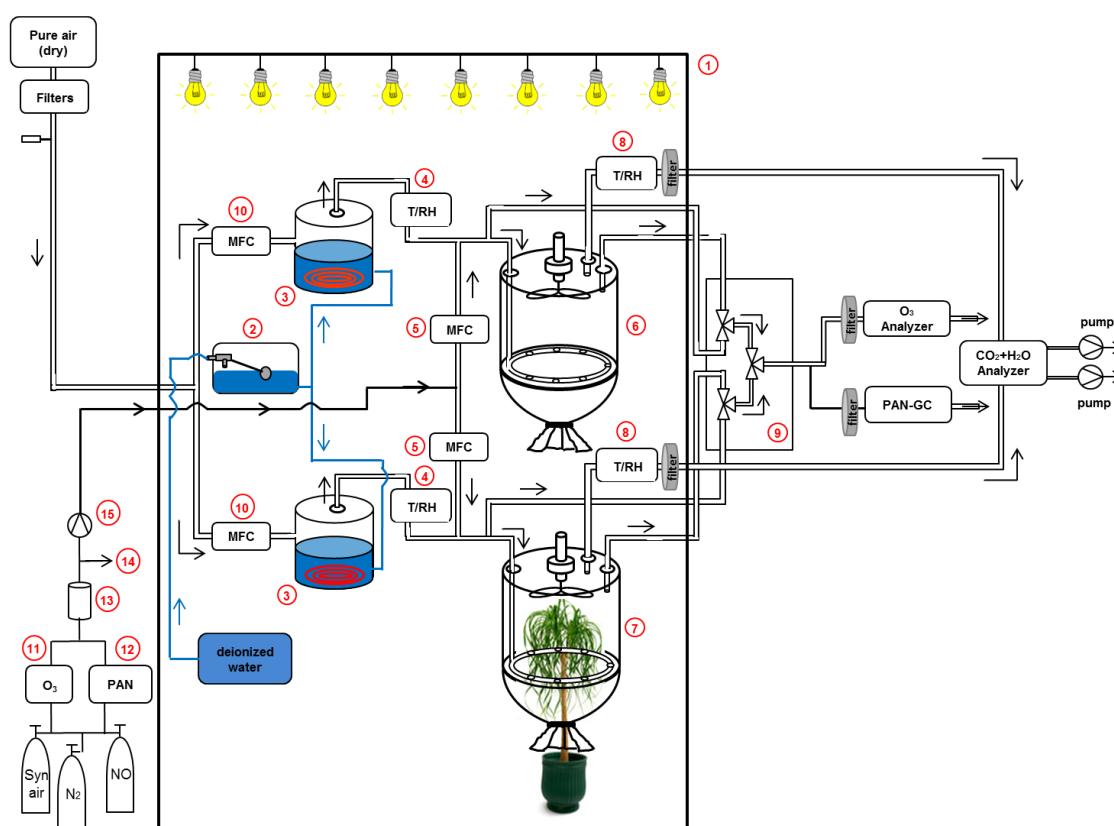


Fig. 1: Flow chart of the dual cuvette system. 1 plant cabinet; 2 water storage tank (see Sect. 2.1.3); 3 ATRAHS (see Sect. 2.1.3); 4 Temperature and relative humidity sensor for humidity regulation (see Sect. 2.1.3); 5 mass flow controller (MFC); 6 dynamic cuvette (reference); 7 dynamic cuvette (sample); 8 Temperature and relative humidity sensor for monitoring; 9 Teflon-valve block; 10 MFC for gas addition; 11 O<sub>3</sub> – primary standard; 12 PAN – calibration unit; 13 mixing vessel; 14 overflow; 15 Teflon membrane pump.

After inserting the plant into the sample cuvette, the relative difference of O<sub>3</sub> and PAN mixing ratios between the sample and the reference cuvette corresponded to O<sub>3</sub> and PAN uptake by

the leaves, respectively. The valve switching between both cuvettes was controlled automatically with an interval of 10 minutes, which matched to the measurement cycle of the PAN GC-ECD. Inlet mixing ratios of both cuvettes were monitored once per hour over the entire experiment. Due to the pressure fluctuation at the moment of the valve switching only the data values between 00:30 min and 09:30 min of each measured position were averaged. The cuvettes were located inside a plant cabinet (VB1014, Vötsch GmbH, Germany) to keep the environmental temperature constant during the experiments (see Sect. 2.2.2). The photosynthetic active radiation (PAR) was measured by a quantum sensor (Model LI-190SA, LiCor Inc., USA). In addition, CO<sub>2</sub> and H<sub>2</sub>O concentrations were measured with an infrared gas analyzer (Li-7000, LiCor Inc., USA) to determine plant photosynthesis and transpiration. The Li-7000 operated in the differential mode to measure the concentration difference of CO<sub>2</sub> and H<sub>2</sub>O between both cuvettes simultaneously

### 2.1.2 Dynamic cuvette

The wall material of the cuvettes was made of FEP foil (Saint Gobain Performance Plastics Corporation, USA) to minimize wall effects for the measured trace gases. All tubing and tubing connections that were in contact with the air flow consisted of PFA-Teflon<sup>®</sup> (Swagelok, USA). A fan (APC Propellers, USA), which had been coated with Teflon<sup>®</sup> by the MPIC mechanical workshop, was installed inside both cuvettes to assure well-mixed conditions in order to reduce the aerodynamic resistance for the trace gas fluxes (Gut et al., 2002). The purified air stream supplied with a certain mixing ratio of O<sub>3</sub> and PAN reached the inner cuvette through the inlet PFA-tube (see Fig. 2). With an additional perforated ring at the bottom of the cuvette the main air stream was divided into several small air streams to improve the distribution of the air addition inside the cuvette. Air samples were withdrawn by the two sampling tubes entering the cuvettes from the top. The surplus of the air stream effused at the vent situated at the bottom of the cuvette (see Fig. 2). To prevent ambient air from entering the cuvette, the flow rates were adjusted such that the cuvettes were slightly over-pressurized. For an accurate performance of the dynamic cuvettes potential deposition of the trace gases on the cuvette walls and the influence of chemical gas phase reactions have to be known and quantified. The deposition rate  $k_{dep,wall}$  represents the amount of molecules which deposit on the foil surface of the cuvette per time and is defined according to Bonn et al. (2013) as Eq. (1):

$$k_{dep,wall} = \ln \left( \frac{vmr_{in,trace\ gas}}{vmr_{out,trace\ gas}} \right) \times \frac{1}{\tau} \quad (1)$$

where  $vmr_{in,trace\ gas}$  is the initial mixing ratio,  $vmr_{out,trace\ gas}$  is the outlet mixing ratio of the trace gas species, respectively, and  $\tau$  the residence time of air in the dynamic cuvette. Under well-mixed conditions,  $\tau$  of air within the dynamic cuvette is determined as the ratio between

the cuvette volume  $V_{cuvette}$  and purging rate  $f_{purg}$ :

$$\tau = \frac{V_{cuvette}}{f_{purg}} \quad (2)$$

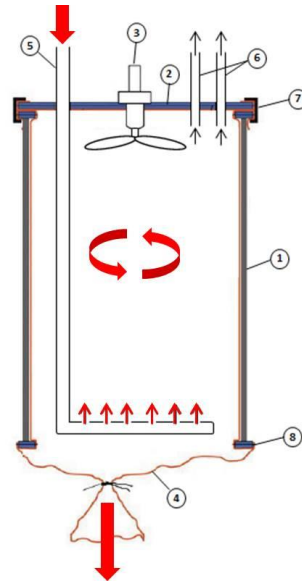


Fig. 2: Layout of the dynamic cuvette as used in this study. 1 PVC frame; 2 acrylic glass cap; 3 fan coated with Teflon; 4 FEP foil; 5 inlet PFA-tube with additional ring; 6 sample tubes; 7 clamps; 8 silicon strip.

The choice of the appropriate residence time in the cuvette is a key factor for the operation of a dynamic cuvette system. On the one hand, it should be short enough to exclude chemical reactions in the cuvette and to follow potential fast changes in the environment. In the case of PAN, the thermal decomposition under higher temperature made it necessary to keep the residence time inside both cuvettes as short as possible. As the lifetime of PAN was about 5 hours at the cuvette temperature of 25 °C (calculated from the rate coefficient suggested by Atkinson et al., (2006)) the thermal decomposition of PAN did not affect the uptake measurements by the leaves. On the other hand, the residence time has to be low enough to receive a sufficient mixing ratio difference caused by the enclosed leaf material that can be resolved by the analytical system. For a dynamic cuvette with well-mixed flow conditions, the residence time is equal to the flushing time as defined in Eq. (2). With a cuvette volume of 70 L and an operating air flow of about 20 L min<sup>-1</sup> for each cuvette the residence time inside the cuvette was 3.4 minutes.

### 2.1.3 Automatic Temperature Regulated Air Humidification System (ATRAHS)

We present an automatic temperature regulated air humidification system (ATRAHS) to control the relative humidity inside the cuvettes. Due to the high operating main flow rate of  $20 \text{ L min}^{-1}$  and the resulting short residence time of the dry air stream inside the humidifier tank for each cuvette, we chose to humidify the main dry air stream directly with the challenge to obtain a high humidification efficiency. ATRAHS consists of two stainless steel tanks (humidifier tank), one for each cuvette, with a tank volume of 1.5 L (see Fig. 3). The tanks were filled with deionized water and heated by a heat element. The dry air stream was purged through the head space of the tank and was thereby humidified due to the high vapor pressure of heated water. An additional tank served as a water reservoir, which was connected to a deionized water supply. The water level in this tank was regulated by a floating valve. Due to the hydrostatic pressure of the water inside the storage tank the humidifier tank was kept on a constant level automatically. With this setup, the humidifier provided an unlimited water reservoir for the humidification procedure at a constant ratio of water level to headspace. Therefore, at a given air flow rate the resulting humidity depended mainly on the water temperature, which was controlled by an electronic control device (V25) developed by the MPIC electronic workshop. The temperature and relative humidity before and inside the cuvettes were determined by two sensors for each dynamic cuvette (Hygromer<sup>®</sup> MP 100 A, Rotronic Messgeräte GmbH, Germany).

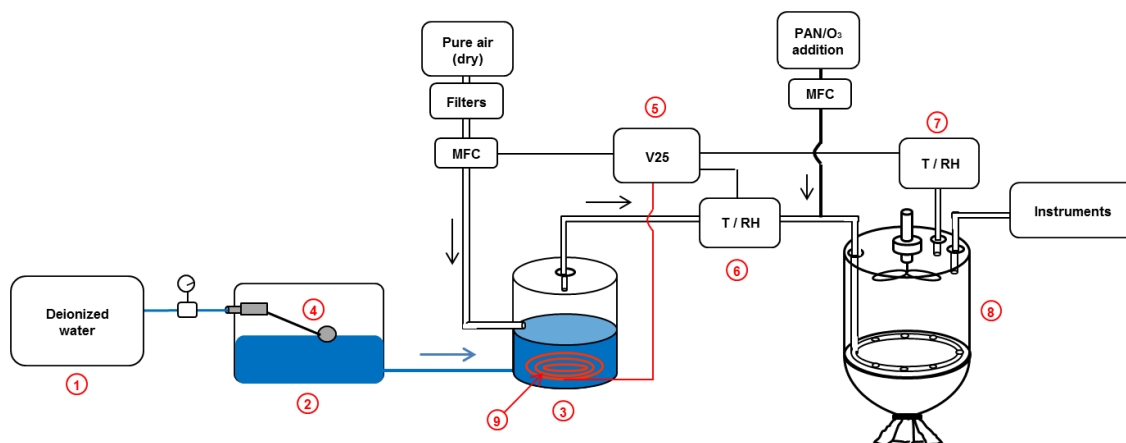


Fig. 3: Flow chart of the automatic temperature regulated air humidification system (ATRAHS). 1 deionized water supply; 2 water storage tank; 3 humidifier tank; 4 float valve; 5 V25 control device; 6 T/RH sensor (initial regulation); 7 T/RH sensor (monitoring); 8 dynamic cuvette; 9 heat element.

A routine was developed to regulate the heating temperature automatically to obtain a constant humidity value inside the cuvettes. The initial humidity of the air stream measured by the humidity sensor in front of the cuvette (see Fig. 3, No. 6) was used for the humidity

regulation with V25. The humidity sensor behind the cuvette (see Fig. 3, No. 7) was needed to monitor the adjusted humidity value inside the cuvette. To avoid prevent the O<sub>3</sub> or PAN from coming into contact with stainless steel and water surface, the gas addition system was installed after the humidifier tank. For testing the humidification system, the relative humidity inside both cuvettes (RH<sub>cuv</sub>) was manipulated in an additional experiment adjusting an initial humidity (RH<sub>in</sub>) level from 50% to 100% for both cuvettes over a time period of 75 hours including light and dark periods (see Sect. 3.1.2).

### 2.1.4 Leaf wetness sensor

The leaf wetness sensors were used to identify and characterize the formation of liquid water films on the leaf surface. The technique is based on the measurement of the electrical resistance of the surface between two electrodes, which are fixed on the leaf with metal clamps (see Fig. 4). The sensor design is based on that published by Burkhardt and Eiden (1994), and has been updated according to suggestions of J. Gerchau (2011, personal communication). Briefly, an oscillator generates an alternating voltage (2 VAC) with an adjustable frequency between 0.5 and 2 kHz. This voltage is applied to the leaf surface, which acts as a resistor in a voltage divider circuit. The resistance of the leaf surface, which is derived directly from the resistive voltage drop, depends on the leaf surface wetness. A major drawback of the old sensor design was the temperature dependence of the signal (e.g., Altimir et al., 2006) caused by changing resistance of the cable between the leaf clamp and the measuring device. This has now been solved by using a miniaturized sensor board measuring the leaf resistance with a voltage divider circuit including a capacitor and a pre-amplifier directly at the clamps of the sensor (see Fig. 4).

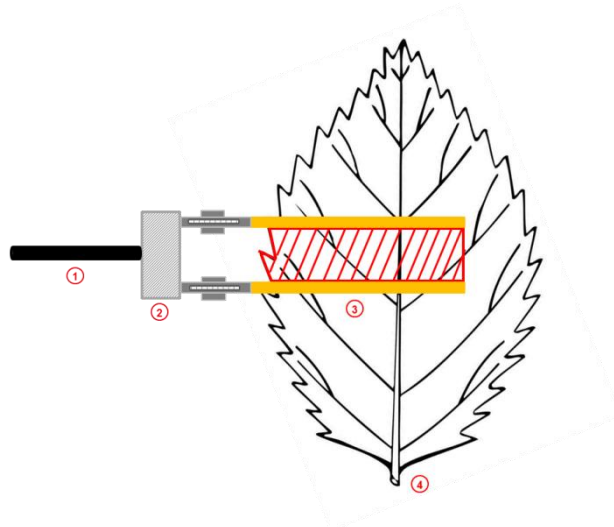


Fig. 4: Draft of the leaf wetness sensor. 1 data cable; 2 sensor; 3 electrode clamps; 4 plant leaf. Modified from Burkhardt and Gerchau (1994).



Additionally, the oscillator can be tuned to four different frequencies from 0.5 to 2 kHz, which allows conductivity measurements also at high ionic strengths (activities), i.e., at low ion mobility. Furthermore, all sensors are now evaluated independently with individual sensor boards as well as individual amplifier and rectifier circuits before A/D conversion in order to avoid interferences between different leaf measurements. In this study, we present measurements of the optimized version of the leaf wetness sensor. For the sample cuvette, three sensors were mounted on plant leaves at different heights to obtain an average value, which was regarded as representative for the entire plant. The background signals were measured by sensors without leaves in the reference cuvette. The net-signals were used to calculate the electrical surface conductance  $G$  in  $\mu\text{S}$ , Eq. (3).

$$G = 1019 \times U^{-1.062} \quad (3)$$

where  $G$  ( $\mu\text{S}$ ) is the electrical surface conductance and  $U$  (mV) is the measured voltage raw signal by the sensor.

## 2.2 Test experiment with $\text{O}_3$ and PAN

A long-term flux measurement was performed over a period of 14 days to demonstrate the quality of the twin-cuvette setup.

### 2.2.1 Plant material and growth conditions

The experiments were performed with 3-year-old tree individuals of *Quercus Ilex* (ordered from Burncoose & South Down Nursery, Gwennap, Redruth, Cornwall, UK), a plant species typical for the Mediterranean region. After delivery, the trees grew up in pots with commercial soil mixture (FloraSelf, Germany) in the institute's own greenhouse under natural growing conditions ( $T_{\text{winter}} = 15 \text{ }^\circ\text{C}$ ,  $T_{\text{summer}} = 30 \text{ }^\circ\text{C}$ ,  $\text{PAR}_{\text{max}} = 1400 \text{ } \mu\text{molm}^{-2}\text{s}^{-1}$ ). The plants were watered daily in the summer period and in the winter period every 3 days. Measurements started after four days of acclimatization of the sample plant inside the cuvette. Measurements were performed with two replicates of the plant species

### 2.2.2 Plant cabinet conditions

The diurnal cycle of the plant was simulated by the plant cabinet system with 13 hours of light and 11 hours of dark period. The light intensity (450 – 650 nm) was kept constant at  $600 \text{ } \mu\text{mol m}^{-2} \text{ s}^{-1}$  for all day light conditions by eight HQI<sup>®</sup>-BT lamps (400 W, OSRAM GmbH, Germany) and six Krypton lamps (100 W, General Electric Company, USA). The cabinet temperature was held constant during the light period at  $T = 28 \pm 0.1 \text{ }^\circ\text{C}$  and at dark period at  $23 \pm 0.1 \text{ }^\circ\text{C}$ .

### 2.2.3 Determination of the leaf area

For a non-destructive determination of the leaf area the shape of every single leaf of the sample plant was drafted by hand and digitalized via a photo scanner (Epson Perfection 3170 Photo). The scans were evaluated by the program “Compu eye, Leaf & Symptom Area” (Bakr, 2005) to obtain the overall leaf area.

### 2.2.4 Application of abscisic acid

Abscisic acid (ABA) is a plant hormone, which affects the closure of the leaf stomata. For the experiments, a branch was cut from the plant under water to prevent embolism. The stock solution of ABA was created by dissolving solid ABA (CAS 14375-45-2, Sigma Aldrich, USA) in 5 mL ethanol and then filling up to 100 mL with deionized water. The nutrient solution was concentrated with 250  $\mu\text{M}$  ABA for the  $\text{O}_3$  experiment and 350  $\mu\text{M}$  for the PAN experiment. For the fumigation of the plant, 60 ppb  $\text{O}_3$  and 310 ppt PAN were used. Additionally, the nutrient solution contained 1 mM of potassium chloride (KCl), 0.1 mM of sodium chloride (NaCl) and 0.1 mM of calcium chloride ( $\text{CaCl}_2$ ) (Chaparro-Suarez et al., 2011). For the ABA experiments, the branch was introduced to the cuvette for 3 days for acclimatization before the measurement started.

### 2.2.5 Calculation of fluxes and plant exchange parameters

As we could assume constant conditions in the cuvettes over the time of 10 min switching intervals, the mixing ratios of all four measured positions (inlet and outlet of both cuvettes) could be used to derive the deposition fluxes of  $\text{O}_3$  and PAN. The fluxes were determined from the differences of trace gas mixing ratios of the reference and sample cuvettes as follows (see e.g. Teklemariam and Sparks, 2004), Eq. (4):

$$F(\text{O}_3, \text{PAN}) = - \frac{f_m \times (\text{vmr}_{\text{out,ref}} - \text{vmr}_{\text{out,sample}})}{A_{\text{leaf}}} \quad (4)$$

where  $F$  is the flux of  $\text{O}_3$  ( $\text{nmol m}^{-2} \text{s}^{-1}$ ) and PAN ( $\text{pmol m}^{-2} \text{s}^{-1}$ ), respectively.  $f_m$  ( $\text{mol s}^{-1}$ ) is the mole flow rate through each cuvette, which is calculated from the volume flow rate  $f_v$  ( $\text{L s}^{-1}$ ) divided by 24.4  $\text{L mol}^{-1}$  (at 25 °C and 1013,25 hpa), i.e. the volume of one mole in air at standard conditions, which can be used as the conditions in the set cabinet were close to standard conditions (see Sect. 2.2.2).  $A_{\text{leaf}}$  ( $\text{m}^2$ ) is the leaf area of the entire plant inside the sample cuvette.  $\text{vmr}_{\text{out,ref}} - \text{vmr}_{\text{out,sample}}$  is the difference of the trace gas mixing ratio between the reference and sample cuvette. The same equation was used to calculate the water flux  $E$  ( $\text{mmol m}^{-2} \text{s}^{-1}$ ) with the mixing ratio difference of the water vapor between both cuvettes.

The deposition velocity  $V_d$  ( $\text{mm s}^{-1}$ ) of  $\text{O}_3$  and PAN was calculated following Eq. (5):

$$V_d(O_3, PAN) = \frac{F(O_3, PAN)}{vmr_{out, sample}} \times V_m \quad (5)$$

where  $V_m$  is the molar volume of 22,4 L mol<sup>-1</sup> at 25 °C.

The stomatal conductance is an important parameter to evaluate the gaseous uptake from the ambient air into the plant leaves. The stomatal conductance of water vapor  $g_{s, calc}(H_2O)$  (mmol m<sup>-2</sup> s<sup>-1</sup>), Eq. (6) was determined from the ratio between the water flux  $E$  (mmol m<sup>-2</sup> s<sup>-1</sup>) and the Air-to-Leaf-Vapor-Pressure-Deficit  $VPD$  (Pa kPa<sup>-1</sup>):

$$g_{s, calc}(H_2O) = \frac{E}{VPD} \quad (6)$$

where  $VPD$  is given according to von Ceammerer and Farquhar (1981) as Eq. (7):

$$VPD = \frac{SVP(T_{leaf})}{P_{sample}} - C_{out, sample}(H_2O) \quad (7)$$

The saturation water vapor pressure  $SVP$  (hPa) was calculated with the Goff-Gratch equation (Goff and Gratch, 1946), which is dependent on the leaf temperature  $T_{leaf}$ .  $P_{sample}$  (kPa) is the pressure in the sample cuvette and  $C_{out, sample}(H_2O)$  (Pa kPa<sup>-1</sup>) is the concentration of water vapor inside the sample cuvette. The stomatal conductances of O<sub>3</sub> and PAN were determined following Eq. (8) from the stomatal conductance to water vapor multiplied by the ratio of the diffusion coefficients of the respective trace gas (O<sub>3</sub>, PAN) and H<sub>2</sub>O:

$$g_{s, calc}(O_3, PAN) = g_{s, calc}(H_2O) * \frac{D_{O_3, PAN}}{D_{H_2O}} \quad (8)$$

The diffusion coefficients of O<sub>3</sub>, PAN and H<sub>2</sub>O are  $D_{O_3} = 0,137$  cm<sup>2</sup> s<sup>-1</sup> (Laisk et al., 1989),  $D_{PAN} = 0,089$  cm<sup>2</sup> s<sup>-1</sup> (Sparks et al., 2003) and  $D_{H_2O} = 0,25$  cm<sup>2</sup> s<sup>-1</sup> (Marrero and Mason, 1972), respectively.

The leaf internal O<sub>3</sub> and PAN mixing ratios were determined according to Teklemariam and Sparks (2004) by following equation Eq. (9):

$$vmr_{int, leaf} = vmr_{out, sample} - \left( \frac{F(O_3, PAN)}{g_{s, calc}(O_3, PAN)} \right) \quad (9)$$

Measured leaf conductance  $g_{s, meas}$  (mmol m<sup>-2</sup> s<sup>-1</sup>) to O<sub>3</sub> and PAN was calculated according to the equation scheme of Teklemariam and Sparks (2004), Eq. (10):

$$g_{s, meas}(O_3, PAN) = \frac{F(O_3, PAN)}{vmr_{out, sample} - vmr_{int, leaf}} \quad (10)$$

For O<sub>3</sub> and PAN,  $vmr_{int, leaf}$  is assumed to be closed to zero (Laisk et al. 1989).

## 2.3 System characterization and quality assurance

### 2.3.1 Evaluation of the twin-cuvette system and O<sub>3</sub> and PAN loss

As mentioned above, the advantage of a twin-cuvette setup was to account for disturbing background effects such as wall deposition, assuming that these effects were equal for both cuvettes. In order to check the accuracy and stability, the mixing ratio measurements of O<sub>3</sub> and PAN were compared when both cuvettes were empty. Inside an empty cuvette, the inner mixing ratio was defined as difference between the inlet and outlet of the cuvette, Eq. (11) and Eq. (12):

$$vmr_{ref,diff} = vmr_{ref,in} - vmr_{ref,out} \quad (11)$$

$$vmr_{sample,diff} = vmr_{sample,in} - vmr_{sample,out} \quad (12)$$

The mixing ratio difference between both cuvettes was defined as follows, Eq. (13):

$$vmr_{diff} = vmr_{sample,diff} - vmr_{ref,diff} \quad (13)$$

By combination of Eqs. (11) – (13) we received Eq. (14):

$$vmr_{diff} = vmr_{ref,out} - vmr_{sample,out} + vmr_{sample,in} - vmr_{ref,in} \quad (14)$$

Given that the inlet mixing ratios between both cuvettes are identical ( $vmr_{diff,in} = vmr_{sample,in} - vmr_{ref,in} = 0$ ), the mixing ratio difference between both cuvettes could be simplified as Eq. (15):

$$vmr_{diff,out} = vmr_{ref,out} - vmr_{sample,out} \quad (15)$$

The described evaluation experiment was conducted over 8 hours at which the inlet O<sub>3</sub> and PAN mixing ratios were held constant at 59.5 ppb and 324 ppt, respectively.

In addition to accounting for effects in the cuvettes, the O<sub>3</sub> and PAN mixing ratios were determined systematically with and without the cuvettes as well as at different positions of the setup to quantify the losses of both gas species on the material surface as tubes, addition pump, cuvette foil and valve block.

### 2.3.2 Calibration procedure

Calibration of the O<sub>3</sub> analyzer and PAN GC-ECD were performed at all inlet and outlet positions of the dual cuvette system using multiple O<sub>3</sub> and PAN mixing ratios (9, 18, 37, 74, 86 ppb and 195, 380, 656, 896 ppt, respectively) (see Fig. 7). The O<sub>3</sub> analyzer was calibrated with a GPT (Gas-Phase-Titration calibrator, Sonimix 6000C2, LN Industries, Switzerland) in combination with a NO<sub>x</sub> analyzer (49i, Thermo Fisher Scientific, USA). A NO standard gas

$10 \pm 0.33$  ppm was used to calibrate the  $\text{NO}_x$  analyzer. The determination of the set  $\text{O}_3$  mixing ratio occurred from the titration of the diluent  $\text{NO}$  mixing ratio by a certain  $\text{O}_3$  level produced with an internal UV lamp of the GPT. The calibration of the PAN GC-ECD was performed via a PAN calibration unit. A mixture of  $\text{NO}$  standard gas ( $2 \pm 0.04$  ppm) and synthetic air stream is enriched with acetone in a permeation cell. PAN is then produced by photolysis of acetone an internal UV lamp in presence of  $\text{NO}$  and  $\text{O}_2$  (Patz et al., 2002). The detection limit (LOD) of the  $\text{O}_3$  analyzer and PAN GC-ECD was determined as  $3\sigma$  of the zero noise level. As the ECD showed a temperature dependency, the entire PAN GC-ECD was placed inside an additional climate cabinet to keep the ambient temperature constant at  $23^\circ\text{C}$ .

### 2.3.3 Random flux error calculation and statistical significance

The precision of the  $\text{O}_3$  analyzer and the GC-ECD was determined by supplying constant initial  $\text{O}_3$  and PAN mixing ratios (59.5 ppb and 324 ppt) and measuring them consecutively at both the inlet and outlet positions of both dynamic cuvettes for eight hours. Determining the precision via the inlet and outlet positions instead of just determining the precision of the gas analyzers itself, ensured to obtain precision values which are representative for the actual measurements of mixing ratio differences required for the flux calculation. The relative precision at each position was determined in Eq. (16) by the standard deviation ( $1\sigma$ ) divided by the mean value.

$$\text{precision} [\%] = \frac{\text{standard deviation} (vmr_{\text{O}_3, \text{PAN}})}{\text{mean value} (vmr_{\text{O}_3, \text{PAN}})} * 100 \quad (16)$$

The random errors of  $F$ ,  $g_{s, calc}$ ,  $g_{s, meas}$  and  $V_d$  were calculated using general representation of the Gaussian error propagation (Bevington and Robinson, 2003), Eq. (17):

$$u(x_{i,j}) = \sqrt{\sum_{i=1}^n \left(\frac{\partial u}{\partial x_i}\right)^2 * (\Delta x_i)^2 + \sum_{i=1}^n \sum_{j=1}^n \left(\left(\frac{\partial u}{\partial x_i}\right) \left(\frac{\partial u}{\partial x_j}\right) \Delta x_i \Delta x_j r(x_i, x_j)\right)}, i \neq j \quad (17)$$

$\Delta u$  is the random error of the respective parameter (i.e.  $F$ ,  $g_s$  and  $V_d$ ), which can be expressed as a function of  $n$  individual quantities ( $x_{i,j}$ ).  $\partial u / \partial x_{i,j}$  are the partial derivatives of the function.  $\Delta x_i$  and  $\Delta x_j$  are the random error of the error-prone variables.  $r(\Delta x_i, \Delta x_j)$  is the correlation coefficient between two dependent variables  $x_i$  and  $x_j$ . In the case that the variables are uncorrelated, the term  $\Delta x_i \Delta x_j r(x_i, x_j)$  is zero.

The significance of the mixing ratio difference between each sampling position of the reference and sample cuvette was proved with an independent two-sample-t-test, using a  $\alpha$ -significance level of 0.05. The Pearson correlation coefficient  $R_{pearson}$  with 95 % confidence interval was calculated with the statistic software described in Mudelsee (2003).

## 3 Results

### 3.1 Performance of the twin-cuvette system

#### 3.1.1 Quality of O<sub>3</sub> and PAN measurements

##### Comparison between the empty sample and reference cuvettes

The comparison of both empty cuvettes (see Sect. 2.3.1) showed only insignificant differences (i.e.  $p > 0.05$  in the t-test) in O<sub>3</sub>, PAN and CO<sub>2</sub> mixing ratio between both inlet and outlet sampling positions of the cuvettes. As mentioned in Sect. 2.3.1, the O<sub>3</sub> and PAN initial mixing ratios were held constant with 59.4 ppb in O<sub>3</sub> and 324 ppt in PAN over a time period of 8 hours (see Fig. 5). For O<sub>3</sub>  $vmr_{diff,in}$  was  $0.05 \pm 0.35$  ppb and  $vmr_{diff,out}$  was  $0.01 \pm 0.33$  ppb. For PAN  $vmr_{diff,in}$  was  $1.29 \pm 7.16$  ppt and  $vmr_{diff,out}$  was  $0.68 \pm 9.35$  ppt (see Table 2).

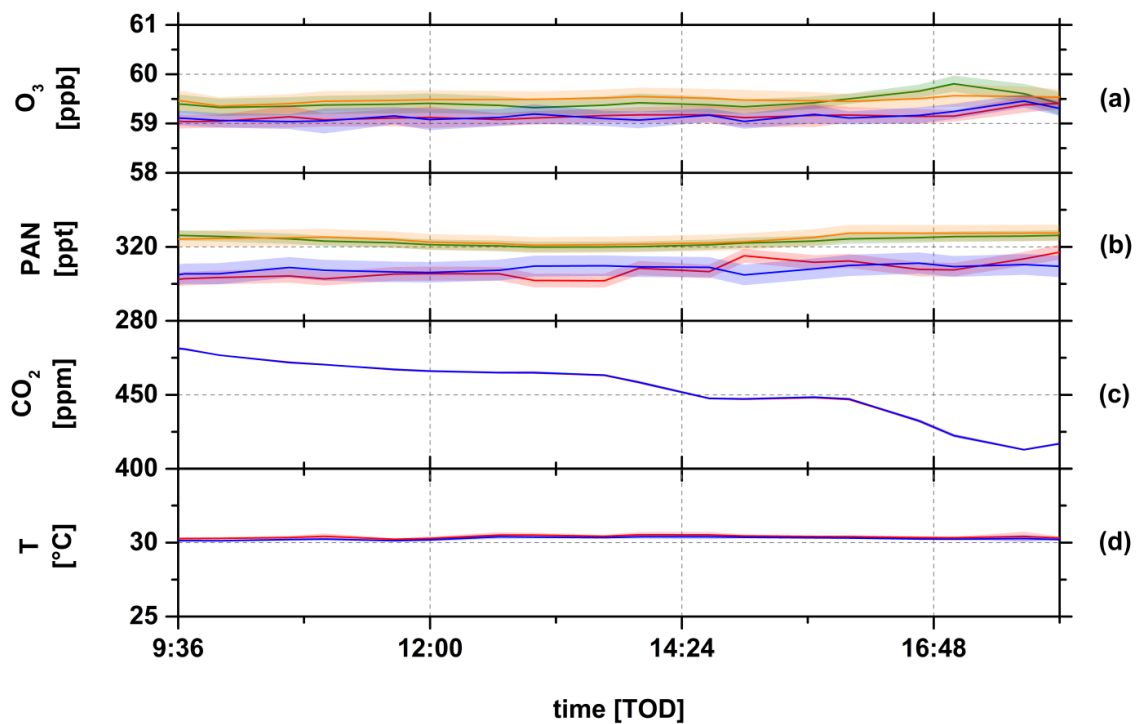


Fig. 5: Comparison of the all key parameters between both empty cuvettes to indicate their identity. a) O<sub>3</sub> mixing ratio, b) PAN mixing ratio, c) CO<sub>2</sub> mixing ratio, — inlet position of the reference cuvette, — inlet position of the sample cuvette, — outlet position of the reference cuvette, — outlet position of the sample cuvette, d) cuvette inner temperature, reference cuvette (red) and sample cuvette (blue). The colored area represents the uncertainty of the calculated mean values over an average time period of 10 min.

Table 2: minimal resolvable mixing ratio difference of O<sub>3</sub> and PAN between both cuvettes.

<b>Sampling positions</b>	<b><math>vmr_{diff,O_3}</math> (ppb)</b>	<b><math>vmr_{diff,PAN}</math> (ppt)</b>
Inlet	0.05 ± 0.35	1.29 ± 7.16
Outlet	0.01 ± 0.33	0.68 ± 9.35

Over the duration of the experiment, the CO<sub>2</sub> mixing ratio declined steadily from 480 to 400 ppm, which was due to the fact that ambient CO<sub>2</sub> was not retained by the air purification. The magnitude of the variation in the CO<sub>2</sub> mixing ratio is considered as not large enough to have a significant effect on the plant metabolism and thus on the uptake of O<sub>3</sub> and PAN. Temperature differences between the cuvettes were also insignificant, although the temperature in the climate cabinet was 5 K less during dark than during light periods (data not shown).

### Precision and detection limit (LOD) of the cuvette system

Table 3: Detection limit (LOD) and precision of the twin-cuvette system at different sampling positions. The determination of the LOD is based on 3 $\sigma$  of the blank value.

<b>Trace gas</b>	<b>Sampling position</b>	<b>LOD (3<math>\sigma</math>)</b>	<b>adjusted mixing ratio</b>	<b>Precision (%)</b>
O <sub>3</sub>	Inlet sample	0.8 ppb	59.4 ppb	0.3
	Inlet reference	0.9 ppb	59.4 ppb	0.3
	Outlet sample	0.9 ppb	58.8 ppb	0.3
	Outlet reference	0.9 ppb	58.8 ppb	0.3
PAN	Inlet sample	1 ppt	324.4 ppt	1.4
	Inlet reference	1 ppt	323.1 ppt	1.1
	Outlet sample	1.2 ppt	307.6 ppt	1.8
	Outlet reference	1.3 ppt	306.6 ppt	1.2

To include the potential influence of cuvette system on the LOD and the precision of the O<sub>3</sub>

and PAN measurements, the calibrations were also performed at different sampling positions of the cuvette system (Table 3). The calibration curves of both analyzers were linear with a slope of  $3.3 \cdot 10^{-2}$  ( $R^2 = 0.99$ ) for the ozone analyzer and 164.2 ( $R^2 = 0.99$ ) for the PAN GC-ECD (see Fig. 7). While a small loss of  $O_3$  and PAN can be observed in the experiments (see Sect. 3.1.3 for detailed analysis of potential losses within the cuvette system), the LOD ranged for  $O_3$  between 0.8 and 0.9 ppb and for PAN between 1 and 1.3 ppt. The precision for  $O_3$  was 0.3 % and for PAN between 1.4 and 1.8 %.

### 3.1.2 Quality of the humidity regulation with ATRAHS

The initial humidity ( $RH_{in}$ ) controlled by ATRAHS was very constant. When increasing the set humidity value gradually from 50% to 90%, the relative humidity became constant within several minutes after each change (see Fig. 6).  $RH_{cuv}$  was 9 % lower than  $RH_{in}$  during the dark period and 12 % lower during the light period, which is caused by the addition of dry air from the  $O_3$  and PAN addition downstream of the  $RH_{in}$  humidity probe. The difference of 3 %  $RH_{cuv}$  between light and dark period was caused to the inner cuvette temperature, which is 3 °C higher than the environmental temperature of the plant cabinet during the light period. In the dark period, both inner temperatures were the same. There was no significant difference of  $RH_{cuv}$  observed between both cuvettes up to a value of 70 % in the light and 80% in the dark period. Above those values,  $RH_{cuv}$  fluctuated strongly, which could be the cause of water condensation inside the cuvettes. The condensation at 80 %  $RH_{cuv}$  did not occur during the dark period, presumably as the temperature difference between the cuvettes and the plant cabinet environment was close to zero, which also explains the adjusting of higher  $RH_{cuv}$  values up to 90 % in the dark period. Furthermore, the heating temperature ( $T_{heater}$ ) of both humidifiers was higher during the light periods, caused by its regulation, which vaporized more water to compensate for the lower relative humidity. Beyond 90%  $RH_{in}$  in the light, the heating temperature began to decrease continuously, which was as a result of decreasing water demand due to the water condensation.

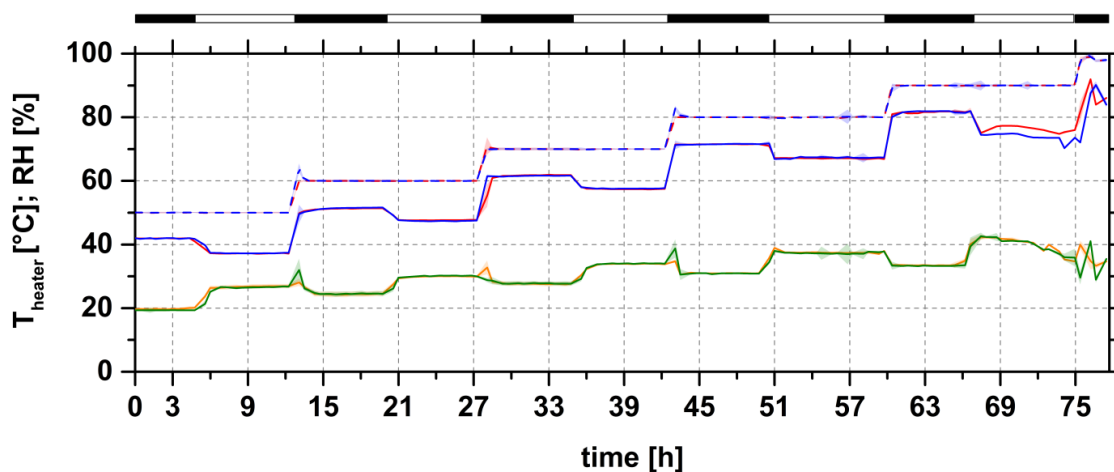




Fig. 6: Relative humidity controlled by ATRAHS at different levels from 50% to 100%. —  $RH_{\text{cuv}}$  of the reference cuvette, —  $RH_{\text{cuv}}$  of the sample cuvette, ---  $RH_{\text{in}}$  of the reference cuvette, ---  $RH_{\text{in}}$  of the sample cuvette, —  $T_{\text{heater}}$  of the reference humidifier, —  $T_{\text{heater}}$  of the sample humidifier. The diurnal cycle of light was simulated by a climate cabinet with 6 hours light period (white balk) and 6 hours dark period (black balk).

### 3.1.3 Loss of $O_3$ and PAN within the system

For both,  $O_3$  and PAN, the calibrations with inclusion of the total setup performed by sampling at different positions of the cuvette setup exhibited a weaker slope than calibrating the analyzers without setup. This indicates a loss of  $O_3$  and PAN inside the setup, caused by tubing, connectors, MFCs, valves, pumps and the cuvette itself (see Fig. 7).

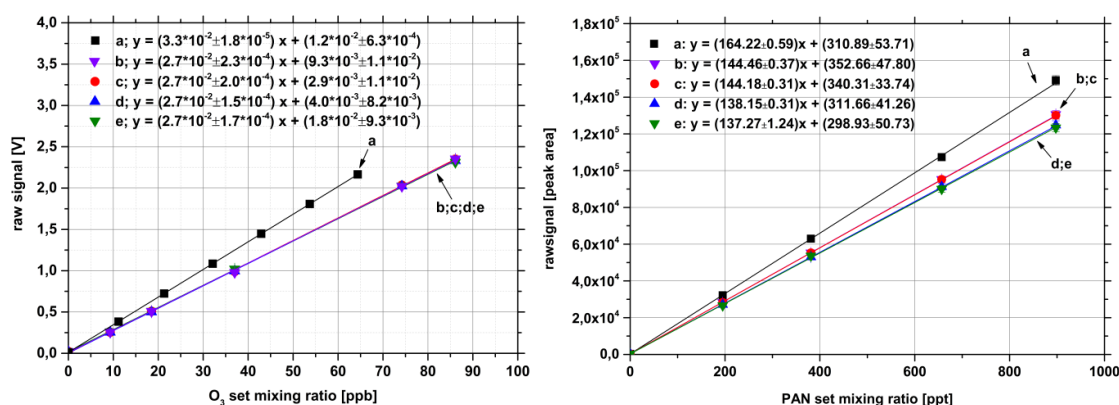


Fig. 7: Multipoint calibration curve of  $O_3$  (left) and PAN (right) at different sampling positions: a without setup, b inlet of the sample cuvette, c inlet of the reference cuvette, d outlet of the sample cuvette, e outlet of the reference cuvette. The linear fit equations are given with the error of slope and offset.

The overall loss measured at the different sampling positions was 18.2 % in  $O_3$  and 16.3 % in PAN mixing ratios. For  $O_3$ , the difference between the inlet and outlet positions was not significant, indicating the major  $O_3$  loss not to be caused by the cuvettes themselves. For PAN, a 5% difference between the cuvette inlet and outlet was found, which is most likely associated with deposition of PAN to the foil surface (see also Sect. 3.1.1, Fig. 5). The  $O_3$  and PAN losses were nearly identical for both the sample and reference cuvettes, confirming the identical behavior of the twin-cuvette system. To determine the loss of  $O_3$  and PAN, which was not attributed to the cuvettes, the  $O_3$  and PAN mixing ratios were measured downstream of the Teflon membrane pump, the MFCs, the cuvettes and the Teflon valves (listed in order of appearance in the flow path, see Fig. 1). As shown in Fig. 8, different slopes of the calibration curves were observed depending on the sampling location, indicating an increase of the  $O_3$  and PAN losses in some parts of the cuvette/piping system.

For example, a loss of  $O_3$  of 6 % and a loss of PAN of 9.5 % was induced by the Teflon pump. As the air inside the Teflon pump heated up to 50 °C, thermal decomposition of PAN could have contributed to the higher loss of PAN. However, as the lifetime of PAN was about 10 min for these conditions and the residence time of the gas stream inside the Teflon pump tube was calculated as  $3.5 \cdot 10^{-2}$  s, a significant contribution of thermal decomposition to the PAN loss at the Teflon pump can be excluded. For  $O_3$ , the highest loss of 9.7 % occurred while the gas stream passed through the MFCs. This  $O_3$  loss is most likely caused by the reaction of  $O_3$  with the inner surface of the MFC, which was made of stainless steel. Furthermore, the MFCs had an operational temperature of nearly 30°C, which could promote the loss process. The  $O_3$  loss between the inlet position and outlet of the dynamic cuvette including the Teflon valve block system was less reaching 3.5 %. For PAN the loss within the cuvette was only slightly higher than for  $O_3$  reaching 5 %.

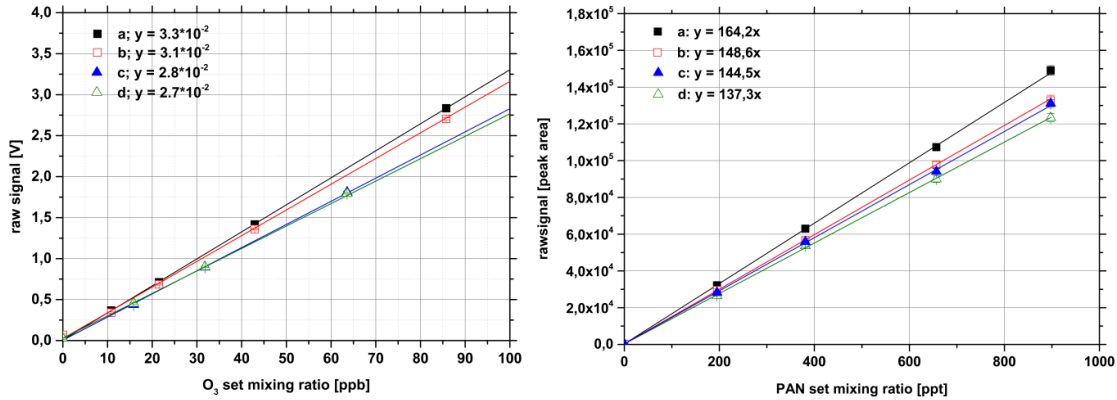


Fig. 8: Systematical determination of the  $O_3$  and PAN loss at different locations of the cuvette setup. a analyzer directly connect with calibration unit without setup, b including teflon pump, c including MFCs for gas addition, d including cuvettes and valve block system

Table 4: Wall deposition rate of  $O_3$  and PAN within the dynamic cuvettes

Dynamic cuvettes	$k_{dep,wall}PAN$ ( $s^{-1}$ )	$k_{dep,wall}O_3$ ( $s^{-1}$ )
Reference	$(2.55 \pm 0.78) \cdot 10^{-4}$	$(2.78 \pm 0.63) \cdot 10^{-5}$
Sample	$(2.54 \pm 0.44) \cdot 10^{-4}$	$(2.76 \pm 0.64) \cdot 10^{-5}$

The wall deposition rate  $k_{dep,wall}$  for PAN was found to range around  $(2.55 \pm 0.78) \cdot 10^{-4} s^{-1}$  in the reference cuvette and  $(2.54 \pm 0.44) \cdot 10^{-4} s^{-1}$  in the sample cuvette (Table 4). In case of  $O_3$ ,  $k_{dep,wall}$  was  $(2.78 \pm 0.63) \cdot 10^{-5} s^{-1}$  in the reference cuvette and  $(2.76 \pm 0.64) \cdot 10^{-5} s^{-1}$  in the

sample cuvette (data for the calculation of  $k_{dep,wall}$  see Fig. 5). The finding that the wall deposition rates for both gases were not significantly different comparing both cuvettes was supporting the use of a twin-cuvette system with an identical construction. The fact that  $k_{dep,wall,PAN}$  exceeded  $k_{dep,wall,O_3}$  by 1 order of magnitude shows the significantly higher wall deposition of PAN than  $O_3$ . Due to the short residence time of 3.4 minutes and a life time of PAN inside the cuvette of 5 hours (see Sect. 2.1.2) thermal decomposition of PAN could be excluded as a reason for the higher deposition of PAN.

## 3.2 Flux measurements under laboratory conditions

### 3.2.1 Test run and flux rates

The twin-cuvette system could be successfully adapted to the needs of the plants and the experimental conditions needed. Measurements were performed under a light/dark cycle with a maximum of  $480 \mu\text{mol photons m}^{-2} \text{s}^{-1}$  in the light period (see Fig. 9a). Leaf temperature ( $T_{\text{leaf}}$ ) rose to  $27 \text{ }^\circ\text{C}$  in the light period and decreased in the dark period to  $22 \text{ }^\circ\text{C}$  (see Fig. 9b). The relative humidity in the reference cuvette represented the background value with a minimum of 22 % during the dark periods and a maximum of 37 % at light periods (see Fig. 9c). The relative humidity in the sample cuvette was significantly enhanced by the transpiration of the plant. During the dark periods the relative humidity of the sample cuvette was 38 %, a similar value as compared to the reference cuvette when the leaf stomata were closed and plant transpiration was inhibited. During the light periods, the humidity level inside the sample cuvette reached 47 %. The water transpiration and  $\text{CO}_2$  exchange of the plant showed a typical behavior related to the light and dark periods. The  $\text{CO}_2$  flux had a minimum of  $-3 \mu\text{mol m}^{-2} \text{s}^{-1}$  and a maximum of  $0.8 \mu\text{mol m}^{-2} \text{s}^{-1}$ , which represents a  $\text{CO}_2$  uptake under light and an emission under dark conditions (see Fig. 9d). The water flux showed a maximum of  $0.9 \text{ mmol m}^{-2} \text{s}^{-1}$  during light periods. At dark periods it was close to zero (see Fig. 9e). There was a slight decreasing trend of water flux over the measurement period, while after 10 days the water flux seemed to become constant. As expected, the stomatal conductance to water vapor  $g_{s,calc}(H_2O)$  followed the same trend as the water flux (see also Fig. 9e). The mixing ratio of  $O_3$  in the reference cuvette was constant at  $55.8 \pm 0.2$  ppb (see Fig. 9f). In the sample cuvette the  $O_3$  mixing ratio followed the plant diurnal cycle with a minimum of 32 ppb during the light period and a maximum of 55 ppb during the dark period, which was close to the reference value as the leaf stomata were closed due to the absence of light.

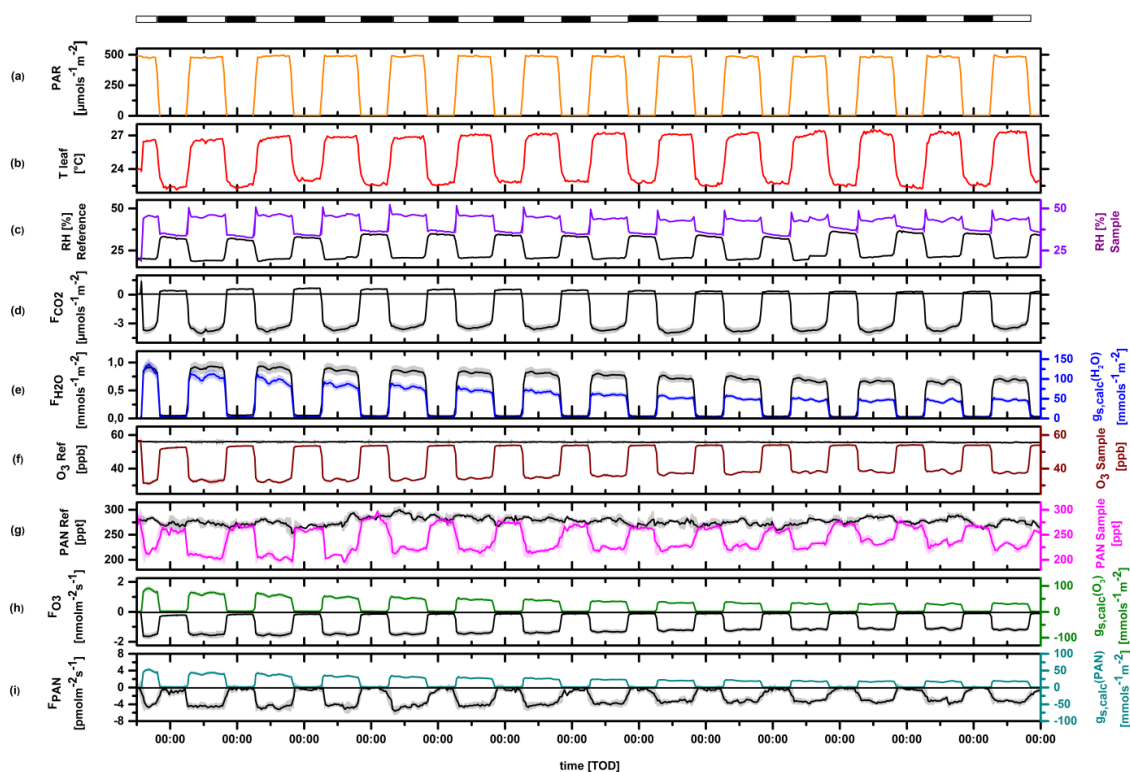


Fig. 9: Long-term flux measurement of *Quercus Ilex* at constant initial mixing ratio ( $O_3 = 57$  ppb, PAN = 280 ppt) over 14 days. a) light density, b) leaf temperature, c) relative humidity of the reference (black) and sample (violet) cuvette, d)  $CO_2$  exchange flux, e) transpiration rate (black) and stomatal conductance to water vapor (blue), f)  $O_3$  mixing ratio of the reference cuvette (black) and sample cuvette (brown), g) PAN mixing ratio of the reference cuvette (black) and sample cuvette (magenta), h)  $O_3$  exchange flux (black) and  $O_3$  conductance (green), i) PAN exchange flux (black) and PAN conductance (dark cyan). The diurnal cycle of light was simulated by a climate cabinet with 13 hours light period (white balk) and 11 hours dark period (black balk). The inner area of the cabinet had a temperature of 25 °C and relative humidity of 50%.

The PAN mixing ratio in the reference cuvette was on average  $277 \pm 5$  ppt during the measurement (see Fig. 9g). The mixing ratio in the sample cuvette followed the plant diurnal cycle similarly as  $O_3$  with a minimum of 200 ppt during light periods and 280 ppt during dark periods. The latter value is close to the reference PAN mixing ratio considering the precision of the PAN measurements (Table 3). The larger scatter in the results for PAN compared to  $O_3$  are explained by the lower temporal resolution of the trace gas analysis. The  $O_3$  and PAN exchange fluxes showed a clear diurnal trend with a maximum of  $-1.6 \text{ nmol m}^{-2} \text{ s}^{-1}$  in  $O_3$  and  $-4 \text{ pmol m}^{-2} \text{ s}^{-1}$  in PAN under light conditions (see Fig. 9h and Fig. 9i, respectively). During dark periods, the minimum exchange flux for both species was close to zero, clearly indicating the role of stomatal control. Additionally, it should be noted that the fluxes during light conditions followed the same decreasing trend as the water flux and stomatal conductance for water vapor in the first 10 days of the experiment. During the light period, the calculated deposition velocity of  $O_3$  (see Sect. 2.2.5) ranged from 0.66 to 1.06  $\text{mm s}^{-1}$  and

for PAN from 0.32 to 0.48 mm s<sup>-1</sup>. During the dark period, the deposition velocity was 0.05 mm s<sup>-1</sup> for O<sub>3</sub> and close to 0 mm s<sup>-1</sup> for PAN at < 50 % RH. The ratio of the deposition velocity between O<sub>3</sub> and PAN was 0.45 ± 0.04 (Table 5). Compared with the only two existing literature values of previous studies, which were performed in the early 70s (Hill, 1971, Garland and Penkett, 1976), our deposition velocity ratio was close to Garland and Penkett (1976).

Table 5: Comparison of the deposition velocity ratio of O<sub>3</sub> and PAN in previous studies.

Location	Method	Plant species	V <sub>d</sub> (PAN) / V <sub>d</sub> (O <sub>3</sub> )	Reference
	Climate chamber	<i>Medicago sativa</i>	0.37	Hill (1971)
Laboratory	Wind tunnel setup	<i>Grass</i>	0.42	Garland and Penkett (1976)
	Twin-cuvette system	<i>Quercus ilex</i>	0.45 ± 0.04	This study

### 3.2.2 Correlation between ambient mixing ratio and uptake of O<sub>3</sub> and PAN

A clear linear relationship was found between the O<sub>3</sub> (R<sub>pearson</sub> = 0.98; CI<sub>95%</sub> = 0.01) and PAN (R<sub>pearson</sub> = 0.97; CI<sub>95%</sub> = 0.08) uptake by the leaf and the respective ambient mixing ratios (see Fig. 10). By increasing the ambient mixing ratio of O<sub>3</sub> from 32 ppb to 105 ppb the exchange flux rose from 2 to 6 nmol m<sup>-2</sup> s<sup>-1</sup>. In case of PAN the increase of the ambient mixing ratio from 100 to 350 ppt resulted in an increase of the PAN exchange flux from 2 to 10 pmol m<sup>-2</sup> s<sup>-1</sup>. The ratio of the exchange fluxes of O<sub>3</sub> and PAN stayed constant at 0.48 ± 0.05 as derived from the ratio of the slopes. However, the observed deposition fluxes were about 50 % larger for similar O<sub>3</sub> and PAN mixing ratios as compared to the results shown in Fig. 9, which can be understood as a seasonal effect as the flux values shown in Fig. 10. This experiment was performed in June, instead of October of the same year.

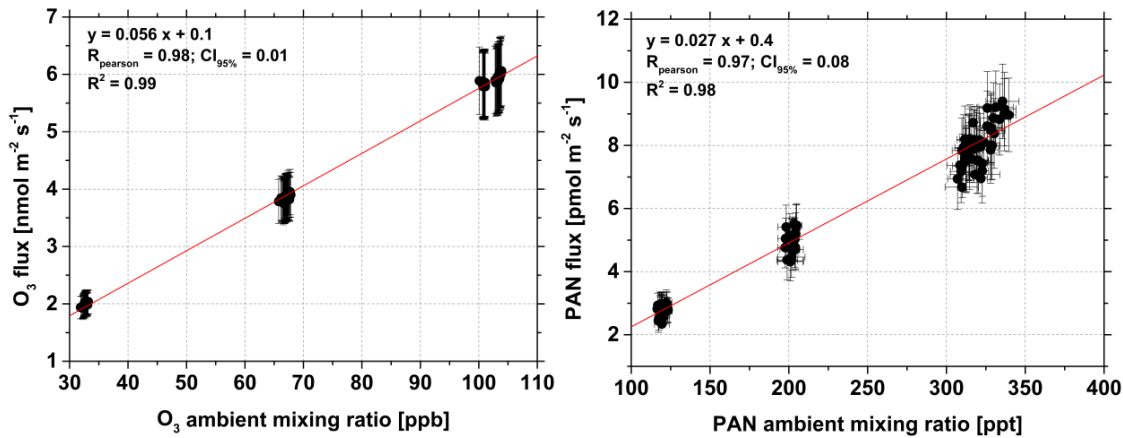


Fig. 11: Behavior of  $O_3$  and PAN flux with rising ambient mixing ratio. Both experiments were performed separately.

### 3.2.3 Application of abscisic acid (ABA)

The ABA nutrient solution ( $c = 250\mu\text{M}$ ) was added to the plant sample after 3 days of acclimatization. After adding the ABA, the measured  $O_3$  mixing ratio in the sample cuvette rose from 72 ppb to 87 ppb within a few hours (see Fig. 11a), which lead to a decrease of the  $O_3$  deposition from  $-4.2 \text{ nmol m}^{-2} \text{ s}^{-1}$  to  $-0.4 \text{ nmol m}^{-2} \text{ s}^{-1}$  (see Fig. 11b) and a decrease of the stomatal conductance for  $O_3$  from  $63 \text{ mmol m}^{-2} \text{ s}^{-1}$  to  $5.5 \text{ mmol m}^{-2} \text{ s}^{-1}$  (see Fig. 11c). In the following light period the  $O_3$  mixing ratio as well as the  $O_3$  flux persisted with the uncertainty at the same value as the reference. The stomatal conductance of  $O_3$  was close to zero, which indicates an inhibition of the stomatal activity. After removing the ABA nutrient solution the  $O_3$  mixing ratio in the sample cuvette decreased from 90 ppb to 82.5 ppb within several days. At the same time, the  $O_3$  flux increased from  $-0.4 \text{ nmol m}^{-2} \text{ s}^{-1}$  to  $-1.8 \text{ nmol m}^{-2} \text{ s}^{-1}$ , which was 42.8 % of the flux value before the plant was treated with ABA. The stomatal conductance to  $O_3$  increased from  $2.2 \text{ mmol m}^{-2} \text{ s}^{-1}$  to  $23 \text{ mmol m}^{-2} \text{ s}^{-1}$ .

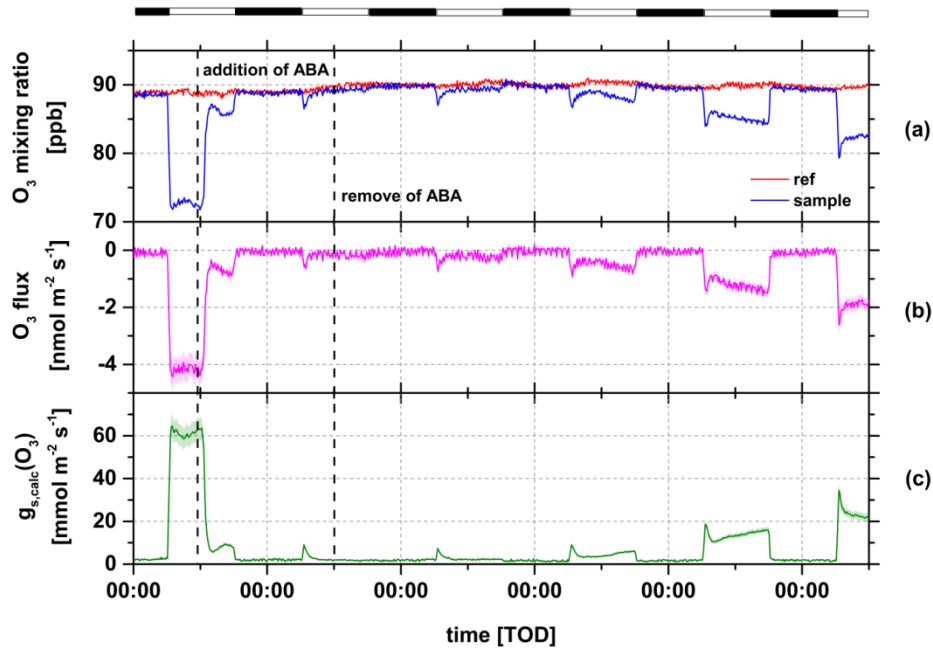


Fig. 11:  $O_3$  mixing ratio (a),  $O_3$  flux (b) and stomatal conductance to  $O_3$  (c) measured at *Quercus ilex* treated with  $250\mu\text{M}$  ABA-nutrient solution. The diurnal cycle of light was simulated by a climate cabinet with 13 hours light period (white balk) and 11 hours dark period (black balk). RH inside both cuvettes was around 40 %.

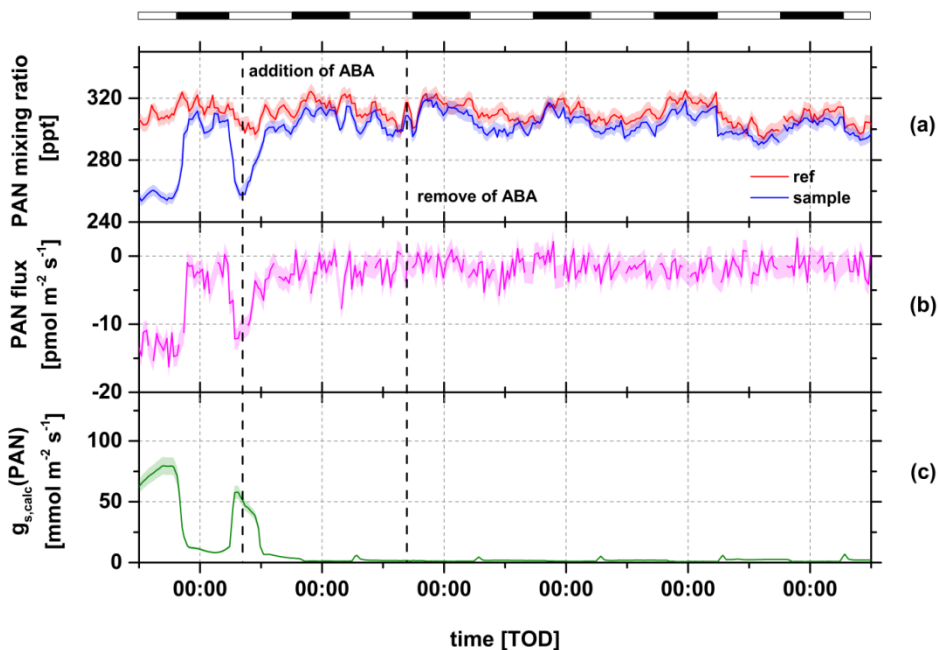


Fig. 12: PAN mixing ratio (a), PAN flux (b) and stomatal conductance to PAN (c) for *Quercus ilex* treated with  $350\mu\text{M}$  ABA-nutrient solution. The diurnal cycle of light was simulated by a climate cabinet with 13 hours light period (white area) and 11 hours dark period (grey shaded area). RH inside both cuvettes was around 40 %.

The PAN experiment and the O<sub>3</sub> experiment (350 μM ABA nutrient solution) were performed separately (see Fig. 12). The PAN mixing ratio in the sample cuvette increased after the ABA addition from 258.4 ppt to 301.4 ppt within a few hours (see Fig. 12a). The PAN deposition decreased from -12.1 pmol m<sup>-2</sup> s<sup>-1</sup> to -1.1 pmol m<sup>-2</sup> s<sup>-1</sup> and then fluctuated between 0 – -4.8 pmol m<sup>-2</sup> s<sup>-1</sup> (see Fig. 12b). According to Table 2 the minimal resolvable deposition flux of PAN was -2.5 pmol m<sup>-2</sup> s<sup>-1</sup>. The stomatal conductance to PAN decreased from 57.9 mmol m<sup>-2</sup> s<sup>-1</sup> to 6.8 mmol m<sup>-2</sup> s<sup>-1</sup> and was close to zero for the remaining time period (see Fig. 12c). Contrary to O<sub>3</sub>, after removing the ABA nutrient solution, no significant change in the fluxes was observed. For O<sub>3</sub> and PAN, the measured stomatal conductance ( $g_{s,meas}$ ) was plotted against the calculated stomatal conductance ( $g_{s,calc}$ ) (see Sect. 2.2.5, Eq. 6) to investigate the partitioning between stomatal and non-stomatal deposition of O<sub>3</sub> and PAN on the plant leaves (see Fig. 13). A clear linear relationship between  $g_{s,meas}$  and the  $g_{s,calc}$  for O<sub>3</sub> ( $R_{pearson} = 0.99$ ;  $CI_{95\%} = 0.07$ ) and PAN ( $R_{pearson} = 0.91$ ;  $CI_{95\%} = 0.1$ ) was found with a slope of  $0.98 \pm 0.01$  for O<sub>3</sub> and  $0.64 \pm 0.02$  for PAN.

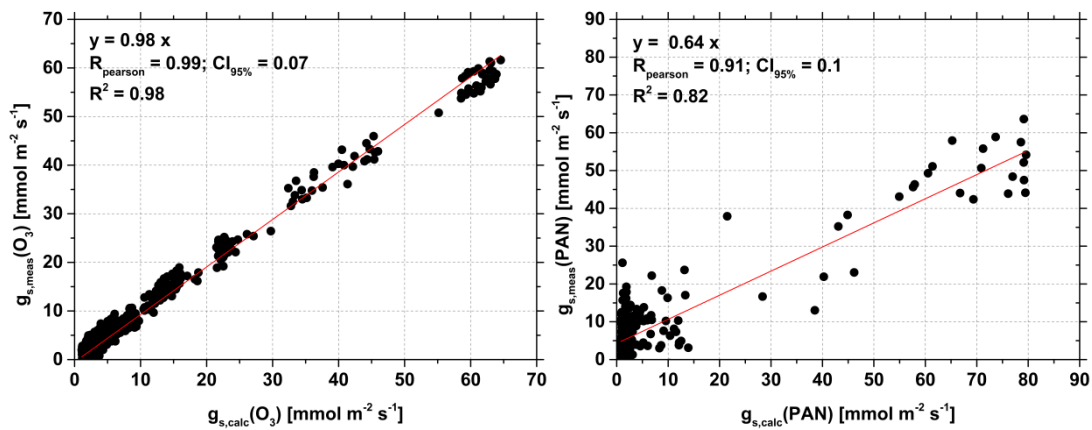


Fig. 13: Relationship between the measured stomatal conductance  $g_{s,meas}$  and calculated stomatal conductance  $g_{s,calc}$  to O<sub>3</sub> (left) and PAN (right)

### 3.2.4 Influence of RH on electrical surface conductance

Of special interest is the question whether plant surfaces may act as a sink for trace gases without taking into account the stomatal deposition. Water soluble compounds can be affected significantly by water films on such surfaces (Burkhardt and Eiden, 1994). Our twin-cuvette system with the automatic temperature regulated humidification system (ATRAHS) can support experimental conditions to investigate such questions (see Fig. 6). As demonstrated, the electrical surface conductance  $G$  of the plant leaves rose with the relative humidity in an exponential way ( $R^2 = 0.96$ ) (see Fig. 14). The critical value of the relative humidity  $RH_{crit}$ , where  $G$  increases exponentially, was found at 60 % in this study. Above this value a formation of a liquid water film on the leaf surface was clearly observed.



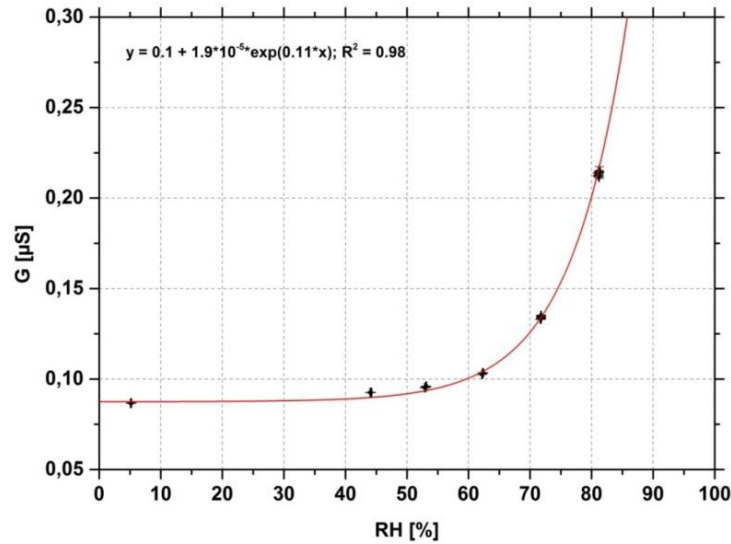


Fig. 14: Relationship between relative humidity and electrical leaf surface conductance.

## 4 Discussion

### 4.1 Performance of the twin-cuvette system

#### 4.1.1 Accuracy and consistency of O<sub>3</sub> and PAN measurements

With the presented twin-cuvette system it is possible to measure stable O<sub>3</sub> and PAN mixing ratios over long time periods under controlled environmental conditions. The resolution of the mixing ratio difference was quite high, so that even small differences in the range of a few hundred ppt in O<sub>3</sub> and several ppt in PAN could be differentiated in the measurement data (see Sect. 3.1.1, Table 2). Especially for the investigations on the flux partitioning, i.e. the discrimination between stomatal and non-stomatal deposition of O<sub>3</sub> and PAN, a measurement system with high precision to resolve the mixing ratio difference was required. The mixing ratios used during the long-term flux experiments (57 ppb for O<sub>3</sub> and 280 ppt for PAN, see Fig. 9) as well as the mixing ratios inside the sample cuvette (58.8 ppb for O<sub>3</sub> and 307.6 ppt for PAN) were far above the measured detection limits of the twin-cuvette setup (0.9 ppb for O<sub>3</sub> and 1.3 ppt for PAN, see also Table 3), but representative for ambient conditions. The good resolution of the mixing ratio difference between both cuvettes (see Table 2) was due to the very high precision and stability of the measured mixing ratio signal of O<sub>3</sub> and PAN within the cuvette system. As these mixing ratio differences are used to calculate the fluxes, the fluxes could be determined with a high sensitivity as well. Furthermore, the twin-cuvette system was tested to be a more precise method to perform flux measurements with reactive

trace gas species under controlled laboratory conditions than a single-cuvette system. As shown in Table 6, the O<sub>3</sub> and PAN fluxes with a single-cuvette system were calculated as  $1.2 \pm 0.2 \text{ nmol m}^{-2} \text{ s}^{-1}$  for O<sub>3</sub> and  $4.2 \pm 0.3 \text{ pmol m}^{-2} \text{ s}^{-1}$  for PAN. This indicates some overestimation at least for PAN when relying on inlet/outlet measurements with a single-cuvette system. The flux overestimation with a single-cuvette system is caused by an underestimation of the O<sub>3</sub> and PAN deposition on the cuvette foil, which had to be considered during the flux calculation with the single-cuvette system. For the twin-cuvette system, such a correction is not needed.

Table 6: Comparison of O<sub>3</sub> and PAN flux between a single-cuvette and dual cuvette measurement system.

Trace gas	Method	Flux (nmol m <sup>-2</sup> s <sup>-1</sup> )
O <sub>3</sub>	Single-cuvette	$1.2 \pm 0.2$
	Dual cuvette	$1.1 \pm 0.1$
PAN	Single-cuvette	$4.2 \cdot 10^{-3} \pm 3.0 \cdot 10^{-4}$
	Dual cuvette	$3.3 \cdot 10^{-3} \pm 2.0 \cdot 10^{-4}$

#### 4.1.2 ATRAHS

To investigate the uptake of trace gases by plant leaves under controlled laboratory conditions, the simulation of environmental parameters such as light, temperature and relative humidity inside the cuvettes is essential (Niinemets et al., 2011). For the non-stomatal deposition of O<sub>3</sub> and PAN to plant leaves, the influence of liquid films on leaf surfaces to the deposition of O<sub>3</sub> and PAN is discussed as an important factor (Fuentes and Gillespie, 1992, Shepson et al., 1992, Doskey et al., 2004, Moravek et al., 2015). To study the effect of different moisture levels on the non-stomatal deposition, the humidity inside the dynamic cuvettes system has to be changed with reliable accuracy. Various methods to humidify the cuvette air exist, which was presented in previous studies. Dynamic plant cuvettes for laboratory studies from Kesselmeier et al. (1996), Kesselmeier et al. (1998), Breuninger et al. (2012) use air humidification to create a proper environmental growth condition for the plant inside the cuvette. Thereby, the dry air stream was flushed through a water tank for humidification. A regulation of the inner relative humidity was not provided. However, many other studies such as Neubert et al. (1993), Fares et al. (2008) and Wildt et al. (1997) did not specify the humidification system used. Thereby, the water vapor content inside the cuvette was defined by the plant transpiration. In the cuvette system from Stokes et al. (1993) and Behrendt et al. (2014), the relative humidity inside the cuvette could be controlled by mixing

a bypass stream of wet air into the dry air stream. Normally, these systems (depending on the relative flow rates of the dry and humidified stream) cannot reach very high values of RH. Additionally, two MFCs are necessary for each cuvette to control both (dry and humid) additive air streams. Thereby, the precision of the adjusted humidity is dependent on the precision of all involved MFCs. Compared to all these methods, ATRAHS provides an opportunity to humidify the air stream directly. With this system, the humidity level inside the cuvettes could be held constant and regulated with high precision. Furthermore, the automatic water-filling mechanism avoids an interruption of the long-term measurements improving the performance of the entire measurement system and preventing data gaps. Due to the mechanical float valve, the water-filling process occurred continuously, so that the change of the water level inside the humidifier tank was very limited. In this case, the regulation of the humidity level by changing the heat temperature was very efficient due to the small volume of new water, which was filled to the humidifier tank. Additionally, only one MFC was needed for each cuvette when using ATRAHS. Thereby, a high precision of 0.3 % of the adjusted relative humidity could be achieved. The only limits are the range of the humidification, which was dependent on the water temperature of the humidifier, thus limited by the environmental temperature. The lowest adjustable humidification limit was 50 % at a temperature of 19.5 °C and flow rate of 20 L min<sup>-1</sup>, which was sufficient for our experiments. To achieve the range below 50 % RH with ATRAHS in the current setup, a cooling system would be needed for the humidifier tank to receive a lower water temperature.

## 4.2 Flux measurements under laboratory conditions

During the long-term experiment a decreasing trend of the water flux was observed over the measurement period, which became constant after 10 days. This effect might be due to the acclimatization process of the plant by changing the location from the greenhouse to the plant cabinet. From previous studies it is known that plant samples need a significant amount of days to adapt for changes in temperature, light intensity and relative humidity (Kesselmeier et al., 1998). Also, as the measurement was performed in October, the onset of winter stress could have played a role in the reduction of the water flux with time as it also effects the transpiration rate (Oh and Koh, 2014). A similar reducing trend could also be observed for the deposition fluxes of O<sub>3</sub> and PAN. To suppress annual behaviors such as the winter dormancy, the plant samples would have had to be grown under very constant environmental condition, which was not possible in our case, considering a growing time of 3 years. During the light periods, the determined deposition velocities ranged for O<sub>3</sub> from 0.66 to 1.06 mm s<sup>-1</sup>, which is comparable to Fares et al. (2008). Values for PAN of 0.32 to 0.48 mm s<sup>-1</sup> were comparable to the study of Teklemariam and Sparks (2004) (see Table 1). During the dark periods the deposition velocity of O<sub>3</sub> was slightly higher than that of PAN (see Sect. 3.2.1). As the leaf

stomata were closed under dark conditions, the  $O_3$  deposition is most likely associated with non-stomatal uptake on the leaf surface. Fuentes and Gillespie (1992) showed that the deposition of  $O_3$  can be reinforced by liquid water films on the leaf surface, which could be formed at high humidity. For example, Burkhardt and Eiden (1994) found that the relationship between humidity and electrical surface conductance of the plant leaves is due to the dissolution of ammonia and migration of ions in the liquid water film along the leaf surface of the plant. Further, atmospheric particles deposited on the leaf surface are likely to become deliquescent within the water vapor transpired by the leaf (Burkhardt et al. 2001). For these reasons we exposed the plant to ambient air, just outside the institute, to simulated natural conditions. Atmospheric particles could deposit on the plant leaves and increase the electrical surface conductance with rising ambient humidity inside the cuvette (see Sect. 3.2.4). The ABA experiment showed a clear effect of ABA on the leaf stomata closure in regard to the deposition fluxes of  $O_3$  and PAN. The linear relationship between the measured and calculated stomatal conductance to  $O_3$  ( $R_{\text{pearson}} = 0.99$ ;  $CI_{95\%} = 0.07$ ) and PAN ( $R_{\text{pearson}} = 0.91$ ;  $CI_{95\%} = 0.1$ ) shows predominantly stomatal uptake of both gas species, which agrees with results of previous studies (Okano et al., 1990, Sparks et al., 2003, Doskey et al., 2004, Fares et al., 2008, Fares et al., 2010). For the calculation of  $g_{s, meas}$  we assumed that  $vmr_{int, leaf}$  ( $O_3$ ) was close to zero (Laisk et al., 1989, Doskey et al., 2004) as well as for PAN (see Sect. 2.2.5, Eq.(10). In case of  $O_3$  at  $< 50\%$  RH, the linear slope of  $0.98 \pm 0.01$  indicates that there is no additional internal leaf resistance and surface deposition of  $O_3$  such as liquid water films as it was reported by Fuentes and Gillespie (1992). That  $O_3$  is rapidly decomposed in cell walls and plasmalemma has already been reported by Laisk et al. (1989). The absence of epicuticular deposition might have been caused by the low relative humidity of 40 % within the cuvettes during this experiment. As a consequence, we could conclude that below 40 % RH the surface deposition had no important contribution to the total  $O_3$  deposition. As observed in Fig. 14, the value of  $RH_{crit}$ , the humidity level where the formation of the leaf surface water film starts, was found at 60 %. However, Jud et al. (2016) observed a contribution of semi-volatile organic compounds, in this case diterpenes of *Nicotiana tabacum*, to non-stomatal sinks of  $O_3$ . These observations demonstrated that special structures or organs can exist on the plant surface as in the case of glandular trichomes of *Nicotiana tabacum*, which may release stored volatile organic compounds impacting gas phase chemistry. Such an incidence may act as a contribution to non-stomatal  $O_3$  sinks which should be kept in mind, especially for highly reactive sesquiterpenes, which may contribute by ozonolysis within the canopy (Jardine et al., 2011). However, sesquiterpene emission from healthy holm oak is negligible (Staudt and Houtellier, 2007). Furthermore, based on the results of our experiment under laboratory conditions, we conclude that due to the short residence time of 3.4 minutes, a contribution of gas phase reactions with  $O_3$  and monoterpenes from the internal leaf tissue to the non-stomatal deposition is low. An effect of ABA on the monoterpene production would affect the monoterpene synthesis on an even

lower level. The gas phase reaction with O<sub>3</sub> is an aspect of non-stomatal O<sub>3</sub> deposition which would become important when discussing a complete forest ecosystem. For PAN the slope ( $m = 0.64 \pm 0.02$ ) was lower than unity. This indicates an additional resistance to PAN deposition, which might be caused by limited uptake and transport in the leaves mesophilic cells. Therefore, the leaf internal PAN mixing ratio should not be zero as a result of the mesophyllic resistance for PAN, which is assumed to be higher than for O<sub>3</sub> (Sparks et al., 2003, Doskey et al., 2004, Teklemariam and Sparks, 2004, Moravek et al., 2015). The results from further detailed investigations on the non-stomatal deposition of PAN and O<sub>3</sub> to leaf surfaces will be presented in a subsequent publication.

## 5 Conclusions

By using a comparative measurement technique with a twin-cuvette system, we are able to perform trace gas exchange measurements with high precision and resolution of the measured trace gas mixing ratios. In our experimental setup, it is possible to control multiple environmental parameters such as light, temperature, trace gas mixing ratio and relative humidity inside the dynamic cuvettes. The comparison of fluxes between a single and the twin - cuvette system revealed an overestimation of fluxes by the single-cuvette system for both O<sub>3</sub> (8.3 %) and PAN (21.4 %), which is due to unconsidered effects of wall deposition. Consequently, the dual cuvette system represents a more precise method to perform flux measurements with reactive trace gas species under controlled laboratory conditions. Furthermore, with ATRAHS the relative humidity inside the cuvette could be controlled with a high precision of 0.3 %. According to our experimental data, ATRAHS is suitable for cuvette systems operated with higher flow rates ( $> 20 \text{ L min}^{-1}$ ), but it could be also possible to use for lower flow rates ( $> 5 \text{ L min}^{-1}$ ), and where humidity values up to 100 % are required. Due to the automatic water-filling mechanism, an interruption to refill the water for humidification during long-term measurements is not necessary, which improves the performance of the entire measurement system and prevents data gaps. O<sub>3</sub> and PAN exchange fluxes were determined with *Quercus ilex* during a long-term experiment of 2 weeks under controlled laboratory conditions. The deposition velocity ratio of O<sub>3</sub> and PAN was determined as  $0.45 \pm 0.04$ . By using O<sub>3</sub> mixing ratios between 32 and 105 ppb and PAN mixing ratios between 100 and 350 ppt a linear dependency of the O<sub>3</sub> flux as well as the PAN flux to its ambient mixing ratio could be observed. Furthermore, we are able to observe and characterize the formation of a water film on the leaf surface by measuring its electrical surface conductance with the leaf wetness sensor. An exponential relationship was observed between the electrical surface conductance and the ambient humidity, with a critical value of the

relative humidity of 60 %. The combination of all these features of the presented twin-cuvette system will give the opportunity to investigate further questions as flux partitioning between stomatal and non-stomatal deposition of O<sub>3</sub> and PAN and the influence of liquid films on a leaf surface.

## References

- Altimir, N., Kolari, P., Tuovinen, J.P., Vesala, T., Bäck, J., Suni, T., Kulmala, M. and Hari, P.: Foliage surface ozone deposition: a role for surface moisture?, *Biogeosciences*, 3, 1-20, 2006.
- Atkinson, R., Baulch, D. L., Cox, R. A., Crowley, J. N., Hampson, R. F., Hynes, R. G., Jenkin, M. E., Rossi, M. J., Troe, J., and IUPAC Subcommittee: Evaluated kinetic and photochemical data for atmospheric chemistry: Volume II – gas phase reactions of organic species, *Atmos. Chem. Phys.*, 6, 3625–4055, doi:10.5194/acp-6-3625-2006, 2006.
- Bakr, E. M.: A New Software for Measuring Leaf Area, and Area Damaged by *Tetranychus Urticae* Koch, Blackwell Verlag, Berlin, vol. 129, 173–175, 2005.
- Behrendt, T., Veres, P. R., Ashuri, F., Song, G., Flanz, M., Mamtimin, B., Bruse, M., Williams, J., and Meixner, F. X.: Characterisation of NO production and consumption: new insights by an improved laboratory dynamic chamber technique, *Biogeosciences*, 11, 5463–5492, doi:10.5194/bg-11-5463-2014, 2014.
- Bevington, P. R. and Robinson, D. K.: *Data Reduction and Error Analysis for the Physical Sciences*, 3rd edn., McGraw-Hill, New York, ISBN: 0-07-247227-8, 2003.
- Bonn, B., Sun, S., Haunold, W., Sitals, R., van Beesel, E., dos Santos, L., Nillius, B., and Jacobi, S.: COMPASS – COMparative Particle formation in the Atmosphere using portable Simulation chamber Study techniques, *Atmos. Meas. Tech.*, 6, 3407–3423, doi:10.5194/amt-6-3407-2013, 2013.
- Breuninger, C., Oswald, R., Kesselmeier, J., and Meixner, F. X.: The dynamic chamber method: trace gas exchange fluxes (NO, NO<sub>2</sub>, O<sub>3</sub>) between plants and the atmosphere in the laboratory and in the field, *Atmos. Meas. Tech. Discuss.*, 4, 5183–5274, doi:10.5194/amtd-4-5183- 2011, 2011.
- Burkhardt, J. and Eiden, R.: Thin water films on coniferous needles, *Atmos. Environ.*, 28, 2001– 2011, 1994.
- Burkhardt, J. and Gerchau, J.: A new device for the study of water-vapor condensation and gaseous deposition to plant-surfaces and particle samples, *Atmos. Environ.*, 28, 2012– 2017, 1994.
- Burkhardt, J., Koch, K., and Kaiser, H.: Deliquescence of deposited atmospheric particle on leaf surfaces, *Water, Air, Soil Pollut., Focus*, 1, 313–321, 2001.
- Chaparro-Suarez, I. G., Meixner, F. X., and Kesselmeier, J.: Nitrogen dioxide (NO<sub>2</sub>) uptake by vegetation controlled by atmospheric concentrations and plant stomatal aperture, *Atmos. Environ.*, 45, 5742–5750, 2011.

- Doskey, P. V., Kotamarthi, V. R., Fukui, Y., Cook, D. R., Breitbeil, F. W., and Wesely, M. L.: Air-surface exchange of peroxyacetyl nitrate at a grassland site, *J. Geophys. Res.-Atmos.*, 109, D10310, doi:10.1029/2004JD004533, 2004.
- Fares, S., Loreto, F., Kleist, E., and Wildt, J.: Stomatal uptake and stomatal deposition of ozone in isoprene and monoterpene emitting plants, *Plant Biol.*, 10, 44–54, 2008.
- Fares, S., Park, J. H., Ormeno, E., Gentner, D. R., McKay, M., Loreto, F., Karlik, J. and Goldstein, A. H.: Ozone uptake by citrus trees exposed to a range of ozone concentrations, *Atmos. Environ.*, 44(28), 3404-3412, doi:10.1026/j.atmosenv.2010.06.010, 2010
- Fuentes, J. D. and Gillespie, T. J.: A gas-exchange system to study the effects of leaf surface wetness on the deposition of ozone, *Atmos. Environ.*, 26, 1165–1173, 1992.
- Garland, J. A. and Penkett, S. A.: Absorption of peroxy acetyl nitrate and ozone by natural surfaces, *Atmos. Environ.*, 10, 1127–1131, 1976.
- Goff, J. A. and Gratch, S.: Low-pressure properties of water from -160 to 212 F, *T. Am. Soc. Heat. Ventil. Engin.*, 52, 95–121, 1946.
- Gut, A., Scheibe, M., Rottenberger, S., Rummel, U., Welling, M., Ammann, C., Kirkman, G. A., Kuhn, U., Meixner, F. X., Kesselmeier, J., Lehmann, B. E., Schmidt, W., Müller, E., and Piedade, M. T. F.: Exchange fluxes of NO<sub>2</sub> and O<sub>3</sub> at soil and leaf surfaces in an Amazonian rain forest, *J. Geophys. Res.-Atmos.*, 107, 8060, doi:10.1029/2001JD000654, 2002.
- Hill, A. C.: Vegetation: a sink for atmospheric pollutants, *JAPCA J. Air Waste Ma.*, 21, 341–346, 1971.
- Horst, T. W. and Weil, J. C.: How far is far enough – The fetch requirements for micrometeorological measurement of surface fluxes (Vol 11, PG 1018, 1994), *J. Atmos. Ocean. Tech.*, 12, 447–447, 1995.
- Jardine, K., Yañez Serrano, A., Arneth, A., Abrell, L., Jardine, A., Artaxo, P., Alves, E., Kesselmeier, J., Taylor, T., Saleska, S., and Huxman, T.: Ecosystem-scale compensation points of formic and acetic acid in the central Amazon, *Biogeosciences*, 8, 3709-3720, 2011.
- Jud, W., Fischer, L., Canaval, E., Wohlfahrt, G., Tissier, A. and Hansel, A.: Plant surface reactions: an opportunistic ozone defence mechanism impacting atmospheric chemistry, *Atmos. Chem. Phys.*, 16, 277-292, 2016.
- Kesselmeier, J., Schäfer, L., Ciccioli, P., Brancaleoni, E., Cecinato, A., Frattoni, M., Foster, P., Jacob, V., Denis, J., Fugit, J. L., Dutaur, L., and Torres, L.: Emission of monoterpenes and isoprene from a Mediterranean oak species *Quercus ilex* L measured within the BEMA (Biogenic Emissions in the Mediterranean Area) project, *Atmos. Environ.*, 30, 1841–1850, 1996.
- Kesselmeier, J., Bode, K., Gerlach, C., and Jork, E. M.: Exchange of atmospheric formic and acetic acids with trees and crop plants under controlled chamber and purified air condition, *Atmos. Environ.*, 32, 1765–1775, 1998.
- Kruit, R. J. W., Jacob, A. F. G., and Holtslaga, A. A. M.: Measurements and estimates of leaf wetness over agricultural grassland for dry deposition modeling of trace gases, *Atmos. Environ.*, 42, 5304–5316, 2008.
- Kulmala, M., Hienola, J., Pirjola, L., Vesala, T., Shimmo, M., Altimir, N. and Hari, P.: A model for NO<sub>x</sub>-O<sub>3</sub>-terpene chemistry in chamber measurements of plant gas exchange,

- Atmos. Environ, 33, 2145-2156, 1999.
- Laisk, A., Kull, O., and Moldau, H.: Ozone concentration in leaf intercellular air space is close to zero, *Plant Physiol.*, 90, 1163–1167, 1989.
- Marrero, T. R. and Mason, E. A.: Gaseous diffusion coefficients, *J. Phys. Chem. Ref. Data*, 1, 3–110, 1972.
- Moravek, A., Foken, T., and Trebs, I.: Application of a GC-ECD for measurements of biosphere–atmosphere exchange fluxes of peroxyacetyl nitrate using the relaxed eddy accumulation and gradient method, *Atmos. Meas. Tech.*, 7, 2097–2119, doi:10.5194/amt-7-2097-2014, 2014.
- Moravek, A., Stella, P., Foken, T., and Trebs, I.: Influence of local air pollution on the deposition of peroxyacetyl nitrate to a nutrient-poor natural grassland ecosystem, *Atmos. Chem. Phys.*, 15, 899–911, doi:10.5194/acp-15-899-2015, 2015.
- Mudelsee, M.: Estimating Pearson’s correlation coefficient with bootstrap confidence interval from serially dependent time series, *Math. Geol.*, 35, 651–665, 2003.
- Neubert, A., Kley, D., Wildt, J., Segschneider, H. J., and Forstel, H.: Uptake of NO, NO<sub>2</sub> and O<sub>3</sub> by sunflower (*Helianthus-annuus* L.) and Tobacco plants (*Nicotiana-tabacum*-L) dependence on stomatal conductivity, *Atmos. Environ.*, 27, 2137–2145, 1993.
- Niinemets, Ü., Kuhn, U., Harley, P. C., Staudt, M., Arneth, A., Cescatti, A., Ciccioli, P., Copolovici, L., Geron, C., Guenther, A., Kesselmeier, J., Lerday, M. T., Monson, R. K., and Peñuelas, J.: Estimations of isoprenoid emission capacity from enclosure studies: measurements, data processing, quality and standardized measurement protocols, *Biogeosciences*, 8, 2209–2246, doi:10.5194/bg-8-2209-2011, 2011.
- Oh, S. and Koh, S. C.: Photosystem II photochemical efficiency and photosynthetic capacity in leaves of tea plant (*Camellia sinensis* L.) under winter stress in the field, *Hortic. Environ. Biotechnol.*, 55, 363–371, 2014.
- Okano, K., Tobe, K., and Furukawa, A.: Foliar uptake of peroxyacetyl nitrate (PAN) by herbaceous species varying in susceptibility to this pollutant, *New Phytol.*, 114, 139–145, 1990.
- Ortega, J. and Helmig, D.: Approaches for quantifying reactive and low-volatility biogenic organic compound emissions by vegetation enclosure techniques – Part A, *Chemosphere*, 72(3), 343-364, doi: 10.1016/j.chemosphere.2007.11.020, 2008
- Pape, L., Ammann, C., Nyfeler-Brunner, A., Spirig, C., Hens, K., and Meixner, F. X.: An automated dynamic chamber system for surface exchange measurement of non-reactive and reactive trace gases of grassland ecosystems, *Biogeosciences*, 6, 405–429, doi:10.5194/bg-6-405-2009, 2009.
- Patz, H. W., Lerner, A., Houben, N., and Volz-Thomas, A.: Validation of a new method for the calibration of peroxy acetyl nitrate (PAN)-analyzers, *Gefahrst. Reinhalt. L.*, 62, 215–219, 2002.
- Shepson, P. B., Bottenheim, J. W., Hastie, D. R., and Venkatram, A.: Determination of the relative ozone and PAN deposition velocities at night, *Geophys. Res. Lett.*, 19, 1121–1124, 1992.
- Sparks, J. P., Monson, R. K., Sparks, K. L., and Lerday, M.: Leaf uptake of nitrogen dioxide (NO<sub>2</sub>) in a tropical wet forest: implications for tropospheric chemistry, *Oecologia*, 127, 214–221, 2001.



- Sparks, J. P., Roberts, J. M., and Monson, R. K.: The uptake of gaseous organic nitrogen by leaves: a significant global nitrogen transfer process, *Geophys. Res. Lett.*, 30, 2189, doi:10.1029/2003GL018578, 2003.
- Staudt, M. and Houtellier, L.: Volatile organic compound emission from holm oak infested by gypsy moth larvae: evidence for distinct responses in damaged and undamaged leaves, *Tree Physiology*, 27, 1433–1440, 2007.
- Stokes, N. J., Lucas, P. W., and Hewitt, C. N.: Controlled environment fumigation chamber for the study of reactive air pollutant effects on plants, *Atmos. Environ.*, 27, 679–683, 1993.
- Teklemariam, T. A. and Sparks, J. P.: Gaseous fluxes of peroxyacetyl nitrate (PAN) into plant leaves, *Plant Cell Environ.*, 27, 1149–1158, 2004.
- Van Hove, L.W.A., Bossen, M. E., de Bok, F. A. M. and Hooijmaijers, C. A. M.: The uptake of O<sub>3</sub> by poplar leaves: the impact of a long-term exposure to low O<sub>3</sub>-concentrations, *Atmos. Environ.*, 33, 907-917. 1999
- Volz-Thomas, A., Xueref, I., and Schmitt, R.: An automatic gas chromatograph and calibration system for ambient measurements of PAN and PPN, *Environ. Sci. Pollut. R.*, 4, 72–76, 2002.
- Von Caemmerer, S. and Farquhar, G. D.: Some relationships between the biochemistry of photosynthesis and the gas exchange of leaves, *Planta*, 153, 376–387, 1981.
- Wang, D., Hinckley, T. M., Cumming, A. B. and Braatne, J.: A comparison of measured and modeled ozone uptake into plant leaves, *Environ. Pollut.* 89(3), 247-254, 1995.
- Wildt, J., Kley, D., Rockel, A., Rockel, P., and Segschneider, H. J.: Emission of NO from several higher plant species, *J. Geophys. Res.-Atmos.*, 102, 5919–5927, 1997.



# Appendix C

## **Investigation of the influence of liquid surface films on O<sub>3</sub> and PAN deposition to plant leaves coated with organic / inorganic solution**

Shang Sun<sup>1</sup>, Alexander Moravek<sup>2</sup>, Ivonne Trebs<sup>3</sup>, Jürgen Kesselmeier<sup>1</sup>, Matthias Sörgel<sup>1</sup>

<sup>1</sup>Max Planck Institute for Chemistry, Biogeochemistry Department, P.O. Box 3060, 55128 Mainz, Germany

<sup>2</sup>University of Toronto, Department of Chemistry, 80 St. George St, M5S 3H6, Toronto, Canada

<sup>3</sup>Luxembourg Institute of Science and Technology (LIST), Environmental Research and Innovation (ERIN), 41, rue du Brill,  
L-4422 Belvaux, Luxembourg

*Correspondence to:* Shang Sun (shang.sun@mpic.de)

Published in Journal of Geophysical Research: Atmospheres

Received 21. Juni. 2016 - Accepted 17. November. 2016 - Accepted article online 21. November. 2016

© Wiley 2016. Used with the permission from Wiley.

DOI: 10.1002/2016JD025519

## Abstract

This study investigates the influence of leaf surface water films on the deposition of ozone (O<sub>3</sub>) and peroxyacetyl nitrate (PAN) under controlled laboratory conditions. A twin cuvette system was used to simulate environmental variables.

We observed a clear correlation between the O<sub>3</sub> deposition on plants (*Quercus ilex*) and the relative humidity (*RH*) under both, light and dark conditions. During the light period the observed increase of the O<sub>3</sub> deposition was mainly attributed to the opening of leaf stomata, while during the absence of light the liquid surface films were the reason for O<sub>3</sub> deposition. This finding was supported by experimentally induced stomatal closure by the infiltration of abscisic acid. In the case of PAN, no relationship with *RH* was found during the dark period, which indicates that the non-stomatal deposition of PAN is not affected by the liquid surface films. Consequently, the ratio of the O<sub>3</sub> and PAN deposition velocities is not constant when relative humidity changes, which is in contrast to assumptions made in many models. The flux partitioning ratio between non-stomatal and stomatal deposition as well as between non-stomatal and total deposition was found to be  $R_{nsto/sto} = 0.21 - 0.40$ ,  $R_{nsto/tot} = 0.18 - 0.30$  for O<sub>3</sub> and  $R_{nsto/sto} = 0.26 - 0.29$ ,  $R_{nsto/tot} = 0.21 - 0.23$  for PAN.

Furthermore, we demonstrate that the formation of the liquid surface film on leaves and the non-stomatal O<sub>3</sub> deposition are depending on the chemical composition of the particles deposited on the leaf cuticles as proposed previously.

## 1 Introduction

Liquid films present on environmental surfaces play an important role in the fate of water soluble atmospheric gases and particles [Burkhardt and Eiden, 1994] by increasing the deposition of trace gases to moist surfaces. Chameides and Stelson [1992] found that the dissolution of trace gases in airborne particulate matter increases with rising water/solid ratio of the particles. Furthermore, already deposited particles can be dissolved by surface water formed by wet precipitation (e.g. fog, dew or rain) [Lindberg et al., 1982] or may become deliquescent by the moisture from stomatal leaf transpiration [Burkhardt et al., 1999]. Depending on their chemical property, deliquescent salt particles can again represent a potential sink for trace gases [Flechard et al., 1999].

Earlier studies on the formation mechanism of liquid water films on homogeneous surfaces found that the condensation of a vapor to liquid on hydrophobic surfaces led to a formation of a grid of small droplets, in which the droplets coalesces with each other to form a well-

defined structure [Lopez et al., 1993]. Additionally, Burkhardt and Eiden [1994] observed for evaporating droplets that their contact angles with surfaces decrease, which is also reinforced by deposited particles on the surfaces [Cape, 1983; Leclerc et al., 1985; Cape, 1988], and could explain the formation of continuous water films on cuticles [Burkhardt and Hunsche, 2013]. Based on the work of Burkhardt and Eiden [1994], Lammel [1999] described three stages of liquid films formation as dry for  $RH < 55\%$ , partially wet for  $RH < 90\%$  and totally wet for  $RH > 90\%$ .

Tropospheric O<sub>3</sub> is known as a threat for ecosystems due to its plant toxicity [Fuhrer et al., 1997]. The removal of O<sub>3</sub> at terrestrial surfaces represents the main sink for boundary layer O<sub>3</sub> in rural areas [Simpson, 1992]. The sink strength is depending on the interaction of all removal pathways for O<sub>3</sub>, which include stomatal as well as non-stomatal deposition [Fares et al., 2012]. Loreto and Fares [2007] showed that stomatal uptake was the main factor of the total O<sub>3</sub> deposition during daytime for typical European ecosystems. On the opposite, Plake et al. [2015] found a non-stomatal contribution of 73 % to the total O<sub>3</sub> deposition at a natural grassland site. For maize crops also Stella et al. [2011] estimated a non-stomatal contribution of 70% during maturity. Non-stomatal O<sub>3</sub> sinks include various pathways such as deposition on leaf cuticle, soil, stems and gas phase reactions. Fuentes and Gillespie [1992] found that the O<sub>3</sub> deposition was enhanced by leaf surface wetness resulting from a dew layer or raindrops. Grantz et al. [1995] came to a similar conclusion that dew formation enhanced ozone deposition to the hypostomatous leaves. On the contrary, the O<sub>3</sub> deposition on leaf cuticles can be limited under dry conditions [Cape et al., 2009]. Altimir et al. [2006] found that the non-stomatal O<sub>3</sub> deposition in the boreal zone was clearly correlated with ambient relative humidity higher than 70 %. They suggest that the non-stomatal O<sub>3</sub> deposition on the leaf cuticle was influenced by the leaf surface water film, which was in line with the conclusion of Fuentes and Gillespie [1992]. Further, Brewer and Smith [1997] showed that leaf surface can hold a variable amount of wetness as a result of dew formation, rain, or ambient moisture. Rudich et al. [2000] found that the formation of the liquid surface film on organic surfaces is depending on the chemical composition and corrugation degree of the surface. Fuentes and Gillespie [1992] came to a similar conclusion that the increased O<sub>3</sub> deposition is ascribed mainly to the presence of compounds in aqueous form, scavenging O<sub>3</sub> by chemical reactions. Based on modelling studies, Potier et al. [2015] concluded that antioxidants leaching out of the leaf into the water film may explain high O<sub>3</sub> deposition rates during wet leaf conditions especially during senescence.

For peroxyacetyl nitrate (PAN), the influence of liquid surface films and ambient humidity on its deposition to surfaces is still largely unknown. PAN is a secondary trace gas, which is produced in the troposphere by photochemical oxidation of volatile organic substances producing peracetic acid radicals (C<sub>2</sub>H<sub>4</sub>O<sub>3</sub>) in the presence of nitrogen dioxide [Tuazon et al.,

1991]. The atmospheric lifetime of PAN is strongly depending on thermal decomposition [Roberts and Bertman, 1992]. Therefore, under conditions with lower temperature PAN serves as a carrier for reactive nitrogen over long distances and can release nitrogen dioxide into the lower atmosphere by thermal decomposition [Crutzen, 1979; Singh and Hanst, 1981; Fischer et al., 2011], contributing to the local increase of nitrogen dioxide and affecting other atmospheric processes such as tropospheric O<sub>3</sub> production [Zhang et al., 2009; Fischer et al., 2011]. Hence, it is important to understand the sources and sinks of PAN. One of the main loss processes for PAN below 7 km height is thermal decomposition [Talukdar et al., 1995]. Further removal processes include dry and wet deposition. However, due to the low water solubility of PAN ( $H^*_{\text{PAN}} = 4.1 \text{ M atm}^{-1}$ , see Kames and Schurath [1995]) the magnitude of its hydrolysis rate constant excludes wet deposition as an important removal process [Kames et al., 1991]. This was in agreement with Hill [1971], Garland and Penkett [1976], Doskey et al. [2004], and Teklemariam and Sparks [2004]. Of high importance with regard to dry and wet deposition is the uptake of PAN by ecosystems. Sparks [2009] concluded that foliar uptake of atmospheric reactive nitrogen by plants could represent a major contribution of global atmospheric input of nitrogen into the ecosystems. This view is supported by previous laboratory experiments with PAN deposition on plants showing a clear correlation between the PAN deposition flux and the stomatal conductance, which implies that stomatal uptake of PAN is the dominant pathway [Okano et al. 1990; Sparks et al. 2003; Teklemariam and Sparks 2004; Sun et al. 2016]. However, non-stomatal deposition of PAN to the leaf cuticles is still a strong matter of discussion [Turnipseed et al., 2006; Wolfe et al., 2009; Moravek et al., 2015], which demonstrates the needs to investigate PAN exchange with vegetation as it is still poorly understood.

The formation of surface water films and its influence on the deposition of trace gases was proposed in many previous studies [van Hove et al., 1989; Fuentes and Gillespie, 1992; Burkhardt and Eiden, 1994; Grantz et al., 1995; Hakan et al., 1995; Burkhardt et al., 1999; Flechard et al., 1999; Klemm et al., 2002]. However, except the work of Fuentes and Gillespie [1992] no detailed studies on this topic exist. In our study, we investigate the influence of induced leaf surface liquid films on the deposition of O<sub>3</sub> and PAN under controlled laboratory conditions. A twin cuvette system described in Sun et al. [2016] was used to simulate environmental variables such as light, temperature, trace gas mixing ratio and humidity. Furthermore, the leaf surface was treated with various organic and inorganic solutions to investigate the electrical surface conductance of the leaves at various relative humidity values. Based on these experiments, the surface deposition of O<sub>3</sub> and PAN is investigated depending on the leaf surface properties and the influence of soluble compounds. The aim of our study is to contribute to a better understanding of underlying mechanisms determining the non-stomatal deposition process of O<sub>3</sub> and PAN to terrestrial vegetation.

## 2 Material and Methods

### 2.1 Plant Material and Growth

All experiments were performed with three years old tree individuals of *Quercus Ilex* ordered from Burncoose & South Down Nursery, Gwennap, Redruth, Cornwall, UK. We choose this particular species as a model plant due to its evergreen character, and, thus a measurable stomatal activity over the whole year. Additionally, this oak species is typical for the Mediterranean area. The trees grew up in pots with commercial soil mixture (FloraSelf, Germany) in the greenhouse of the Max Planck Institute for Chemistry under natural growing conditions ( $T_{\text{winter}} = 15^{\circ}\text{C}$ ,  $T_{\text{summer}} = 30^{\circ}\text{C}$ ,  $\text{PAR}_{\text{max}} = 1400 \mu\text{molm}^{-2}\text{s}^{-1}$ ). The greenhouse was not hermetically isolated, so that the tree samples inside the greenhouse were exposed to ambient air conditions. Furthermore, the plants were watered daily in the summer period and every 3 days in the winter period.

### 2.2 O<sub>3</sub> and PAN flux measurements

The flux measurements were performed with a dynamic twin-cuvette system under controlled environmental conditions (temperature, light, relative humidity, trace gas mixing ratio) (see Figure 1). The dual-cuvette system consisted of the sample (plant) cuvette and an empty reference cuvette, both identical in construction to rule out any bias by cuvette surfaces and is described in detail in Sun et al. [2016]. In short, both cuvettes (volume 70 L) are housed in a temperature controlled plant cabinet (VB1014, Vötsch GmbH) and O<sub>3</sub> and PAN mixing ratios are alternately measured downstream of both cuvettes. The fluxes of O<sub>3</sub> (in nmol m<sup>-2</sup> s<sup>-1</sup>) and PAN (in pmol m<sup>-2</sup> s<sup>-1</sup>) were calculated by the difference of the trace gas mixing ratio between the reference and sample cuvettes as:

$$F(\text{O}_3, \text{PAN}) = \frac{f_m \times (\text{vmr}_{\text{out,ref}} - \text{vmr}_{\text{out,sample}})}{A_{\text{leaf}}} \quad (1)$$

where  $\text{vmr}_{\text{out,ref}} - \text{vmr}_{\text{out,sample}}$  is the difference of the trace gas mixing ratio between the reference and sample cuvette.  $f_m$  (mol s<sup>-1</sup>) is the mole flow rate through each cuvette, which is calculated from the volume flow rate  $f_v$  (L min<sup>-1</sup>) divided by 24.4 L mol<sup>-1</sup> (at 25 °C and 1013.25 hPa), i.e. the volume of one mole in air at standard conditions.  $A_{\text{leaf}}$  (m<sup>2</sup>) is the leaf area of the entire plant inside the sample cuvette and was determined by digitally scanning all leaves of the sample tree after completion of the flux experiments (for further details see Sun et al. [2016]).

O<sub>3</sub> was measured by a UV photometric analyzer (Model 49i, ThermoScientific, USA) and PAN was measured using an automatic gas chromatograph (Meteorologie Consult GmbH, Germany) with electron capture detection [Volz-Thomas et al., 2002; Moravek et al., 2014]. In addition, CO<sub>2</sub> and H<sub>2</sub>O concentrations were measured with an infrared gas analyzer (Li-7000, LiCor Inc., USA) to determine plant photosynthesis and transpiration. For the latter, Eq. (1) was used to calculate the water flux  $E$  (mmol m<sup>-2</sup> s<sup>-1</sup>) with the mixing ratio difference of the water vapor between both cuvettes.

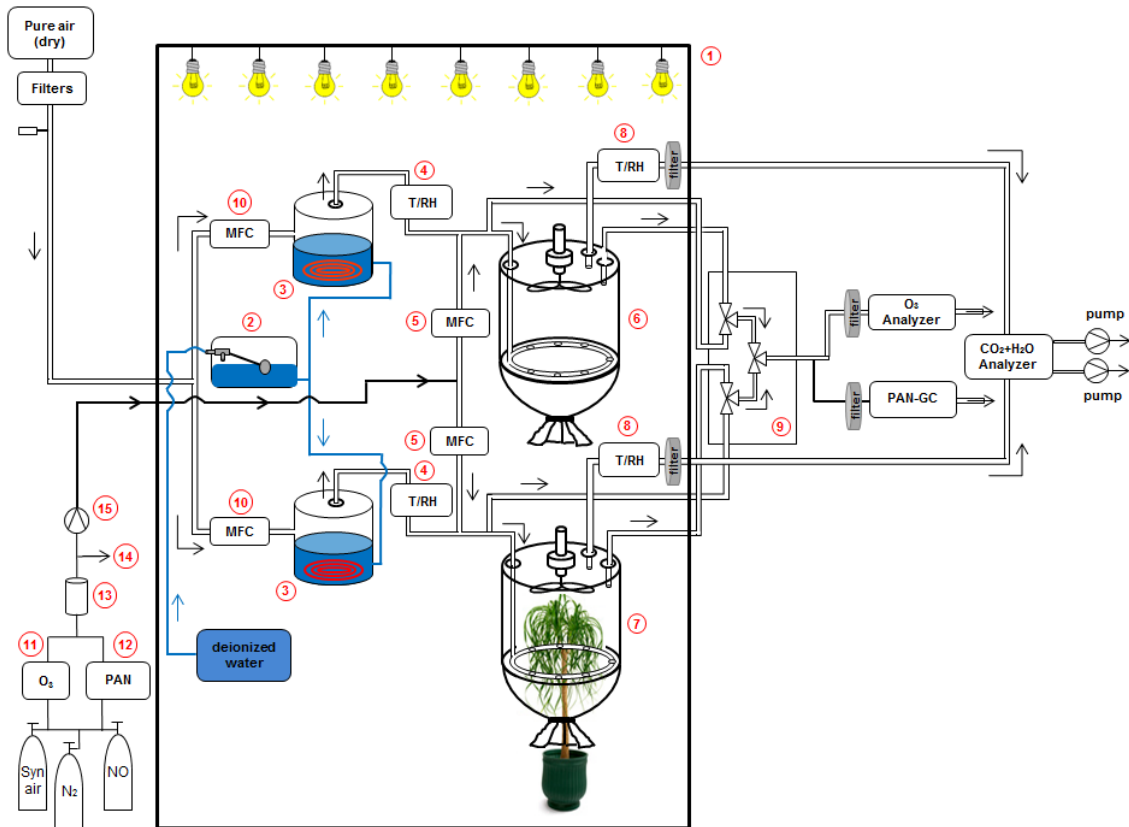


Fig. 1: Flow chart of the dual cuvette system after Sun et al. 2016. 1 plant cabinet, 2 water storage tank, 3 humidification system (ATRAHS, see Sun et al. 2016), 4 Temperature and relative humidity sensor for humidity regulation, 5 mass flow controller (MFC), 6 dynamic cuvette (reference), 7 dynamic cuvette (sample), 8 Temperature and relative humidity sensor for monitoring, 9 Teflon- valve block, 10 MFC for gas addition, 11 O<sub>3</sub> – primary standard, 12 PAN – calibration unit, 13 mixing vessel, 14 overflow, 15 Teflon membrane pump.

During the experiments, light conditions were simulated by the plant cabinet system, while the photosynthetic active radiation (PAR) was measured by a quantum sensor (LiCor Inc., USA). During daytime conditions, the light intensity (450 – 650 nm) was kept constant at 600  $\mu\text{mol m}^{-2} \text{s}^{-1}$  for all by 8 HQI<sup>®</sup>-BT (400 W, OSRAM GmbH, Germany) and 6 Krypton (100 W, General Electric Company, USA) lamps. The relative humidity inside the cuvettes was regulated by the Automatic Temperature Regulated Air Humidification System



(ATRAHS, see Sun et al. [2016]), which allowed for a precise regulation of a relative humidity (*RH*) in the cuvettes. The formation of liquid surface films on the leaf was determined by three leaf wetness sensors, which were mounted on the plant leaves at different heights. The updated sensors according to Sun et al. [2016] was not prone to signal drifts compared to the older version described in Burkhardt and Eiden [1994]. The background signals were measured by sensors without leaves in the reference cuvette. For detailed description of the wetness sensor see Burkhardt and Eiden [1994] and Sun et al. [2016].

The stomatal conductance of water vapor  $g_s(H_2O)$  (mmol m<sup>-2</sup> s<sup>-1</sup>) was determined from the ratio between the water flux  $E$  (mmol m<sup>-2</sup> s<sup>-1</sup>) and the air to leaf vapor pressure deficit  $VPD$  (Pa kPa<sup>-1</sup>) according to von Caemmerer and Farquhar [1981], see Eq. (2):

$$g_{s,calc}(H_2O) = \frac{E}{VPD} \quad (2)$$

where  $VPD$  was derived as

$$VPD = \frac{SVP(T_{leaf})}{P_{sample}} - C_{out,sample}(H_2O) \quad (3)$$

The saturation water vapor pressure  $SVP$  (hPa) was calculated with the Goff-Gratch-Equation (Goff and Gratch, 1946), which is depending on the leaf temperature  $T_{leaf}$  (see Eq. (3)). For this, the leaf temperature was measured by thermocouples (Type E, OMEGA Engineering, Inc., USA) at four different positions of the plant.  $C_{out,sample}(H_2O)$  (Pa kPa<sup>-1</sup>) is the concentration of water vapor inside the sample cuvette and  $P_{sample}$  (kPa) is the pressure in the sample cuvette, which was also measured by pressure sensors (HCX series, First Sensor AG, Germany).

Generally, the stomatal flux of O<sub>3</sub> and PAN is given by the difference of the total flux and the non-stomatal flux

$$F_{sto}(O_3, PAN) = F_{nsto+sto}(O_3, PAN) - F_{nsto}(O_3, PAN) \quad (4)$$

where  $F_{sto}$  is the stomatal flux of O<sub>3</sub> and PAN in nmol m<sup>-2</sup> s<sup>-1</sup> and pmol m<sup>-2</sup> s<sup>-1</sup>, respectively. For this case  $F_{nsto+sto}$  equals the total flux of O<sub>3</sub> and PAN measured during the light period, i. e. when plant stomata were open (see Sect. 2.3).  $F_{nsto}$  is the non-stomatal flux measured in the absence of light in the period “dark\_cont” (see Sect. 2.3), which was verified by measurements under light and dark conditions by closing the stomata with abscisic acid (see also 2.4 and 3.2).

$F_{sto}$  was calculated as the difference of the linear fit equations of  $F_{nsto}$  and  $F_{nsto+sto}$  (see Figure 2):

$$F_{sto} = (m_{F_{nsto+sto}} - m_{F_{nsto}}) \times RH + b_{F_{nsto+sto}} - b_{F_{nsto}} \quad (5)$$

where  $m_{F_{nsto+sto}}$  is the linear slope and  $b_{F_{nsto+sto}}$  is the intercept of the total flux of O<sub>3</sub> and PAN.  $m_{F_{nsto}}$  is the linear slope and  $b_{F_{nsto}}$  is the intercept of the non-stomatal flux.  $RH$  is the relative humidity in the sample cuvette.

The deposition velocity  $V_d$  (mm s<sup>-1</sup>) of O<sub>3</sub> and PAN was calculated as:

$$V_d(O_3, PAN) = \frac{F(O_3, PAN)}{vmr_{out, sample}} \times V_m \quad (6)$$

where  $V_m$  is the molar volume of 24.55 L mol<sup>-1</sup> at 26 °C (air temperature in the cuvette).

The electrical surface conductance  $G$  (μS) was determined according to *von der Heyden* [2013] and *Sun et al.* [2016] after the following equation:

$$G = 1018.7 \times U^{-1.062} \quad (7)$$

where  $U$  (mV) is the measured voltage raw signal by the leaf wetness sensor (for detailed description see *Sun et al.* [2016]).

## 2.3 Flux experiment 1: stomatal and non-stomatal flux partitioning under outdoor air conditions

Two different flux experiments were performed enclosing the above ground parts of a potted complete tree of *Quercus ilex*, one with alternating light and dark conditions and one under continuous dark conditions. The sample trees (one sample and one replicate) were grown outside under a plastic tarp (shelter open to all sides) for nearly one month, in order to capture particles from the outdoor air but being shielded against rain and strong sunlight. This allowed us to investigate the flux partitioning between stomatal and non-stomatal deposition of O<sub>3</sub> and PAN for more realistic conditions with outdoor air exposed leaves. For the first experiment, the diurnal cycle was simulated with a light/dark period of 12 h each over a period of six days. The light and dark periods of this experiment are referred to as “light” and “dark\_alter”. To test the impact of humidity,  $RH$  was increased every day by 10 % (24 h), from initially 30 % to 80 % on the last day. For “dark\_alter”, the initial  $RH$  was 45 % due to the technical limit of the humidification system. For the second experiment “dark\_cont”, the O<sub>3</sub> and PAN deposition was measured for three days under continuous dark conditions with the same tree as in the first experiment to determine the deposition under stomatal closure. The  $RH$  was increased by 10 % every 12 hours also from initially 45 % to 80 % at the end. For both experiments, O<sub>3</sub> mixing ratio of  $51.5 \pm 0.7$  ppb and PAN mixing ratio of  $574.7 \pm 6.9$  ppt were used for fumigation. Due to the warming effect of the lamps, the cuvette temperature was  $T = 26 \pm 0.1$  °C during light conditions and  $20 \pm 0.1$  °C during the dark conditions. For both experiments, the sample tree was acclimatized inside the cuvette under respective conditions for three days before the start of the experiment. The experiments were performed

in February 2015 whereas the seasonal effect on the plant metabolism has to be considered. To investigate the chemical composition of the particles deposited to the leaf surface under outdoor conditions below the plastic tarp, the leaves were rinsed with deionized water after the experiment and the collected water sample was analyzed for the total organic carbon (TOC), dissolved organic carbon (DOC), Cl<sup>-</sup> and Br<sup>-</sup>.

## 2.4 Flux experiment 2: effect of liquid surface film composition on non-stomatal deposition

To investigate the effect of the liquid surface film on the deposition of O<sub>3</sub> and PAN, individual plant branches of *Quercus ilex* (grown outside under plastic tarp) were cut from the tree stem under water (to prevent embolism) and dipped into a nutrient solution (for the detailed chemical composition see Sun et al. [2016]). After cleaning, the leaves were treated with artificial solutions containing inorganic and organic compounds to simulate a qualitative environmental pollution by airborne particles (Table 1). The humic acid spray solution was also analyzed for the same organic compounds (TOC, DOC, Cl<sup>-</sup> and Br<sup>-</sup>) as the leaf wash water sample (see Sect. 2.3).

Table 1: Compositions of the spray solutions for the leaf surface coating. The inorganic and halogen solutions were generated with deionized water. The humic acid solution was generated with 0.05 M NaOH and deionized water. The pH of all solutions was 7.

	Substance	concentration
inorganic	SO <sub>4</sub> <sup>2-</sup>	7 mmol L <sup>-1</sup>
	NO <sub>3</sub> <sup>-</sup>	1.8 mmol L <sup>-1</sup>
	NO <sub>2</sub> <sup>-</sup>	5 mmol L <sup>-1</sup>
	NH <sub>4</sub> <sup>+</sup>	1.8 mmol L <sup>-1</sup>
Halogen	Cl <sup>-</sup>	15 mmol L <sup>-1</sup>
	Br <sup>-</sup>	15 mmol L <sup>-1</sup>
Organic	humic acid	-

To investigate the effect of non-stomatal deposition, the cut plant branches were treated with plant hormone abscisic acid (ABA) prior to the experiment to initiate the closure of the leaf stomata. The application procedure is described in detail by Sun et al. [2016]. The inorganic, organic and halogenic solutions were sprayed on the plant leaf surface of the individual cut

branches. The compounds of the inorganic solution used for wetting the leaves were representative for fine particulate matter [Li et al., 2015]. For the organic solution, a humic acid solution was prepared by dissolving 10 g solid humic acid (30 – 40 %, CAS 1415-93-6, Roth, Germany) in 20 mL 0.05 M NaOH. After filtration, the filtrate was filled up with deionized water to 100 mL final volume. The resulting pH was 7. After drying of the wetted surfaces, the branch, which was still dipped into the nutrient solution, was introduced into the cuvette. Subsequently, ABA was added to the nutrient solution inducing stomatal closure. The experiment of each coated branch was performed under controlled environmental conditions for two days ( $T = 20 - 26$  °C, diurnal cycle of light = 6h/6h).  $RH$  was varied between 40 % – 80 % by increasing with 10 % steps. Untreated (outdoor air) and tree treated with inorganic solution were also measured at  $RH = 5$  %.

### 3 Results

#### 3.1 Flux experiment 1: stomatal and non-stomatal flux partitioning under outdoor air conditions

Figure 2 shows the deposition flux of O<sub>3</sub> and PAN in relation to relative humidity inside the cuvettes (a-b) and the corresponding stomatal (leaf) conductance (c-d). As shown in Figure 2a, the O<sub>3</sub> deposition in the light period ( $F_{\text{nsto+sto}}$ ) is strongly correlated with the relative humidity. This correlation diminishes during the intermittent dark period (dark\_alter, magenta line). However, a strong correlation of O<sub>3</sub> deposition with increasing relative humidity is also found in the dark under constant darkness (dark\_cont, black line, denoted also as  $F_{\text{nsto}}$ ). The deposition of PAN behaves very similar for the light period (Figure 2b). However, under dark conditions, there is no correlation with  $RH$ , neither in the intermittent dark periods nor under constant darkness. Consequently, the calculated stomatal fluxes for O<sub>3</sub> and PAN show a different slope relative to the total flux ( $F_{\text{nsto+sto}}$ ). When relating the fluxes to the stomatal conductance (Figure 2c-d), the role of the stomatal uptake becomes evident. Under light conditions there is a clear correlation between stomatal opening and increasing uptake for both gases. The strong decrease of uptake under dark conditions is clearly linked to the reduction or absence of the stomatal deposition pathway. Plotting the stomatal conductance against the relative humidity supports these finding as shown in Figure 3. There is a clear increase of stomatal conductance with  $RH$  under light conditions in the cuvette. In the dark, no significant stomatal conductance was observed (see Figure 2c-d).

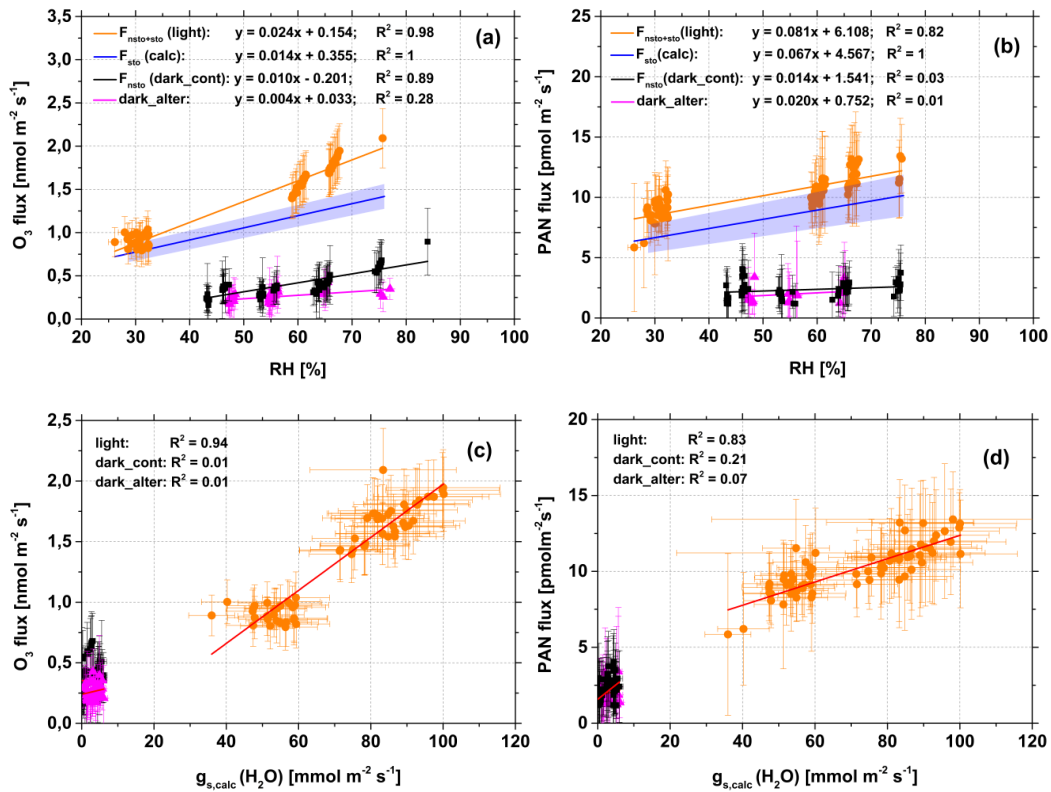


Fig. 2: O<sub>3</sub> and PAN fluxes at various humidities (a-b) and in relation to stomatal conductance (c-d) during light (orange,  $F_{nsto+sto}$ ) and two different dark periods, “dark\_alter” (magenta) and “dark\_cont” (black,  $F_{nsto}$ ) (see Sect. 2.3).  $F_{sto}$  (blue) was calculated from the difference of the linear fit equation between  $F_{nsto+sto}$  and  $F_{nsto}$  (see Sect. 2.2, Eq. (4) and (5)). The whole plant of *Quercus ilex* (exposed to outdoor air condition, under plastic tarp) was introduced to the cuvette without ABA-treatment for three days of acclimatization to adapt for the cuvette conditions (see Sect. 2.3). The cabinet temperature was  $26 \pm 0.1$  °C during the light period and  $20 \pm 0.1$  °C during the dark period. The Gaussian propagated uncertainties of the fluxes consider the error of the measured O<sub>3</sub> and PAN mixing ratio differences and operating flow rate (see Eq. (1)).

The data as shown in Figure 2 demonstrate the different contribution of stomatal and non-stomatal deposition for O<sub>3</sub> and PAN. Figure 4 shows the dependence of the flux ratios  $R_{nsto/sto}$  and  $R_{nsto/tot}$  on the relative humidity. For O<sub>3</sub>,  $R_{nsto/sto}$  increased with rising RH from 0.21 at 40 % RH up to 0.40 at 80 % RH and  $R_{nsto/tot}$  increased from 0.18 – 0.30 within the same RH range. For PAN,  $R_{nsto/sto}$  decreased from 0.29 at 40 % RH to 0.26 at 80 % RH and  $R_{nsto/tot}$  decreased from 0.23 – 0.21 within the same RH range. This decreasing trend for PAN is insignificant considering the measurement uncertainty.

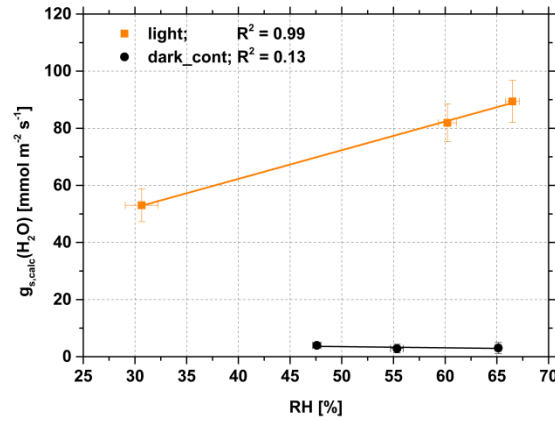


Fig. 3: Relationship between stomatal conductance and  $RH$  under light (orange) and dark\_cont (black) conditions measured in the cuvette. The environmental conditions of the cuvettes are the same as shown in Fig. 2.

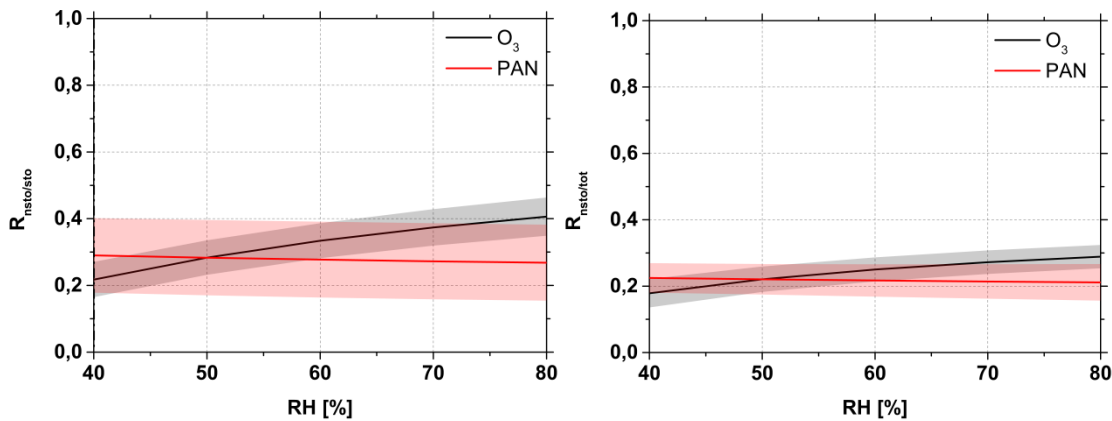


Fig. 4: Calculated partitioning ratio  $R_{nsto/sto}$  between non-stomatal and stomatal deposition flux (left) and  $R_{nsto/tot}$  between non-stomatal and total deposition flux (right) of O<sub>3</sub> (black) and PAN (red) versus  $RH$ . The red and grey uncertainty areas of the partitioning ratios were propagated considering the errors of the stomatal and non-stomatal fluxes of O<sub>3</sub> and PAN.

These differences may be related to the existence of liquid surface films, which were monitored by the surface conductance measurements. The electrical surface conductance ( $G$ ) shows an exponential behavior with  $RH$  and ranged between 0.13 and 0.23  $\mu\text{S}$  during the period “dark\_alter” and between 0.14 and 0.26  $\mu\text{S}$  during the light period (see Figure 5). A clear difference between the light and “dark\_alter” was observed above 50 %  $RH$ , with the  $G$  values of the light period being higher than ones of the period “dark\_alter”. The critical value of the relative humidity  $RH_{crit}$ , where  $G$  increases exponentially, was at  $\sim 40$  % during the light period and  $\sim 50$  % during the period “dark\_alter”.

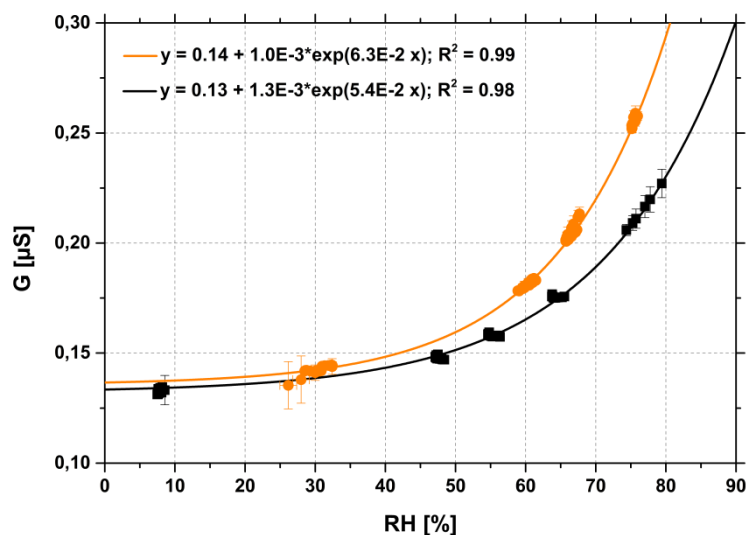


Fig. 5: Electrical surface conductance at various relative humidity values (30% - 80%) during light (orange) and period “dark\_alter” (black). For the dark condition, G values were measured additionally at 8%.

### 3.2 Flux experiment 2: effect of liquid surface film composition on non-stomatal deposition

For a better understanding of the contribution of non-stomatal deposition, the exchange of O<sub>3</sub> and PAN was investigated by addition of the hormone ABA to the nutrient solution of individual plant branches, which caused stomatal closure. In case of O<sub>3</sub>, the deposition flux and RH reveal an exponential relationship under light and dark conditions (see Figure 6 and Figure 7). In the presence of light, the O<sub>3</sub> deposition to the cleaned leaves (see Figure 6a) was 0.16 nmol m<sup>-2</sup> s<sup>-1</sup> at 40 % RH and increased with rising RH to a maximum of 0.25 nmol m<sup>-2</sup> s<sup>-1</sup> at 75 % RH. In the case of leaves carrying particles derived from outdoor air incubation (see Figure 6b) the increase of the O<sub>3</sub> flux with increasing RH was significantly stronger than for cleaned leaves, a pattern which was comparable to the O<sub>3</sub> flux of the leaves treated with the inorganic solution (see Figure 6c). The O<sub>3</sub> flux to leaves treated with humic acid (see Figure 6d) varied only from 0.21 nmol m<sup>-2</sup> s<sup>-1</sup> at 40 % RH to 0.42 nmol m<sup>-2</sup> s<sup>-1</sup> at 75 % RH and that to leaves treated with halogen compounds increased from 0.35 – 0.55 nmol m<sup>-2</sup> s<sup>-1</sup> within the same RH range (see Figure 6e). A common feature of all different leaf surface coatings was the clear increase of the O<sub>3</sub> flux above 60 % RH. In contrast, the PAN flux was not correlated with RH for all leaf treatments under light, with flux values fluctuating between 0.3 and 5.7 pmol m<sup>-2</sup> s<sup>-1</sup>. In the case of the cleaned leaves, G showed a slightly exponential relationship to RH from 0.09 μS at 40 % RH to 0.13 μS at 75 % RH. For the leaves exposed to outdoor air under plastic tarp, the G value varied from 0.08 to 0.21 μS at RH from 5 – 75 %, which was higher than for the cleaned leaves. For the leaves treated with inorganic solution G was even stronger than for the first both cases with values ranging from 0.08 – 0.27 μS for RH between

40 % and 75 %. The weakest relationship between  $G$  values and  $RH$  was found for the humic acid treated leaves with 0.07 – 0.11  $\mu\text{S}$  at 40 – 75 %  $RH$  and the strongest relationship was observed for the halogen treated leaves with 0.15 – 1.13  $\mu\text{S}$  at 40 – 75 %  $RH$ .

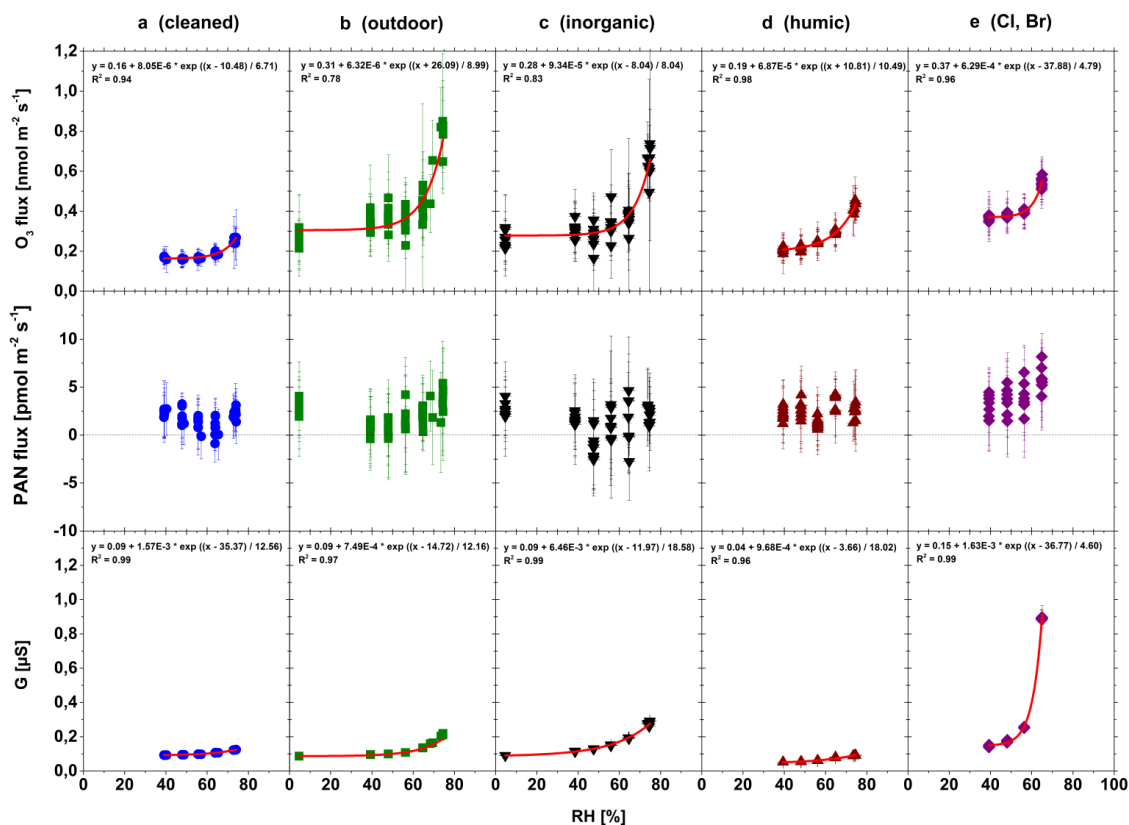


Fig. 6: O<sub>3</sub>, PAN flux and electrical surface conductance  $G$  at various  $RH$  (5 % - 80 %) during the light period under ABA induced stomatal closure. Cleaned leaf surface (column a), exposed with outdoor air (column b), treated with inorganic solution (column c), treated with humic acid (column d) and treated with Cl, Br (column e). The increasing trend was fitted with an exponential growth function.

Under dark conditions a similar pattern was found. The O<sub>3</sub> flux to the cleaned leaves (see Figure 7a) increased from 0.14  $\text{nmol m}^{-2} \text{s}^{-1}$  at 44 %  $RH$  to 0.27  $\text{nmol m}^{-2} \text{s}^{-1}$  at 80 %  $RH$ . For the leaves exposed to outdoor air (see Figure 7b) the O<sub>3</sub> flux ranged from 0.24  $\text{nmol m}^{-2} \text{s}^{-1}$  at 5 %  $RH$  to 0.51  $\text{nmol m}^{-2} \text{s}^{-1}$  at 80 %  $RH$ . The O<sub>3</sub> flux to the leaves treated with inorganic solution (see Figure 7c) showed a similar trend as for leaves polluted with outdoor air ranging from 0.23 to 0.45  $\text{nmol m}^{-2} \text{s}^{-1}$ . Under the treatment with humic acid (see Figure 7d) the O<sub>3</sub> flux to leaves varied between 0.14  $\text{nmol m}^{-2} \text{s}^{-1}$  at 44 %  $RH$  and 0.46  $\text{nmol m}^{-2} \text{s}^{-1}$  at 80 %  $RH$ . The O<sub>3</sub> flux to leaves treated with halogen compounds increased from 0.28 to 0.61  $\text{nmol m}^{-2} \text{s}^{-1}$  at 44 % to 72 %  $RH$  (see Figure 7e). In contrast, for the PAN flux no correlation with increasing  $RH$  was found under all conditions. The  $G$  values measured under dark condition were found to be lower than those under light conditions for the same  $RH$  values.  $G$  was 0.08



– 0.12 μS at 44 % – 80 % *RH* for the cleaned leaves, 0.08 – 0.21 μS at 5 % – 80 % *RH* for the ambient air polluted leaves, 0.08 – 0.28 μS at 5 % – 80 % *RH* for the inorganic treated leaves, 0.05 – 0.11 μS at 44 % – 80 % *RH* for the humic acid treated leaves and 0.15 – 1.11 μS at 44 % – 72 % *RH* for halogenic treated leaves.

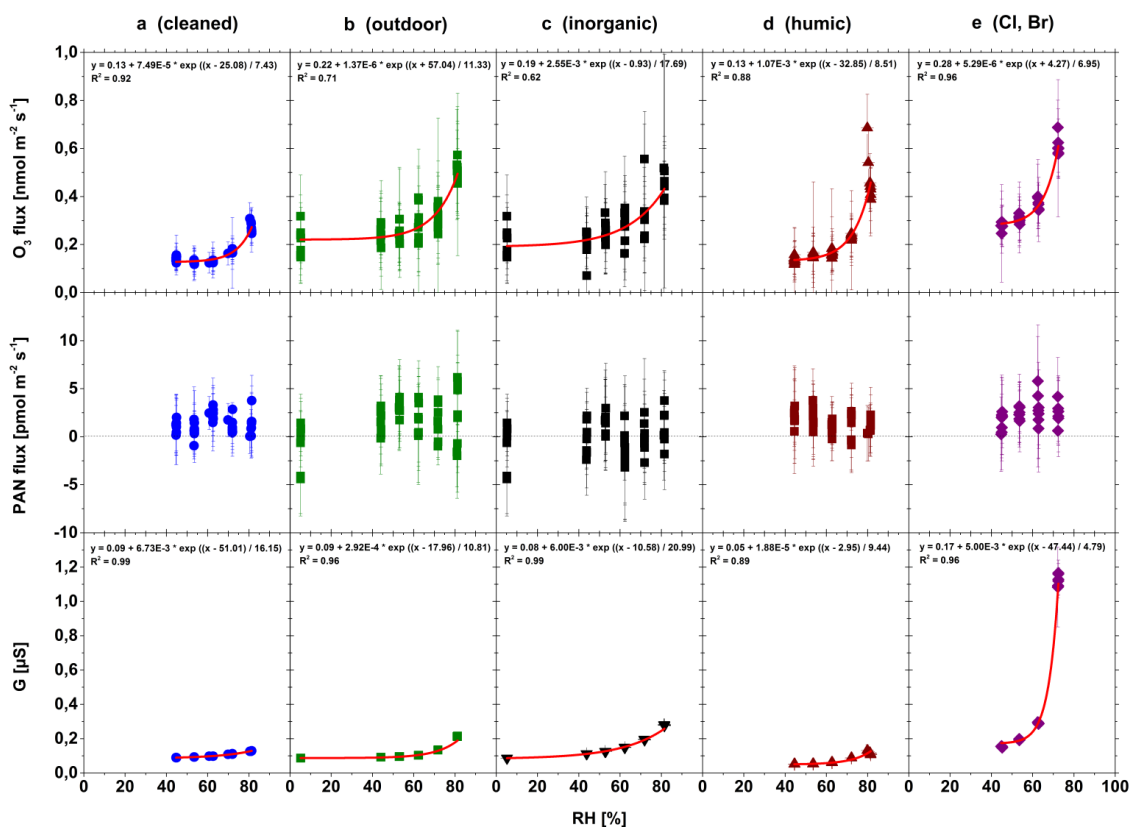


Fig. 7: O<sub>3</sub>, PAN flux and electrical surface conductance *G* at various *RH* (5 % - 80 %) during the dark period under ABA induced stomatal closure. Cleaned leaf surface (column a), exposed with outdoor air (column b), treated with inorganic solution (column c), treated with humic acid (column d) and treated with Cl, Br (column e). The increasing trend was fitted with an exponential growth function.

As we found particles originating from air pollution to affect the non-stomatal deposition after exposure to outdoor air, we determined the loading of the leaf surface by foliar rinsing and subsequent chemical analysis. The DOC concentration of the rinsing water sample was 2.7 mg L<sup>-1</sup> and the TOC concentration was 3.7 mg L<sup>-1</sup>. Hence, 73 % of the total organic carbon was contained in the dissolved fraction. The Br<sup>-</sup> concentration was negligible with < 0.05 mg L<sup>-1</sup> (see Table 2). The Cl<sup>-</sup> concentration was 1.04 mg L<sup>-1</sup>. As expected, the humic acid solution showed a higher TOC concentration of 180 mg L<sup>-1</sup> than the rinsing water sample. The DOC concentration contributed with 130 mg L<sup>-1</sup> to 72 % of the TOC.

Table 2: The content of the total organic carbon (TOC), dissolved organic carbon (DOC), Cl<sup>-</sup> and Br<sup>-</sup> derived from foliar rinsing of the branch leaves (*Quercus ilex*) exposed to outdoor air, and of the humic acid spray solution. nd: not determined.

	DOC mg L <sup>-1</sup>	TOC mg L <sup>-1</sup>	Br <sup>-</sup> mg L <sup>-1</sup>	Cl <sup>-</sup> mg L <sup>-1</sup>
Test method		EN 1484	DIN EN ISO 10304-1	
Leaf wash water	2.7	3.7	< 0.05	1.04
Humic acid	130	180	nd	nd

## 4 Discussion

### 4.1 Stomatal and non-stomatal deposition after exposure to outdoor air conditions

The measured O<sub>3</sub> deposition flux was linearly correlated with increasing *RH* during the light and “dark\_cont” periods (see Figure 2a-b). Under light conditions it is well known that, besides other environmental variables, relative humidity influences the stomata response [Lange et al., 1971; Farquhar et al., 1987; Schulze et al., 1987; Monteith, 1995]. We showed in this study that the stomatal conductance increased with rising *RH* in the dynamic cuvette (Figure 3), which can be explained by the decrease of the peristomatal water loss results in a restitution of the turgescence and consequently inducing the stomata to open under elevated humidity condition [Lange et al., 1971]. As a result, the stomatal uptake of O<sub>3</sub> will be enhanced at high *RH* (see Figure 2c-d). Under dark conditions the stomatal uptake of O<sub>3</sub> is expected to be negligible [Mikkelsen et al., 2004] due to the low stomatal activity. However, a slight opening of the leaf stomata in the absence of light cannot be fully excluded. Mairgareth et al. [2007] concluded that the stomatal conductance at night is regulated by diverse range of C<sub>3</sub> and C<sub>4</sub> plants similar to the daytime regulation. However, our observed O<sub>3</sub> deposition during periods “dark\_alter” and “dark\_cont” could be mainly attributed to non-stomatal deposition of O<sub>3</sub> as the O<sub>3</sub> flux and  $g_{s,calc}(H_2O)$  did not correlate (see Figure 2c). The same non-correlated trend can also be observed for the O<sub>3</sub> flux and  $g_{s,calc}(H_2O)$  of the plant branch treated with ABA, where stomatal closure was induced by the addition of the plant hormone. The influence of surface water evaporation on the calculation of the stomatal conductance

from the measured water vapor flux was found to be quite small during our experiments, as a comparison of the ABA experiment with the Flux experiment 1 under light condition shows that the averaged stomatal conductance of the ABA experiment is only 4.3 % of that from the flux experiment 1 under light condition. In contrast to “dark\_cont”, no correlation was found between the O<sub>3</sub> deposition flux and the rising *RH* during the “dark\_alter” conditions. We assume that the different experimental performances (see Sect. 2.3) might be responsible for the different results. At the first experiment “dark\_alter”, the plant sample was influenced by the diurnal cycle of light, while the second experiment “dark\_cont” was performed completely under dark conditions. The periodical influence by the light could be responsible for the non *RH*-correlated O<sub>3</sub> deposition. Furthermore, considering the error bars, it has to be kept in mind that the data points of „dark\_cont“ and “dark\_alter” do not differ significantly from each other, especially between 40 – 65 % *RH*. However, we are confident that the data from “dark\_cont” are largely reliable due to their agreement with the data from the ABA experiment (see Fig. 6 and 7).

In many previous field studies, O<sub>3</sub> deposition was observed at night [Fowler et al., 2001; Gerosa et al., 2005; Altimir et al., 2006; Rannik et al., 2009; Plake et al., 2015]. One cause of the nocturnal O<sub>3</sub> loss is the surface deposition to plants [Fowler et al., 2001; Altimir et al., 2006]. Fuentes and Gillespie [1992] observed a correlation between the O<sub>3</sub> deposition flux and the leaf surface moisture. Our experiments confirm the observed enhancement of the O<sub>3</sub> deposition with rising *RH* (see Figure 2a-b) under different simulated environmental conditions. The observed electrical surface conductance (*G*) correlated with *RH*, which indicated the formation of liquid surface films on the leaves above 40 – 50 % *RH* (see Figure 5). This is in accordance with Burkhardt and Gerchau [1994], who detected leaf wetness at a humidity level of 70 % *RH*. Furthermore, Altimir et al. [2006] identified a threshold for the generation of a liquid surface film at 60 % - 70 % *RH*. The variation of these values may be due to the assumption that  $RH_{crit}$  could be depending on the chemical composition of the surface [Sumner et al., 2004]. As already mentioned above (Sect. 1), the formation of liquid films occurred via different growth stages to form continuous liquid surface films. This could be shown by the exponential increase of the *G*-value through these different stages (Figure 5). Furthermore, we observed significant higher *G* values above 40 – 50 % *RH* during the light period than for the dark period, which can be explained by the general temperature dependency of the electrical conductivity itself. Kuyucak and Chung [1994] described in a simple microscopic model the temperature dependence of conductivity in electrolyte solutions and ionic channel in bio membranes. They concluded the hydration process of ions to be the key factor for the temperature dependency and explained it by the influence of ion-dipole and dipole-dipole bonding on the effective radius and mass of the ions, which led to an increase of the conductivity with rising temperature. Further possible explanation could be based on the

deliquescence of salt crystals deposits on the leaf surface. Zeng *et al.* [2014] showed that depending on the type of salt crystals, the deliquescence relative humidity (*DRH*), at which the salt crystals start to become liquid decreases with rising temperature. Accordingly, the *DRH* will be reduced under light conditions due to the higher cuvette temperature. Therefore, the deliquescence process under light conditions starts at a lower *DRH* than under dark conditions (~ 40 % *RH<sub>crit</sub>* during the light period and ~ 50 % *RH<sub>crit</sub>* during the dark period), which explains the higher *G* value of the formed water film under light conditions than under dark conditions. Also, this implies that under light conditions the liquid surface film exhibited a slightly higher contribution to the O<sub>3</sub> deposition, as shown in Figure 6 and Figure 7.

In the case of PAN, a similar linear correlation with *RH* was found in the presence of light (see Figure 2b), which was mostly due to the stomatal uptake of PAN. In the dark period, no relationship with *RH* was found at all, which may be related to the chemical and physical properties of PAN. Compared with O<sub>3</sub>, PAN has a lower solubility in water. The Henry's law constant for PAN in acidic water was reported by Holdren *et al.* [1984] as  $5 \pm 1 \text{ M atm}^{-1}$  at 10°C and  $4.1 \text{ M atm}^{-1}$  at 20°C in distilled water [Kames and Schurath, 1995]. Additionally, the deposition velocity of PAN to water surfaces was found to be low (approximately  $8.0 \cdot 10^{-3} \text{ cm s}^{-1}$ ; [Garland and Penkett, 1976]). Therefore, the aqueous partitioning of PAN is assumed to be less than for O<sub>3</sub>.

As mentioned in Sect. 3.1,  $R_{nsto/sto}$  ( $0.21 - 0.40 \pm 0.05$  for O<sub>3</sub> and  $0.29 - 0.26 \pm 0.11$  for PAN) and  $R_{nsto/tot}$  ( $0.18 - 0.30 \pm 0.04$  for O<sub>3</sub> and  $0.21 - 0.23 \pm 0.10$  for PAN) was related to *RH* (40 – 80 %) (see Figure 4). As we performed flux measurement of above ground parts of trees under controlled laboratory conditions with a low residence time of 3.4 min inside the cuvette, gas phase reactions as discussed in [Jud *et al.*, 2016] and other non-stomatal sink pathways such as soil deposition can be excluded [Sun *et al.*, 2016]. Depending on the *RH*, up to 30 % of the total O<sub>3</sub> deposition flux and 20 % of the total PAN deposition flux is associated with the non-stomatal deposition to leaf and stem surfaces. The seasonal effect on the plant could play a role (experiments were conducted in the month of February), which may result in limiting plant transpiration and stomatal activity [Oh and Koh, 2014]. As the stem surface was maximal 4 % of the leaf surface, the loss of O<sub>3</sub> and PAN to the stem could be neglected.

To our knowledge no comparable and conclusive laboratory studies on the flux partitioning of O<sub>3</sub> and PAN have been conducted in the past. Instead we can compare our branch/leaf-level studies with studies on ecosystem scale, where we have to face much more complexity, however. Fares *et al.* [2012] modeled  $R_{nsto/tot}$  (O<sub>3</sub>) of 0.44 for orange orchard trees for the winter time considering cuticular and gas phase sinks as the non-stomatal contribution. For our experiment the gas phase contribution to the O<sub>3</sub> sink was negligible due to the short residence time within the cuvettes [Sun *et al.*, 2016]. Furthermore, liquid water films are supposed to serve as a diffusion barrier for cuticular plant emissions, which scavenge O<sub>3</sub> as in the case of *Nicotiana tabacum* [Jud *et al.*, 2016]. Therefore, if compounds emitted through the

leaf cuticles are supposed to play a role in non-stomatal loss of O<sub>3</sub>, the deposition flux should decrease as soon as the formation of a liquid film is observed due to the formation of a diffusion barrier for both O<sub>3</sub> ( $D_{\text{O}_3,\text{air}} = 0.137 \text{ cm}^2 \text{ s}^{-1}$  [Laisk et al., 1989]  $\gg D_{\text{O}_3,\text{H}_2\text{O}} = 1.76 \cdot 10^{-5} \text{ cm}^2 \text{ s}^{-1}$  [Johnson and Davis, 1996]) and the excreted compounds. As O<sub>3</sub> fluxes always increased with *RH* (see Figure 2a), we rather believe that the compounds dissolved in the liquid film are responsible for the larger uptake. This is indicated as well by the higher fluxes of O<sub>3</sub> towards leaves exposed to ambient air (deposited particles) than towards the same leaves cleaned with purified water (see Figure 6 and Figure 7). For a mixed hardwood forest, Hogg et al. [2007] determined  $R_{\text{nsto}/\text{tot}}$  of 0.63 and even  $R_{\text{nsto}/\text{sto}} > 1$ , which showed the dominance of the non-stomatal deposition. Furthermore, Lamaud et al. [2009] determined the partitioning of O<sub>3</sub> deposition over maize crops and obtained values ranging between 0.5 and 0.8 for  $R_{\text{nsto}/\text{tot}}$ , for *RH* ranging between 50 % and 90 %. Additionally, Plake et al. [2015] found a non-stomatal contribution of 73 % to the total O<sub>3</sub> deposition at a natural grassland site. The results from these previous studies exceed our value of  $R_{\text{nsto}/\text{tot}}(\text{O}_3) = 0.3$ . This discrepancy might be due to the fact that under field conditions additional environmental factors are important for the deposition process. In contrast, laboratory experiments are more suitable to investigate the underlying mechanisms of non-stomatal surface deposition of O<sub>3</sub> and PAN on plants because different factors can be analyzed separately. Our experiments under controlled laboratory conditions show that even without the influence of additional environmental factors the cuticular deposition of O<sub>3</sub> significantly contributes to the total O<sub>3</sub> deposition, even at  $< 50 \%$  *RH*. This conclusion seems to be contradictory to the results of Sun et al. [2016], where no contribution of non-stomatal deposition of O<sub>3</sub> at 40 % *RH* under laboratory conditions is reported. However, on the one hand the tree sample used for the experiment in Sun et al. [2016] was completely grown under greenhouse conditions. Therefore, the composition of the deposited particles on the leaf surface was most likely different and was potentially less reactive to O<sub>3</sub>. On the other hand, comparing the measured non-stomatal fluxes and their uncertainties in both studies,  $0.20 \pm 0.14 \text{ nmol m}^{-2} \text{ s}^{-1}$  at 42 % *RH* of this study (see Figure 2a) and  $0.12 \pm 0.10 \text{ nmol m}^{-2} \text{ s}^{-1}$  (almost indistinguishable from zero) at 40 % *RH* of Sun et al. [2016], it cannot be excluded that at 40 % *RH* a small non-stomatal sink was also present in Sun et al. [2016].

For PAN, the  $R_{\text{nsto}/\text{sto}}$  as well as the  $R_{\text{nsto}/\text{tot}}$  values declines slightly with higher *RH*, which seems to be due to the decrease of the non-stomatal contribution of PAN. However, the decrease is insignificant considering the uncertainty (see Sect. 3.1, Figure 4). Shepson et al. [1992] assumed that the non-stomatal deposition of PAN would decrease with higher surface wetness caused by the low solubility of PAN in water and less open leaf area, where PAN can deposit. However, this assumption has not been validated by field studies yet. Both Schrimpf et al. [1996] and Moravek et al. [2015] could not find a significant dependency of non-

stomatal deposition of PAN on *RH* for a corn field and a natural grassland site, respectively. *Cape et al.* [1997] concluded that the PAN deposition close to the leaf surface is only dependent on its hydrolysis rate in aqueous film, which is quite low ( $H = 4.1 \text{ M atm}^{-1}$  at 20 °C). *Turnipseed et al.* [2006] found an increase of non-stomatal deposition under wet conditions for a pine forest ecosystem. They suspect that there is a reactive uptake process responsible for the enhanced deposition. Although, the work of *Frenzel et al.* [2000] provides some evidence for enhanced PAN uptake, this was not observed for the compounds we used.  $F_{nsto}$  values derived in field studies are typically based on nighttime fluxes, where turbulent transport is typically limited and therefore flux uncertainties are often quite large. Additionally, it cannot be excluded that the leaf stomata were open in the absence of light, as the nighttime stomatal opening and transpiration have implications for plant growth and physiology [*Mairgareth et al.*, 2007]. Therefore, a contribution of the stomatal pathway cannot be completely excluded at nighttime. *Turnipseed et al.* [2006] showed that almost 50 % of the daytime PAN deposition was due to non-stomatal processes and they suggest them to be the dominant deposition pathways in the upper canopy. Furthermore, *Wolfe et al.* [2009] found 21 - 35 % of the PAN deposition flux to be non-stomatal for a pine forest. *Moravek et al.* [2015] determined stomatal and non-stomatal pathways of PAN deposition for a grassland ecosystem of equal strength under daytime conditions. The non-stomatal contribution of ~20 % to the total PAN deposition, as found in our study, was at the lower end of the non-stomatal deposition values as reported for field studies. These different conclusions suggest that the deposition of PAN is depending on many environmental parameters such as light, relative humidity, temperature and consistency of natural surfaces. The studies, where the PAN deposition was concluded as mainly stomatal controlled were performed under laboratory conditions [*Okano et al.*, 1990; *Sparks et al.*, 2003; *Teklemariam and Sparks*, 2004], while the significant contribution of non-stomatal PAN deposition was observed in field studies (*Turnipseed et al.*, 2006; *Wolfe et al.*, 2009; *Moravek et al.*, 2015]. However, the term “non-stomatal” comprises much more contributions if derived from field measurements. Furthermore, the environmental conditions in the field are much more complex than it can be simulated in the laboratory. Hence, the challenge for future studies is to identify the reasons for the observed non-stomatal PAN deposition in the field. A further interesting point would be the comparison of the O<sub>3</sub> and PAN deposition between different plant species. As well-known, the stomatal behavior differs between the plant species [*Tardieu and Simonneau*, 1997]. Therefore, the contribution of water films to the non-stomatal deposition in relation to the total deposition of O<sub>3</sub> should vary among different plant species due to the variation of their stomatal conductance. However, for our experiments, the focus was on the demonstration of a convenient experimental setup and the application of *Quercus ilex* as a model species to show the effect of water films on the deposition of O<sub>3</sub> and PAN.

In state of the art regional and global deposition models the non-stomatal PAN deposition is typically derived assuming a certain reactivity of PAN with the underlying surface. E.g. in the EMEP model [Simpson et al., 2012] the non-stomatal deposition pathway is based on the non-stomatal conductance of sulfur dioxide ( $G_{ns}SO_2$ ) and O<sub>3</sub> ( $G_{ns}O_3$ ):

$$G_{ns}(PAN) = 10^{-5} \times H_{*,PAN} \times G_{ns}(SO_2) + f_{0,PAN} \times G_{ns}(O_3) \quad (8)$$

$H_{*,PAN}$  is the solubility index for PAN, which is very low compared to SO<sub>2</sub> ( $H_{*,PAN} = 4.1 \text{ M atm}^{-1}$  at 20°C [Kames and Schurath, 1995],  $H_{*,SO_2} = 10^5 \text{ M atm}^{-1}$ ), which is why the first term can be neglected for PAN.  $f_{0,PAN}$  is the reactivity index for PAN, which is assumed to be 0.1 according Wesley [1989]. In comparison, the reactivity of O<sub>3</sub> is considered  $f_{0,O_3} = 1$ , resulting in a much larger deposition than PAN. However, as also discussed in Moravek et al. [2015], depending on the used  $f_0$ -factors the results differ considerably. For example, in GEOS-chem a PAN reactivity of  $f_0 = 1$  was recently implemented [Fischer et al, 2014], which implied equal strength of PAN and O<sub>3</sub> non-stomatal deposition. Assuming  $f_{0,O_3} = 1$ ,  $f_{0,PAN}$  can be inferred also from the ratio of velocities of PAN and O<sub>3</sub> ( $V_d(PAN) / V_d(O_3)$ ). In our study, the ratio of the non-stomatal deposition velocities is the highest with 0.95 at 40% RH and decreases with increasing RH to 0.40 at 80% RH (Figure 8).

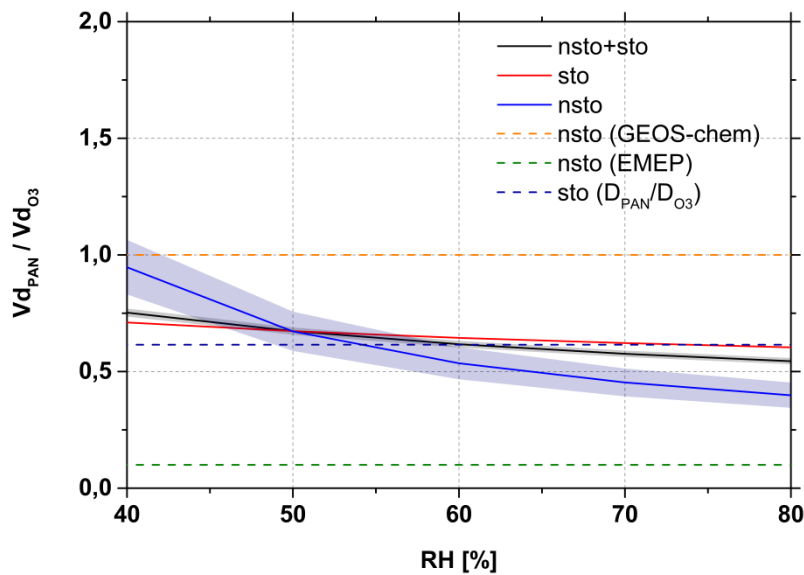


Figure 8: Deposition velocity ratio between PAN and O<sub>3</sub> of different deposition pathways nsto+sto (black), sto (red) and nsto (blue) in relation to RH compared with various modelled deposition velocity ratio as GEOS-chem (orange dashed), EMEP (green, dashed) and  $D_{PAN}/D_{O_3}$  (blue, dashed). The shaded uncertainty areas of the deposition velocity ratios were propagated considering the errors of the stomatal and non-stomatal fluxes and deposition velocities of O<sub>3</sub> and PAN

Hence, during dry conditions the reactivity of both PAN and O<sub>3</sub> can be considered as equal,

whereas at humid conditions the non-stomatal O<sub>3</sub> uptake becomes more dominant. Also Zhang et al. (2003) found in the revised deposition model that during nighttime when the canopies are wetted by dew, the O<sub>3</sub> deposition velocity is higher compared to dry conditions. This shows the importance of incorporating the *RH* dependency of the non-stomatal O<sub>3</sub> uptake, especially in models where  $G_{ns}(PAN)$  is estimated as a function of  $G_{ns}(O_3)$  (see Eq. (8)). For the stomatal  $V_d$ -ratio, the values compare well with the ratio of PAN to O<sub>3</sub> diffusion coefficients given as  $D_{PAN}/D_{O_3} = 0.61$  [Wesley, 1989]. This indicates that there is no additional mesophyll resistance for PAN uptake (assuming no mesophyll resistance for O<sub>3</sub>) as the difference in the stomatal uptake of PAN and O<sub>3</sub> can be solely attributed to the differences in the diffusion into the stomata. Our values of 0.4 – 0.5 for the non-stomatal  $V_d$  – ratio in a range of 65 – 80 % *RH* is comparable with the nighttime results of previous field studies such as Hill (1971), Garland and Penkett (1976), Shepson et al. (1992) and Wolfe et al. (2009). Further, Wolfe et al. (2009) found a  $V_d$  – ratio of 1.3 at daytime, which indicates a higher  $V_d(PAN)$  than  $V_d(O_3)$ . At our laboratory study, we did not observe a  $V_d$  – ratio > 1 under daytime conditions. Our max  $V_d$  – ratio was 0.75 at 40 % *RH*.

## 4.2 Influence of leaf surface and liquid surface films on non-stomatal deposition

Based on the findings by Fuentes and Gillespie [1992], who argued that dissolved substances in the water film are able to scavenge O<sub>3</sub> via chemical reactions, we treated the leaf surface of sample branches with various inorganic and organic chemical compounds (see Sect. 2.4, Table 1) and measured the deposition flux of O<sub>3</sub> and PAN under light and dark conditions as well as at various *RH*. As a complete closing of the leaf stomata in the absence of light cannot be assumed, the plant material was treated with ABA to exclude the influence of the stomatal deposition of O<sub>3</sub> and PAN. The experimental data showed that the *G* values were different depending on the used chemical compounds under both light and dark conditions (see Figure 6 and Figure 7) with the following sequence of increasing *G* values:  $G_{humic} < G_{cleaned} < G_{outdoor} < G_{inorg} < G_{halogen}$ . The highest *G* values were found for the leaves treated with chloride / bromide solution and the lowest in the case of humic acid treated leaves. This is in disagreement with the idea that the lowest *G* values would be expected for the cleaned plant leaves. However, it is likely that the cleaning process did not remove all deposited particles and compounds on the leaf surface. Burkhardt et al. [2001] concluded that hygroscopic salt particles liquitate at elevated humidity on the surface of plant leaves and can form amorphous crusts, which cannot be removed easily by washing and leads to a higher wettability of the leaves with increasing age. The lowest *G* values of the humic acid solution can also be explained by high molecular organic substances, which have lower electrical conductivity than inorganic salt, resulting from its weaker electrolytic dissociation [Lockhart, 1981].



Furthermore, humic acid is able to reduce the ionic mobility and thus decrease the electrical conductivity [Riggle and Wandruszka, 2004]. The G values of the leaves treated with inorganic solution were slightly higher than that of the leaves exposed to outdoor air, which can be explained by the chemical composition of the leaf surface liquid films. The inorganic solution comprises different inorganic salts (see Table 1), which have high dissociation potential in aqueous solution. In the case of the leaves exposed to outdoor air the surface was coated with a mixture of different organic and inorganic compounds (see Table 2), where the electrical conductivity of the inorganic compounds may be compensated by the organic fraction, resulting in a lower total electrical conductance. The halogenic solution consists of chloride and bromide, and showed the highest G values due to its higher ionic concentration compared to the inorganic solution (see Table 1).

The O<sub>3</sub> fluxes for leaves exposed to the outdoor air showed similar values as the flux for the leaves treated with inorganic solution. As mentioned in Sect. 2.4, the compounds of the inorganic solution were selected from the relative fractions of a typical fine particulate matter [Li et al., 2015], considering that the concentration of the artificial solution on the leaf surface might be higher than its primary solution due to dry out. Nevertheless, the measurements of outdoor exposed leaves and those of the inorganic solution treatment (“typical inorganic aerosol composition”) are quite similar with respect to both, conductivity values and O<sub>3</sub> fluxes, which might imply a dominant role of inorganic components as O<sub>3</sub> is well known to react efficiently with these species [Hoigné et al., 1985; Liu et al., 2001]. However, we observed a clear enhancement of the O<sub>3</sub> deposition flux with rising RH by the humic acid treated leaves as well (see Figure 6d and Figure 7d), which represents the reactivity potential of the organic compounds with O<sub>3</sub>. It is well known that O<sub>3</sub> is able to react with double bonded molecules such as alkenes [Criegee, 1975; Geletneky and Berger, 1998]. Humic acid are known to destroy O<sub>3</sub> in solution [e.g. Hoigné and Bader, 1983; Staehelin and Hoigné, 1985]. However, TOC and DOC values were about a factor of 50 higher on humic acid treated leaves. As shown in Table 2, 86 % of the TOC was dissolved in the aqueous solution. A recent study on tobacco plants [Jud et al., 2016] showed that specific compounds excreted by the plants react very efficiently with O<sub>3</sub> at the leaf surface. Whether this process will be enhanced (higher reaction rates in solution) or hindered (lower diffusion) by formation of the liquid film remains open. Another mechanism was proposed by Potier et al. [2015] that reproduced the increase of O<sub>3</sub> deposition by adjusting the reaction rate of O<sub>3</sub> in epicuticular liquid films to values corresponding to the reaction rate with ascorbate in plant cells in modelling study. They conclude that during senescence, especially when leaves are wet, apoplastic anti-oxidants leak out to the leaf surface and react with O<sub>3</sub>. Furthermore, Feng and Legube [1991] found that the radical decomposition of O<sub>3</sub> in water by fulvic acid (fraction of humic acid with lower molecular weight) is promoted with rising pH, while there is no radical decomposition of O<sub>3</sub> at a strong acidic pH (pH =2). In this study, the pH of the humic acid solution was 7,

although the resulting pH of the rewetted surface film might differ from that of the original solution but could not be measured in this study. There are some indications that evaporating films get more acidic [Klemm, 1988]. Nevertheless, the radical decomposition of O<sub>3</sub> by the fulvic acid could also contribute to the observed enhancement of the O<sub>3</sub> deposition. The leaves treated with chloride and bromide showed the strongest enhancement of the O<sub>3</sub> deposition with rising *RH*. Obviously, these halogen compounds dissolved in the water films on the leaf surface are able to scavenge O<sub>3</sub> very efficiently [Razumovskii et al., 2010; Rayne and Forest, 2014]. Both reaction pathways (reaction with humic/fulvic acids and halogens) are well known as side reactions in drinking water ozonation [e.g. Haag and Hoigné, 1983; Hoigne and Bader, 1983; Hoigné et al., 1985; Staehelin and Hoigné, 1985; Liu et al., 2001; Levanov et al., 2003]. As Hoigné et al. (1985) found that most inorganic compounds only react with O<sub>3</sub> in their dissociated form. In acidic solutions, most of them are strongly or fully shielded when their reactive site becomes protonated. Therefore, the reactivity of such compounds to O<sub>3</sub> decreases with declining pH. Therefore, depending on the chemical compounds on the leaf surface, the surface deposition of O<sub>3</sub> may decline when liquid films become acidic.

In general, we observed a clear contribution of non-stomatal O<sub>3</sub> deposition in relation to *RH* and surface coatings for all experiments.

As mentioned in Sect. 4.1, our results revealed a contribution of ~20 %, (see Figure 4) of non-stomatal deposition for PAN to the total deposition, but no clear relationship between the deposition flux and *RH* was found for the different leaf surface coatings. On the one hand, the results revealed that PAN is chemically inert against the used compounds and imply that the variation of the deposition of PAN on plants is mainly controlled by plant stomata. This conclusion confirms results of previous laboratory studies by Okano et al. [1990], Sparks et al. [2003] and Teklemariam and Sparks [2004]. On the other hand, a larger non-stomatal deposition pathway has been observed in past field experiments (see discussion in Sect. 4.1). As an additional sink for atmospheric PAN, gas phase reactions with PAN are also possible and may contribute to the larger non-stomatal PAN deposition. For example, reaction of PAN with aldehydes was reported by Wendschuh et al. [1973]. It was concluded that the addition of aldehydes to PAN resulted in the oxidation of the aldehyde to the corresponding acid with a yield of approximately 85 %. Nevertheless, in our laboratory measurements we found no evidence for an additional PAN loss in the liquid phase. If at all, there was a slight decrease in non-stomatal PAN uptake due to the formation of the water films.

## 5 Conclusion

We demonstrate the suitability of a laboratory dynamic twin-cuvette system for simultaneous measurements of O<sub>3</sub> and PAN deposition fluxes to plants. The system allows for systematic determination and investigation of stomatal and non-stomatal deposition pathways including the formation of liquid water films on the leaves.

We observed a clear correlation between the O<sub>3</sub> deposition to plants (*Quercus ilex*), the relative humidity and the stomatal conductance at both, light and dark conditions. During the light period the increase of the O<sub>3</sub> deposition was partly explained by opening of leaf stomata under rising *RH*, while during the absence of light liquid surface films were responsible for the enhancement of the O<sub>3</sub> deposition as proven by experiments with plants treated with ABA. In the case of PAN, a similar linear correlation with *RH* was found in the presence of light, which was due to the stomatal uptake of PAN. In the dark period, no relationship with *RH* was found, which may be explained by the lower aqueous partitioning for PAN.

The flux partitioning ratio between non-stomatal and stomatal deposition as well as between non-stomatal and total deposition was found to be  $R_{nsto/sto} = (0.21 - 0.40) \pm 0.05$ ,  $R_{nsto/tot} = (0.18 - 0.30) \pm 0.04$  for O<sub>3</sub> and  $R_{nsto/sto} = (0.26 - 0.29) \pm 0.11$ ,  $R_{nsto/tot} = (0.21 - 0.23) \pm 0.10$  for PAN at 40 – 80 % *RH* and the annual season of February (plant activity). The nonstomatal contributions found in our study are in the lower range or below the contributions calculated from field experiments. As in our laboratory setup environmental variables (light, temperature, humidity) were controlled and the residence time of air inside the cuvette was low, the change in fluxes could be related to stomatal opening and the formation of liquid water films. On the contrary, additional factors (esp. gas phase reactions, different compounds on leaf surface) are expected to play a role under field conditions, which may explain the higher non-stomatal contribution. The determined  $V_d$ -ratios between PAN and O<sub>3</sub> for the different depositions pathways: non-stomatal = 0.40 – 0.95, stomatal = 0.61 – 0.71 and total = 0.55 – 0.75, in relation to the relative humidity may help improving the estimation of the deposition velocity for PAN in models.

The formation of the leaf surface films was found to be depending on the chemical composition of the particles deposited on the leaf cuticles, which is in line with *Burkhardt et al.* [2001]. Accordingly, the O<sub>3</sub> deposition was also influenced by the species of the deposited particles dissolved in the liquid surface films, which provide a chemical loss pathway in the liquid phase. The experimental data show that the *G* values were depending on the used chemical compounds under both light and dark conditions.

Finally, we show that the liquid surface film significantly contributes (up to 30 %) to the total deposition of O<sub>3</sub>, which varied with changing humidity. For PAN, a significant contribution (~ 20 %) of non-stomatal deposition was observed, which was not significantly affected by

liquid surface films. Therefore, the variation of the deposition of PAN to plants appears to be mostly stomatal controlled, which is in line with other laboratory studies. Furthermore, we demonstrated that the formation of the liquid surface film on leaves and the non-stomatal O<sub>3</sub> flux were depending on the chemical composition of the particles deposited on the leaf cuticles. These differences in the non-stomatal uptake ratio affect the deposition velocities of PAN and O<sub>3</sub>, which is currently not considered in state-of-the-art deposition models.

## References

- Altimir, N., P. Kolari, J. P. Tuovinen, T. Vesala, J. Bäck, T. Suni, M. Kulmala, and P. Hari (2006), Foliage surface ozone deposition: a role for surface moisture?, *Biogeosciences*, 3, 1-20.
- Brewer, C. A. and W. K. Smith (1997), Patterns of leaf surface wetness for montane and subalpine plants, *Plant Cell Env.*, 20, 1–11.
- Burkhardt, J. and R. Eiden (1994), Thin water films on coniferous needles, *Atmospheric Environment*, 28(12), 2001-2011.
- Burkhardt, J. and J. Gerchau (1994), A new device for the study of water-vapor condensation and gaseous deposition to plant-surfaces and particle samples, *Atmospheric Environment*, 28(12), 2012-2017.
- Burkhardt, J., H. Kaiser, H. Goldbach, and L. Kappen (1999), Measurements of electrical leaf surface conductance reveal recondensation of transpired water vapour on leaf surfaces, *Plant Cell and Environment*, 22, 189–196.
- Burkhardt, J., K. Koch, and H. Kaiser (2001), Deliquescence of deposited atmospheric particles on leaf surfaces, *Water, Air and Soil Pollution, Focus*, 1, 313-321.
- Burkhardt, J. and M. Hunsche (2013), „Breath figures” on leaf surfaces formation and effects of microscopic leaf wetness, *Plant science*, 4(422), doi: 10.3389/fpls.2013.00422, 1 – 9.
- Cape J. N. (1983), Contact angles of water droplets on needles of Scots pine (*Pinus sylvestris*) growing in polluted atmospheres, *New Phytol*, 93, 293-299.
- Cape J. N. (1988), Chemical interactions between cloud droplets and trees. In *Acid Deposition at High Elevation Sites* (edited by Unsworth M. H. and Fowler D.), pp. 639-649.
- Cape, J. N. (1997), Photochemical Oxidants - What Else is in the Atmosphere besides

- Ozone?, *Phyton, Annales Rei Botanicae, Horn*, 37, 45-58.
- Cape, J. N., R. Hamilton, and M. R. Heal (2009), Reactive uptake of ozone at simulated leaf surfaces: implications for 'non-stomatal' ozone flux, *Atmospheric Environment*, 43, 1116-1123.
- Chameides, W. L. and A. W. Stelson (1992), Aqueous-Phase Chemical Processes in Deliquescent Sea-Salt Aerosols: A Mechanism That Couples the Atmospheric Cycles of S and Sea Salt, *Journal of Geophysical Research-Atmospheres*, 97(D18), 20565-20580.
- Criegee, R. (1975), Mechanism of Ozonolysis, *Angewandte Chemie international edition*, 14(11), 745-752.
- Crutzen, P. J. (1979), Role of NO and NO<sub>2</sub> in the chemistry of the troposphere and stratosphere, *Annual Review of Earth and Planetary Sciences*, 7, 443-472.
- Doskey, P. V., V. R. Kotamarthi, Y. Fukui, D. R. Cook, F. W. Breitbeil, and M. L. Wesely (2004), Air-surface exchange of peroxyacetyl nitrate at a grassland site, *J. Geophys. Res.-Atmos.*, 109, D10310, doi:10.1029/2004JD004533.
- Farquhar, G. D. (1987), Feedforward Response of Stomata to humidity, *Australian Journal of Plant Physiology*, 5(6), 787-800.
- Fares, S., R. Weber, J. H. Park, D. Gentner, J. Karlik, and A. H. Goldstein (2012), Ozone deposition on orange orchard: Partitioning between stomatal and non-stomatal sinks, *Environmental Pollution*, 169, 258-266..
- Feng, X. and B. Legube (1991), Enhancement of radical chain-reactions of ozone in water in the presence of an aquatic fulvic-acid, *Ozone-science and Engineering*, 13(3), 349-363.
- Fischer, E. V., D. A. Jaffe, and E. C. Weatherhead (2011), Free tropospheric peroxyacetyl nitrate (PAN) and ozone at Mount Bachelor: potential causes of variability and timescale for trend detection, *Atmospheric Chemistry and Physics*, 11(12), 5641-5654.
- Fischer, E. V., D. J. Jacob, R. M. Yantosca, M. P. Sulprizio, D. B. Millet, J. Mao, F. Paulot, H. B. Singh, A. Roiger, L. Ries, R. W. Talbot, K. Dzepina, and S. Pandey Deolal (2014), Atmospheric peroxyacetyl nitrate (PAN): a global budget and source attribution, *Atmos. Chem. Phys.*, 14, 2679-2698, doi:10.5194/acp-14-2679-2014.
- Flechar, C. R., D. Fowler, M. A. Sutton, and J. N. Cape (1999), A dynamic chemical model of bi-directional ammonia exchange between semi-natural vegetation and the atmosphere, *Quarterly Journal of the Royal Meteorology Society*, 125, 2611-2641.
- Fowler D., C. Flechar, J. N. Cape, R. L. Storeton-West, and M. Coyle (2001), Measurements of ozone deposition to vegetation quantifying the flux, the stomatal and non-stomatal components, *Water Air and Soil Pollution*, 130(1-4), 63-74.

- Frenzel, A., S. Kutsuna, K. Takeuchi, T. Ibusuki (2000), Solubility and reactivity of peroxyacetyl nitrate (PAN) in dilute aqueous salt solutions and in sulphuric acid, *Atmospheric Environment*, 34, 3641 – 3644.
- Fuentes, J. D. and T. J. Gillespie (1992), A gas-exchange system to study the effects of leaf surface wetness on the deposition of ozone, *Atmospheric Environment*, 26(6), 1165-1173.
- Fuhrer, J., L. Skärby, and M. R. Ashmore (1997), Critical levels for ozone effects on vegetation in Europe, *Environmental Pollution*, 97(1-2), 91-106.
- Garland, J. A. and S. A. Penkett (1976), Absorption of peroxyacetyl nitrate and ozone by natural surfaces, *Atmos. Environ.*, 10, 1127-1131.
- Geletneky, C. and S. Berger (1998), The Mechanism of ozonolysis revisited by O-17-NMR spectroscopy, *European Journal of organic chemistry*, 8, 1625-1627.
- Gerosa, G., M. Vitale, A. Finco, F. Manes, A. B. Denti, and S. Cieslik (2005), Ozone uptake by an evergreen Mediterranean Forest (*Quercus ilex*) in Italy. Part I: Micrometeorological flux measurements and flux partitioning, *Atmospheric Environment*, 39(18), 3255-3266.
- Goff, J. A. and S. Gratch (1946), Low-pressure properties of water from -160 to 212 F, *Transactions of the American Society of Heating and Ventilating Engineers*, 52, 95-121.
- Grantz, D. A., X. J. Zhang, W. J. Massman, G. Den Hartog, H. H. Neumann, and J. R. Pederson (1995), Effects of stomatal conductance and surface wetness on ozone deposition in field-grown grape, *Atmospheric Environment*, 29(21), 3189-3198.
- Haag, W.R. and J. Hoigné (1983), Ozonation of Bromide-Containing Waters: Kinetics of Formation of Hypobromous Acid and Bromate, *Environ. Sci. Technol.*, 17, 261-267.
- Hakan, P., G. P. Karlsson, H. Danielsson, and N. G. Selldén (1995), Surface wetness enhances ozone deposition to a pasture canopy, *Atmospheric Environment*, 29(22), 3391-3393.
- Hill, A. C. (1971), Vegetation: a sink for atmospheric pollutants, *JAPCA J. Air Waste Ma.*, 21, 341-346.
- Hogg, A., J. Uddling, D. Ellsworth, M. A. Carroll, S. Pressley, B. Lamb, and C. Vogel (2007), Stomatal and non-stomatal fluxes of ozone to a northern mixed hardwood forest, *Tellus Series B-Chemical and Physical Meteorology*, 59(3), 514-525.
- Hoigné, J. and H. Bader (1983), Rate constants of reactions of ozone with organic and inorganic compounds in water – II – Dissociating organic compounds, *Water Res.*, 17, 185 – 194.
- Hoigné, J., H. Bader, W. R. Haag, and J. Staehelin (1985), Rate constants of reactions of ozone with organic and inorganic compounds in water – III – Inorganic compounds and

- radicals, *Water Res.*, *19*(8), 993-1004.
- Holdren M.W., C. W. Spicer, and J. M. Hales (1984), Peroxyacetyl nitrate solubility and decomposition rate in acidic water, *Atmospheric Environment*, *18*, 1171–1173.
- Johnson, P. N. and R. A. Davis (1996), Diffusivity of Ozone in Water, *J. Chem. Eng. Data*, *41*, 1485- 1487.
- Jud, W., L. Fischer, E. Canaval, G. Wohlfahrt, A. Tissier, and A. Hansel (2016), Plant surface reactions: an opportunistic ozone defence mechanism impacting atmospheric chemistry, *Atmos. Chem. Phys.*, *16*, 277-292.
- Kames, J., S. Schweighöfer, and U. Schurath (1991), Henry's law constant and hydrolysis of Peroxyacetyl nitrate (PAN), *Journal of Atmospheric Chemistry*, *12*(2), 169-180.
- Kames J. and U. Schurath (1995), Henry's law and hydrolysis-rate constants for peroxyacetyl nitrates (PANs) using a homogenous gas-phase source, *Journal of Atmospheric Chemistry*, *21*, 151–164.
- Klemm O. (1988), Säure / Base- und redoxchemische Simulation des Verdampfens von Niederschlagswasser von Fichtennadeln. PhD thesis, Bayreuth, Germany, pp. 214.
- Klemm, O., C. Milford, M. A. Sutton, G. Spindler, and E. van Putten (2002), Acclimatology of leaf surface wetness, *Theoretical and Applied Climatology*, *71*, 107–117.
- Kuyucak, S. and S.-H. Chung (1994), Temperature dependence of conductivity in electrolyte solutions and ionic channels of biological membranes, *Biophysical Chemistry*, *52*, 15-24.
- Laisk, A., O. Kull, and H. Moldau (1989), Ozone concentration in leaf intercellular air space is close to zero, *Plant Physiol.*, *90*, 1163–1167.
- Lamaud, E., B. Loubet, M. Irvine, P. Stella, E. Personne, and P. Cellier (2009), Partitioning of ozone deposition over a developed maize crop between stomatal and non-stomatal uptakes, using eddy-covariance flux measurements and modelling, *Agricultural and Forest Meteorology*, *149*(9), 1385-1396.
- Lammel G. (1999), Formation of nitrous acid: Parameterization and comparison with observations, Max Planck Institute for Meteorology, Hamburg, Germany, report No. 286, pp. 36.
- Lange, O. L., R. Lösch, E.-D. Schulze, and L. Kappen (1971), Response of stomatal to changes in humidity, *Planta*, *100*(1), 76-86.
- Leclerc M. Y., Thurtell G. W. and T. J. Gillespie (1985), Laboratory simulation of evaporation of water droplets on artificial soybean leaves, *Agric. For. Met.*, *36*, 105-111.
- Levanov, A.V., I. V. Kuskov, A. V. Zosimov, E. E. Antipenko, and V. V. Lunin (2003), Acid Catalysis in Reaction of Ozone with Chloride Ions, *Kinetics and Catalysis*, *44*, 740-746.

- Li, Y. J., B. P. Lee, L. Su, J. C. H. Fung, and C. K. Chan (2015), Seasonal characteristics of fine particulate matter (PM) based on high-resolution time-of-flight aerosol mass spectrometric (HR-ToF-AMS) measurements at the HKUST Supersite in Hong Kong, *Atmospheric Chemistry and Physics*, 15(1), 37-53.
- Lindberg, S. E., R. C. Harriss, and R. R. Turner (1982), Atmospheric deposition of metals to forest vegetation, *Science*, 215, 1609–1611.
- Liu, Q., L. M. Schurter, C. E. Muller, S. Aloisio, J. S. Francisco, and D. W. Margerum (2001), Kinetics and Mechanisms of Aqueous Ozone Reactions with Bromide, Sulfite, Hydrogen Sulfite, Iodide, and Nitrite Ions, *Inorg. Chem.*, 40, 4436-4442.
- Lockhart, N. C. (1981), Electrical conductivity and the surface characteristics of kaolinitic clays and clay-humic acid complexes, *Clays and Clay Minerals*, 19(6), 423-428.
- Lopez, G. P., Biebuyck, H. A., Frisbie, C. D. and G. M. Whitesides (1993), Imaging of Features on Surfaces by Condensation Figures, *Science*, 260, 647 – 649.
- Loreto, F. and S. Fares (2007), Is ozone flux inside leaves only a damage indicator? Clues from volatile isoprenoid studies, *Plant Physiology*, 143, 1096-1100.
- Mairgareth, A. C., H. R. James, and A. D. Lisa (2007), Nighttime Stomatal Conductance and Transpiration in C<sub>3</sub> and C<sub>4</sub> Plants, *Plant Physiology*, 143, 4-10.
- Mikkelsen, T. N., H. Ro-Poulsen, M. F. Hovmand, N. O. Jensen, K. Pilegaard, and A. H. Egeløv (2004), Five-year measurements of ozone fluxes to a Danish Norway spruce canopy, *Atmospheric Environment*, 38, 2361–2371.
- Monteith, J. L. (1995): A reinterpretation of stomatal response to humidity, *Plant, Cell and Environment*, 18, 357-364.
- Moravek, A., T. Foken, and I. Trebs (2014), Application of a GC-ECD for measurements of biosphere-atmosphere exchange fluxes of peroxyacetyl nitrate using the relaxed eddy accumulation and gradient method, *Atmospheric Measurement Techniques*, 7(7), 2097-2119.
- Moravek, A., P. Stella, T. Foken, and I. Trebs (2015), Influence of local air pollution on the deposition of peroxyacetyl nitrate to a nutrient-poor natural grassland ecosystem, *Atmospheric Chemistry and Physics*, 15, 899-911.
- Oh, S. and S. C. Koh (2014), Photosystem II photochemical efficiency and photosynthetic capacity in leaves of tea plant (*Camellia sinensis* L.) under winter stress in the field, *Horticulture Environment and Biotechnology*, 55(5), 363-371.
- Okano, K., K. Tobe, and A. Furukawa (1990), Foliar uptake of peroxyacetyl nitrate (PAN) by herbaceous species varying in susceptibility to this pollutant, *New Phytol.*, 114, 139–145.



- Plake, D., P. Stella, A. Moravek, J.-C. Mayer, C. Ammann, A. Held, and I. Trebs (2015), Comparison of ozone deposition measured with the dynamic chamber and the eddy covariance method, *Agriculture and Forest Meteorology*, 206, 97-112.
- Potier, E., J. Ogée, J. Jouanguy, E. Lamaud, P. Stella, E. Personne, B. Durand, N. Mascher, and B. Loubet (2015), Multilayer modelling of ozone fluxes on winter wheat reveals large deposition on wet senescing leaves, *Agriculture and Forest Meteorology*, 211-212, 58-71.
- Rannik, Ü., I. Mammarella, P. Keronen, and T. Vesala (2009), Vertical advection and nocturnal deposition of ozone over a boreal pine forest, *Atmospheric Chemistry and Physics*, 9(6), 2089-2095.
- Rayne, S. and K. Forest (2014), A G4MP2 and G4 theoretical study on reactions occurring during the ozonation of bromide containing waters, *Computational and Theoretical Chemistry*, 1031, 22-33.
- Razumovskii, S. D., M. L. Konstantinova, T. V. Grinevich, G. V. Korovina, and V. Ya. Zaitsev (2010), Mechanism and Kinetics of the Reaction of Ozone with Sodium Chloride in Aqueous Solutions, *Kinetics and Catalysis*, 51(4), 492-496, doi: 10.1134/S0023158410040051.
- Riggle, J. and R. Wandruszka (2004), Dynamic conductivity measurements in humic and fulvic acid solutions, *Talanta*, 62, 103-108.
- Roberts, J. M. and S. B. Bertman (1992), The Thermal Decomposition of Peroxyacetic Nitric Anhydride (PAN) and Peroxymethacrylic Nitric Anhydride (MPAN), *International Journal of Chemical Kinetics*, 24(3), 297-307.
- Rudich, Y., I. Benjamin, R. Naaman, E. Thomas, S. Trakhtenberg, and R. Ussyshkin (2000), Wetting of hydrophobic organic surfaces and its implications to organic aerosols in the atmosphere, *J. Phys. Chem. A*, 104, 5238-5245.
- Schrimpf, W., K. Lienaerts, K. P. Müller, J. Rudolph, R. Neubert, W. Schübler, and I. Levin (1996), Dry deposition of peroxyacetyl nitrate (PAN): Determination of its deposition velocity at night from measurements of the atmospheric PAN and (222) Radon concentration gradient, *Geophysical Research Letters*, 23(24), 3599-3602.
- Schulze, E.-D., N. C. Turner, T. Gollan, and K. A. Shackel (1987), Stomatal Responses to Air Humidity and Soil Drought. In Stomatal Function, *Stanford University Press*, California, 311-322. (Edited by Zeiger, E., Farquhar, G.D. and Cowan, I. R).
- Shepson, P. B., J. W. Bottenheim, D. R. Hastie, and A. Venkatram (1992), Determination of the relative Ozone and PAN deposition velocities at night, *Geophysical Research Letters*, 19(11), 1121-1124.
- Simpson, D. (1992), Long-period modelling of photochemical oxidants in Europe. Model

- calculations for July 1985, *Atmospheric Environment*, 26(9), 1609-1634.
- Simpson, D., A. Benedictow, H. Berge, R. Bergström, L. D. Emberson, H. Fagerli, C. R. Flechard, G. D. Hayman, M. Gauss, J. E. Jonson, M. E. Jenkin, A. Nyríri, C. Richter, V. S. Semeena, S. Tsyro, J.-P. Tuovinen, Á. Valdebenito, and P. Wind (2012), The EMEP MSC-W chemical transport model – technical description, *Atmos. Chem. Phys.*, 12, 7825-7865, doi:10.5194/acp-12-7825-2012.
- Singh, H. B. and P. L. Hanst (1981), Peroxyacetyl nitrate (PAN) in the unpolluted atmosphere: An important reservoir for nitrogen oxides, *Geophysical Research Letters*, 8(8), 941-944.
- Sparks, J. P., J. M. Roberts, and R. K. Monson (2003), The uptake of gaseous organic nitrogen by leaves: A significant global nitrogen transfer process, *Geophysical Research Letters*, 30(23), 2189.
- Sparks, J. P. (2009), Ecological ramifications of the direct foliar uptake of nitrogen, *Oecologia*, 159(1), 1-13.
- Stahelin, J. and J. Hoigné (1985), Decomposition of Ozone in Water in the Presence of Organic Solutes Acting as Promoters and Inhibitors Of Radical Chain Reactions, *Environ. Sci. Technol.*, 19(12), 1206 – 1212.
- Stella, P., E. Personne, B. Loubet, E. Lamaud, E. Ceschia, P. Béziat, J. M. Bonnefond, M. Irvine, P. Keravec, N. Mascher, and P. Cellier (2011), Predicting and partitioning ozone fluxes to maize crops from sowing to harvest: the Surf atm-O<sub>3</sub> model, *Biogeosciences*, 8, 2869-2886.
- Sumner, A. L., E. J. Menke, Y. Dubowski, J. T. Newberg, R. M. Penner, J. C. Hemminger, L. M. Wingen, T. Brauers, and B. J. Finlayson-Pitts (2004), The nature of water on surfaces of laboratory systems and implications for heterogeneous chemistry in the troposphere, *Physical chemistry Chemical Physics*, 6(3), 604-613.
- Sun, S., A. Moravek, L. von der Heyden, A. Held, M. Sörgel, and J. Kesselmeier (2016), Twin-cuvette measurement technique for investigation of dry deposition of O<sub>3</sub> and PAN to plant leaves under controlled humidity conditions, *Atmos. Meas. Tech.*, 9, 599–617, doi:10.5194/amt-9-599-2016.
- Talukdar, R. K., J. B. Burkholder, A. M. Schmoltner, J. M. Roberts, R. R. Wilson, and A. R. Ravishankara (1995), Investigation of the loss processes for Peroxyacetyl nitrate in the atmosphere - UV photolysis and reaction with OH, *Journal of Geophysical Research – Atmospheres*, 100(D7), 144163-14173.
- Tardieu, F. and T. Simonneau (1997), Variability among species of stomatal control under fluctuating soil water status and evaporative demand: modelling isohydric and anisohydric

- behaviours, *Journal of Experimental Botany*, 49, 419-432.
- Teklemariam, T. A. and J. P. Sparks (2004), Gaseous fluxes of peroxyacetyl nitrate (PAN) into plant leaves, *Plant Cell and Environment*, 27(9), 1149-1158.
- Tuazon, E. C., W. P. L. Carter, and R. Atkinson (1991), Thermal-decomposition of peroxyacetyl nitrate and reactions of acetylperoxy-radicals with NO and NO<sub>2</sub> over the temperature-range 283-313 K, *Journal of Physical Chemistry*, 95(6), 2434-2437.
- Turnipseed, A. A., L. G. Huey, E. Nemitz, R. Stickel, J. Higgs, D. J. Tanner, D. L. Slusher, J. P. Sparks, F. Flocke, and A. Guenther (2006), Eddy covariance fluxes of peroxyacetyl nitrates (PANs) and NO<sub>y</sub> to a coniferous forest, *Journal of Geophysical Research-Atmospheres*, 111(D9), D09304.
- Van Hove, L. W. A., E. H. Adema, W. J. Vredenberg, and G. A. Pieteres (1989), A study of the adsorption of NH<sub>3</sub> and SO<sub>2</sub> on leaf surfaces, *Atmos. Environ.*, 23, 1479-1486.
- Volz-Thomas, A., I. Xueref, and R. Schmitt (2002), An automatic gas chromatograph and calibration system for ambient measurements of PAN and PPN, *Environmental Science and Pollution Research*, 4, 72-76.
- Von Caemmerer, S. and G. D. Farquhar (1981), Some relationships between the biochemistry of photosynthesis and the gas exchange of leaves, *Planta*, 153, 376-387.
- Von der Heyden, L. (2013): Charakterisierung und Kalibrierung von Blattfeuchtesensoren in einer Tauchkammer, Bachelor thesis, Universität Bayreuth.
- Wendschuh, P. H., C. T. Pate, and Jr. J. N. Pitts (1973), The reaction of peroxyacetyl nitrate with aldehydes, *Tetrahedron Letters*, 31, 2931-2934.
- Wesley, M. L. (1989): Parametrization of surface resistances to gaseous dry deposition in regional-scale numerical models, *Atmospheric Environment*, 23(6), 1293-1304.
- Wolfe, G. M., J. A. Thornton, R. L. N. Yatawelli, M. McKay, A. H. Goldstein, B. LaFranchi, K. E. Min, and R. C. Cohen (2009), Eddy covariance fluxes of acyl peroxy nitrates (PAN, PPN and MPAN) above a Ponderosa pine forest, *Atmospheric Chemistry and Physics*, 9(2), 615-634.
- Zhang, L., J. R. Brook, and R. Vet (2003), A revised parameterization for gaseous dry deposition in air-quality models, *Atmos. Chem. Phys.*, 3, 2067-2082, doi:10.5194/acp-3-2067-2003.
- Zhang, J. M., T. Wang, A. J. Ding, X. H. Zhou, L. K. Xue, C. N. Poon, W. S. Wu, J. Gao, C. Zuo, J. M. Chen, X. C. Zhang, and S. J. Fan (2009), Continuous measurement of peroxyacetyl nitrate (PAN) in suburban and remote areas of western China, *Atmospheric Environment*, 43(2), 228-237.

Zeng, G., J. Kelley, J. D. Kish, and Y. Liu (2014), Temperature-Dependent Deliquescent and Efflorescent Properties of Methanesulfonate Sodium Studied by ATR-FTIR Spectroscopy, *Journal of Physical Chemistry A*, 118(3), 583-591.

# Appendix D

## **Case study: Emission of Trimethylamine from *Chenopodium vulvaria* - first results from quantifying plant emissions of amines and their potential effects on atmospheric new particle formation**

Shang Sun<sup>1</sup>, Albrecht Neftel<sup>2</sup>, Joerg Sintermann<sup>2</sup>, Carina Sauvage<sup>1</sup>, Bettina Derstroff<sup>1</sup>, Katharina Bohley<sup>3</sup>, Gudrun Kadereit<sup>3</sup>, Jonathan Williams<sup>1</sup>, Christopher Pöhlker<sup>1</sup>, Jürgen Kesselmeier<sup>1</sup>, Matthias Sörgel<sup>1</sup>

<sup>1</sup>Max Planck Institute for Chemistry, Biogeochemistry Department, P.O. Box 3060, 55128 Mainz, Germany

<sup>2</sup>Agroscope, Institute for Sustainability Science, 8046 Zurich, Switzerland

<sup>3</sup>J. G. University, Institute for Special Botany, 55099 Mainz, Germany

*Correspondence to:* Shang Sun (shang.sun@mpic.de)

Manuscript to be submitted

## Abstract

In this study, we investigated the emission of trimethylamine (TMA) by terrestrial vegetation, especially *Chenopodium vulvaria*, and the potential impact on atmospheric new particle formation. The analysis of the leaf anatomy of *Chenopodium vulvaria* showed that the emission of TMA can be related to the epidermal gland vesicles, which were very fragile and can be destroyed easily by handling or even slight air streams. Depending on the intensity of the mechanical stimuli, high amounts of TMA ( $> 8 \text{ nmol m}^{-2} \text{ s}^{-1}$ ) can be emitted by the plant. A screening of different flowering plants showed that plant emissions of TMA might not be restricted to specialized plants. Their potential impact on the atmospheric new particle formation could be demonstrated qualitatively by the ternary nucleation systems with sulfuric acid – TMA – H<sub>2</sub>O and formic acid – TMA – H<sub>2</sub>O. Sulfuric acid was used to test if enhanced formation can be reproduced according to recent publications (e.g. Almeida et al. 2013). A new approach was to study the nucleation with organic acids. For formic acid, the particle concentration was about 3 orders of magnitude less than for sulfuric acid whereas for the other tested organic acids (acetic acid and tartaric acid) no particle formation was observed.

## 1 Introduction

Amines comprise a wide range of nitrogenous organic compounds such as aliphatic methylamines (MA). The most common species in the atmosphere are monomethylamine (MMA), dimethylamine (DMA) and trimethylamine (TMA) (Ge et al., 2011a). In the atmosphere amines play a role as bases that neutralize acids such as sulfuric and nitric acid. Due to their semi-volatile property they exist in the gas phase as well as the particle phase. Their major sources are both natural and anthropogenic (Ge et al., 2011a; Lee and Wexler, 2013). Schade and Crutzen (1995) concluded that TMA could be the species which is predominantly emitted by agriculture. But other amine species could also be released. Further, biodegradation of organic matter could also serve as a major source of amines (Ge et al., 2011a). Many marine plants and bacteria contain MA (MMA, DMA and TMA), which are produced in the metabolism of marine organisms (Wang and Lee, 1994; Calderón et al., 2007). On the global scale, the knowledge about the flux of most amines is limited (Ge et al., 2011a). Schade and Crutzen (1995) suggest that animal husbandry, the ocean, and biomass burning are the major emission sources of MA. Additionally, terrestrial vegetation is also assumed to be a potential source for amines (Schade and Crutzen, 1995; Ge et al., 2011a). A few studies since the end of the 19<sup>th</sup> century until 1975 described high amounts of MA-

emission from certain plant species, which was associated with their plant tissues or with blossoms during flowering (Wicke, 1862; Smith, 1971, 1975). Wicke (1862) described emission of TMA from a certain plant species *Chenopodium vulvaria* as one of the first scientists. Additionally, he observed a kind of “fog”- forming under a glass dome in the presence of HCl vapor exposed close to the plant, which could be one of the first observed NPF under controlled environmental conditions.

Despite the low atmospheric concentration of amines (DMA = 0.5 ppb (Okita, 1970), TMA = 0.6 -1.6 ppb (Fujii and Kitai, 1987)), previous studies have already shown that amines may play an important role in the New aerosol Particle Formation (NPF) (Almeida et al., 2013; Glasoe et al., 2015). In the atmosphere, NPF is frequently derived from gas-phase precursors. High uncertainty exists in the estimation of the global secondary aerosols budget, which is caused by an uncertain contribution of the gas-phase precursors to the NPF (Spracklen et al., 2011). It becomes more clear that, instead of a binary system of sulfuric acid and water, a ternary system of sulfuric acid, water and a neutralizing compound as  $\text{NH}_3$  or amines is a key system in NPF (Chen et al., 2012; Almeida et al., 2013; Kurten et al., 2014). Furthermore, the contribution of organic acids with amines to NPF is still unexplored and should not be neglected. For example, Dawson et al. (2012) found out that amines are able to form stable clusters with methanesulfonic acid. Also oxidation products of organic compounds can contribute to NPF (Riccobono et al., 2014) or are able to nucleate even without sulfuric acid (Tröstle et al., 2016). However, such kind of vegetation dependent amine emission in relation to its key role in the NPF has not been elucidated yet (Sintermann and Neftel, 2015).

In this study, we focus on the plant species *Chenopodium vulvaria*, which is known to be a strong TMA-emitter (Dessaignes, 1856). But TMA emission rates from that plant species were not determined systematically up to now. In this study, we investigate the TMA emission from *Chenopodium vulvaria* in our dynamic cuvette system (Sun et al., 2016). As TMA plays a key role in the atmospheric NPF, the results should give a perception of the contribution of the TMA emission from the terrestrial vegetation to the global NPF. Additionally, we have screened several typical European plant species at their flowering state with a GC-NCD to determine further potential TMA-emitters qualitatively. Furthermore, we investigate in a nucleation tube system the NPF- process of the ternary nucleation system based on inorganic / organic acids, water and TMA.

## 2 Material and Methods

### 2.1 Plant growth condition

The experiments were performed with *Chenopodium vulvaria*, which is a typical plant species for the Mediterranean region. The plant samples (height = 30 cm) were grown as seedlings and treated with a commercial fertilizer (WUXAL<sup>®</sup> Top N, MANNA GmbH, Germany). For the experiments the seedlings were treated with three fertilization levels (0.2, 0.4 and 1.14 g L<sup>-1</sup> of urea). The growth conditions were kept constant inside a greenhouse under natural growth conditions ( $T_{\text{winter}} = 15^{\circ}\text{C}$ ,  $T_{\text{summer}} = 30^{\circ}\text{C}$ ,  $\text{PAR}_{\text{max}} = 1400 \mu\text{molm}^{-2}\text{s}^{-1}$ ). The plant samples were watered every two days.

### 2.2 Leaf sectioning of *Chenopodium vulvaria* and extraction of the sap of bladder cells for chemical identification of TMA

Fresh leaves were harvested and immediately fixed in formaldehyde, acetic acid and 70% ethanol [1:1:18], followed by dehydration in an ascending ethanol series. For embedding, Technovit 7100 (Heraeus Kulzer, Germany) was used following the manufacturer's manual. Right after embedding the blocks were put into an oven at 60°C for four hours to shorten curing time. Sectioning was done using a rotary microtome (Leitz Wetzlar, Germany) with a d-knife at 5–10  $\mu\text{m}$  thickness. Sections were stained for three minutes with a dye containing 3 parts Eosin Y (C.I. 45380; Merck, Germany) and 10 parts Azure II (C.I. 52010/52015; Merck, Germany), shortly rinsed with 70% ethanol and immediately rinsed with distilled water. For isolating the sap from the bladder cells of *Chenopodium vulvaria*, glass capillaries were heated above an ethanol burner and drawn to a fine tip. With these, bladders from the abaxial side of the leaf were punctured one at a time and the liquid extracted under a stereo microscope. For the identification of TMA, Dragendorff's reagent (CAS 39775-75-2, Sigma-Aldrich Inc., USA) was used to detect TMA in the liquid of the bladder cells chemically.

### 2.3 TMA-emission measurement with GC-NCD

#### 2.3.1 Performance of the GC-NCD and peak identification

For the analysis of organic nitrogen species, a system which consists of an ENtech 7200 commercial preconcentrator, an Agilent 6850 gas chromatograph (GC) and an Agilent 255 nitrogen chemiluminescence detector (NCD) was built. During the pre-concentration process sample air is drawn past an empty stainless steel silonite coated trap which is cooled to  $-10^{\circ}\text{C}$



with liquid nitrogen to remove water. Subsequently trace gases are adsorbed on a Tenax trap at -45 °C. By heating this trap to 180 °C and flushing with He, the analytes are revolatilized and transferred to an additional cryofocussing stage at -190 °C before injection to the GC. The GC houses a combination of a HP-5 (30 m; 0,32 mm; 0,25 µm) and a Restek 1701-CB-0,5 (5 m; 0,25mm; 0,5 µm) column. A ramped temperature and carrier gas flow program is used to ensure good peak separation and shape. In the dual plasma burner of the NCD the eluting compounds react in a combustion process to NO. In a reaction cell NO reacts with ozone in a chemiluminescence reaction emitting light in the near infrared range, which is detected by a photomultiplier. GC operation, data acquisition and data analysis is done with Agilent Open Lab Chemstation.

Peak identification was done using a permeation source. Pure liquid samples of TMA (offered from the Chemical storage of the University of Mainz) were filled into GC vials with Teflon septum sealed screw caps. Those were put into a centrifuge tube (56 mm; 145 mm) equipped with a glass impinger top. The source was constantly flushed with 300 ml/min synthetic air. The outlet of the source was split up into one line to a rotameter and one line to a sample inlet of the pre-concentration unit. The rotameter works as control of the total flow through the source and excess during sampling from the sample outlet.

### 2.3.2 Screening experiment

The screening experiment was performed under laboratory and normal indoor light conditions. Four different plant species (*Crataegus monogyna*, *Sorbus aucuparia*, *Pyrus communis* and *Chenopodium vulvaria*) were analyzed to determine the emission of TMA qualitatively (1 sample for each plant species). The flowers of the first three species were collected from different outdoor areas nearby our institute and measured immediately after collection. *Chenopodium vulvaria* were grown under greenhouse conditions as described in Sect. 2.1. A simplified single cuvette system, derived from the setup shown in Fig. 1, was used to perform the measurement with the GC-NCD. The dynamic cuvette had a volume of 17.5 L and the operation flow rate with synthetic air as carrier gas was 2 L min<sup>-1</sup> to optimize the measured concentration signal of TMA. The air stream was humidified by passing through a water tank containing deionized water without fine controlling of the relative humidity within the cuvette. Including the plant transpiration the relative humidity inside the cuvette was at 60 %. After a blank measurement the plant sample was put inside the cuvette for several hours to obtain a time course of the TMA emission. Between each measurement of the plant species the cuvette was purged with synthetic air for 24 hours to remove the TMA from the wall material.

## 2.4 TMA-emission measurement with PTR-TOF-MS

### 2.4.1 Performance of the PTR-TOF-MS

Trimethylamine (TMA) was measured online by using a PTR-TOF-MS (Proton-Transfer-Reaction-Time-Of-Flight-Mass-Spectrometer, Ionicon Analytik GmbH, Innsbruck, Austria). The technique is based on the protonation of sample molecules by  $\text{H}_3\text{O}^+$  ions, which are produced in a hollow cathode discharge. The protonated molecular ions are accelerated by an electrical field to the same kinetic energy and are transferred into the time of flight mass spectrometer. Here the sample ions are separated by their mass-to-charge-ratio, which determines their velocity. Molecules with a proton affinity higher than water can be measured. More details can be found elsewhere (Graus, 2010; Veres et al., 2013). For the TMA measurements a time resolution of 10 s was chosen, the drift pressure was set to 2.2 mbar and the drift voltage to 600 V (E/N 137 Td). Post-acquisition data analysis was performed using the program “PTR-TOF DATA ANALYZER”, which is described by Müller et al. (2013). For calibration 1,3,5-trichlorobenzene was used as an internal standard. After the measurements the instrument was calibrated for TMA by means of a permeation source (Macherey-Hagel GmbH & Co. KG, Germany) with a permeation rate of  $321 \text{ ng min}^{-1} \pm 15\%$  at  $40 \text{ }^\circ\text{C}$ . A known mixing ratio of TMA was also flushed through the chamber to determine wall losses.

### 2.4.2 Twin-cuvette setup

The TMA emission measurements with PTR-TOF-MS were performed with a modified version of the dual-cuvette system described in Sun et al. (2016) under controlled environmental conditions (temperature, light, relative Humidity, trace gas mixing ratio) in a plant cabinet (VB1014, Vötsch GmbH) (see Fig. 1). Two dynamic cuvettes with a volume of 17.5 L were used. Considering an operation flow rate of  $5 \text{ L min}^{-1}$ , the flushing time of each cuvette was 3.5 min. The measurement of TMA and plant photosynthesis ( $\text{CO}_2$  and  $\text{H}_2\text{O}$ ) occurred via two different methods. For determination of the plant photosynthesis and transpiration, the  $\text{CO}_2$  and  $\text{H}_2\text{O}$  mixing ratio between the reference and sample cuvette were measured simultaneously with an infrared gas analyzer (Li-7000, LiCor Inc., USA) in dual mode.

The emission flux of TMA from the plant was determined from the difference of its mixing ratio in the empty cuvette and those in the same cuvette after introducing the plant, see Eq. (1).

$$F(\text{TMA}) = \frac{f_m * (vmr_{out,ref} - vmr_{out,sample})}{A_{leaf}} \quad (1)$$

where  $vmr_{out,ref} - vmr_{out,sample}$  is the difference of the TMA mixing ratios.  $f_m$  ( $\text{mol s}^{-1}$ ) is the mole flow rate through each cuvette, which is calculated from the volume flow rate  $f_v$  of  $5 \text{ L min}^{-1}$  divided by  $24.4 \text{ L mol}^{-1}$  (at  $25 \text{ }^\circ\text{C}$  and  $1013.25 \text{ hpa}$ ), i.e. the volume of one mole in air at standard conditions and  $A_{leaf}$  ( $\text{m}^2$ ) is the leaf area of the entire plant inside the sample cuvette that was determined by digitally scanning all leaves of the sample tree (for further details see Sun et al., 2016).

TMA was measured online by using a PTR-TOF-MS (Proton-Transfer-Reaction-Time-Of-Flight-Mass-Spectrometer, Ionicon Analytik GmbH, Innsbruck, Austria). The 1.5 meter sampling tube for the PTR-TOF-MS was completely heated ( $45 \text{ }^\circ\text{C}$ ) to minimize the TMA loss within the tubes. The photosynthetic active radiation (PAR) was measured by a quantum sensor (LiCor Inc., USA). For detailed description of the cuvette setup, see also Sun et al. (2016).

### 2.4.3 TMA-Emission experiment with *Chenopodium vulvaria*

Two different experiments were performed to determine the emission behavior of TMA by *Chenopodium vulvaria*. For the first experiment, plant samples grown under three different fertilization levels (see Sect. 2.1) were used to quantify the TMA emission flux for 36 h under alternating light/dark conditions of 13/11h. One plant sample for each fertilization level was used for the measurement. The plants were introduced to the cuvette after 6 h of blank measurement, respectively. The cabinet temperature was  $T = 30 \pm 0.1 \text{ }^\circ\text{C}$  during light period and  $23 \pm 0.1 \text{ }^\circ\text{C}$  during the dark period. The relative humidity ( $RH$ ) was  $60 - 70 \%$  within the cuvette including the plant.

For the second experiment, the TMA emission flux was measured for 3 days under same conditions as the first experiment. After introducing the plant into the cuvette, the emission behavior of the plant was analyzed under artificial (by mechanical stimuli) and natural (by changes in light and  $RH$ ) stress condition.

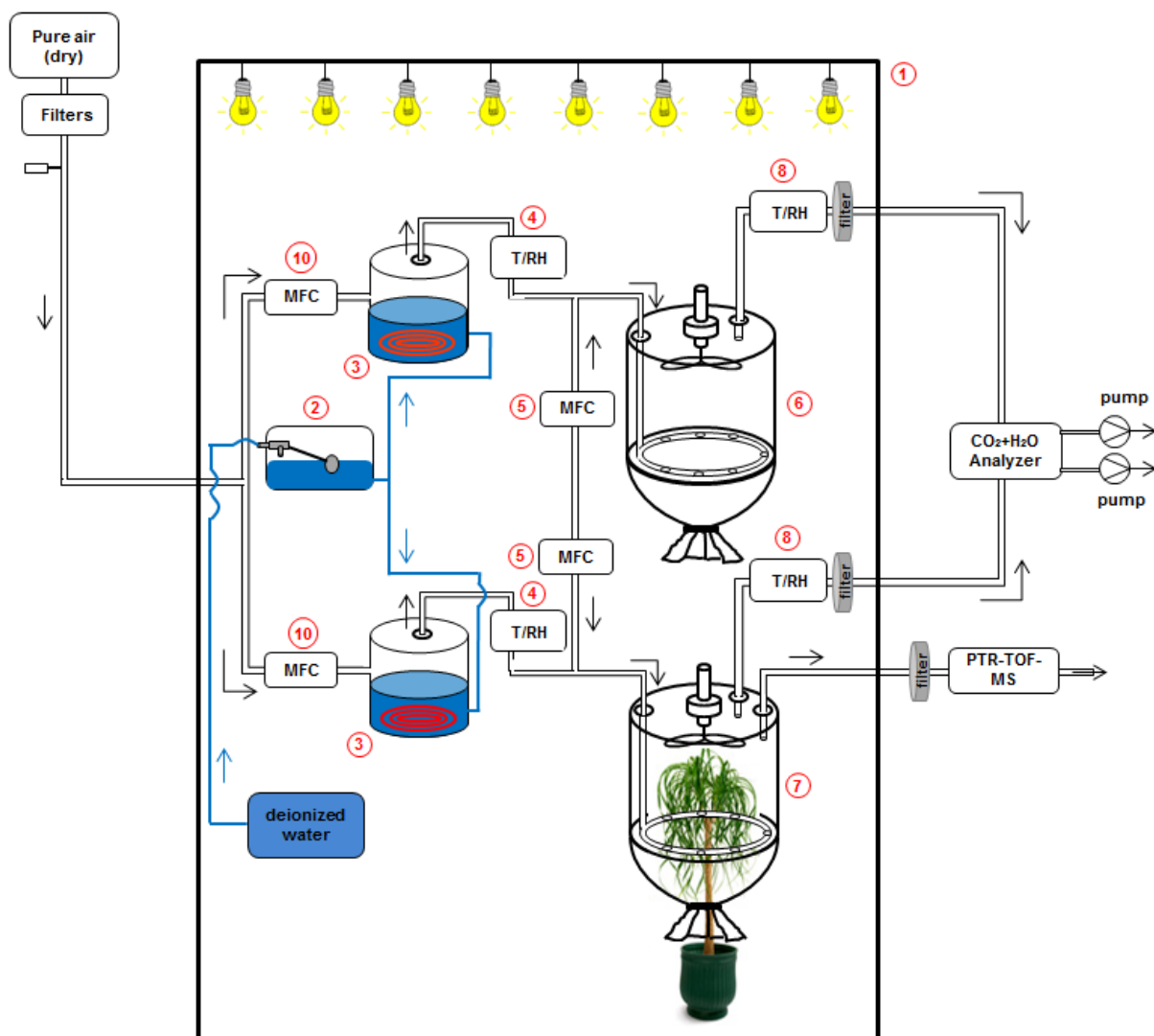


Fig. 1: Flow chart of the dual cuvette system. 1 plant cabinet, 2 water storage tank, 3 ATRAHS, 4 Temperature and relative humidity sensor for humidity regulation, 5 mass flow controller (MFC), 6 dynamic cuvette (reference), 7 dynamic cuvette (sample), 8 Temperature and relative humidity sensor for monitoring

## 2.5 Investigation of new particle formation

### 2.5.1 Setup of the flow reactor

The nucleation experiments were performed with a flow reactor (Fig. 2) under laboratory conditions. The flow reactor, with a length of 2 meters and a diameter of 2.5 cm, was made of stainless steel for minimizing the wall loss of the particles caused by the electrostatic charge. Considering a total volume of 0.98 L and an operation flow rate of  $1 \text{ L min}^{-1}$ , a residence time of 1 minute could be achieved. The temperature within the flow tube was constantly  $23 \text{ }^\circ\text{C}$ . The gas addition of TMA occurred via permeation tubes (Macherey – Nagel GmbH & Co. KG, Germany) with a permeation rate of  $321 \text{ ng min}^{-1} \pm 15 \%$  at  $40 \text{ }^\circ\text{C}$ , which equates to a

mixing ratio of 664 ppb. The temperature of the TMA permeation tube was controlled by a temperature controlled aluminum block at  $40\text{ }^{\circ}\text{C} \pm 0.3\text{ }^{\circ}\text{C}$  constantly.

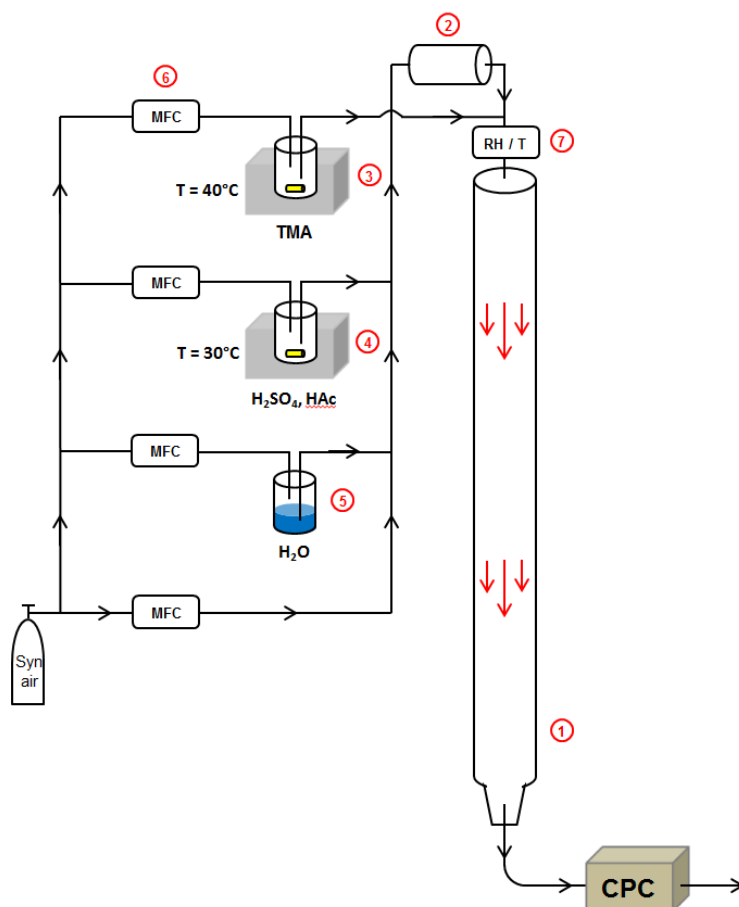


Fig. 2: Flow chart of the nucleation reactor. 1 – flow tube reactor; 2 – mixing volume; 3 – tempered permeation cell for TMA; 4 – tempered permeation cell for the acids; 5 – humidifier; 6 – mass flow controller (MFC); 7 – temperature and humidity sensor. The temperature within the flow tube was constantly  $23\text{ }^{\circ}\text{C}$  and the  $RH$  was 40 %.

For the formic acid (and HAc) a similar permeation tube (permeation rate =  $7.3\text{ ng min}^{-1} \pm 10\%$  at  $30\text{ }^{\circ}\text{C}$  which equate to 25 ppb) was used to add the gas into the system. The addition of the sulfuric acid occurred via a permeation source, which contained a 50 % diluted solution of 98 %  $\text{H}_2\text{SO}_4$ . The temperature was held constant at  $30\text{ }^{\circ}\text{C}$  as well. Furthermore, synthetic air was used as carrier gas to flush all the permeation sources and the flow reactor. The relative humidity was set by the synthetic air stream over a water reservoir at  $23\text{ }^{\circ}\text{C}$  resulting in 40 %  $RH$ . Additionally, a mixing vessel arranged for a well-mixed condition of all components before the gas stream entered the flow reactor. At last, the final relative humidity and temperature of the gas stream was measured via a temperature and humidity sensor (Model 145, MSR Electronics GmbH, Switzerland). A butanol condensation particle counter (CPC)

(Model 3775, TSI Inc., USA) with a particle size detection limit of 2 nm measured the total particle number at the bottom of the flow reactor.

### 2.5.2 Nucleation experiment

For investigating the influence of gaseous TMA on the new particle formation process, several experiments were performed with sulfuric acid, formic acid, acetic acid and tartaric acid under laboratory condition. The total flow rate through the reactor was 1 L min<sup>-1</sup> resulting in a residence time of 1 minute. For the blank measurement only the carrier gas enriched with 50 % H<sub>2</sub>SO<sub>4</sub> was added into the system. After the blank was stable, TMA was added by varying its mixing ratio incrementally (0, 66, 99, 132 and 166 ppb). The same procedure was also made for formic acid with a mixing ratio of 5 ppb and 300 ppb TMA. Furthermore, 50 % acetic acid and Tartaric acid were tested qualitatively as well.

## 3 Results

### 3.1 Leaf anatomic structure and reservoir for TMA

Gland vesicles with a diameter of 40 - 100 µm are evenly distributed at the bottom of the leaf (Fig. 3). The semitransparent vesicles contain a foul-smelling fluid, which could be released by a stress situation for the plant, such as minimal mechanical stimuli such as touching or slight air streams (e.g. a person passing the plants in the greenhouse without touching them).

The leaf cross section of *Chenopodium vulvaria* (Fig. 4) shows the inner structure of the leaf consisting of palisade parenchyma, spongy parenchyma and leaf stomata. The vascular bundle containing xylem and phloem is located in the center of the cross section. An intact gland vesicle, containing a liquid substance, is connected by a stalk to the epidermis cell as can be seen on the right upper side of the leaf. The rest of the gland vesicle structures, which are distributed around the cross section, are either fragments destructed during the sectioning process or intact glands cut outlying the stalk.

### 3.2 Chemical identification of TMA within bladder cells

The chemical identification of TMA by the Dragendorff's reagent was not valid because of insufficient amounts of extract. Conducting this identification method by hand was very difficult, due to the small size and delicacy of the bladder cells. Additionally, each bladder

cell only contains a very small volume of liquid and a high number of bladders would be needed to extract sufficient amounts of extract. The use of a motorized cannula holder (comparable to those used in in-vitro fertilization) might simplify the process and increase yield and accuracy of the method.

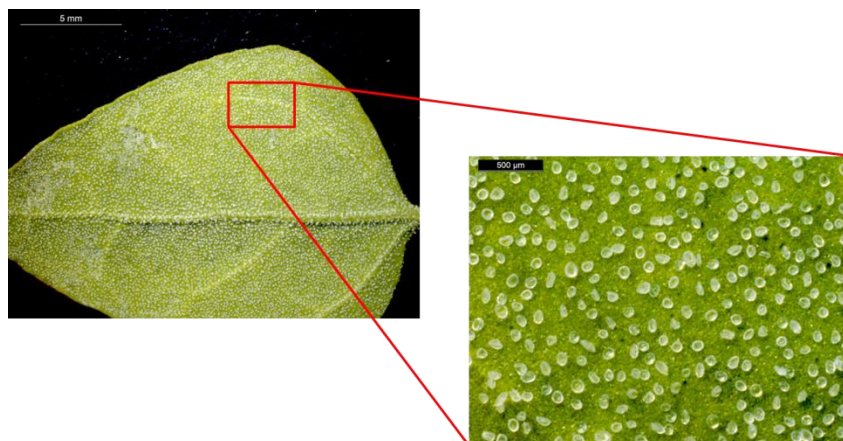


Fig. 3: Gland vesicles on the bottom of the leaf surface of *Chenopodium vulvaria*.

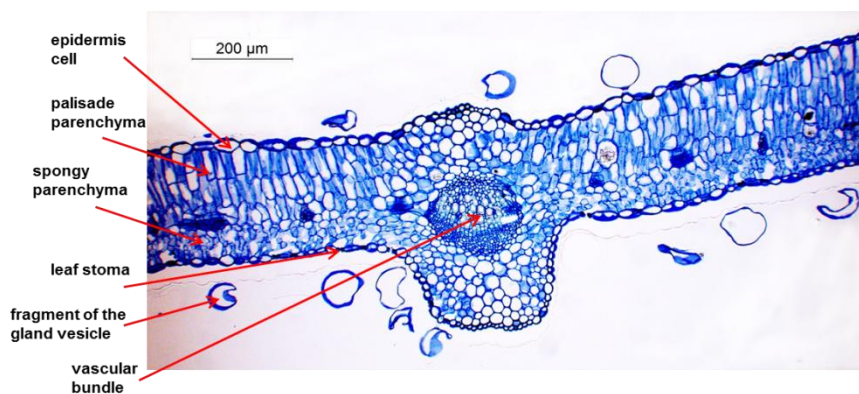


Fig. 4: Leaf cross section of *Chenopodium vulvaria*. Gland vesicles arranged on the top and bottom of the leaf epidermis were sectioned missing and hitting the stalk (epidermal connection).

### 3.3 Identification of TMA

TMA was identified with two different systems, GC-NCD and PTR-TOF-MS. Fig. 5 shows the GC-NCD-chromatogram of air sampled from the empty reference cuvette and the plant cuvette. The reference chromatogram shows only a single peak at 3.6 min, which was suggested as the TMA peak. The plant chromatogram shows overall four different peaks at 2.15, 2.38, 2.68 and 3.35 min of retention time (RT). The latter one was the object of interest and was assumed to be the emitted TMA signal, which differed significantly from the

reference peak with a retention time shift of 0.25 min. The peak at 2.38 min RT was identified as acetonitrile and the other two peaks (2.15 and 2.68) were not identified.

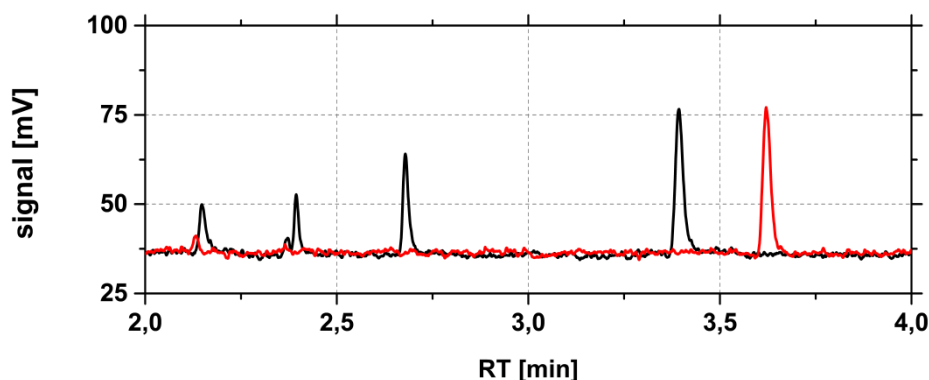


Fig. 5: Identification of TMA by GC-NCD. Chromatogram of reference TMA (red line) and plant TMA-volatiles emitted by *Chenopodium vulvaria* (black line).

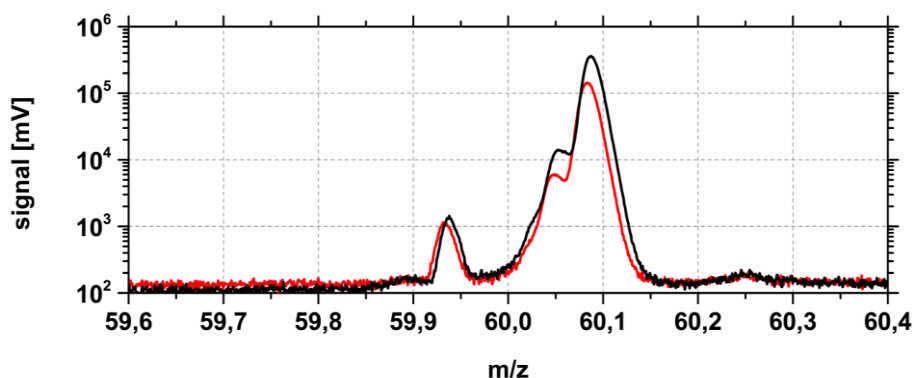


Fig. 6:  $m/z$  spectra of reference TMA (red line) and TMA emitted by *Chenopodium vulvaria* (black line) measured by PTR-TOF-MS.

Figure 6 shows the mass spectra of both air samples, containing reference and emitted TMA respectively. The range between 59.6  $m/z$  and 60.4  $m/z$  was chosen to specify the identification of TMA. The graph shows three different peaks for both samples. The first one was found at 59.94  $m/z$ . The second peak at 60.05 seems to overlap with the dominant peak at 60.1. Both spectra conform each other and the TMA (atom mass = 59.1u) peak was identified at 60.1  $m/z$  after protonation.

### 3.4 Screening experiment with GC-NCD

The screening experiment was performed with four different plant species (Fig. 7) to investigate the TMA emission qualitatively. Figure 7 shows the developing TMA mixing



ratios over time for all four enclosed plant species. The RT 3.35 was assumed to be TMA, whose emission, as reflected by the mixing ratio fluctuations, can be observed with all four plant species. RT 2.37 was identified as acetonitrile. Additionally, other nitrogen containing substances (RT 2.13, 2.29, 2.34 and 2.65) were also measured by the GC-NCD, but without identification. The mixing ratio of TMA was on average significantly higher than the other substances. The highest TMA mixing ratio could be observed for *Pyrus communis* with 22 ppt followed by *Crataegus monogyna* and *Sorbus aucuparia* with 15 ppt and *Chenopodium vulvaria* with 11 ppt. The mixing ratios of most of the other substances were high at the beginning of the measurements and declined afterward to the background level.

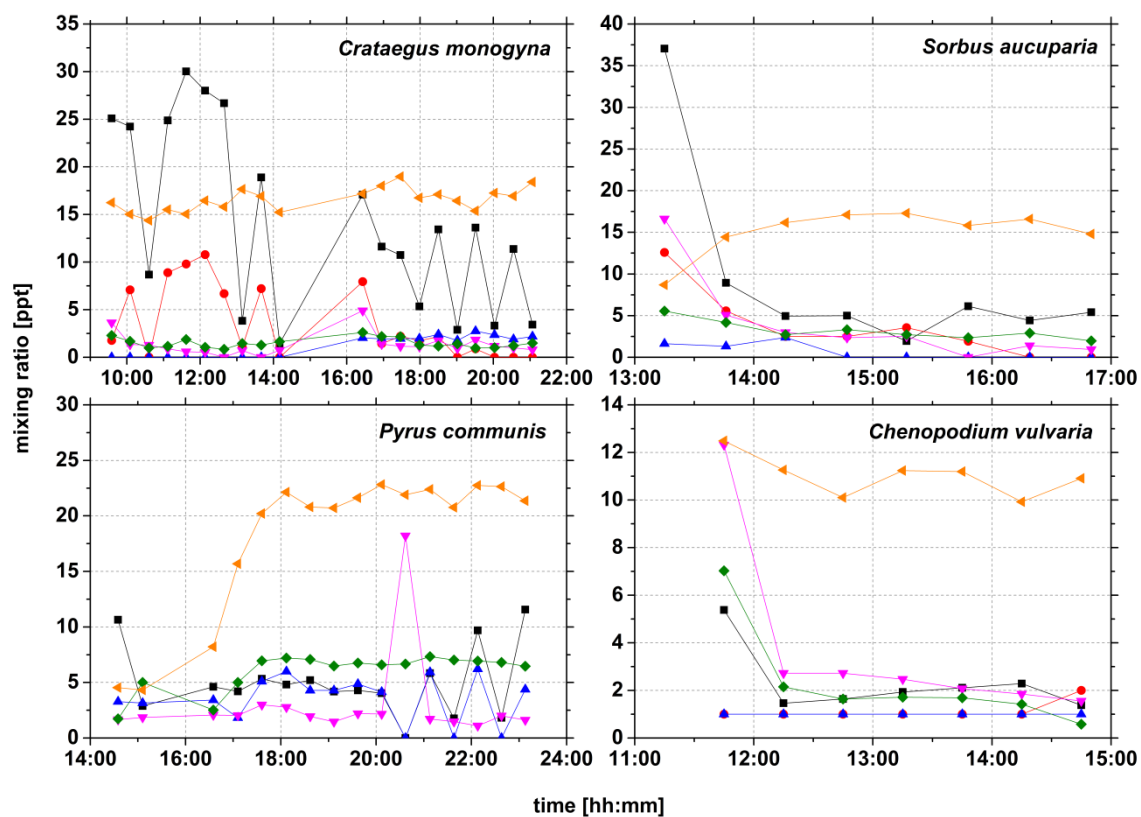


Fig. 7: TMA screening experiment with four different plant species. *Crataegus monogyna*, *Sorbus aucuparia* and *Pyrus communis* were measured at flowering period. Enclosure mixing ratios reflect emission capacities. Emitted substances were characteristic for their retention time (RT). ■ RT 2.13, ● RT 2.29, ▲ RT 2.34, ▼ RT 2.37(acetonitrile), ◆ RT 2.65, ◀ RT 3.35 (assumed to be TMA).

### 3.5 Emission of TMA from *Chenopodium vulvaria*

Figure 8 shows the TMA emission from plant samples grown under three different fertilization levels (see Sect. 2.1). A dominant peak could be observed for all three plant samples after the plant was put inside the cuvette. For the highest fertilized plant sample

(ChenVP1S) the mixing ratio peak increased up to 103 ppb, which was the highest observed TMA mixing ratio of all plant sample (Fig. 8, left) under these enclosure measurement conditions. For the medium fertilized sample (ChenWP1S) the TMA mixing ratio reached 9 ppb and the low fertilized sample (ChenNOP1S) 13 ppb. The emission flux (see Fig. 8, right) followed the same trend as indicated by the mixing ratios. Subsequently, the TMA emission decreased within several hours reaching steady state mixing ratios of 3.1 ppb for ChenVP1S and 1.5 ppb for ChenWP1S and ChenNOP1S. A substantial difference between all samples in mixing ratios as well as in emission fluxes could only be observed at the start of incubation when inserting the plant into the cuvette. It can be noted that at the steady state the TMA emission of ChenVP1S was higher than the other two fertilized samples.

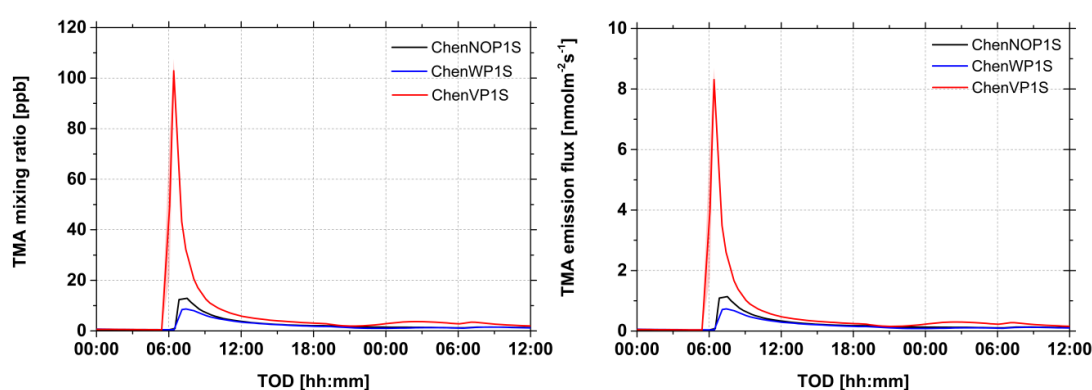


Fig. 8: Emitted trimethylamine (TMA) from *Chenopodium vulvaria*. Mixing ratio (left) and emission flux (right). Plant samples growth under various fertilization levels low (black line), middle (blue line) and high (red line) (see Sect. 2.1).

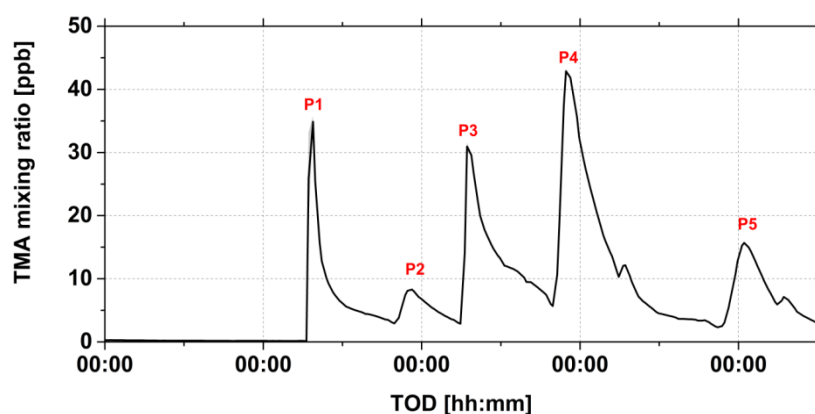


Fig. 9: Emitted TMA from *Chenopodium vulvaria*. TMA peaks occurred under mechanical stimuli via shaking.  $RH$  was 60 – 70 % within the cuvette including the plant.

Figure 9 shows the TMA emission behavior of *Chenopodium vulvaria* within 4 days of measurement. At the introducing of the plant sample into the cuvette, an emission peak of

TMA was observed similar as in the experiment above (Fig. 9, P1). Furthermore, four additional peaks (P2 - P5) could be observed, whereby P3 was triggered by touching the plant stem. The reasons for P2, P4, and P5 were discussed in Sect. 4.3.

### 3.6 Influence of TMA on atmospheric new particle formation

The effect of TMA on the new particle formation process was investigated with a flow reactor described in Sect. 2.5. Figure 10 shows the measured particle concentration, which clearly increased with rising TMA mixing ratio to a maximum of  $3.5 \times 10^4 \text{ cm}^{-3}$  at the highest TMA mixing ratio of 166 ppb. After removing the addition of TMA, the particle concentration decreased incrementally to the background level.

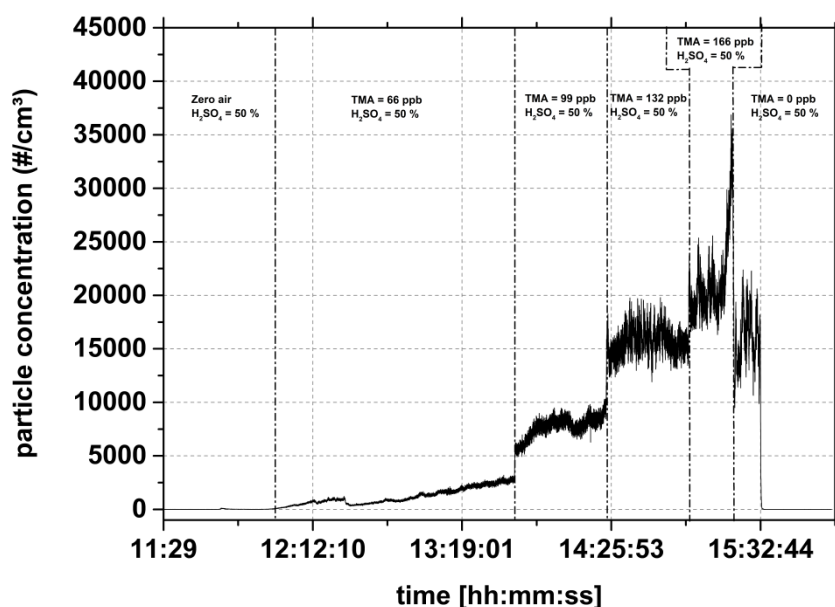


Fig. 10: Ternary nucleation system with sulfuric acid,  $\text{H}_2\text{O}$  and TMA. The concentration of sulfuric acid was constant at 50 %, while the TMA mixing ratio was varied stepwise between 66 – 166 ppb. The blank was measured with 50 % sulfuric acid in synthetic air without TMA addition. Temperature inside the flow tube was 23 °C and the relative humidity was 30 %.

In case of the nucleation system with formic acid,  $\text{H}_2\text{O}$  and TMA (Fig. 11) the new particle formation is also depending on the presence of gaseous TMA. Formic acid mixing ratio was 5 ppb which is typical for environmental conditions according to Grosjean (1989). TMA mixing ratio was 300 ppb, which was much higher than it can be found under ambient condition. At the beginning, the particle concentration increased rapidly up to  $70 \text{ cm}^{-3}$  upon TMA addition and stabilized at  $40 \text{ cm}^{-3}$ .

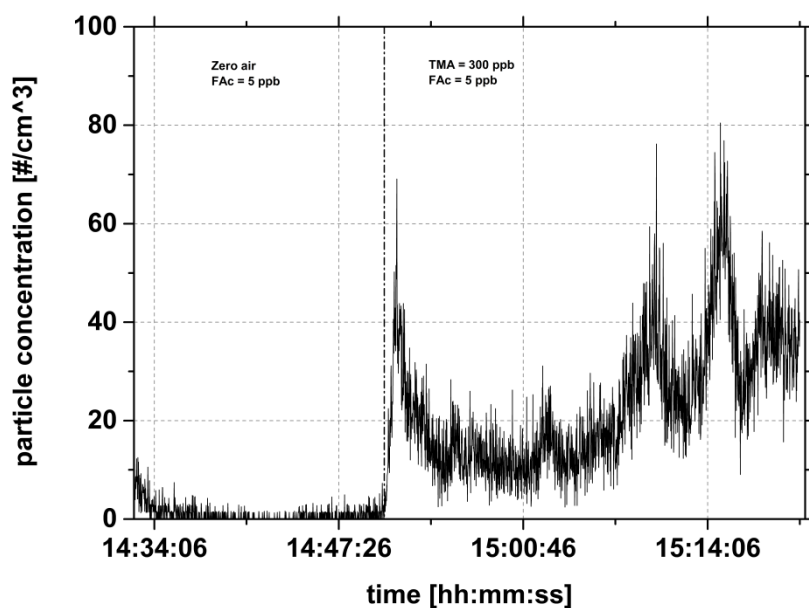


Fig. 11: Ternary nucleation with formic acid (FAC), H<sub>2</sub>O and TMA. The blank was measured with 5 ppb FAC in the presence of synthetic air. The TMA mixing ratio was 300 ppb. Temperature inside the flow tube was 23 °C and the relative humidity was 30 %.

## 4 Discussion

### 4.1 Leaf anatomic structure and reservoir for TMA

*Chenopodium vulvaria* is a well-known TMA-emitter (Dessaignes, 1856; Wicke, 1862). The TMA is released from gland vesicles on the surface of the leaves, which makes an accurate determination difficult (Cromwell, 1949). The factors controlling the release of TMA from the gland vesicles have not yet been fully investigated (Cromwell, 1949). At our leaf anatomic analysis (Fig. 3 and Fig. 4) we showed the gland vesicles are well distributed at both sides of the plant leaf. The glands were very fragile and easily ruptured by handling or even slight air streams. Additionally, the connecting part between the gland vesicles and the leaf epidermis (a stalk) is very fragile as well, whose destruction could lead to a splitting of the entire gland vesicle (see Fig. 4). In both cases, the contained TMA can be easily released into the atmosphere.

The production of TMA within the leaves of *Chenopodium vulvaria* was investigated by Cromwell (1949), who suggested that the synthesis of TMA derived from choline. The production process was assumed to be occurring by metabolizing choline to a compound other than TMA before it reached the possible production site (Cromwell and Richardson, 1966). This assumption supports the conclusion of Cromwell (1949), who suggested the

production of TMA was restricted to the epidermal glands, where the TMA concentration was higher than in the leaf tissues. On the one hand, enzymatic breakdown of choline by certain members of Enterobacteriaceae has been reported by Dyer and Wood (1947), who showed that TMA was produced at pH 7.2 from choline, but not from betaine. On the other hand, Steele (1949) suggested that the TMA production of *Chenopodium vulvaria* is a result of decomposition of betaine. As the conclusive studies to that topic are very rare, the existent explanations about the production pathway of TMA within the leaves are disputed and needs further process studies to describe it in detail.

## **4.2 Screening experiment with different plant species and their potential contribution to the emission of volatile TMA**

Four different plant species (*Crataegus monogyna*, *Sorbus aucuparia*, *Pyrus communis* and *Chenopodium vulvaria*) were analyzed with a GC-NCD to investigate the TMA emission qualitatively. For the first three plant species the measurement was performed during their flowering period (see Fig. 7). It has been observed by former studies that various groups of plant species emit high amount of methylamines (MA) with blossoms during the flowering period (Smith, 1971, 1975). Accordingly, our screening experiment showed that all of the investigated plant species emit an amount of TMA, assuming the identification of the TMA peak with GC-NCD was correct. Already in the middle of the 19<sup>th</sup> century, Wicke (1862) concluded that TMA can be found in the blossoms of these mentioned species above. But such in-situ measurement of volatile TMA in the gas phase was not possible at that time and even until nowadays conclusive studies of TMA-emission by plants are very limited.

However, the contribution to the global emission of volatile TMA from terrestrial vegetation is strongly dependent on the abundance and phenology of emitting plant species (Sintermann and Neftel, 2015). For example, *Crataegus monogyna* is commonly habituated in North Africa and from Europe to West Asia (Christensen, 1992) and has been introduced to America and Australia (Sintermann and Neftel, 2015). Its flowering period is between April and May (Gyan and Woodell, 1987). *Sorbus aucuparia* is present in almost the whole of Europe, from Iceland and North Russia to the mountains of central Spain, Italy and Caucasus (Fitter, 1978; Welter and Ruben Sutter, 1982; Hultén and Fries, 1986). Additionally, it was introduced to North America as an ornamental tree (Raspé et al., 2000). In central Europe, *Sorbus aucuparia* flowers from May to June. *Chenopodium vulvaria* is originally wide spread in countries bordering the Mediterranean and eastward to Afghanistan and Mongolia (Jalas and Suominen, 1980; Meusel et al., 1992). From the historical literature it is clear that during the 18<sup>th</sup> and 19<sup>th</sup> centuries, *Chenopodium vulvaria* was common in parts of northern Europe. In nowadays, the population in the northern Europe declines, which is caused by the habitat change. In European countries the native range and distribution of *Chenopodium vulvaria* is

focused in the southern part, while in the northern part the native range is still unknown (Groom, 2015). In this study, all of these plant species were found to be a TMA-emitter and represent a terrestrial source of volatile TMA. Because of their wide geographical distribution and depending on the flowering period, a potential contribution to the global budget of volatile TMA can be assumed.

### 4.3 Emission of TMA from *Chenopodium vulvaria*

In this study, flux measurements of TMA were performed with *Chenopodium vulvaria* to determine the emission potential. We observed a strong influence of the emission of TMA by mechanical stimuli. Main emission peaks occurred when introducing the plant into the cuvettes (Fig. 8 and Fig. 9, p1) and touching the plant stem outside of the cuvette during the experiment (Fig. 9, p3). As mentioned in Sect. 4.1, the glands were very fragile and could easily be destroyed by handling, which led to a release of TMA even over  $8 \text{ nmol m}^{-2} \text{ s}^{-1}$ . As the emission is affected by the intensity of the mechanical stimuli, we could not observe a significant relationship between the fertilization levels and the emission rate of TMA. However, we could observe further TMA emission peaks (Fig. 9, p2, p4, p5), which were not related to the mechanical stimuli of the plant. We assumed that the occurrence of these emission peaks were due to the changes in environmental parameters such as light and *RH*, which occurred during the transition from light to dark period. This is in accordance with the suggestion of Cromwell (1949), who assumed the relative humidity and temperature to be the driving factors of the emission of TMA. We assume that these environmental factors may not impact the release of the TMA from the gland vesicles, but the release of the adsorbed TMA on the leaf surface.

In general, cuvette measurements of TMA flux from plants are not trivial. One of the critical points is the relative humidity inside the cuvette. Due to the high water solubility of TMA ( $H^*_{\text{TMA}} = 9.2 \text{ M atm}^{-1}$ , see Christie and Crisp, 1967) a significant wall loss of TMA within the cuvette could be assumed at higher *RH*. As in our experiment the *RH* inside the cuvette was up to 70 %, a significant amount of gaseous TMA could be taken up by water films formed on the cuvette wall material and release it in turn under drier conditions. This process represents the major source of uncertainty for the measured emission flux. Hence, the challenge for future studies will be to investigate the emission of TMA by plants under more suitable conditions with an optimal range of humidity. This will improve the quality of the measured emission flux significantly and lead to a more precise estimation of the contribution of emitted TMA by plants.

#### 4.4 Influence of TMA on atmospheric new particle formation

The important role of amines in relation to new aerosol particle formation (NPF) was investigated by recent studies as Almeida et al., 2013, Kurten et al., 2014 and Glasoe et al., 2015. Almeida et al. (2013) found that DMA could influence the atmospheric new particle formation more efficiently than ammonia. At a volume mixing ratio above 3 ppt, DMA was able to enhance particle formation rate more than 1000-fold compared with ammonia. Kurten et al. (2014) showed on the molecular level the stabilization of sulfuric acid by DMA resulting in a concentration increase of stable molecular clusters up to 6 orders of magnitude. The higher stabilization efficiency of DMA was explained by its chemical property as a stronger base compared with ammonia (Ortega et al., 2012). Glaseo et al. (2015) investigated the effect of various amines on the sulfuric acid nucleation process and found that in the case of TMA the effect on the particle formation rate was the strongest followed by DMA and MMA. The aim of our nucleation experiments was to gain a first insight into the ternary nucleation process, which could be potentially induced by organic substances as formic acid, acetic acid and tartaric acid. We used sulfuric acid to validate our nucleation reactor. The results (Fig. 10) confirmed previous studies, which found an enhancing effect of TMA on the ternary nucleation process with sulfuric acid. Every single increase of the TMA mixing ratio caused an abrupt increase of the particle number concentration up to  $3.5 \cdot 10^4 \text{ cm}^{-3}$ . In the case of the nucleation experiment with formic acid and TMA an enhancement of the particle concentration could be observed as well, but of 3 orders of magnitude lower than with sulfuric acid (Fig. 11). For acetic and tartaric acid no significant enhancement of the particle concentration was observed in our experiments (data not shown). Dawson et al. (2012) showed that TMA and DMA could form a stable cluster with methane sulfuric acid, respectively. One of the key components were  $\text{H}_2\text{O}$  molecules, which were required for forming methane sulfuric acid hydrate acting as a particle precursor on the one hand and the methane sulfuric acid – amine –  $\text{H}_2\text{O}$  complex to form particles on the other hand. Formic acid and acetic acid are also able to form hydrates with binding  $\text{H}_2\text{O}$  molecules on the carbonyl oxygen and hydroxyl hydrogen atoms (Soffientini et al., 2015). Furthermore, an increase in the total coordination number of these organic acids could be reached by binding more  $\text{H}_2\text{O}$  molecules (Takamuku et al., 2007). Therefore, Soffientini et al., 2015 assumed that the combination of these effects makes the hydrated acid molecules “stickier” and benefits nucleation processes. However, a significant influence of TMA on organic acid induced new particle formation could not be excluded. On this point, more process studies are needed to investigate the underlying mechanism of the nucleation process with organic acid and TMA in relation to environmental factors like relative humidity.

## 5 Conclusion

The results of our study give a new insight into the emission of TMA by terrestrial vegetation and their potential impact on atmospheric new particle formation. The emission of TMA from *Chenopodium vulvaria* was attributed to the epidermal gland vesicles, which were evenly distributed on both sides of the leaf. Due to its fragility, the contained liquid TMA can be easily released by handling or even slight air streams, whereupon a high amount of TMA ( $> 8 \text{ nmol m}^{-2} \text{ s}^{-1}$ ) can be emitted by the plant. Thus, under natural conditions with mechanical stimuli (like wind) *Chenopodium vulvaria* could contribute with high emissions of TMA locally. Additionally, environmental factors such as light and relative humidity could be assumed as a potential driver for TMA emission, as they govern uptake and release of adsorbed/soluble TMA.

Further TMA emitting plant species (*Crataegus monogyna*, *Sorbus aucuparia*, *Pyrus communis* and *Chenopodium vulvaria*) were investigated by screening experiments. For the first three species, the emission of TMA occurred at the flowering period. All these plant species represent an emission source of volatile TMA. Due to their wide geographical distribution and depending on the flowering period, a potential contribution to the global budget of volatile TMA can be assumed.

The impact of volatile TMA on the atmospheric new particle formation could be demonstrated qualitatively on the ternary nucleation system with sulfuric acid – TMA – H<sub>2</sub>O and formic acid – TMA – H<sub>2</sub>O. The enhancing effect of volatile TMA on the particle concentration was in the case of sulfuric acid 3 orders of magnitude higher than with formic acid. For the other tested organic acids (acetic acid and tartaric acid) no significant enhancement of the particle concentration was observed. However, for formic acid a small effect on the particle formation could be observed. Thus, an influence of TMA on organic acid induced new particle formation could not be completely excluded.



## References

- Almeida, J. et al.: Molecular understanding of sulphuric acid–amine particle nucleation in the atmosphere, *Nature*, 502, 359–363, 2013.
- Calderón, S.M., Poor, N.D. and Campbell, S.W.: Estimation of the particle and gas scavenging contributions to wet deposition of organic nitrogen. *Atmospheric Environment*, 41, 4281-4290, 2007.
- Christie, A. O. and Crisp, D. J.: Activity coefficients of the n-primary, secondary and tertiary aliphatic amines in aqueous solution, *J. appl. Chem.*, 17, 1967.
- Cromwell, B. T.: The Micro-estimation and Origin of Trimethylamine in *Chenopodium vulvaria* L., *Biochem. J.*, 45, 84, 1949.
- Cromwell, B. T. and Richardson M.: Studies on the biogenesis of some simple amines and quaternary ammonium compounds in higher plants, *Phytochemistry*, 5, 735-746, 1966.
- Dawson, M. L., Varner, M. E., Perraud, V., Ezell, M. J., Gerber, R. B., and Finlayson-Pitts, B. J.: Simplified mechanism for new particle formation from methanesulfonic acid, amines, and water via experiments and abinitio calculations, *Proceedings of the National Academy of Sciences*, 109, 18719–18724, 2012.
- Dessaignes, M.: Trimethylamine obtenue de l'urine humaine, *C. R. Acad. Sei. (Paris)*, 43, 670-671, 1856.
- Ge, X., Wexler, A. S. and Clegg, S. L.: Atmospheric amines – Part I. A review, *Atmospheric Environment*, 45, 524-546, 2011.
- Groom: Piecing together the biogeographic history of *Chenopodium vulvaria* L. using botanical literature and collections. *PeerJ*, 3, 723, 2015.
- Chen, M., Titcombe, M., Jiang, J., Jen, C., Kuang, C., Fischer, M. L., Eisele, F. L., Siepmann, J. I., Hanson, D. R., Zhao, J., and McMurry, P. H.: Acid-base chemical reaction model for nucleation rates in the polluted atmospheric boundary layer, *Proceedings of the National Academy of Sciences*, 109, 18 713–18 718, 2012.
- Glusoe, W. A., Volz, K., Panta, B., Freshour, N., Bachman, R., Hanson, D. R., McMurry, P. H. Jen, C.: Sulfuric acid nucleation: An experimental study of the effect of seven bases, *Journal of Geophysical Research-Atmospheres*, 120(5), 1933-1950, 2015.
- Graus, M., Müller, M. and Hansel, A.: High Resolution PTR-TOF: Quantification and Formula Confirmation of VOC in Real Time, *J. Am. Soc. Mass. Spectrom.*, 21(6), 1037-1044, doi:10.1016/j.jasms.210.02.006, 2010
- Grosjean, D.: Organic acids in southern California air: ambient concentrations, mobile source emissions, in situ formation and removal processes, *Environ. Sci. Technol.*, 23, 1506 –

- 1514, 1989.
- Gyan, K. Y. and Woodell, S. R. J.: Flowering Phenology, Flower Colour and Mode of Reproduction of *Prunus spinosa* L. (Blackthorn); *Crataegus monogyna* Jacq. (Hawthorn); *Rosa canina* L. (Dog Rose); and *Rubus fruticosus* L. (Bramble) in Oxfordshire, England, *Functional Ecology*, 1, 261, doi:10.2307/2389429, 1987.
- Christensen, K. I.: Revision of *Crataegus* sect. *Crataegus* and nothosect. *Crataeguineae* (Rosaceae-Maloideae) in the Old World, American Society of Plant Taxonomists, Ann Arbor, Mich., 00101, 1992.
- Fitter, A., *ed.* (1978) An Atlas of the Wild Flowers of Britain and Northern Europe. *Collins, London, UK.*
- Fujii, T. and Kitai, T.: Determination of trace levels of trimethylamine in air by gas chromatography/surface ionization organic mass spectrometry, *Analytical Chemistry*, 59, 379-382, 1987.
- Hultén, E. & Fries, M., *eds* (1986) Atlas of North European Vascular Plants. North of the Tropic of Cancer, Vol. II. *Koeltz Scientific Books, Königstein, Germany.*
- Jalas J. and Suominen J.: Atlas florae Europaeae, Vol.5, Helsinki: The Committee for Mapping the Flora of Europe and Societas Biologica Fennica Vanamo 1980.
- Kurten, A. et al.: Neutral molecular cluster formation of sulfuric acid-dimethylamine observed in real time under atmospheric conditions, *Proceedings of the National Academy of Sciences*, 111, 15019–15024, 2014.
- Lee, D, Wexler, A. S: Atmospheric amines e Part III: Photochemistry and toxicity, *Atmospheric Environment*, 71, 95 – 103.
- 2013.
- Meusel, H, Jäger, E. and Weinert, E.: Vergleichende Chorologie der Zentraleuropäischen Flora, Vol. 1, Jena: Gustav Fischer, 1992.
- Müller, M., Mikoviny, T., Jud, W., D’Anna, B. and Wisthaler, A.: A new software tool for the analysis of high resolution PTR-TOF mass spectra, *Chemometrics Intell. Lab. Sys.*, 127, 158 – 165, doi:10.1016/j.chemolab.2013.06.011, 2013.
- Okita, T.: Filter method for the determination of trace quantities of amines, mercaptans, and organic sulphides in the atmosphere, *Atmospheric Environment*, 4, 93-102 1970.
- Ortega, I. K., Kupiainen, O., Kurtén, T., Olenius, T., Wilkman, O., McGrath, M. J., Loukonen, V., and Vehkamäki, H.: From quantum chemical formation free energies to evaporation rates, *Atmospheric Chemistry and Physics*, 12, 225–235, doi:10.5194/acp-12-225-2012, 2012.

- Raspé, O., Findlay, C. and Jacquemart, A. L.: *Sorbus aucuparia* L., *Journal of Ecology*, 88(5), 910–930, doi: 10.1046/j.1365-2745.2000.00502.x, 2000.
- Riccobono, F. et al.: Oxidation Products of Biogenic Emissions Contribute to Nucleation of Atmospheric Particles, *Science*, 344, 717–721, 2014.
- Schade, G.W. and Crutzen, P.J.: Emission of aliphatic amines from animal husbandry and their reactions: potential source of N<sub>2</sub>O and HCN, *Journal of Atmospheric Chemistry*, 22, 319-346, 1995.
- Sintermann, J. and Neftel, A.: Ideas and perspectives: on the emission of amines from terrestrial vegetation in the context of new atmospheric particle formation, *Biogeosciences*, 12(11), 3225-3240, 2015.
- Spracklen, D. V., Jimenez, J. L., Carslaw, K. S., Worsnop, D. R., Evans, M. J., Mann, G. W., Zhang, Q., Canagaratna, M. R., Allan, J., Coe, H., McFiggans, G., Rap, A., and Forster, P.: Aerosol mass spectrometer constraint on the global secondary organic aerosol budget, *Atmospheric Chemistry and Physics*, 11, 12 109–12 136, 2011.
- Smith, T. A.: The occurrence, metabolism and functions of amines in plants, *Biological Reviews*, 46, 201–241, 1971.
- Smith, T. A.: Recent advances in the biochemistry of plant amines, *Phytochemistry*, 14, 865–890, 1975.
- Sun, S., Moravek, A., von der Heyden, L., Held, A., Sörgel, M. and Kesselmeier, J.: Twin-cuvette measurement technique for investigation of dry deposition of O<sub>3</sub> and PAN to plant leaves under controlled humidity conditions, *Atmospheric Measurement Techniques Discuss*, 8, 12051-12104, doi:10.5194/amtd-8-12051-2015, 2015
- Takamuku, T., Kyoshoin, Y., Noguchi, H., Kusano, S. and Yamaguchi, T.: Liquid structure of acetic acid–water and trifluoroacetic acid–water mixtures studied by large-angle X-ray scattering and NMR, *J. Phys. Chem., B* 111, 9270–9280, 2007.
- Tröstle et al.: The role of low-volatility organic compounds in initial particle growth in the atmosphere, *Nature*, 533, 527 – 531, 2016
- Veres, P. R., Faber, P., Drewnick, F., Lelieveld, J., and Williams, J.: Anthropogenic sources of VOC in a football stadium: Assessing human emissions in the atmosphere, *Atmos. Environ.*, 77, 1052–1059, doi:10.1016/j.atmosenv.2013.05.076, 2013.
- Wang, X.C. and Lee, C.: Sources and distribution of aliphatic amines in salt marsh sediment. *Organic Geochemistry*, 22, 1005-1021, 1994.
- Welter, M. & Ruben Sutter, H.C., eds (1982) *Atlas de Distribution des Ptéridophytes et des Phanérogames de la Suisse. Birkhäuser Verlag, Basel, Switzerland.*

Wicke, W.: Beobachtungen an *Chenopodium vulvaria* über die Ausscheidung von Trimethylamin, *Annalen der Chemie und Pharmacie*, 124, 338–340, 1862.

# Appendix E

## Curriculum vitae

Geburtsdatum / -ort 03.05.1985 / Xi´An (VR China)  
Staatsangehörigkeit deutsch  
Familienstand ledig



## Ausbildung und Studium

---

Feb. 2013 – Nov. 2016 Promotionsstudium im Fachbereich Chemie am Max-Planck-Institut für Chemie in Zusammenarbeit mit der Johannes Gutenberg Universität in Mainz, Abteilung Biogeochemie  
Research topic: Biosphere-atmosphere exchange of reactive trace gases and aerosols

Nov. 2010 – Feb. 2013 Goethe Universität Frankfurt am Main  
Master-Studiengang Umweltwissenschaft  
Master Arbeit: *Construction, Online-Untersuchung und Modellierung von Parametern zur Beschreibung atmosphärischer Nukleation durch Simulationskammerstudien (COMPASS)*, Note: „sehr gut“  
Abschluss: Master of Science in Umweltwissenschaften  
Note: „sehr gut“

Okt. 2006 – Nov.2010	Goethe Universität Frankfurt am Main Bachelor-Studiengang Chemie Bachelor Arbeit: <i>In vivo assessment of mitochondrial/rhodamine 123 fluorescence</i> , Note: „sehr gut“ Abschluss: Bachelor of Science in Chemie, Note: „gut“
Juni. 1999 – Juni. 2006	Wöhler-Gymnasium, Frankfurt am Main Abschluss: Allgemeine Hochschulreife (Abitur)
Aug.1998 – Juni. 1999	Paulsen-Gymnasium, Berlin

### Stipendium

---

Feb. 2013 – vsl. Aug. 2016	Max-Planck-Stipendium zur Förderung der Forschung am Max-Planck-Institut für Chemie.
----------------------------	--

### Fortbildungen

---

2015	Workshop „Digital Research Communication“
2015	Summerschool „Advanced Course on Applied Time Series Analysis“, Climate Risk Analysis GmbH, Germany
2014	Schulung Autodesk Inventor Professionals 2014
2013	Trainingskurs LabVIEW-Grundlagen 1 und 2
2005	Praktikumskurs bei Provadis, Industriepark Höchst

### Tätigkeit in der Lehre

---

SS 15 und WS 15/16	Betreuung des Praktikums Analytische Chemie an der Johannes Gutenberg Universität in Mainz.
SS 16	Betreuung des botanischen Praktikums F2 an der Johannes Gutenberg Universität in Mainz.
Feb. – Mrz. 2016	Betreuung des Schülerpraktikums in Gasphasenanalytik am Max-Planck-Institut für Chemie

---

## Wissenschaftliche Vorträge / Präsentationen

---

17. – 22. April. 2016      Teilnahme an der European Geosciences Union mit eigenem Vortrag und eigener Poster-Präsentation
- Vortrag: Influence of liquid water films on the O<sub>3</sub> and PAN deposition on plant leaves treated with organic / inorganic compounds
- Poster: Emission of Trimethylamine from *Chenopodium vulvaria* and their potential impact on the atmospheric new particle formation

## Publikationen

---

- Erstautorenschaft      Sun, S., Moravek, A., von der Heyden, L., Held, A., Sörgel, M. and Kesselmeier, J.: Twin-cuvette measurement technique for investigation of dry deposition of O<sub>3</sub> and PAN to plant leaves under controlled humidity conditions, *Atmospheric Measurement Techniques*, 9, 599-617, doi: 10.5194/amt-9-599-2016, 2016
- Zweitautorenschaft      Bonn, B., Sun, S., Haunold, W., Sitals, R., van Beesel, E., dos Santos, L., Nillius, B. and Jacobi, S.: COMPASS – COMparative Particle formation in the Atmosphere using portable Simulation chamber Study techniques, *Atmospheric Measurement Techniques*, 6(12), 3407-3423, 2013.
- Weitere Publikationen      Bonn, B., Bourtsoukidis, E., Sun, S. T., Bingemer, H., Rondo, L., Javed, U., Li, J., Axinte, R., Li, X., Brauers, T., Sonderfeld, H., Koppmann, R., Sogachev, A., Jacobi, S. and Spracklen, D. V.: The link between atmospheric radicals and newly formed particles at a spruce forest site in Germany, *Atmos. Chem. Phys.*, 14, 10823-10843, doi:10.5194/acp-14-10823-2014, 2014

## Weitere Kenntnisse

---

- Sprachkenntnisse:      Chinesisch (Muttersprache)  
                                   Deutsch (Abitur)  
                                   Englisch (fließend in Wort und Schrift)  
                                   Latein (Großes Latinum)

EDV-Kenntnisse:

Betriebssysteme:

- Microsoft Windows (sehr gute Kenntnisse)
- OS X (sehr gute Kenntnisse)
- Linux (Grundkenntnisse)

Text- und Bildverarbeitungsprogramme:

- MS Office (sehr gute Kenntnisse)
- Adobe Photoshop (gute Kenntnisse)

Programmiersprachen:

- MATLAB<sup>®</sup> v2010a (sehr gute Kenntnisse)
- LabVIEW (Grundkenntnisse)

Analytikprogramme:

- OriginLab (sehr gute Kenntnisse)
- Biostatistic Prism Graphpad (sehr gute Kenntnisse)

SAP NetWeaver (sehr gute Anwenderkenntnisse)

## Interessen

---

Engagement

Übungsleiter bei Sportvereinen  
(TVE Eschersheim, TSG Ginnheim)

Hobbys

Ausgebildeter Choreograph/Tanzsporttrainer Lizenzstufe C

## Sonstiges

---

Führerscheinklasse B

Frankfurt am Main, 24.11.2016

Shang Sun